PARAMETRIC STUDY AND OPTIMIZATION OF WEDM PROCESS PARAMETERS OF PURE TITANIUM

A thesis submitted
in fulfilment of the requirements
for the award of the degree
of

DOCTOR OF PHILOSOPHY

by

ANISH KUMAR
Reg. No. 950908010

DEPARTMENT OF MECHANICAL ENGINEERING

THAPAR UNIVERSITY

PATIALA-147004

2014

PREFACE

This research work was carried out by the author under the guidance of **Dr. Vinod Kumar**, Associate Professor, Department of Mechanical Engineering, Thapar University, Patiala and **Dr. Jatinder Kumar**, Assistant Professor, Department of Mechanical Engineering, National Institute of Technology (N.I.T), Kurukshetra, Haryana.

WEDM machine (Four-axis Electronica Sprintcut-734 CNC WEDM), Surface roughness (SJ-301) measuring instruments, Weighing machine apparatus and other facilities available at the Central Tool Room, Ludhiana were used for the research work. For analyzing the microstructure of the machined samples, Scanning Electron Microscope (SEM), Energy Dispersive X-ray analysis (EDX) and X-ray Diffraction (XRD) set-ups available at Indian Institute of Technology (I.I.T), Ropar were used.

Several research papers were published out of the present research work. **The list of Journals/Conferences in which the papers find place is given below:**

Journals (SCI-Indexed)

1. Kumar, Anish, Kumar, Vinod, Kumar, Jatinder, "Multi-response optimization of process parameters based on response surface methodology for pure titanium using WEDM process", *International Journal of Advanced Manufacturing Technology*, Vol.68, Iss.9, 2013, pp.2645-2668. **(SCI-Indexed; Thomson Reuters)**
2. Kumar, Anish, Kumar, Vinod, Kumar, Jatinder, "Investigation of machining parameters and surface integrity of pure titanium after Wire Electric Discharge Machining (WEDM)", *Proceedings of Institutions of Mechanical Engineering, Part B: Journal of Engineering Manufacture*, Vol.227, Iss.7, 2013, pp.972-992. **(SCI-Indexed; Thomson Reuters)**
3. Kumar, Anish, Kumar, Vinod, Kumar, Jatinder, "Experimental Investigation on Material Transfer Mechanism in WEDM of Pure Titanium (Grade-2)", *Advances in Materials Science and Engineering*, 2013, pp.1-20, DOI: dx.doi.org/10.1155/2013/847876. **(SCI-Indexed; Thomson Reuters)**
4. Kumar, Anish, Kumar, Vinod, Kumar, Jatinder, "Surface integrity and material transfer investigation of pure titanium for rough cut surface after wire electro discharge machining", *Proceedings of Institutions of Mechanical Engineering, Part B:*

Journal of Engineering Manufacture, 2014, Vol.228, No.8, pp. 880-901. **(SCI-Indexed; Thomson Reuters)**

5. Kumar, Anish, Kumar, Vinod, Kumar, Jatinder, "Microstructure analysis and material transformation of pure titanium and tool wear surface after wire electric discharge machining process", *Machining Science and Technology*, Vol. 18 Iss. 1, 2014, pp.47-77. **(SCI-Indexed; Thomson Reuters)**
6. Kumar, Anish, Kumar, Vinod, Kumar, Jatinder, " Semi-empirical model on MRR and overcut in WEDM process of pure titanium multi-objective desirability approach", *Journal of the Brazilian Society of Mechanical Sciences and Engineering*, 2014, DOI 10.1007/s40430-014-0208-1 **(SCI-Indexed; Thomson Reuters)**

CONFERENCES (International)

1. Kumar, Anish, Kumar, Vinod, Kumar, Jatinder, "Effect of Machining Parameters on MRR during CNC WEDM of Pure Titanium", *Proceedings of the 5th International Conference on Advances in Mechanical Engineering (ICAME-2011)*, National Institute of Technology, Surat, June 06-08, 2011, pp.541-545, Gujarat, India.

(Anish Kumar)

ACKNOWLEDGEMENTS

"God doesn't require us to succeed; he only requires that you try"

— Mother Teresa

The present thesis work is a living testimony to the numerous contributions of a galaxy of distinguished personalities whom I had the good fortune of associating with. I deem it an honor and duty to acknowledge the help and cooperation I received from these luminaries. First of all, I express profound sense of obligation to the "Omnipresent" for showering immense blessings on me and my family, which culminated into the success of this great endeavor.

The author wishes to express my heartfelt, deep sense of unbound gratitude and indebtedness to my supervisors **Dr. Vinod Kumar**, Associate Professor, Department of Mechanical Engineering, Thapar University, Patiala and **Dr. Jatinder Kumar**, Assistant Professor, Department of Mechanical Engineering, National Institute of Technology, Kurukshetra, Haryana for having given me an opportunity to do research in the area of WEDM process for inspiring guidance given throughout this research work.

Heartfelt thanks are due to Prof. Prakash Gopalan (Director, Thapar University, Patiala) and Dr. P.K. Bajpai (Dean, Research and Sponsored Projects, Thapar University, Patiala), Dr. Ajay Batish (Prof. & Head, Mechanical Engineering Department, Thapar University, Patiala), Dr. Kulbir Singh (Prof. & Head, Material Science and Engineering Department), Dr. Tarun Nanada (PhD coordinator) for their encouragement and support during this research work.

I am indebted to Mr. S.P.Singh and Mr. Sharanpreet of Central Tool Room, Ludhiana for providing me free hand in working on EDM Wire Cut machine tool, without which the present work could have been somewhere at its half-way and I thank them with a heart full of reverence.

The author is also thankful to Dr. Harpreet Singh and Ms. Narinder Kaur (Lab Superintendent), IIT, Ropar for providing laboratory facilities (SEM, XRD, and EDX).

I am thankful to Dr. N. K. Batra, Professor and Head, Department of Mechanical Engineering, MMEC, Mullana (Ambala) for his timely recommendations, suggestions, support and for

providing necessary departmental facilities, services and peaceful ambience for research work.

I present my heartfelt thanks to Sh. Tarsem Kumar Garg, Chairman, Maharishi Markandeshwar University and Dr N. P. Mehta, Director, M.M. Engineering College, Maharishi Markandeshwar University (MMU), Ambala, for the motivation and their unstinted support in matter pertaining to my leave.

Many thanks to my friends and colleagues in MMU and others, Dr. Rajesh Khanna, Mr. Rahul Dev Gupta, Dr. R. C. Sharma, Dr. M. P. Garg, Dr. Sandeep Jindal, Dr. Kapil Goel, Dr. Vivek Jain, Dr. J.S.Saini, Mr. Jatinder Chabbra, Mr. Atul Sharma and Mr. Vishal Gupta who always stood with me.

I avail the privilege to pour on paper my regards to my parents, Sh. Romesh Kumar Kaushik and Smt. Raj Rani. They had given me unequivocal support throughout, as always, for which my mere expression of thanks likewise does not suffice.

No amount of thanks is enough, finally, for my beloved wife Renu Sharma who held the key to my success. Her patience and encouragement kept my motivation up. Despite all odds, she single handedly and intelligently managed all family matters as well as my two naughty kids (Ailesh and Devesh) along with her job.

I thank all the souls who helped me in this herculean task. Finally, I bow my head to the **ALMIGHTY** for all the blessings he has showered on me.

(**Anish Kumar)**

CERTIFICATE

Certified that the thesis entitled "**PARAMETRIC STUDY AND OPTIMIZATION OF WEDM PROCESS PARAMETERS OF PURE TITANIUM**" which is being submitted by Mr. Anish Kumar, to the Department of Mechanical Engineering, Thapar University, Patiala, in the fulfillment of the requirements for the award of the degree of **DOCTOR OF PHILOSPHY,** is a record of bonafide research work carried out by him under our guidance and supervision. The matter presented in this thesis has not been submitted either in part or full to any other University or Institute for the award of any degree.

(Dr. Vinod Kumar)
Associate Professor
Department of Mechanical Engineering
Thapar University, Patiala, Punjab,
INDIA
(Supervisor)

(Dr. Jatinder Kumar)
Assistant Professor
Department of Mechanical Engineering
National Institute of Technology (N.I.T)
Kurukshetra, Haryana, INDIA
(Co-Supervisor)

ABSTRACT

Titanium has been recognized as an element (symbol Ti; atomic number 22 and atomic weight 47.9) for at least 200 years. High strength, low density and excellent corrosion resistance are the main property that makes titanium attractive for a variety of applications. The major application of the material is in the aerospace industry, both in airframes and engine components. Non aerospace applications take advantage mainly of their excellent strength properties, for example steam turbine blades, superconductors, missiles etc. or corrosion resistance, for example marine services, chemical, petrochemical, electronics industry, biomedical instruments etc. Pure titanium offers good corrosion resistance in most environments, excluding those containing fluoride ions where it cannot compete with some ceramics, tantalum and various high-nickel alloys. In fluoride-free environments, titanium is cost effective when competing with high-alloy, corrosion-resistant materials such as Hastalloy. When compared with stainless steel, titanium has a much superior technical performance but would not be selected over commodity products such as ferritic and austenitic stainless steels as it is not cost-effective. Several problems such as chatter formation, lower cutting speed and generation of deformed machined surface are observed during conventional machining of titanium and its alloys. Thus, there is a crucial need for reliable and cost effective methods for machining of pure titanium. Over the passage of time, there have been great advancements in development of cutting tools including coated carbides, cubic boron nitrides and polycrystalline diamond. These tools have been successfully applied in machining of steels, high temperature alloys such as nickel based alloys and cast iron, but none of these is found truly applicable in machining of titanium alloys. Attempts have been made for cryogenic machining of titanium alloys by cooling the work piece or tools using a cryogenic coolant. But, even these approaches have inherent limitations. Some studies have proved that use of cutting fluids may improve machinability of titanium alloys using conventional machining. However, toxicity of cutting fluids seriously degrades the quality of machining environment. Keeping in view the difficulties associated with conventional machining of titanium, attempts can be made for machining of these using non conventional machining such as, electric discharge machining (EDM), abrasive water jet machining (AWJ), laser beam machining (LBM), ultrasonic machining (USM). Non conventional machining techniques such as AWJ, LBM can be used, but, the cost of

equipment is high, height of the work-piece is a constraint as well as the accuracy and surface finish problems come into picture. Ultrasonic machining imparts better surface characteristics on the work piece; however, metal removal rate is very low, coupled with a relatively higher tool wear rate. On the other hand, a technique such as wire electric discharge machining (WEDM) seems to be a better choice as it can machine parts with complicated geometries and intricate shapes. This research work is mainly focused on WEDM of pure titanium (grade-2). An attempt has been made to model the eight response variables i.e. machining rate, surface roughness, material removal rate (MRR), overcut, dimensional deviation, wire wear ratio, surface crack size density and recast layer thickness in WEDM process using response surface methodology. The experimental plan is based on Box-Behnken design. The six parameters i.e. pulse on time, pulse off time, peak current, spark gap voltage, wire feed and wire tension have been varied to investigate their effect on output responses. These responses have been optimized using multi-response optimization through desirability. The ANOVA has been applied to identify the significance of developed model. The test results confirm the validity and adequacy of the developed RSM model. Finally, the optimum parametric setting has been designed for the optimization of process. An attempt has also been made to construct a micro-model for prediction of material removal rate and surface roughness using dimensional analysis. The present research work is also mainly focused on the investigation of integrity of the work surface and wire electrode surface after machining with WEDM. Experimental results showed that pulse on time, pulse off time and peak current significantly affected the surface integrity with the formation of deep-wide overlapping craters, pock marks, debris, micro cracks and recast layer. Both carbides and oxides were formed either in free form and/or in compound form due to decomposition of de-ionized water, machined samples and wire material. The compounds like titanium dioxide (rutile) (TiO_2), ($TiO_{0.325}$), Ti_2O_3, Ilmenite (Fe_2Ti_4O), titanium carbides (TiC) and copper titanium dioxide (Cu_3TiO_4) were formed due to phase transformations that were analyzed through X-ray diffraction and energy dispersive X-ray method. The effect of process parameters on the wear of wire surface has also been considered.

LIST OF TABLES

LIST OF FIGURES

CONTENTS

CHAPTER 1

INTRODUCTION

With the development of technology, the scientists and technologists in the field of manufacturing are facing more and more challenges. Technologically advanced industries such as aeronautics, nuclear reactors and automobiles have been demanding high strength temperature resistant (HSTR) materials having high strength to weight ratio. Researchers in the area of materials science are developing materials having higher strength, hardness, toughness and other diverse properties. This also needs the development of improved cutting tool materials so that productivity is not hampered. The conventional machining processes, in spite of recent technical advancements, are inadequate to machine complex shapes in hard, high strength temperature resistant alloys and die steels. Keeping these requirements into mind, a number of Non-traditional machining (NTM) processes have been developed. These can be classified depending upon the type of energies used,

(1) Mechanical Processes: In mechanical processes metal removal takes place either by the mechanism of simple shear (conventional machining) or by erosion mechanism where high velocity particles are used as transfer media and pneumatic/hydraulic pressure acts as source of energy. It includes Abrasive Jet Machining, Ultrasonic Machining, and Water Jet Machining etc.

(2) Chemical Processes: Chemical processes involve the application of resistant material (acidic or alkaline in nature) to certain portion of the work-piece. The desired amount of material is removed from the remaining area of work surface by the subsequent application of an etchant that converts the work-piece material into a dissolvable metallic salt. It includes chemical machining, photochemical machining etc.

(3) Electrochemical Processes: Electrochemical processes involve removal of metal by the mechanism of ion displacement. High current is required as the source of energy and electrolyte acts as transfer media. It includes Electrochemical Machining, Electro Chemical Grinding, and Electro- Jet Drilling etc.

(4) Thermal Processes: Thermal processes involve the application of very intense local heat. Here melting or vaporizing small areas at the surface of the work piece

removes material. The source of energy used is amplified light radiation (Laser Jet Machining,), ionized substance (Iron Beam Machining and Plasma Arc Machining,) and high voltage (Electric discharge machining).

Non-traditional machining processes are called advanced manufacturing processes since they are established in modern industries. In addition, non-traditional machining processes do not use sharp cutting tools. Traditional machining processes such as turning; drilling, shaping and milling are not suitable for machining of extremely hard and brittle materials and may have many difficulties in machining such materials. In such circumstances, conventional processes may not be feasible, satisfactory or economical due to the following characteristics:

a) The tool must be harder than the work piece.
b) There is a direct mechanical contact between the tool and the work piece.
c) It is difficult to machine complicated shapes and obtain close tolerances.

In the recent manufacturing scenario, innovations/improvements in engineering design and ever increasing demands on material performance have resulted in the development and emergence of a spectrum of material alloy combinations engineered for a variety of purposes and applications.

1.1 TITANIUM AND ITS MACHINABILITY

Titanium has been developed in order to satisfy the needs for a class of strong and light weight materials for aircraft engines and airframe manufacturing. Titanium has been recognized as an element (Symbol Ti, atomic number 22, atomic weight 47.9) for at least 200 years. Titanium is the ninth most abundant element in earth's crust and fourth most commonly used structural metal. In nature, it occurs only as a mineral (ore) in combination with O_2 or Iron. Titanium products are available in both commercially pure and alloy grades. These can be grouped into three categories according to the predominant phase, or phases in their microstructure namely, alpha, alpha-beta and beta. Although each of these three general alloy types require specific and different mill processing methodologies, each offers a unique combination of properties, which may be advantageous for a given application. It was recognized in 1950's as a desirable material for aerospace applications. In 1960s and 1970s, titanium was considered for use in vessels and heat exchangers in corrosive environment. Today, these alloys have a wide variety of applications in modern aerospace, marine, automobile sector, atomic power plant reactors, and medical implants owing to their high strength to weight ratios, high strength

and toughness at elevated temperatures, excellent corrosion resistance, fracture resistance and low modulus of elasticity [Yang, 1999]. Pure titanium offers good corrosion resistance in most environments [Hong et al., 2001].

The aerospace industry is the single largest market for titanium products. Titanium's high corrosion resistance is also a valuable characteristic. When exposed to the atmosphere, titanium forms a tight, tenacious oxide film that resists many corrosive materials. Microstructure and mechanical properties in metals are intimately coupled. On a microscopic level, the interaction of crystalline structures in pure titanium and its alloys determines the mechanical properties of that alloy. On a macroscopic level, thermo-mechanical processing manipulates the formation of crystalline phases. The major applications of pure titanium as under [Wood, 1972]:

1. Extensively used for sea water piping's, reactor vessels and heat exchangers.
2. Orthopedic applications, such as implants and prosthesis
3. Airframe and aircraft engine parts
4. Marine chemical parts, Fish breeding cages, Handrails, Buildings, Structures and Monuments, Wheelchairs, Condenser tubing
5. Titanium is used for heart valves.
6. The Apollo capsules were made largely of pure titanium and many parts of the space shuttle are made of the metal.
7. The metal is used for the production of engine parts, portable computers, car accessories, sports equipment (golf clubs, tennis rackets, bicycles or underwater sport equipment).

1.2 PROBLEMS ENCOUNTERED IN MACHINING TITANIUM WITH CONVENTIONAL MACHINING

Titanium is branded as 'difficult to machine' material owing to its distinct properties already discussed. The machining characteristics of titanium and its alloys in conventional machining have been summarized as following:

1. Titanium and its alloys are poor thermal conductors. As a result, the heat generated when machining titanium cannot dissipate quickly; rather, most of the heat is concentrated on the cutting edge and tool face [Ezugwu and Wang, 1997; Takeyama and Murata, 1962; Almeida et. al., 2006].

2. Titanium has strong alloying tendency or chemical reactivity with the tool materials at tool operating temperatures. A temperature above 700° C provides an ideal environment for diffusion of tool material atoms across tool/chip and tool/work piece interfaces. This leads to dissolution of tool materials and therefore rapid destruction of the cutting edge [Nabhani, 2001; Leigh et al., 2000].
3. During machining, titanium alloys exhibit thermal plastic instability that leads to unique characteristics of chip formation. The shear strains in the chip are not uniform; rather, they are localized in a narrow band that forms serrated chips [Amin et. al, 2007; Ginting and Nouari, 2007].
4. The thin chips produced when machining titanium alloy, combined with narrow shear zone and short chip/tool contact lengths result in high temperature closer to edge of the cutting tool and this leads to failure of tools when machining Ti-6Al-4V alloy with carbide tools [Nabhani, 2001].
5. Titanium is more "springy" than steel i.e. work piece tends to move away from tool unless heavy cuts are maintained. Slender parts tend to deflect under tool pressure and it can cause chatter, tool rubbing and hence tolerance problems [Donachie, 2000].
6. During machining of titanium with Tungsten Carbide inserts (with a rake angle of 10^{o}), deformation of metal is increased with an increase in speed. The depth of the deformed layer and extent of deformation depends upon cutting parameters such as cutting speed, tool geometry etc. It was observed that work surface is severely hardened. This hardness decreases sharply with an increase in depth beneath the surface [Jeelani, 1983].

Above discussion reveals that conventional machining processes are unable to provide good machining solutions for titanium. Thus, there is a crucial need for reliable and cost effective methods for machining of pure titanium [Kumar, 2009]. Attempts have been made for cryogenic machining of titanium alloys by cooling the work piece or tools using a cryogenic coolant. But, even these approaches have inherent weaknesses [Hu et al., 2002]. Some studies have proved that generous use of cutting fluids may improve machinability of titanium alloys using conventional machining. However, toxicity of cutting fluids seriously degrades the quality of machining environment [Sreejith and Nagoi, 2000].

Keeping in view the difficulties associated with conventional machining of titanium, attempts can be made for machining of these using non conventional machining such as,

Ultrasonic machining imparts better surface characteristics on the work piece; however, metal removal rate is very low, coupled with a relatively higher tool wear rate [Kumar, 2009]. On the other hand, a technique such as wire electric discharge machining (WEDM) seems to be a better choice as it can machine parts with complicated geometries and intricate shapes [Qin et al., 2003].

Therefore, in the present investigation, an attempt has been made to explore the use of wire electric discharge machining (WEDM) for machining of pure titanium (grade-2).

1.3 WIRE ELECTRIC DISCHARGE MACHINING

Wire electric discharge machining was first introduced to the manufacturing industry in late 1960s [Jameson, 2001]. By 1975, its popularity was rapidly increasing, as the processes and its capabilities were better understood by the industry [Benedict, 1987]. It was only towards the end of 1970s, when computer numerical control (CNC) system was introduced into WEDM that brought about a major evolution of the manufacturing process. As a result, the broad capabilities of the WEDM process were extensively exploited for any through hole machining application owing to the wire, which has to pass through the part to be machined. Its broad capabilities have allowed it to encompass production in aerospace and automotive industries and virtually all areas of conductive material machining [Spedding and Wang, 1997]. This is because wire EDM provides the best alternative, or sometimes the only alternative, for machining conductive, exotic and high strength and temperature resistive (HSTR) materials with the scope of generating intricate shapes and profiles [Puri and Bhattacharya, 2003a,b; Joshi and Das, 2010].

1.3.1 Process principle of wire electric discharge machining

WEDM employs continuously moving electrode in the form of a wire. As shown in Figure 1.1, the wire is moving on the spool, feeds through the workpiece, and is taken up on a second spool. The wire electrode is made of different materials (copper, brass, zinc coated, diffusion annealed etc.) of diameter ranging from 0.05-0.35mm. The gap between the wire and the work piece is flooded with de-ionized water, which acts as a dielectric. There is no mechanical contact between the wire and the work piece in WEDM. The gap between the wire and the workpiece usually ranges from 0.025mm to 0.050mm and is continuously maintained by a computer controlled positioning system. The wire is kept under tension by tensioning device to overcome the inaccuracies in the machined parts and is guided by two support members juxtaposing with the workpiece. The material is

removed by the series of electrical discharges [Mcgeough, 1988]. The wire is kept straight by a mechanical tensioning device and is fed into the work piece by a numerically controlled mechanism or a micro processor. A varying degree of taper ranging from 15º

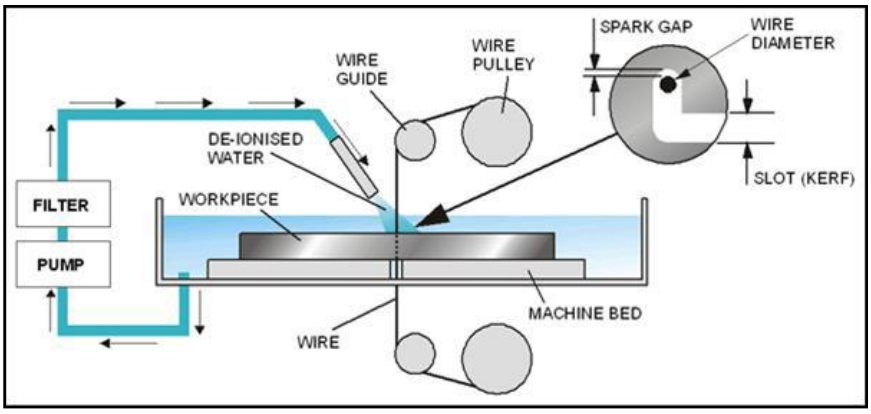

Figure 1.1 Schematic diagram of WEDM system [Guitrau, 1997]

for a 100 mm thick to 30º for a 400 mm thick work piece can be obtained on the cut surface using micro processor control [Benedict, 1987]. The objective of removing a defined quantity of metal from the work piece with every single spark demands for controlled energy flux from power source to the working gap. The power supply of an EDM process should be able to control the parameters of voltage, current, duration and frequency of a pulse. Power generators in WEDM usually are transistor-controlled RC systems that provide higher machining rate and larger gap size to reduce wire rupture risks. In the power system, the discharge frequency can be controlled by adjusting the pulse on time and pulse off tine of the transistors that control the charging pulse for the capacitor connected in parallel with the machining gap. Advanced features included are the anti-electrolysis circuitry that prevents the risk of electrolysis while cutting work pieces that are in the machine for extended periods. De-ionized water serves as the dielectric in a WEDM. The role of dielectric in serving as a medium for discharge is important. It serves a dual role both as an insulator and a conductor. Prior to the discharge, de-ionized water acts as an insulator, allowing the electrical potential between the wire and work piece to be built to certain intensity without bleeding it off through the fluid [Roger, 2010]. Dielectric also performs additional functions such as solidifying and flushing away the debris as well as keeping the wire and work piece cool. The role of discharge channel is crucial in assuring that each discharge cycle is same, else, difference in cutting speed, surface roughness and width of slot may be observed. Thus, maintaining a specific condition of the de-ionized water dielectric is essential to obtain consistent

results from WEDM. Dielectric gets contaminated by the debris removed which consists of the metal removed from the work piece as well as worn out metal from wire. Moreover, significant contamination is produced by the metal salts which are produced during the discharge and gets dissolved into the water. These dissolved salts increase the conductivity of water, causing spark to bleed off prior to the actual occurrence of the discharge, adversely affecting the consistency and efficiency of the discharge. In order to maintain the quality of the dielectric fluid, wire-EDM utilizes mechanical and chemical filtration processes.

Positioning system is necessary for the WEDM machine to follow a programmed path in order to create a specific part. The machine tool comprises of a main work table, an auxiliary table and a wire drive mechanism. The work piece is mounted and clamped on the main work table. The main table moves along X and Y axes, in steps of 0.5µm, by means of servo motors. As the material removal or machining proceeds, the work table carrying the work piece is displaced transversely along a predetermined path which is stored in the controller. The utmost requirement from the positioning system is that it must operate in an adaptive control mode to maintain a constant gap between the wire and the work piece.

In WEDM, electrode is a wire. These wires can range in diameter from 0.03 to 0.3 millimeters (0.001 to 0.012 inches). The traveling wire is continuously fed from spool to the work piece and goes finally to the waste-wire box. A number of forces act on the wire causing it to depart from the programmed path. These forces include the mechanical forces produced by the pressure from the gas bubbles formed by the plasma of the erosion mechanism, the hydraulic forces induced by the flushing, the electro-static forces acting on the wire and the electro-dynamic forces inherent to the spark generation [Dauw and Beltrami, 1994; Kinoshita et al., 1984]. Thus, along its traveling path, the wire is supported under tension, between a pair of wire guides which are disposed on both (lower and upper) sides of the work piece. This tension reduces the amount of vibration in the wire and deflection due to the flow of the dielectric fluid around the wire and due to other forces exerted on it.

1.3.2 Material removal mechanism in WEDM process

The WEDM process is described as:

Step: 1- As shown in Figure.1.2, the spark is initiated by power supply, which generates volts and amperes. The voltage and amperage control the spark between the wire

electrode and the workpiece. The de-ionized water surrounds the wire electrode and the workpiece.

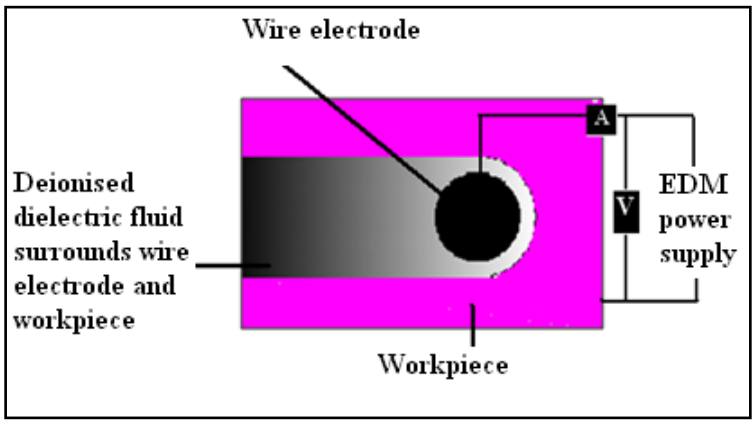

Figure 1.2 Schematic diagram of power supply [Guitrau, 1997]

Step: 2- During pulse-on cycle time, the dielectric fluid acts as resistor until enough voltage is applied. The fluid ionizes and the spark occurs between the wire electrode and the workpiece. The controlled spark erodes, precisely melts and vaporizes the workpiece material (Figure. 1.3).

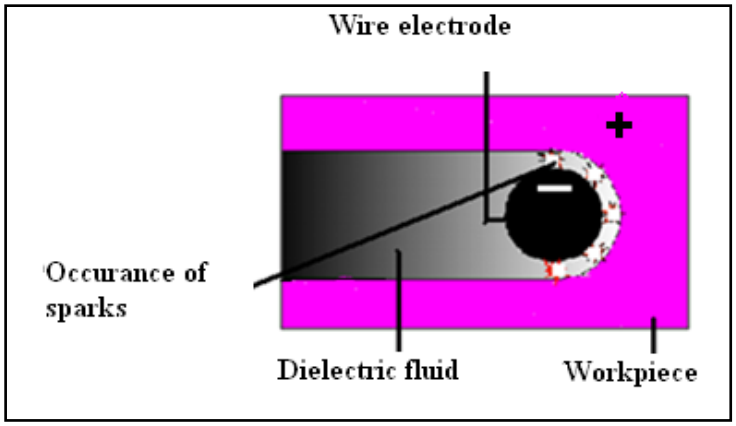

Figure 1.3 Schematic diagram of occurrence of sparks [Guitrau, 1997]

Step: 3 - The sparking process is completed during the pulse-off cycle time. The pressurized dielectric fluid immediately cools the material and the eroded particles are flushed out (Figure. 1.4).

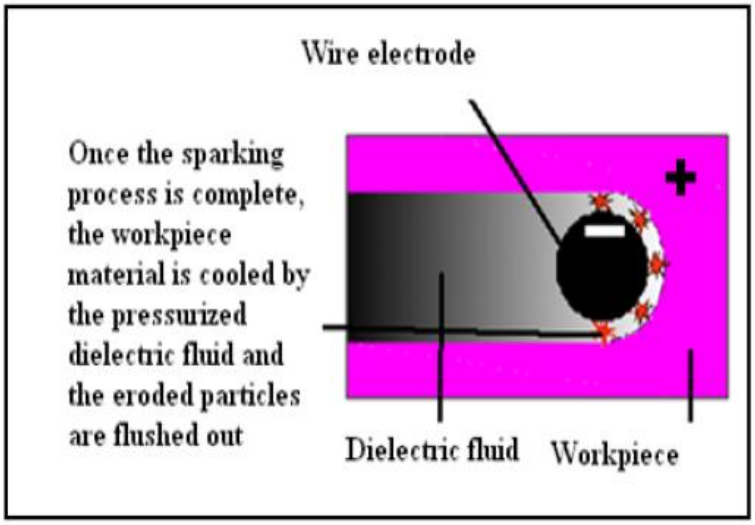

Figure 1.4 Schematic of cooling of the workpiece by the pressurized fluid [Guitrau, 1997]

Step: 4 -The pressurized dielectric fluid flushes the debris/ chips away and quenches the surface of the workpiece. The debris are collected by the filtration system of WEDM (Figure. 1.5).

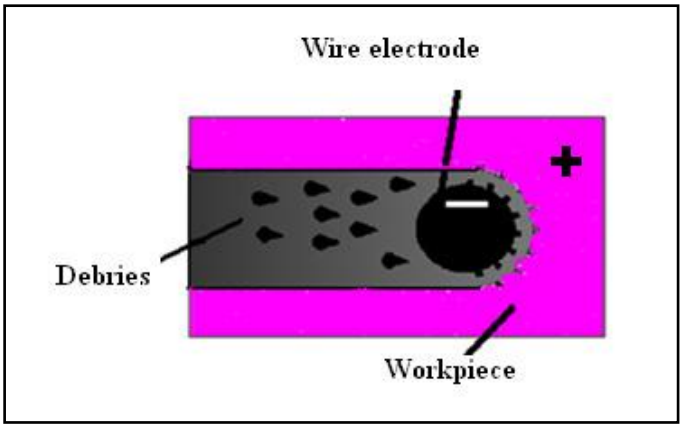

Figure 1.5 Schematic diagram of removal of eroded particles [Guitrau, 1997]

1.3.3 Process capabilities

The capabilities of WEDM process are as follows:

1. WEDM process provides an effective solution for machining of materials like titanium, molybdenum, zirconium and tungsten carbide with intricate shapes and profiles, which are difficult to machine by conventional machining methods [Sarkar et al., 2008].

2. It is capable of achieving very small corner radii as it utilizes wire electrode of very small diameter (0.03-0.3 mm).
3. Mechanical stresses are eliminated because no direct contact between tool and workpiece.
4. The movement of work piece is controlled by computer numerical control system (with positional accuracy of ± 0.5 μm) and wire is fed continuously through the work piece by a micro processor, enabling parts of complex shapes to be machined with high accuracy [Rao and Pawar, 2010].
5. It eliminates the need for pre shaped electrodes, which are commonly required in sinking EDM to perform roughing and finishing operations.

1.3.4 Applications of WEDM

WEDM has been called non-traditional machining processes because it erodes metal with electrical discharges instead of cutting tools which form chips. It has been replacing drilling, milling, grinding, and other traditional machining operations in many industries throughout the world. WEDM is widely used to manufacture components with intricate shapes and profiles. It has been commonly used in the automotive, aerospace, mould, tool and die making industries. Applications can also be found in the field of medical, optical, jewellery and dental parts processing. Owing to high process capability, it is widely used in manufacturing of cam wheels, special gears, bearing cage, various press tools, dies, and similar intricate parts (Sarkar et al., 2005).

1.3.4.1 Tool and Die Making Industries

WEDM is far most widely used machining process in precision mold and die industry. Its chief applications are in the manufacture and reconditioning of press tool and forging dies as well as moulds for injection moldings. The examples are:

1. Sheet metal press dies
2. Stamping and extrusion tools and dies
3. Fixtures and gauges
4. Various types of blanks and punches
5. Variety of miniature and micro-parts
6. Grinding wheel form tools

1.3.4.2 Medical and Surgical Industries

Manufacturing in the medical market demands superior accuracy, requires top precision, and needs the flexibility to accommodate the incredible demands of a constantly-changing and rapidly evolving industry. WEDM specializes in manufacturing medical

devices, tools and implants for all aspects of the field including diagnosis, therapy and surgery. The categories of medical field parts manufactured by WEDM are:

1. Surgical screws, bolts and hardware.
2. Medical implantation hand tools for inserting and extraction or recovery of implants.
3. Surgical Cathodes and syringe components.
4. Bone / Jaw reamers for Dental implants.
5. Go / No Go Gauges for Medical inventory quality control.
6. Breathing Regulator valves for oxygen masks.
7. Various splints and supports for orthotic and prosthetic devices.
8. Knee joint, shoulder joint and hip joint support apparatuses.
9. Tooling and dies for manufacturing, and stamping medical equipment and tools.
10. Metallic materials are widely used in dental implants, orthodontic appliances as bands, arch wires, ligature wires, hooks, tubes, brackets and springs, and orthopedic devices as implants and prosthesis for fractured bones healing.

1.3.4.3 Aircraft and Aerospace Industries

WEDM plays a significant role in the manufacturing process for products in the aircraft and aerospace industries. The following components are manufactured in the field of aircraft and aerospace with WEDM,

1. Rocket guidance systems
2. Airframes for the aerospace industry
3. Satellite structural component
4. Fin deployment actuator housing for a missile
5. Turbine blades
6. Gyroscopes
7. Jet engine blade sets
8. Turbine diffusers

1.3.4.4 Automobile Industries

The demand for WEDM process is increasing among automobile industries to enhance the performance of high-speed automotive engines. Few of the items manufactured by WEDM in automotive fields are:

1. Engine mountings
2. Car engine prototypes
3. Fuel metering valves

4. Gears and rear housing support for formula-1 race cars

1.3.4.5 General applications

Owing to high process capability WEDM is generally used in manufacturing of following parts.

1. Prototype and special form inserts manufacturing
2. Printer components such as magnetic reader heads, printer hammer etc
3. Cam wheel
4. Special gears
5. Stators for stepper motors
6. Watch parts
7. Metallic and Plastic gears
8. Grinding tools
9. Collets
10. Flexures
11. Keyways
12. Extreme tapers
13. Bottling industry
14. Graphite and copper electrodes
15. Containers- beverage, food and perfume etc.,

1.3.5 Advantages of WEDM

1. An important number of CNC features, such as automatic threading of the wire and restarting the operation in the case of wire rupture, improve the performance of WEDM as a manufacturing process.
2. WEDM can machine any complicated profile in electrically conductive materials.
3. Physical and metallurgical properties of the work material, such as strength, hardness, toughness, microstructure, etc. are no barriers to its application.
4. The process generates high surface finish.
5. Complicated contours in hard materials can be produced to a high degree of accuracy and surface finish.
6. It eliminates the geometrical changes occurring in the machining of heat-treated steels.
7. WEDM process simplifies the fabrication of precision work pieces.
8. WEDM produces a sharp, burr-free edge, so it is a highly desirable machining choice for work pieces such as medical implants and die openings.

9. Tool manufacturing and storage is avoided, as the process does not require a special shaped electrode for the purpose of a tool.
10. The time utilization of WEDM is high as it can continuously work throughout the day.
11. Small batch productions including prototypes can be economically machined as most of the CNC programming is easily done.
12. It avoids wastages and rejections due to initial planning and checking of the program.
13. The process can be readily applied to electrically conductive and semi-conductive materials.
14. Although the metal removal is due to thermal effects, there is no heating in the bulk of the material.
15. Heat treatment is usually unnecessary.
16. During machining, the work piece is not subjected to mechanical deformation as there is no physical contact between the tool and work.

1.3.6 Limitations of WEDM

1. Its application is limited to small thicknesses and conductive materials.
2. Material removal rate is comparatively low.
3. Electrolysis can occur in some materials.
4. Not suitable for very large work pieces.
5. High capital cost.
6. Precision uniform wire is required

1.4 OBJECTIVE OF THE STUDY

The study was aimed to investigate the machining characteristics of pure titanium under the different parametric conditions in wire electric discharge machining and to model these for their application in the concerned manufacturing industry.

1.5 ISSUES

1. Material removal rate (MRR) and surface quality of pure titanium as work material have been explored in wire electrical discharge machining in conjunction with the following process parameters; pulse on time , pulse off time, peak current, spark voltage, wire feed rate and wire tension setting.
2. The relationships between different machining parameters (pulse on time, pulse off time, peak current, spark voltage, wire feed rate, wire tension setting) and

machining characteristics (Material removal rate, Surface quality) have been established in this regard.

3. The results obtained have been optimized using suitable optimization technique (Desirability approach).

1.6 SCOPE OF WORK

The work has been limited to wire electrical discharge machining of pure titanium as work material under the different experimental conditions by varying the process parameters (pulse on time, pulse off time, peak current, spark voltage ,wire feed rate, wire tension setting) using suitable optimization technique. The results obtained have been modeled for their application in manufacturing industry.

1.7 PHASES OF RESEARCH

- Literature review
- Design of experiment
- Experimentation work
- Optimizing the results

1.7.1 Design of Experiment

Response surface methodology (RSM) has been used for designing and planning the experiments.

A pilot experimentations was carried out before designing the final experimentation, to explore the trends of influence of the various parameters (pulse on time, pulse off time, peak current, spark voltage, wire feed rate and wire tension setting) on the response variables of interest (MRR, Surface quality). This helped in deciding the number of levels to be used (along with their values) for each factor.

In contrast to the final experimentation, which employed RSM technique for planning of experiments (where two or more factors are simultaneously varied); the pilot experimentation was based on a "one factor at a time" approach.

1.7.2 Experimentation work

The experimentation has been done on CNC wire electrical discharge machining set-up on pure titanium as work material, so as to find out the impact of following machining parameters on MRR, surface quality.

1. Pulse on time (T_{on})
2. Pulse off time (T_{off})
3. Peak current (Ip)

4. Spark voltage (SV)
5. Wire feed rate (WF)
6. Wire tension (WT)

1.7.3 Optimizing the Results

The results obtained have been optimized using desirability approach.

1.8 ORGANIZATION OF THESIS

The thesis has been divided into six chapters. Brief description of the contents of each chapter has been given as following:

Chapter: 1 contains introduction to non-traditional machining methods, titanium and its applications, wire EDM process, the process capabilities, applications and advantages of Wire EDM process. Problems that occur during machining of titanium with conventional machining techniques have also been discussed. Various aspects of WEDM process, including the basic principle, material removal mechanism and its limitations have also been included. Objectives, scope and overall methodology of the work have also been described.

Chapter: 2 contain detailed literature review on the research work reported in the past by various researchers in the field of WEDM. Literature review also presents a discussion on various optimization techniques used by different researchers. This chapter also includes the surface integrity aspects of WEDM surface which depend upon surface topography and surface metallurgy. Gaps in the literature have also been identified.

Chapter: 3 highlights the pilot experimentation performed using one factor at a time approach to sort out the significant process parameters and to fix the range of these process parameters in order to avoid the wire breakage. Finally, main experimentation plan and the experimental observations are presented.

Chapter: 4 provide an overview of the different methods of experimental design. Box – Behnken design and response surface methodology, the approaches used in the present study are then presented in detail. The theoretical aspects of model adequacy building and checking using regression analysis are also discussed.

Chapter: 5 outlines the parametric influence on response measures along with the line diagrams and surface plots. Multi response optimization of process parameters using desirability approach is then presented. Thereafter, results of confirmatory experiments are presented. The surface integrity of machined surfaces was also analyzed through

energy dispersive X-rays, scanning electron microscope and X-ray diffraction techniques. The parametric influence and optimization of surface integrity in terms of number of micro-cracks, length of micro-cracks, surface crack size density and recast layer thickness is also discussed.

Chapter: 6 This chapter outlines the micro-models both for MRR and surface roughness by using dimensional analysis method.

Chapter: 7 is all about the conclusions of this research work. This chapter also highlights limitation of the study and scope for future work in this area. This chapter is followed by references.

CHAPTER 2

LITERATURE REVIEW

2.1 INTRODUCTION

Over the years, the WEDM process has remained as a competitive and economical machining option fulfilling the demanding machining requirements imposed by the short product development cycles and the growing cost pressures. However, the risk of wire breakage and bending has undermined the full potential of the process drastically reducing the efficiency and accuracy of the WEDM operation [Ho et al., 2004]. A significant amount of research has explored the different methodologies of achieving the ultimate WEDM goals of optimizing the numerous process parameters analytically with the total elimination of the wire breakages thereby also improving the overall machining reliability. For better understanding, a detailed literature survey has been carried out by considering the effects of WEDM parameters on the performance characteristics such as MRR, surface roughness, Kerf width, cutting speed, electrode wear ratio, surface integrity etc., in various classes of work material.

The literature review is divided into three sections. First section deals with the processing of titanium and its alloys using WEDM. Second section highlights WEDM carried out on materials other than titanium and its alloys ranging from aluminum to metal matrix composites in the past. All aspects related to WEDM including effects and optimization of process parameters, monitoring and control of inaccuracies induced by wire are discussed in detail. Some discussion on the different optimization techniques used by the various researchers is also done. Finally objectives of the present work have been formulated after identifying gaps existing in the literature. The detailed literature review is presented here:

2.1.1 Wire electric discharge machining of titanium and its alloys

Wire electrical discharge machining (WEDM) is a process of causing intermittent discharge between wire electrode and work piece, through a working fluid. There is relative movement of work piece and wire electrode for cutting the work piece into a desired configuration such as various types of metal moulds, dies, punches, machine

components, etc. WEDM is an indispensable machining technique used to produce complex two- and three- dimensional shapes through difficult to machine electrical conductive metals [Pandey and Shan, 1980]. The performance measures in WEDM are cutting speed, surface finish and form accuracy. The main machining parameters, which affect the performance of WEDM are; pulse-on time, pulse-off time, wire speed, wire tension, servo reference mean voltage, type of wire and dielectric fluid pressure etc.. Several studies have been undertaken in the past in order to improve the performance characteristics, namely the cutting speed, surface roughness and wire wear ratio etc. This section presents the contribution of researchers in the area of processing of Ti and its alloys using WEDM. The related contribution is discussed below.

[Kuriakose and Shunmugam, 2005] optimized the WEDM process parameters in machining Ti-6Al-4V alloy by using non-dominated sorting genetic algorithm. The sorting procedure employed a fitness assignment scheme which prefers non-dominated solutions and used a sharing strategy which preserves diversity among the solutions. Authors found that there was no single optimal combination of cutting parameters, as the influence of process parameters on the cutting velocity and the surface finish were quite opposite. Also, none of the solution in the Pareto-optimal set was better than any other solution in the set. The process engineer can select optimal combination of parameters from the Pareto optimal solution set, depending on the requirements.

[Sarkar et al., 2006] studied wire electric discharge machining of γ titanium alumnide (γ-Ti Al) alloy. A feed forward back propagation neural network model was developed to predict the response parameters namely cutting speed, surface roughness and wire offset as a function of six different control parameters viz. pulse on time, pulse off time, peak current, wire tension, dielectric flow rate and servo reference voltage. Twenty seven optimum parametric combinations were presented which can be utilized as technology guidelines for effective machining of this alloy. Experimental results demonstrated that machining model is suitable to satisfy the practical machining requirements.

[Sarkar et al., 2008] investigated modeling and optimization of wire electrical discharge machining of γ-TiAl in trim cutting operation. A second-order mathematical model, in terms of machining parameters, was developed for surface roughness, dimensional shift and cutting speed using response surface methodology (RSM). The experimental plan was based on face centered, central composite design (CCD). The trim cutting operation was optimized for a given machining condition by desirability function approach and

Pareto optimization algorithm. The residual analysis and experimental results indicated that the proposed models could adequately describe the performance indicators within the limits of the factors that are being investigated.

[Sarkar et al., 2010] presented an integrated approach to optimization of WEDM Of γ-TiAl with assistance of artificial neural network (ANN) modeling. Two ANN models based upon Bayesian regularization and early stopping method had been used to study the influence of process parameters on cutting speed and surface roughness. Pareto optimization was applied to determine the maximum cutting speed corresponding to the required surface roughness for trim cutting process. By combining results of single and multi-pass cutting a machining strategy based upon the novel concept of critical surface roughness was developed for selecting the machining process parameters.

[Pasam et al., 2010] experimentally investigated the WEDM of titanium alloy (Ti6Al4V). The behavior of eight control parameters such as Ignition pulse current (A), Short pulse duration(B), Time between two pulses(C), Servo speed(D), Servo reference voltage(E), Injection pressure(F), Wire speed(G) and Wire tension(H) on surface finish was studied using Taguchi parameter design. A mathematical model was developed by means of linear regression analysis to establish relationship between control parameters and surface finish as process response.

[Liao and Yu, 2004] introduced a term named as specific discharge energy (SDE), which is real energy required removing a unit volume of material. Specific discharge energies of different materials were compared and then materials having close value of SDE such as Ti-6Al-4V, stainless steel and Inconel 718 were selected. Their machinibility characteristics under identical machining conditions were evaluated and compared. A quantitative relationship between machining characteristics and machining parameters was obtained through dimensional analysis. Experimental results indicated that materials having close values of SDE demonstrated very close machining characteristics such as machining speed, groove width and surface finish of machined surface under same machining conditions.

[Miller et al., 2005] discussed wire electric discharge machining of cross section with minimum thickness and compliant mechanisms. Effects of WEDM process parameters, particularly the spark cycle time and spark on time on thin cross section cutting of Nd-Fe-B magnetic material, carbon bipolar plate and pure titanium were investigated. The study

generated an envelope of feasible wire EDM process parameters for commercially pure titanium which can be utilized for production of micro features on Ti components. Scanning electron microscopy observations of EDMed surface, subsurface and debris lead to a hypothesis, to explain the limiting factor for wire EDM cutting of thin sections based upon the thermal and electrostatic stress induced fracture in the test pieces.

[Poros and Zoboruski, 2009] investigated volumetric efficiency in WEDM of Ti6Al4V taking into consideration both process parameters (discharge time and working voltage) and material properties (melting point, electrical conductivity, thermal expansion, density and heat capacity of work piece). A semi empirical model was developed to examine variation of WEDM efficiency by using different wire materials, different process parameters by applying dimensional analysis. It was observed that application of longer discharge and higher working voltage resulted in a better efficiency of cutting. Comparisons of power indexes in dimensional analysis indicated that thermal properties such as melting point and thermal expansion coefficient were more significant than process parameters in machining of Ti6Al4V. The highest volumetric efficiency obtained was 17.75mm^3/min.

[Hseigh et al., 2009] investigated WEDM characteristics of Ti-Ni-X ternary shape memory alloys. Specimens were operated on a Soddick A305 CNC WEDM machine. Experimental results showed that maximum feed rate without wire breakage of wire electrode for $Ti_{35.5}Ni_{49.5}Zr_{15}$ and $Ti_{50}Ni_{49.5}Cr_{0.5}$ alloys in WEDM process exhibited a reverse relationship with product of alloy's melting temperature and thermal conductivity. Authors observed that the surface roughness of machined Ti-Ni-X alloy increased with growing pulse duration where as thickness of recast layer decreased. The specimen hardness reached 875 HV and 807 HV for WEDMed Ti-Ni-Zr and Ti-Ni-Cr alloys. The hardening effect arose from the formation of oxides ZrO_2, $TiNiO_3$, Cr_2O_3 and deposition of particles of consumed brass wire electrode in the recast layer. It was concluded that WEDMed Ti-Ni-X alloys exhibit a nearly perfect shape recovery at normal bending stress.

[Aspinwall et al., 2008] discussed machining of Ti-6Al-4V and Inconel-718 using two high specification WEDM machines with pulse generators designed to provide minimum work piece integrity damage. Operating parameters were selected to provide target work piece surface roughness values for all occurred cuts. Consequently, the cut surfaces were analyzed for exploring any change in micro hardness and micro structure. Results of

analysis revealed that the thickness of average recast layer obtained was less than 11µm and several trim passes showed no apparent recast or damage.

[Qin et al., 2003] reported wire EDM cutting induced hydride precipitation in surface layer of Ti-46Al-2Cr alloy. The existence of hydride in surface layer of TiAl intermetallic alloys play a detrimental role in determining their mechanical properties if hydride layer is not carefully removed. This hydride layer has a poor thermal stability as other titanium hydrides and was removed by vacuum annealing at 400-600ºC. The wire EDM induced micro cracks have also been found on the surface penetrating into the matrix up to 10-30µm of thickness of material; much deeper than the recast layer induced by wire-EDM.

2.1.2 Wire Electric Discharge Machining of Non-Titanium Materials

Many researchers have carried out efforts to investigate the effects of process parameters of WEDM on different response characteristics namely, cutting speed/rate, MRR, surface roughness, dimensional deviation, overcut on a wide variety of materials ranging from conventional steels to metal matrix composites and ceramics. Optimization of the response characteristics is performed to produce optimal sets of process parameters satisfying a number of process yield criteria simultaneously.

[Scott et al., 1991] used a factorial-design method to determine the optimal combination of control parameters in WEDM, with measures of machining performance being the metal removal rate and the surface finish. Based on the analysis of variance (ANOVA), it was found that discharge current pulse duration and pulse frequency were significant control factors for both the metal removal rate and the surface roughness. A total number of 729 experiments were conducted. Thirty two machining settings which resulted in a better metal removal rate and surface roughness were determined by two distinct techniques namely, explicit enumeration of all possible combinations and the dynamic programming approach.

[Spedding and Wang, 1997] attempted the optimization of process parameters of WEDM using response surface methodology and artificial neural network. A response surface model based on rotatable central composite experiment design and a 4-16-3 size back propagation neural network was developed. The pulse-width, the time between two pulses, wire mechanical tension and the wire feed were selected as the input parameters, whilst the cutting speed, the surface roughness and the surface waviness were the responses. The two models were compared for goodness of fit. Verification experiments

were carried out to check the validity of the developed models. It was concluded that both models provide accurate results for the process.

[Lok and Lee, 1997] analyzed processing of advanced ceramics (Sialon and Al_2O_3-TiC) using the wire-cut EDM process. The volumetric material removal rate for processing these ceramic materials was found to be very low as compared with alloy steels and the surface roughness achieved was inferior to that obtained with the die sinking EDM process. The extent of sub surface damage resulted from this thermal process was evaluated further by flexural strength data obtained from three point and four point quarter bend test methods. The results showed that WEDM process is a viable material processing method for machining of advanced ceramics, but work has to be carried out to further study the ways and means of improving the surface finish and surface integrity of the machined ceramics.

[Rozenek et al., 2001] experimentally investigated effect of machining parameters (discharge current, pulse-on time, pulse-off time, voltage) on machining rate and surface roughness during WEDM of metal matrix composites $AlSi_7Mg/SiC$ and $AlSi_7Mg/Al_2O_3$. It was observed that machining rate of WEDM cutting composites significantly depends on the kind of reinforcement. The maximum cutting speed of $AlSi_7Mg/SiC$ and $AlSi_7Mg/Al_2O_3$ composites were approximately 3 times and 6.5 times lower than the cutting speed of aluminum alloy respectively. Current and pulse on time had considerable influence on cutting rate and surface finish.

[Tosun and Cogun, 2003] investigated the effect of cutting parameters on wire wear ratio, material removal rate and mean surface roughness in WEDM of AISI 4140 steel with brass wire using regression analysis technique. It was observed that, wire wear ratio increased with increase in pulse duration and open circuit voltage. It gets decreased with increase in wire speed due to the reducing number of craters on wire per unit length of wire. The minimum value of wire wear ratio was observed at open circuit voltage of 80V, pulse duration of 300 ns, wire speed of 12.5 m/min and dielectric flushing pressure equal to 1.2 Pa. A very low value of experimental error was observed indicating the high accuracy in results.

[Puri and Bhattacharya, 2003a] investigated the variation of the geometrical inaccuracy caused by cutting speed and wire lag in machining of die steel using WEDM. It was observed that for the minimum geometrical inaccuracy, the difference between the offset

values for the rough cut and the trim cut should be as high as possible. The average cutting speed was affected by pulse-on time, pulse-off time and pulse-peak current for rough cutting; and pulse-on time and constant cutting speed during trim cutting. The surface roughness was influenced by pulse-peak voltage during rough cutting and pulse-on time, pulse-peak voltage, spark gap set voltage, dielectric flow rate, wire offset and constant cutting speed during trim cutting. The factors responsible for geometrical inaccuracy due to wire lag were pulse-on time, pulse-off time and pulse-peak current during rough cutting; and pulse-peak voltage, wire tension, wire offset, servo spark gap set voltage and constant cutting speed during trim cutting. Optimum parameter settings have also been obtained and reported.

[Hewidy et al., 2005] developed a mathematical model based upon response surface methodology for correlating the inter relationship of various WEDM parameters such as peak current, duty factor, wire tension and water pressure on the metal removal rate, wire wear ratio and surface roughness in machining of Inconel 601 material. Results showed that the volumetric metal removal rate generally increased with the increase of the peak current and water pressure. This trend is valid up to a certain limit, a further increase in peak current leads to a decrease in MRR. Wire wear ratio increased with the increase in peak current. Surface roughness increased with the increase of peak current and decreased with the increase of duty factor and wire tension.

[Yan et al., 2005] adopted WEDM for the machining of Al_2O_3p/6061Al composites. In the experimentation, machining parameter of pulse-on time was changed to explore its effect on machining performance, including the cutting speed, the width of cutting slit and surface roughness. The process experienced frequent wire breakage during the machining of Al_2O_3p/6061Al composite, so the location and reason of wire breakage was also investigated. The experimental results indicated that the cutting speed, surface roughness and the width of slit of cutting test material significantly depend on volume fraction of reinforcement (Al_2O_3 particles). Test results also revealed that in machining Al_2O_3p/6061Al composite, a very low wire tension, a high flushing rate and a high wire speed were required to prevent wire breakage. An appropriate servo voltage, a short pulse-on time and a short pulse off time which are normally associated with a high cutting speed, had little effect on the surface roughness.

[Ozdemir and Ozek, 2006] investigated the machinability of nodular cast iron by WEDM using different machining parameters viz. voltage, current, wire speed and pulse duration.

Results demonstrated that the increase in surface roughness and cutting rate clearly followed the trend indicated with increasing discharge energy as a result of an increase of current and pulse on time. Increased discharge energy produced larger and deeper discharge craters. Three zones were identified in rough regimes of machining for all samples: decarburized layer, heat effected layer and bulk metal. High machining efficiency was obtained when the proper electrical parameters are selected. Irrespective of the amount of energy impinged on the material, a coarse surface is always obtained. The variation of surface roughness and cutting rate with machining parameters was mathematically modeled by using regression analysis method. Among the several functions tried, the power function was found to be the best fit model.

[Manna and Bhattacharyya, 2006] carried out an experimental investigation to determine the machine parameter settings during WEDM of aluminum reinforced silicon carbide metal matrix composites. Taguchi's L_{18} orthogonal array was used to plan the experiments as well as to determine the signal to noise ratios. ANOVA and F- test values were used to indicate the significant machining parameters affecting the MRR, surface roughness and spark gap. Mathematical models relating input process parameters and output responses were established using Gauss elimination method for effective machining of Al/SiC metal matrix composites. Open gap voltage and pulse on period were the most significant and influencing parameters for controlling the metal removal rates where as wire tension and wire feed rate emerged as the most significant parameters for surface roughness. Spark gap was dominantly dictated by wire tension and spark gap voltage.

[Chiang and Chang, 2006) optimized machining parameters namely cutting radius of work piece, on time of discharging, off time of discharging, arc on time of discharging, arc off time of discharging, servo voltage and wire feed with consideration of multiple performance characteristics such as surface removal rate and maximum surface roughness in WEDM of Al_2O_3 particle reinforced aluminum 6061. Response table and response graph of each level of machining parameters were obtained from grey relation grade and the optimal levels of machining parameters were selected.

[Ali, 2006] investigated the effect and optimization of machining parameters on the material removal rate (MRR) and surface roughness (SR) in the WEDM of Al-Cu-TiC-Si particulate matrix composite. The settings of the machining parameters were determined using Taguchi experimental design method. The variation of MRR and surface roughness

with the machining parameters was mathematically modeled using a nonlinear regression analysis method. The optimal machining parameters for the objective of maximizing MRR and minimizing surface roughness were performed. Confirmatory experiments indicated that, the MRR increased 1.58 times and surface roughness decreased 1.11 times with optimal machine settings.

[Mahapatra and Patnaik, 2007] attempted wire electric discharge machining of D2 steel to explore the effects of process parameters such as discharge current, pulse duration, pulse frequency, wire speed and wire tension on MRR, surface finish and kerf characteristics. Regression was used to develop the mathematical models for response functions. Finally, genetic algorithm (NSGA) was employed to optimize the WEDM process with multiple objectives. Results of optimization revealed that WEDM process parameters can be adjusted to achieve better MRR, surface roughness as well as kerf characteristics.

[Ramakrishnan and Karunamoorthy, 2008] presented the development of artificial neural network (ANN) models and multi response optimization using Taguchi's robust design approach to predict and select the best cutting parameters of WEDM. Inconel- 718 was selected as the work material. Experiments were planned using Taguchi's L_9 array. Experiments were performed under different cutting conditions of pulse on time, wire tension, delay time, wire feed speed and ignition current intensity. Output responses namely material removal rate, surface roughness and wire wear ratio were optimized concurrently using signal to noise ratios. ANOVA was employed to identify the level of importance of the machining parameters on the multiple performance characteristics. It was identified that, the pulse on time and ignition current had more influence on the output responses than the other parameters.

[Saha et al., 2008] analyzed the wire electrical discharge machining of tungsten carbide cobalt composite. A second order multi-variable regression model and a feed-forward back-propagation neural network model had been developed to correlate the input process parameters, such as pulse-on time, pulse-off time, peak current and capacitance with the process performance measures namely cutting speed and surface roughness. The neural network and regression model exhibited the parametric effect on the cutting speed and surface roughness. The SEM analysis confirmed that the machined surface was characterized by loosely bounded WC grains and a lot of micro cracks, which were radialy spread over the machined surface. It was also observed that at high energy levels, the size of the micro cracks increases.

[Jin et al., 2008] discussed the development of reliable multi-objective optimization based on Gaussian process regression (GPR) to optimize the high-speed wire cut electric discharge machining process and showed the superiority of GPR models over the regression models in terms of accuracy and feature scaling and probabilistic variation.

[Rao et al., 2009] discussed influence of parameters such as discharge current, voltage, wire speed, tension on WEDM machining of Brass for optimization of cutting speed, MRR and spark gap using four wires of different Cu percentage. It was observed that cutting speed decreases as thickness of work piece increases owing to larger material need to be removed at larger thickness. With increase in current, there was an upward trend in the spark gap. MRR increases with an increase in discharge current.

[Rao and Pawar, 2010] discussed development of mathematical models using response surface modeling for correlating the inter relationship of various WEDM parameters and responses namely machining speed (mm/min) and surface roughness (Ra). Artificial Bee Colony (ABC) technique was then applied to find optimal combination of process parameters to achieve a maximum cutting speed for a desired value of surface finish. It was observed that convergence rate of ABC algorithm is very high and it can be used effectively in the optimization of multi -variable problems.

[Datta and Mahapatra, 2010] derived the quadratic mathematical models to represent the process behavior of wire electrical discharge machining (WEDM) operation. Experiments were conducted taking into account six process parameters: discharge current, pulse duration, pulse frequency, wire speed, wire tension and dielectric flow rate; to be varied at three different levels. Data related to the process responses viz. material removal rate (MRR), surface roughness and kerf were measured for each of the experimental run. Grey relational analysis was adopted to convert this multi-objective criterion into an equivalent single objective function called overall grey relational grade, which was optimized (maximized) by using Taguchi technique. Mathematical models to highlight parametric influence on three selected process responses were developed using response surface methodology.

[Kumar et al., 2010] investigated on WEDM parameters on machining Inconel 800 super alloy. The process parameters considered in this research work were gap voltage, pulse on time, pulse off time and wire feed. Taguchi's L_9 Orthogonal Array was used to conduct experiments. Optimal levels of process parameters were identified using Grey Relational

Analysis and the relatively significant parameters were determined by Analysis of Variance. The variation of output responses with process parameters was mathematically modeled by using non-linear regression analysis method and the models were checked for their adequacy results.

[Tzeng et al., 2011] analyzed the dependence of MRR and surface roughness on WEDM parameters during cutting of pure Tungsten profiles. A hybrid method including a back propagation neural network model (BPNN), genetic algorithm (GA) and RSM was used to determine the optimal parameter settings of WEDM. The results show that both RSM and BPNN/GA methods are effective tools for the optimization of WEDM process parameters.

[Sadeghl et al., 2011] discussed effects of process parameters on surface roughness and metal removal rate in WEDM of AISI D5 steel alloy. Regression was used to model the process and Tabu search algorithm was opted for optimization. It was found that discharge current and pulse interval were more influential on MRR and surface roughness than open circuit voltage.

[Satish et al., 2011] investigated the effect of WEDM parameters such as pulse on time, pulse off time, gap voltage and wire feed on MRR and surface roughness in machining of Al6063 alloy reinforced with varying percentage of SiC. The experiments were conducted as per Taguchi's L_9 array. Results of ANOVA and regression analysis indicated that the influence of gap voltage was more significant than other parameters for MRR. Voltage, pulse on time, wire feed and pulse off time were found to be the order of influence as percentage of SiC increased in the MMC. Surface roughness increased with the increase in percentage volume fraction of SiC particles in MMC's.

[Somashekhar et al., 2012] carried out micro WEDM of aluminum to optimize MRR, overcut and surface roughness. Series of experiments were conducted with three factors at three levels full factorial experiments developed using design of experiments with gap voltage, capacitance and feed rate as input parameters. The system model was created with statistical based regression analysis using experimental data. The model was employed to maximize the MRR and minimize the surface roughness and overcut using the simulated annealing scheme. It was observed that model is capable of predicting the response characteristics as a function of different control variables.

[Yang et al., 2012] conducted statistical based experimentation to investigate the effect of different process parameters viz. pulse on time, pulse off time, arc off time, servo voltage, wire feed, wire tension and water pressure on average surface roughness (Ra) and corner deviation in the tungsten work pieces cut using WEDM. Experiments were planned using Taguchi's L_{18} array and results of these were utilized to train the back propagation neural network (BPNN) model to predict the MRR, surface roughness and corner deviation properties. Simultaneous optimizations of these objectives were carried out using response surface methodology (RSM) and simulated annealing. Results of the two optimization techniques are compared with the confirmatory experiments and it was concluded that both RSM and BPNN integrated simulated annealing are effective tools for optimization of parameters of WEDM.

[Mukherjee et al., 2012] compared performance of non-traditional optimization algorithms such as Genetic Algorithms, Particle Swarm Optimization, Sheep Flock Algorithm, Ant Colony Optimization, Artificial Bee Colony Optimization and Biography Based Optimization (BBO) for selection of optimum set of WEDM machine parameters such as pulse on time, pulse off time, SV etc to achieve optimized value of responses such as MRR, corner deviation, cutting width and dimensional shift. Authors considered mathematical modeling of two WEDM processes already reported in literature (Hweidy et al. (2005) and Mahaptra and Patnaik (2007)). It was concluded that BBO algorithm had superiority over others in terms of convergence towards optimal solutions.

Few attempts have been made for optimization of single response characteristic using Taguchi's signal to noise ratios, regression analysis. [Luo, 1995] evaluated the energy distribution of high-speed WEDM as a function of wire speed, wire diameter and cutting width to obtain machining conditions for high-speed cutting. It was experimentally confirmed that a stable high cutting speed can be achieved without detriment to the electrode wire only by applying discharge pulses with high power density and then raising the pulse density to the greatest possible extent. Extreme long discharge duration causes low energy efficiency, while excessively high pulse density resulted in incurable instability with low discharge efficiency.

[Huang and Liao, 1997, 1999] focused on the determination of the number of finish cutting operations and process parametric setting in wire electrical discharge machining utilizing the concept of Taguchi quality design. Six different machining parameters were chosen as the control factors whereas the machining performances of the finish cutting

process were gap width, surface roughness, white layer depth and finish cutting area ratio. It was shown that the pulse on time and the distance between the wire periphery (D_{ww}) and the work piece surface in finish cutting were the two dominant factors influencing the machining performances. It was also established that a negative and medium D_{ww} was appropriate in order to obtain a smaller surface roughness, whereas a larger D_{ww} should be chosen for smaller white layer depth.

[Guo et al., 2002] analyzed the WEDM characteristics of particle reinforced material (Al_2O_3 in 6061 Al alloy). Taguchi's method of orthogonal design was adopted to determine the main factors that affect the machining process. The results showed that the electrical discharge energy was closely related to machining stability. It was found that electric parameters have little influence on the surface roughness whereas these were important for the cutting rate. Whether the high energy or the low energy was used, a coarse surface was always obtained. It was concluded that, in operation, large pulse duration, a high voltage, a large machining current and a proper pulse interval can be selected to have high machining efficiency.

[Kozak et al., 2004] analyzed the machining of low electrical conductive material (Si_3N_4) by WEDM. It was observed that there was a significant change in cutting velocity depending upon the position of clamp which was used to fix the work piece on the machine table. As the cut approaches the clamp, an increase in MRR was observed. A reduction in MRR occurs when the wire moves away from the clamp. It was found that actual MRR depends on the individual machining geometry and relative position of wire electrode with respect to clamping. To reduce the energy loss due to drop voltage in the work piece, the machining of Si_3N_4 was carried out with silver paint applied over the work piece. A significant increase in MRR was observed due to silver coating.

[Liao et al., 2004] directed their research efforts towards developing a pulse generating circuit that can be switched for both roughing and finishing operations. The various controlling factors including pulse generating circuit, conductivity of dielectric, resistance in the circuit, capacitance in the circuit, applied voltage, table feed rate and pulse off time were chosen to conduct experiments according to Taguchi's L_{18} mixed orthogonal array. ANOVA and F- test values were utilized to identify the significant factors affecting the surface finish. It was observed that the machining voltage, current-limiting resistance, type of pulse-generating circuit and capacitance were the significant parameters affecting the surface roughness in finishing operation.

[Hascalyk and Caydas, 2004] investigated the machining characteristics of *AISI D*5 tool steel in WEDM process with master brass wire. Various parameters were manipulated during experiments to find out their effect on surface roughness and metallurgical structure. Pulse interval time, table feed rate and wire tension were fixed parameters. Authors showed through experimental investigations that intensity of discharge energy affects significantly the amount of recast layer, surface roughness and micro cracking. Wire speed and dielectric fluid pressure do not have much influence.

[Puri and Bhattacharya, 2005] attempted to model the white layer depth through response surface methodology in a WEDM of die steel, comprising a rough cut followed by a trim cut. Experimental plan of rotatable Central Composite Design involving four variables with five levels had been employed to carry out the experimental investigation. Subsequently to establish the mathematical model correlating the input process parameters and output response i.e. recast layer, regression analysis was adopted. It was found that the white layer depth increased with increase in pulse on time during rough cutting and decreased with increase in pulse on time in trim cutting.

[Patil and Brahmankar, 2006] investigated the effect of various control parameters such as pulse-on time, pulse-off time, ignition pulse current, wire speed, wire tension, and flushing pressure on the cutting speed and surface finish of Al/SiC metal matrix composites using Taguchi methods. Mathematical models relating the machining performance and machining parameters were formulated and optimal settings for each performance measure were obtained. A comparative study on unreinforced alloy revealed the effect of reinforcement on the machining process. It was found that the cutting speed for unreinforced alloy was higher as compared with MMC. Wire breakage was found to pose limitation on attaining higher cutting speed in the case of machining of MMC.

[Han et al., 2007] presented influence of machining parameters (including pulse duration, discharge current, sustained pulse time, pulse interval time, polarity effect and dielectric) on surface finish in the finish cutting of WEDM. Experiments proved that the surface roughness can be improved by decreasing both pulse duration and discharge current. It was observed that when the pulse energy per discharge is constant, shorter pulses and longer pulses resulted in the same surface roughness but different surface morphology and different material removal rates. The metal removal rate, when a shorter pulse was used was much higher than when the pulse duration is long.

[Mathew et al., 2007] conducted statistical based experimental investigations to analyze the effect of different process parameters on over cut in the micro slots produced using µ-WEDM operation on aluminum and stainless steel. The results revealed that the dominant process parameters influencing the machining performance were gap voltage, resistance and pulse on-time.

[Kanalyasiri and Boonmung, 2007] presented an investigation of the effects of machining variables on the surface roughness of wire electrical discharge machined DC53 die steel. The machining variables investigated were pulse-peak current, pulse-on time, pulse-off time, and wire tension. The authors developed a mathematical model using the multiple regression method to formulate the effect of pulse-on time and pulse-peak current to the surface roughness. The developed model was validated with experimental data.

[Mohammadi et al., 2008] presented the design of a precise, flexible and corrosion resistant rotary spindle which was mounted on a five axis wire EDM machine to rotate the work piece for carrying out wire electric discharge turning. Several experiments based upon Taguchi's L_{18} array were conducted to access the effect of power, pulse off time, voltage, servo wire speed, wire tension and rotational speed on metal removal rate. S/N ratio as well as regression analysis revealed that power, voltage and servo had considerable effect on MRR where as rotational speed and wire tension emerged as the least significant.

[Liu and Guo, 2009] studied the behavior of wire electric discharge machining of Al_2O_3 particle reinforced aluminum alloy 6061. The effect of machining voltage, current, pulse duration, and electrolyte concentration on material removal rate was evaluated. The results suggested that for achieving the highest metal removal rate (MRR), applied current was the most influential among current, pulse duration and electrolyte concentration.

[Newton et al., 2009] investigated to determine the main WEDM parameters which contributed to recast layer formation in Inconel-718. It was found that average recast layer thickness increased primarily with energy per spark, peak discharge current and current pulse duration. Over the range of parameters tested, the recast layer was observed to be between 5 µm and 9 µm in average thickness, although highly variable in nature. The recast material was found to possess in-plane tensile residual stresses, as well as lower hardness and lower elastic modulus than the bulk material.

[Manna, 2009] investigated the effect of various cutting parameters of WEDM viz. open circuit voltage , pulse on time, pulse off time, peak current, wire feed rate, wire tension and spark gap set voltage on wire crater depth , electrode wear rate and surface roughness in machining of E0300 die steel. Taguchi methods based L_{18} mixed orthogonal array was used to determine S/N ratios, analysis of variance and F-test values for indicating the most significant parameters affecting the electrode performance and machined surface finish. The significant parameters were considered for verification of optimal machining performance through confirmation tests with respect to chosen reference parameter settings. Considering the significant WEDM parameters, mathematical models were also developed for wire crater, electrode wear rate and surface finish.

[Pal et al., 2009] attempted modeling of WEDM of TiC/Fe metal matrix composites by normalized radial basis function network (NRBFN) with traditional as well as enhanced k means clustering technique. The effect of pulse on time, pulse off time, wire feed and average gap voltage on cutting speed and kerf width were explored. It was found out that average gap voltage lead to decrease in cutting speed but increase in kerf width. Pulse on time, pulse off time and wire feed had less effect on cutting speed and kerf width as compared to gap voltage. NRBFN with enhanced k means clustering technique yielded better results in respect of the closeness to the experimental results than NRBFN with traditional k means technique.

[Rakwal and Bamberg, 2009] investigated slicing of germanium wafers from single crystal, gallium doped ingots using WEDM. Seventy two experiments were planned using a full factorial design experiments to establish the kerf generated by brass wire and 108 experiments to analyze kerf produced by Molybdenum wire. Consequently cleaning of germanium wafers after slicing was demonstrated using degreasing agents and chemicals. It was concluded that slicing late of WEDM process was found to be relatively slow and cost of Molybdenum wire per wafer was relatively high.

[Shah et al., 2009] investigated seven machining parameters in addition to varying material thickness on machining responses such as MRR, kerf and surface roughness of tungsten carbide samples machined by WEDM. The design of experiments was based on Taguchi orthogonal designs with 8 control factors at three levels. The results showed that material thickness has little effect on material removal rate and kerf.

[Parashar et al., 2010] reported the statistical and regression analysis of kerf width using designed experiments for WEDM operations. Each experiment was performed under

different cutting conditions of gap voltage, pulse on time, pulse off time, wire feed and dielectric flushing pressure to ascertain the kerf width obtained in each case. The results revealed that pulse on time and dielectric flushing pressure are the most significant factors, while gap voltage, pulse off time and wire feed are the less significant factors to the kerf width of wire EDMed SS 304L.

[Rao et al., 2010] considered Wire-cut electric discharge machining of Aluminum-24345 in the research work. Experimentation was done by using Taguchi's L_{18} (2^1x3^7) orthogonal array under different levels of parameters. The response of surface roughness was considered for improving the machining efficiency. Optimal combinations of parameters were obtained using Taguchi's signal to noise ratios. The confirmation experiment showed that the significant improvement in surface finish (1.03μm) was obtained with this method. Multiple linear regression models were developed for correlating the process parameters and machining performance.

[Patil et al., 2010] proposed a semi empirical model for material removed rate in WEDM, based upon thermo physical properties of work piece and machining parameters such as pulse on time and average gap voltage. The model was developed using dimensional analysis and non linear estimation techniques such as Quasi Newton and Simplex. Predictability of the proposed model was more than 99% for silicon carbide particulate reinforced metal material composites. The experiments and model prediction showed significant role of coefficient of thermal expansion of the work materials in the WEDM of these materials. However limitation of this model was that this model could not address the regions of wire breakage that may take place when the machine is operated at full range of machine parameters.

[Abdulkareem et al., 2011] explored the effects of wire electric discharge machining (WEDM) variables on surface topography of stainless steel. The effects of pulse current and gap voltage on surface topography during wet and dry WEDM of stainless steel were investigated. It was observed that wet wire EDM produced better surface integrity as compared to the dry wire EDM. During dry wire EDM, adhesion of machining debris on the inter electrode surface was one of the factors that was responsible for poor surface finish on the work piece. Increase in both pulse current and gap voltage also contributed to poor surface integrity of work piece during dry wire EDM.

[Pragya et al., 2012] discussed the effect of four input process parameters (servo voltage, pulse on time, pulse off time and wire feed rate) on wire breakage frequency and the microstructure of cut surface during WEDC of SiC/6061/Al MMC. The objective of the study was to bracket the optimum range of input parameters for determining the effects of input process parameters on the average cutting rate, MRR and surface roughness. It was concluded that to achieve lower value of wire breakage frequency, lower values of voltage, pulse on time and higher values of pulse off time and wire feed rate should be used. At any given value of process parameters, MMC with higher percentage of non conductive particles gives the highest value of wire breakage frequency. Minimum value of surface roughness was obtained at lower values of voltage and pulse on time and higher values of pulse off time and wire feed rate.

[Weingartner et al., 2012] evaluated the influence of high speed rotating work pieces on wire electric discharge machining. Single discharge experiments were conducted inside a grinding machine in a self designed wire electrical discharge dressing device on a brass wheel of diameter 75mm. It was observed that the shape and size of eroded craters produced during the making were found to be highly influenced by the applied relative speed. Volume of eroded craters are increased as the relative speed is increased indicating that higher melting efficiencies are achieved for higher relative speeds.

Many researchers have tried to improve the efficiency of WEDM by having an insight into the process regarding exploration of the causes that led to degradation of its performance such as wire breakage, inaccuracies induced due to wire vibration as well as wire lag and development of control systems to control these.

[Kinoshita et al., 1982] analyzed the various types of wire breaking. It was observed that the pulse frequency of gap voltage rises abruptly and lasts for approximately 5–40ms before wire breakage. Authors developed a monitoring and control system that switches off the pulse generator and servo system once a sudden rise of pulse frequency is detected to prevent the wire from breaking. However, the machining efficiency was much reduced by such control strategy. It was pointed out that the ratio between the equilibrium clearance and the amplitude of wire vibration is the most appropriate value to judge the short circuit.

[Rajurkar and Wang, 1991] experimentally investigated the material removal rate for varying machining parameters. The experimental findings were used in a developed

thermal model to analyze the wire rupture (breakage) phenomena. The identified causes leading to wire rupture were failure under excessive thermal loads, failure through short circuiting and wire vibration, the most important among these being the thermal load.

[Rajurkar and Wang, 1993] analyzed the wire rupture phenomena with a thermal model. An extensive experimental investigation was carried out to determine the process performances such as machining rate and surface finish with all the control parameters of a WEDM machine in the study. The relationship between the machining rate and surface finish under optimal machine settings was determined by means of a multi-objective model.

[Beltrami and Dauw, 1994] monitored and controlled the wire position online by means of an optical sensor equipped with a control algorithm, which enables virtually, any contour to be cut at a relatively high cutting speed. Authors reported that the vibration of the wire was substantially reduced when the wire and wire guides were completely submerged in the working fluid tank filled with deionized water.

[Tosun et al., 2003 a] experimentally investigated the effects of the pulse duration, open circuit voltage, wire speed and dielectric flushing pressure on the dimensions of craters produced in the wire due to sparking. It was found that increasing the pulse duration, open circuit voltage and wire speed increases the crater diameter and crater depth, whereas increasing the dielectric fluid pressure decreases these factors to some extent. The mathematical relationships between the crater diameters, crater depth in terms of cutting parameters were established by the regression analysis method. It was concluded that the most effective parameters for determining the crater depth and crater diameter are open circuit voltage and pulse duration as revealed by analysis of variance and the F-test. Wire speed and dielectric flushing pressure are less effective factors for determining the crater diameter and crater depth.

[Puri and Bhattacharyya, 2003b] investigated the effect of wire vibration in WEDM. It was reported that the variable nature of various forces acting along or upon the wire leads to wire vibration. The maximum amplitude of the vibration depends upon the ratio of H/L(H- Height of the job, L- Span of the wire between guides). It was found that the higher the thickness/ height of the work piece, the larger will be the maximum amplitude of the vibration for a given span of the wire guides and amplitude.

[Sanchez et al., 2007] discussed the influence of work thickness, corner radius and number of trim cuts on the accuracy of WEDM corner cutting of AISI D2 tool steel work material. It was found that wire lag was responsible for the back-wheel effect in corner cutting and deviation was larger in case of the test-piece with smaller corner radius. It was not possible to achieve an optimum fit along the whole corner (both at 45°and at the exit). There was a reduction in dimensional error up to 50% in case of corners between 30°and 135°. It was affirmed from the study that to achieve a good fit to the ideal corner geometry, the approach of limiting the cutting speed during trim cuts must take into account the variable excess or lack of material produced by the previous cuts.

[Cabanes et al., 2008] discussed the results of the analysis of an experimental database that reproduces unexpected disturbances that generally appear during normal operation of WEDM. The results of analysis revealed new symptoms that allow one to predict wire breakage. The symptoms were related to the occurrence of an increase in discharge energy, peak current as well as increase or decrease in delay time. This study contributed to improve the process performance through a wire breakage monitoring and diagnostic system. This system measured the relevant magnitudes by visual instrumental system and detected low quality cutting regimes through diagnostic system in advance and predicted wire breakage. This provides anticipation time intervals that range from tens of milliseconds to seconds to supervision system to readjust process parameters to avoid wire breakage.

[Shichun et al., 2009] analyzed the kerf width in micro WEDM, which is explained by breakdown distance and wire vibration amplitude. The wire lateral vibration model in micro WEDM process was built and relationship between machining parameters and wire vibration was analyzed. It was observed that open voltage not only determines the breakdown distance but also affects the wire vibration in the process and was considered a key factor to influence kerf width.

[Ho et al., 2004] reviewed the work carried out from the spin-off from the EDM process to the development of the WEDM. Authors concluded that WEDM is a well-established non-conventional material removal process capable of meeting the diverse machining requirements posed by the metal cutting industries. However the development of newer and more exotic materials has challenged the viability of the WEDM process in the future manufacturing environment. Hence continuous improvement needs to be made to the current WEDM traits in order to extend the machining capability and increase the

machining productivity and efficiency. With the continuous trend towards unattended machining operation and automation, the WEDM process has to be constantly improved to maintain as a competitive and economical machining operation in the modern times from manufacturing arena. The authors believed that the WEDM process, due to its ability to efficiently machine parts made up of difficult to machine materials and with complicated geometries, have its own application area unmatched by other manufacturing processes.

[Huang et al., 2013] studied the effects and optimization of cutting parameters on surface roughness (Ra) and material removal rate (MRR) in the wire electrical discharge machining (WEDM) of high hardness tool steel YG15. In addition, comparative analysis of finish and rough cutting is drawn to analyze the difference between rough cutting and finish cutting. Then, regression models and signal-to-noise ratio are used to obtain the optimum cutting parameter combination. Finally, the results present the optimized MRR and Ra of the rough and finish process, respectively, and confirm the efficiency and abilities of the model.

[Ikrem et al., 2013] This paper reports the effect and optimization of eight control factors on material removal rate (MRR), surface roughness and kerf in wire electrical discharge machining (WEDM) process for tool steel D2. It has been found that pulse on-time is the most significant factor affecting the surface roughness, kerf and material removal rate

[Yeh et al., 2013] investigated on wire electrical discharge machining (WEDM) to process polycrystalline silicon ingot, and their surface characteristics. At first, two different dielectrics, pure water and pure water with sodium pyrophosphate powder, were experimented to compare their effects on cutting speed and surface roughness. The findings in this study prove that using phosphorous dielectric on WEDM could be applied onto polycrystalline silicon cutting. In addition, pure water with sodium pyrophosphate powder increases both working efficiency and improves infiltration of the phosphorous element on the surface.

2.2 OPTIMIZATION TECHNIQUES IN PROCESS PARAMETER OPTIMIZATION

Literature review indicates that a large number of researchers have utilized Taguchi's DOE technique for plan of experimentation as well as optimization of process parameters.

Taguchi's method can only find the best set of specified process parameters combinations which include the discrete settings of the process parameters. The application of conventional Taguchi method is unreasonable, when the variable of a process parameter is continuous [Yang, 2012]. Using Taguchi method, each performance characteristic is separately analyzed and therefore, parameter settings can be optimized with respect to one characteristic at a time. But for WEDM process, engineers are required to determine the parametric settings that simultaneously optimize the performance characteristics [Gauri and Chakarborty, 2010].

Few authors have employed artificial neural networks for modeling and analysis of WEDM processes. Neural networks present a number of disadvantages including their black box nature, large computational burden and proneness to over fitting of the data [Hu and Hwang, 2002]. Application of neural networks requires large number of samples to train the model and large number of layers of non linear elements are required for establishing arbitrary input- output mapping [Saha et al., 2009].

It is also observed from the literature review that traditional methods of optimization such as mathematical programming techniques, method of feasible direction, min-max, weighted sum methods etc. do not fare well over a broad spectrum of problem domains. These methods change the multi- objective problem into a single objective, with the corresponding weights based upon their relative importance. The serious drawback of these is that the decision maker must have sufficient knowledge of ranking of objective functions [Kuriakose and Shunmugam, 2005]. Moreover, these methods are not adequate for handling multi objective optimization problems because they cannot find all solutions in a single run, there by requiring them to be applied as many times the number of desired Pareto optimal solutions. Also they may not be robust and stay to obtain a local optimal solution [Sardinas and Santana, 2006].

[Rao, P.V., 2002] carried out the study and development of a surface roughness prediction model for machining mild steel, using Response Surface Methodology (RSM). The experimentation was carried out with TiN-coated tungsten carbide (CNMG) cutting tools, for machining mild steel work-pieces covering a wide range of machining conditions. A second order mathematical model, in terms of machining parameters, was developed for surface roughness prediction using RSM. The objective function of surface roughness was optimized using genetic algorithms.

[Kuriakose and Shunmugam, 2005] carried out WEDM of Ti-6Al-4V alloy with an objective to explore the effect of process parameters on cutting velocity and average surface roughness. Empirical models for cutting velocity and average surface roughness are obtained using regression analysis. Multi objective optimization of the objective functions is carried out using Non-dominated Sorting Algorithm (NSGA). Optimization results indicated that for same surface roughness, better values of cutting speed can be obtained using recommended machine settings.

[Mandal et al., 2007] have attempted to model and optimize the complex EDM process using soft computing techniques. Artificial Neural Network (ANN) was used to model the process and Non Dominated Sorting Algorithm-II (NSGA-II) was employed to optimize the process. Testing results demonstrated that the model is suitable for predicting the response parameters. A Pareto optimal solution set based upon NSGA-II is obtained.

[Kanagarajan et al., 2008] investigated electric discharge machining of Tungsten Carbide and Cobalt composites. Effect of machining parameters such as pulse current, pulse on time, electrode rotation and flushing pressure on metal removal rate and surface finish is modeled empirically using regression equations. NSGA-II is then used to optimize the processing conditions. A non dominated solution set was obtained and reported. Confirmatory experiments reveal that optimal values of MRR and surface roughness obtained using NSGA and actual experiment results are in close agreement.

[Prasad et al., 2009] carried out empirical modelling of input parameters of WEDM to investigate the effect of these on MRR and surface roughness using response surface methodology. The regression equation obtained is utilized as fitness function in multi objective optimization of MRR and surface roughness using NSGA. To obtain better convergence the algorithm is run for 200 generations. A solution set consisting of 40 non dominated solutions is obtained and reported.

[Kondayya et al., 2010] presented the application of an integrated evolutionary approach for modeling and optimization of a wire electrical discharge machining (WEDM) process. The proposed methodology was in two parts. In the first part, a novel application of genetic programming (GP) was proposed. GP is an evolutionary modelling algorithm which uses principles similar to genetic algorithms to model highly non-linear and complex processes, resulting in accurate and reliable models. Two important aspects of machining performance of WEDM, namely metal removal rate and surface roughness, were modeled based on experimental data using GP in terms of four prominent input

variables. The work presented was a fully fledged evolutionary approach for optimization of the process.

[Kumar et al., 2011] discussed Electrochemical Machining (ECM) of 25Al/15%SiC composites. A multiple regression model was used to represent relationship between input and output variables. Multi objective optimization method based upon NSGA-II was then used to optimize the ECM process. A solution set comprising of 31 solutions was presented and selected experiments were performed to validate the optimization results.

[Scott et al, 2004] have presented a study for the optimization of cutting parameters, which are effective for material removal rate and surface finish. They found that the surface finish increases with increasing discharge current, pulse duration and wire speed.

[Fonda.et al, 2008] investigated the effect of Ti–6Al–4V's thermal and electrical properties on the EDM productivity. In this study, temperature measurements have been made for Ti–6Al–4Vworkpieces with various duty factors to clarify the essential causes of difficulty in machining titanium alloys and observe the optimal duty factor in terms of productivity and quality. The resulting temperature measurements show that as the duty factor increases, the internal workpiece temperature also increases. Beyond a certain duty factor, the temperature begins to steadily increase, which causes poor EDMing productivity and quality. Optimal duty factor in terms of productivity and quality is found at around 7%.

[Wansheng et al., 2002] introduces ultrasonic vibration into micro-EDM: Ti–6Al–4V as work piece material with 2mm thickness, carbide YG6X electrode, 20 kHz ultrasonic vibration and 2 mm amplitude; holes with diameter of 0.2mm and depth/diameter ratio of more than 15 can be drilled.

[Chow et al., 2000] Applying powder in dielectric fluid for EDMing of titanium alloy was done by in micro-slit machining operation. Their experimental results indicated that adding Al and Si_C powder in kerosene caused the MRR to increase. They also found that Si_C powder exhibits better performance over Al powder. Both powders can extend the gap between the electrode and the workpiece.

[Minami et al., 1998] proposed a coloring method of titanium alloy using WEDM during the finishing without any other post treatment. When machining in water, a molten and resolidified surface created by electrical discharge process was colored directly by the interference phenomenon of light in the anodic oxide film formed with electrolysis

reaction. The thickness of the oxide film controlled by the average working voltage determined the color tone.

[Chen et al., 1999] investigating the influence of kerosene and distilled water as dielectric on Ti–6A1–4V work pieces they found that carbide is formed on the work piece surface while using kerosene while oxide is formed on the work piece surface while using distilled water. The debris size of Ti–6Al–4V alloy in distilled water is greater than that in kerosene and compared with kerosene, the impulsive force of discharge in distilled water is smaller but more stable.

[Asokan et al., 2000] pointed that EDM of titanium alloys is slightly complicated as compared to Nickel based super alloys, owing to the material properties. It was well-known that titanium alloys have high electrical resistivity (low conductivity) and therefore becomes very difficult to machine by EDM process. They have used EDM for drilling hole of Ti-64 with copper as an electrode and distilled water as dielectric fluid. They concluded that the machining current, On/Off time and capacitance effected the MRR and the dimensional accuracy of materials, and various standard technologies for setting the machining parameters according to workpiece material have been established.

2.3 GAPS IDENTIFIED IN THE LITERATURE REVIEW

Literature review in this chapter reveals that a substantial amount of work on different aspects of machining with WEDM has been reported. However, applicability of WEDM for pure titanium is still at the infant stage and has a long way to go. On the basis of literature review, following gaps in the literature have been identified:

1. A thorough scrutiny of the literature clearly indicated that, there is almost no study reported on WEDM of pure titanium.
2. The predictive modeling for the effects of machining parameters in WEDM of pure titanium is another aspect that has not been explored. So, experimental investigations regarding WEDM of pure titanium, leading to predictive models (for different responses) could be carried out.
3. Technology charts or operator reference manuals are not available for effective machining of pure titanium using WEDM. So, there is a need to generate optimal sets of process parameters satisfying a number of performance measures such as

machining rate, surface roughness, material removal rate (MRR), dimensional deviation, overcut and wire wear ratio.

4. Most of the researchers have carried out multi objective optimization of objective functions using traditional optimization techniques such as Taguchi method, min-max method, weighted method etc. Multi objective optimization of process parameters is needed to be done using some evolutionary optimization techniques such as response surface methodology (RSM), as literature survey reports a lot about limitations of traditional optimization techniques.
5. Very limited work has been reported on evaluation of the surface integrity of pure titanium after machining. The novelty of present research work is the investigation of the surface integrity of the machined samples of pure titanium and wire surface topography, analyzed through energy dispersive X-ray analysis (EDX), scanning electron microscope (SEM) and X-ray diffraction (XRD) techniques. The influence of process conditions on surface topography, recast layer, heat affected zone, formation of micro-cracks and debris analysis was considered in the present study.
6. No significant literature has been found relating to optimization of surface integrity in terms of number of micro-cracks, length of micro-cracks, surface crack density and recast layer thickness after processing with WEDM.

CHAPTER 3
DESIGN OF STUDY

3.1 INTRODUCTION

WEDM is a stochastic process and a large number of control factors influence the process in a complex way. Any alteration even in a single parameter may produce undesirable results leading to loss of productivity, deterioration in surface quality or both apart from the unpredictable results on the material properties such as change in micro hardness and microstructure. The solution of this lies in the process analysis to generate optimal machining parameters which may involve detailed experimentation and subsequent analysis of results. In experimental studies, input variables called as control factors are changed and their effects on output performance measures (responses) are observed. Each control factor can take several values during the course of experimentation. Such values of control factors are called levels or treatments. An experiment (also called trial or run) is a combination of parameters at different levels whose effect on the output is of primary concern.

For conduct of experiments, a scientific approach is necessary to plan the experiments, so as to assign equal importance to all control factors in addition to preserving robustness of the process. A properly planned and executed set of experiments is of prime importance for deriving clear and accurate conclusions from the experimental observations. The one factor at a time (OFTA) approach is a method used to plan the experiments by varying one factor at a time keeping all other factors at fixed levels. This method is effective only when emphasis is only to estimate main effects of the factors on responses, provided the experimental error is not too large as compared to factor effects such as screening experiments where it is desirable to isolate insignificant factors [Montgomery, 2002]. This method suffers from serious drawbacks that are given below:

(i). OFTA approach require more number of runs to estimate effect of factors for the same precision as obtained in statistically designed experiments.

(ii). OFTA fails to address interactions existing between the parameters assuming that each factor behaves independently.

(iii). OFTA takes into account the effect of only one parameter at a time. In actual machining process, cumulative effects of different control factors yield the output.

Thus, true optimal settings cannot be obtained when OFTA approach is followed for design of experiments.

Keeping in view above mentioned limitations, Sir Ronald A. Fisher devised factorial experiment designs, which focus on simultaneous change in a number of factors at a time [Montgomery, 2002]. A very useful strategy named as design of experiments was established. Design of experiments (DOE) is defined as, "A collection of mathematical and statistical technique that are useful for modeling and analysis of problems in which a response of interest is influenced by several variables and objective is to optimize this response" [Montgomery, 2002]. [Antony, 2003] defined as, "planning, designing and analyzing the experiments, so that valid and objective conclusions can be effectively and efficiently drawn". By statistically designed experiments, appropriate data can be collected, which can be analyzed by statistical methods resulting into valid and objective conclusions. In fact, feasibility of statistical analysis is possible only when the experiments are statistically designed. Design of experiments offers a number of advantages that are as follows [Alder et al., 1975; Peterson, 1985; Ferreira et al., 2007]:

(i). The use of design of experiments offers advantages such as reduction in the number of experiments that need to be performed, which leads to efficient use of materials and time.

(ii). Estimation of the experimental error incurred in the phase of experimentation.

(iii). It allows assessment of the relevance and statistical significance of a factor and is able to evaluate the interaction effects among the factors as well.

(iv). Empirical modeling of output response in terms of process parameters can be done.

(v). Optimal combination of process parameters generating maximum or minimum yield criteria can be obtained with a flexibility to set the relative priorities among the yield criteria or response functions.

The research on experimentation strategies has been further propagated to full factorial designs, fractional factorial designs [Peterson, 1985], Response Surface methodology (RSM) [Myers, 1990; Montgomery, 2002] and Taguchi methodology by extracting maximum from the concepts of DOE. Literature reveals that, generally, one factor at a time approach is used for carrying out of screening experiments or preliminary investigation of the process. For detailed experimentation and analysis Response Surface

methodology or Taguchi methodology is preferred. Taguchi's methodology for design of experiments is widely reported in the literature [Mahapatra and Patnaik, 2006; Kuriokase and Shagunmun, 2005], but it has certain inherent weaknesses that are as follows [Myers, 2002; Box, 1988; Hunter, 1989] :

(i). Taguchi's methodology makes use of signal to noise ratios (S/N ratios) that summarize the observations and provide information about mean and standard deviation of one measure in analyzing data from a robust design view point. The S/N ratios and loss function confound location (mean) and dispersion (variance) effects. In other words, the signal to noise ratio and loss function contain information concerning both mean and the variability and the singular effect of variables on these two measures cannot be assessed.

(ii). In Taguchi's methodology, interaction effects are assumed to be negligible unless they are explicitly recognized. In addition, the generally accepted method of creating these designs does not always achieve optimum design resolution to mitigate the problem of effect confounding.

(iii). This methodology lacks in building mathematical models that describe, how the performance changes as a function of control and noise variables. Such mathematical models not only provide a basis for developing an understanding of the phenomenon of interest, but are also required for suggesting directions for further improvement.

(iv). The results obtained using Taguchi's method are not truly optimal as in most cases optimization techniques are not employed. In addition sequential nature of experimentation is not pursued.

(v). Simultaneous optimization of more than one objective functions cannot be carried out; unless some another technique such as Grey relation analysis is employed on the already obtained results.

Considering these limitations of Taguchi's method, the present study utilizes RSM for designing the experiments and carrying out detailed investigation on WEDM of pure titanium (grade-2). The following section briefly describes RSM.

3.2 RESPONSE SURFACE METHODOLOGY

RSM is a combination of mathematical and statistical techniques used in empirical study of relationships and optimization where several independent variables or factors influence

a dependent variable or response. It was developed by Box and Wilson in 1951 while working on a chemical investigation, based on the pioneering works of [Fisher, 1931], in connection with agricultural experimentation [Box 1952; Box and Hunter, 1957]. The response surface function gives a complete summary of the results of the experiment and also enables to predict the response for the combination of the values of factors that are not tested experimentally. RSM also quantifies the relationship between controllable input parameters and obtained response surfaces [Kwak, 2005]. Further it assists in developing predictive models. This methodology has been successfully used in agricultural and chemical fields and also in production engineering works as in turning, milling, grinding, extrusion, press working, welding, etc. The design procedure of RSM is as follows [Gunaraj and Murugan 1999]:

(i). Designing of a series of experiments for adequate and reliable measurement of the response of interest.

(ii). Developing a mathematical model of the second order response surface with the best fittings.

(iii). Finding the optimal set of experimental parameters that produce a maximum or minimum value of response.

(iv). Representing the direct and interactive effects of process parameters through two and three dimensional plots.

If all variables are assumed to be measurable, the response surface can be expressed as follows:

$$y = f(x_1, x_2, x_3, \ldots, x_n) \quad \ldots (3.1)$$

Where

y = output response

x_i = i^{th} independent variable (Control factor)

The goal is to optimize the response variable y. It is assumed that independent variables are continuous and controllable by experiments with negligible errors. It is required to find a suitable approximation for true functional relationship between independent variables and the response surface. In RSM, dependant variable (response variable) is viewed as a surface to which a mathematical model is fitted. Usually a two factor interaction or second-order surface is utilized in RSM that is given by following equations [Kwak, 2005; Gunaraj and Murugan, 1999].

$$y = \beta_0 + \sum_{i=1}^{k} \beta_i x_i + \sum_{i=1}^{k} \beta_{ii} x_i^2 + \sum_{i<j} \beta_{ij} x_i x_j + \varepsilon \qquad \ldots (3.2)$$

where

y = output response

x_i = i^{th} control factor

β = regression coefficient

ε = random error

Regression coefficients (β) are sometimes called partial regression coefficients as β_i measures the expected change in y per unit change in x_i when x_j are held constant. The assumed surface y contains linear, squared and cross product terms of the variables x_i.

3.2.1 Estimation of Regression Coefficients

The method of least squares is typically used to estimate the regression coefficients in a multiple linear or quadratic regression model [Gunaraj and Murugan, 1999]. In general Equation (3.2) can be written in matrix form.

$$y = X\beta + \varepsilon \qquad \ldots (3.3)$$

Where y is defined to be a matrix of measured values, X to be a matrix of independent variables. The matrixes β and ε consist of coefficients and errors, respectively.

$$y = \begin{bmatrix} y_1 \\ y_2 \\ . \\ . \\ y_n \end{bmatrix} \quad X = \begin{bmatrix} 1 & X_{11} & X_{21} & . & X_{1k} \\ 1 & X_{21} & X_{22} & . & X_{2k} \\ . & . & . & . & . \\ . & . & . & . & . \\ 1 & X_{n1} & X_{n2} & . & X_{nk} \end{bmatrix} \quad \beta = \begin{bmatrix} \beta_0 \\ \beta_1 \\ . \\ . \\ \beta_k \end{bmatrix} \quad \varepsilon = \begin{bmatrix} \varepsilon_0 \\ \varepsilon_1 \\ . \\ . \\ \varepsilon_n \end{bmatrix}$$

In general, y is an n×1 vector of observations, X is an n×k matrix of levels of independent variables, β is a k×1 vector of regression coefficients and ε is an n×1 vector of random errors. The aim is to find the vector of least square estimators, b that minimizes L that is as follows:

$$L = \sum_{i=1}^{n} \varepsilon_i^2 = \varepsilon'\varepsilon = (y - X\beta)'(y - X\beta)$$
$$= y'y - \beta'X'y - y'X\beta + \beta'X'X\beta$$
$$= y'y - 2\beta'X'y + \beta'X'X \qquad \ldots (3.4)$$

Since $\beta'X'y$ is a 1×1 matrix, or scalar, and its transpose $(\beta'X'y)' = y'X\beta$ is the same scalar. The least square estimators must satisfy

$$\left.\frac{\partial L}{\partial \beta}\right|_b = -2X'y + 2X'Xb = 0$$

$$X'Xb = X'y \quad \ldots (3.5)$$

Equation 3.5 is set of normal equations in matrix form. Multiply both sides of this by inverse of $X'X$. Thus, least square estimator of β is [Kwak, 2005; Gunaraj and Murugan 1999]:

$$b = (X'X)^{-1}X'y \quad \ldots (3.6)$$

The fitted regression model is

$$\hat{y} = Xb \quad \ldots (3.7)$$

Where $\hat{y}$ = estimate of y

3.2.2 Model Adequacy Checking Tests

Model adequacy checking is necessary to (a) Examine the fitted model to ensure that it provides an adequate approximation to the true system and (b) to verify that none of the least square assumptions are violated. The various techniques used for it are described below [Myers, 2002].

3.2.2.1 Sum of Squares of Residuals Technique

The difference between observation y_i and fitted value $\hat{y}$ is called residual (e). The n×1 vector of residuals is denoted by

$$e = y - \hat{y} \quad \ldots (3.8)$$

The method of least square produces an unbiased estimator of the parameter β in the multiple regression models. The important parameter is the sum of squares of the residuals (SS_E)

$$SS_E = \sum_{i=1}^{n} (y_i - \hat{y})^2 = \sum_{i=1}^{n} (e_i)^2 = e'e \quad \ldots (3.9)$$

From (3.7 and 3.8) substituting $e = y - \hat{y} = y - Xb$,

$$ss_E = (y - Xb)'(y - Xb)$$

$$= y'y - b'X'y \quad \ldots (3.10)$$

The above equation is called error or residual sum of squares with n-k-1 degrees of freedom.

Total sum of squares (SS_T) is given by following equation with n-1 degrees of freedom

$$SS_T = y'y - \left(\sum_{i=1}^{n} y_i\right)^2 \Big/ n$$

It is necessary to test for significance of the model. This test procedure involves partitioning the total sum of squares into sum of squares due to model (regression) and sum of squares due to error [Myers, 2002].

$$SS_T = SS_R + SS_E$$

$$SS_R = b'X'y - \left(\sum_{i=1}^{n} y_i\right)^2 \Big/ n \text{ with k degrees of freedom} \quad \ldots (3.11)$$

4.2.2.2 Test for Significance of Regression

F Statistics is a test for comparing model variance with residual (error) variance. It is the ratio of mean square of regression (MS_R) to the mean square of error (MS_E).

Where

$$MS_R = \frac{SS_R}{k}$$

$$MS_E = \frac{SS_E}{n-k-1}$$

If model F value exceeds $F_{\alpha,k,n-k-1}$, then the model is considered valid. Alternatively, p-value approach to hypothesis testing can be utilized, according to which if p-value of the F statistics of the model is lower than the confidence interval (α), the model is considered valid.

R^2 is a measure of amount of reduction in the variability of y obtained by using the regressor variables x_1, x_2,..,x_n in the model and is defined by ratio of sum of squares due to regression to the total sum of squares ($\frac{SS_R}{SS_T}$) . The domain for R^2 = 0 to 1. A larger value of R^2 does not necessarily imply that regression model is good one. Adding a variable to the model will always increase R^2, regardless of whether the additional variable is statistically significant or not. Thus, it is preferred to use an adjusted R^2 statistics that is defined as follows:

$$R^2_{adj} = 1 - \frac{SS_E/(n-k)}{SS_T/(n-1)}$$

Adjusted R^2 is a measure of the amount of variation around the mean explained by the model, adjusted for the number of terms in the model. The adjusted R-square decreases as the number of terms in the model increases, if those additional terms don't add value to the model.

Adequate Precision is a term that measures signal to noise ratios. It compares the range of the predicted values at the design points to the average prediction error. Ratios greater than 4 indicate adequate model discrimination.

3.2.2.3 Test for Lack of Fit

It is frequently useful to obtain two or more observations (replicates) on the response at the same settings of independent variables. As replicates of the central point are made, it is possible to estimate pure error associated with repetitions. Thus, sum of the square for residuals can be dismembered into two more parcels: the sum of the square due to pure error (SS_{PE}) and the sum of the square due the lack of fit (SS_{LOF}), as shown below:

$$SS_{RES} = SS_{PE} + SS_{LOF}$$

$$SS_{PE} = \sum_{i=1}^{m}\sum_{j=1}^{n_i}(y_{ij} - \bar{y}_i)^2$$

$$SS_{LOF} = \sum_{i=1}^{m} n_i\ (\bar{y}_i - \hat{y}_i)^2$$

$$MS_{PE} = \frac{SS_{PE}}{n_i - 1}$$

$$MS_{LOF} = \frac{SS_{LOF}}{m - k}$$

Where

y_{ij}	=	j^{th} observation on the response at y_i
n_i	=	number of observations at i^{th} level
m	=	levels of x_i
$n_i - 1$	=	degrees of freedom associated with SS_{PE}
$m - k$	=	degrees of freedom associated with SS_{LOF}

Another way to evaluate the model is the *lack of fit test*. If the mathematical model is well fitted to the experimental data, MS_{LOF} will reflect only the random errors inherent to the system. Additionally, MS_{PE} is also an estimate of these random errors and it is assumed that these two values are not statistically different. This is the key idea of the lack of fit test. It is possible to use the *F* distribution to evaluate if there is some statistical difference between these two media, in the same way that the significance of regression was verified:

$$\frac{MS_{LOF}}{MS_{PE}} \approx F_{(dlof\ ,dpe)}$$

where, *dlof* and *dpe* are the degree of freedom associated with the lack of fit and the pure error respectively. If this ratio is higher than tabulated value of *F*, it is concluded that there is evidence of a lack of fit and that the model needs to be improved. However, if the value is lower than tabulated value, the model fitness can be considered satisfactory. To apply a lack of fit test, the experimental design must be performed with authentic repetitions at least at its central points.

3.3 RESIDUAL ANALYSIS

The residuals from least square fit play an important role in judging the model adequacy. A check on the normality assumption may be made by constructing a normal probability plot of residuals. If residuals plot is approximately along a straight line, then the normality assumption is satisfied. Various types of residuals are evaluated for judging the adequacy of the model, that are as follows [Myers, 2002; Montgomery, 2002]:

3.3.1 Standardized and Studentized Residuals

Scaled residuals such as standardized and studentized residuals convey more information than ordinary least square residuals.

Standardized residuals $d_i = \frac{e_i}{\hat{\sigma}}$ i= 1, 2…., n

Where $\hat{\sigma} = \sqrt{MS_E}$

These standardized residuals have mean zero and approximately unit variance and are useful in looking out for outliers. Most of the standardized residuals should lie in the interval $-3 \leq d_i \leq 3$. Any observation with a studentized residual outside this limit may represent something as simple as data recording error or something of more serious

concern. The studentized residual is the number of standard deviations that separate the actual and predicted response values. It is calculated by the ratio of residual to the estimated standard deviation of the residual.

Studentized residual = $\frac{e_i}{\sqrt{\hat{\sigma}^2(1-h_{ii})}}$

Where

h_{ii} = measure of location of the ith point in x space.

The studentized residuals have constant variance equal to 1 regardless of the location of x_i, when the form of the model is correct.

3.3.2 Prediction Error Sum of Squares Residuals

The prediction error sum of squares (PRESS) provides a useful residual scaling. To calculate PRESS, ith observation is selected and the regression model is fitted to remaining n-1 observations. The equation developed so is utilized to predict the withheld observation y_i. Denoting this predicted value by $\hat{y}_{(i)}$, now find the prediction error for point i as $e_i = y_i - \hat{y}_{(i)}$. This prediction error is called ith PRESS residual. This procedure is repeated for each observation. Then PRESS statistics is defined as sum of squares of the n such PRESS residuals in the following manner

$$PRESS = \sum_{i=1}^{n} {e_i}^2 = \sum_{i=1}^{n} (y_i - \hat{y}_i)^2$$

PRESS is used to compute an approximate R^2 for prediction

$$R^2{}_{prediction} = 1 - \frac{PRESS}{SS_T}$$

$R^2{}_{prediction}$ Indicate predictability of the regression model. Within 95% confidence interval, usually it is desirable to have $0.95 \leq R^2{}_{prediction} \leq 1$. It means that it is expected from the model to explain most the variability arising in predicting new observations.

3.4 ANALYSIS OF VARIANCE

Analysis of variance (ANOVA) is a technique for analyzing experimental data in which one or more response (or dependent) variables are measured under various conditions identified by one or more classification variables. In ANOVA, variation in the response is

separated into variation attributable to differences between the classification variables and variation attributable to random error. To accomplish this, Sum of squares due to error (SS_E), Sum of squares due to regression (SS_R) and Total Sum of squares (SS_T) are utilized. The (SS_T) is divided into following four parts as shown in Table 3.1 to ascertain contribution of first order terms, second order terms, lack of fit element to measure the deviations of the response from the fitted surface and estimation of the experimental error from center runs [Pecas and Henriques, 2003].

Table 3.1: Analysis of variance using multiple regressions [Marcos et al., 2008]

Variation Source	Sum of Squares (SS)	Degrees of Freedom	Mean Square (MS)
Regression	$SS_R = \sum_{i=1}^{m}\sum_{j=1}^{n_i}(\hat{y}_i - \bar{y})^2$	$p-1$	$MS_R = \frac{SS_R}{p-1}$
Residuals	$SS_{residual} = \sum_{i=1}^{m}\sum_{j=1}^{n_i}(y_{ij} - \hat{y}_i)^2$	$n-p$	$MS_{residual} = \frac{SS_{residual}}{n-p}$
Lack of fit	$SS_{LOF} = \sum_{i=1}^{m}\sum_{j=1}^{n_i}(\hat{y}_i - \bar{y}_i)^2$	$m-p$	$MS_{LOF} = \frac{SS_{LOF}}{m-p}$
Pure error	$SS_{PE} = \sum_{i=1}^{m}\sum_{j=1}^{n_i}(y_{ij} - \bar{y}_i)^2$	$n-m$	$MS_{PE} = \frac{SS_{PE}}{n-m}$
Total	$SS_T = \sum_{i=1}^{m}\sum_{j=1}^{n_i}(y_{ij} - \bar{y})^2$	$n-1$	

Where,

n = number of observations

m = total number of levels in the design

p = number of parameters of model

$\bar{y}$ = overall mean

$\hat{y}_i$ = estimated value by the model for the level *i*;

y_{ij} = replicates performed in each individual levels;

$\bar{y}_i$ = mean of replicates performed in the same set of experimental conditions.

Based upon results obtained from ANOVA, mathematical models consisting of significant terms of individual and interaction effects are built for responses of interest.

3.5 BOX- BEHNKEN DESIGNS

Box–Behnken designs (BBD) are one class of the experimental designs for response surface methodology. They are rotatable or nearly rotatable based on three-level incomplete factorial designs [Box and Behnken, 1960]. Rotatable means that the model would possess a reasonably stable distribution of scaled prediction variance throughout the experimental design region [Montgomery, 2002]. The special arrangement of the BBD levels allows the number of design points to increase at the same rate as the number of polynomial coefficients. For example, for three factors, the design can be constructed as three blocks of four experiments consisting of a full two-factor factorial design with the level of the third factor set at zero [Souza et al., 2005].

BBD allows calculations of the response function at intermediate levels and enables estimation of the system performance at any experimental point within the range studied through careful design and analysis of experiments. Another advantage of the BBD is that it does not contain combinations for which all factors are simultaneously at their highest or lowest levels. Thus, these designs are useful in avoiding experiments performed under extreme conditions, for which unsatisfactory results might occur [Ferreira et al., 2007; Myers and Montgomery, 2002]. Therefore, for three factors BBD, its graphical representation can be seen as a cube that consists of the central point and the middle points of the edges as shown in Figure 3.1 [Ferreira et al., 2007; Myers and Montgomery, 2002]. However, it can also be viewed as consisting of three interlocking 2^2 factorial designs and a central point (Figure. 3.2). BBD requires three levels of each factor instead of five as in the case of Central Composite Designs (CCD), which results in fewer experimental trials to evaluate multiple variables and their interactions and is more convenient and less expensive to run than CCD with the same number of factors [Ragonese et al., 2002] as indicated in Table 3.3.

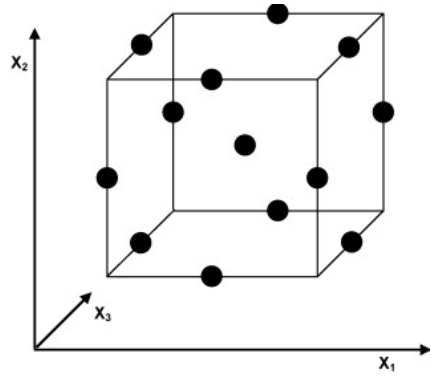

Figure 3.1 Box–Behnken designs as derived from a cube [Souza et al., 2005]

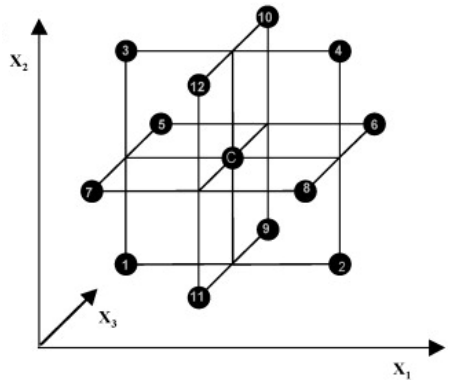

Figure 3.2 Representation of Box Behnken Design as Interlocking 2^2 factorial experiments [Souza et al., 2005]

Table 3.2 Comparative study of different designs on the basis of number of experiments [Source: www. It1.nist.gov, 2011]

No. of Factors	Number of Experiments		
	Central Composite Design	Full Factorial Design	Box -Behnken Design
2	13	9	11
3	20	27	15
4	30	81	27
5	50	243	46
6	86	729	54
7	152	2187	62

CHAPTER 4
EXPERIMENTATION

4.1 INTRODUCTION

Optimum utilization of capabilities of WEDM process requires selection of appropriate sets of machining parameters. This can mainly be achieved by understanding the interrelationship between large numbers of parameters affecting the process and identifying the optimal machining conditions as the process is complex and stochastic in nature. Thus, experiments are to be performed on a given machine tool in order to understand the effect of different process parameters on performance measures i.e. machining rate, surface roughness, material removal rate (MRR), overcut, dimensional deviation, wire wear ratio, surface crack size density and recast layer thickness.

In the present work experiments are performed on a 4- axis Sprintcut-734 WEDM machine manufactured by Electronic India Ltd. Pune, India, as shown in Figure 4.1 and available at Central Tool Room, Ludhiana, India. Table 4.1 provides specifications of the selected machine tool.

4.2 SPECIFICATIONS OF WORK PIECE MATERIAL

Pure titanium (ASTM grade-2) required for experimentation was procured from M/s Anand Metals, Mumbai, India. Table 4.2 shows chemical composition of pure titanium and Table 3.3 shows its mechanical properties.

4.3 PROCESS PARAMETERS OF WEDM

WEDM process is a complex machining process controlled by a large number of process parameters. A change in a single parameter may influence the process in a complex way. Thus, a thorough and deep insight into the process parameters is essential. Process parameters of WEDM can be divided into two categories:

(i). Electrical parameters: Pulse on time, pulse off time, peak current, and spark gap voltage.

(ii). Non-electrical parameters: Wire feed, wire tension and water pressure.

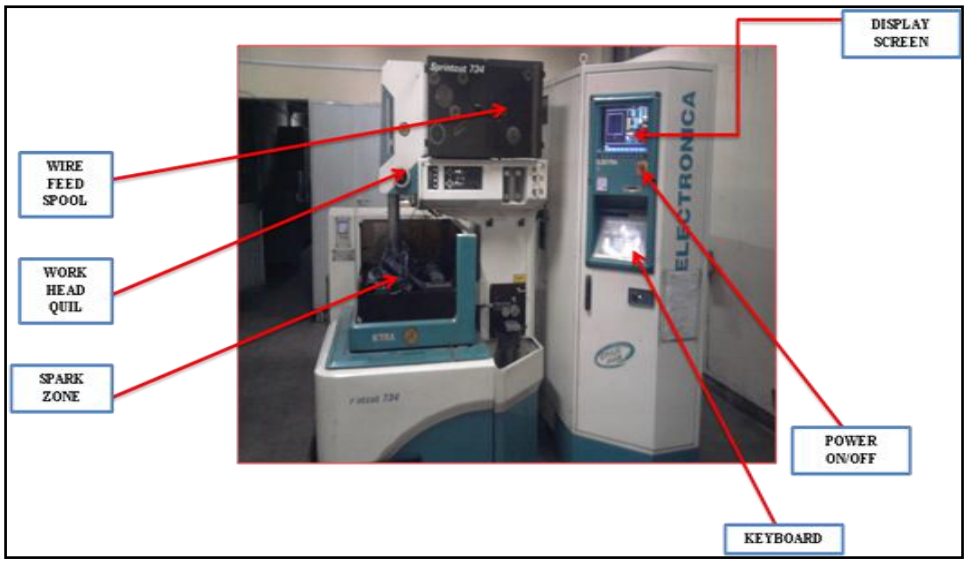

Figure 4.1 Four-axis Electronica Sprintcut-734 CNC WEDM [Source: Central Tool Room, Ludhiana]

Table 4.1 Specifications of Electronica Sprintcut-734 WEDM [Source: Electronica Sprintcut Machine tool Manual, 2002]

Electrical Specifications		
1.	Input power supply	3 Phase, AC 415 V, 50 Hz
2.	Connected load	15 KVA
3.	Average power consumption	6 to 7 KVA
4.	Overload protection	With SIEMENS contractor and 3 phases thermal overload relay.
Mechanical Specifications		
1.	Table size	650 mm ×440 mm
2.	Maximum work piece size	600 mm×780 mm×200 mm
3.	Maximum work piece weight	400 kg
4.	Main table traverse (X×Y)	300 mm× 400 mm
5.	Auxiliary table traverse (U×V)	± 40 mm × ± 40 mm
6.	Vertical table traverse (Z)	225 mm
7.	Main table feed rate	900 mm/min
8.	Resolution	0.0005 mm
9.	Maximum taper cutting angle	± 30.8 / 50 mm
10.	Control of axis	X, Y, U, V, Z simultaneous / independent
11.	Wire electrode	0.25 mm (Standard) 0.20 mm, 0.15 mm (Optional)

Table 4.2 Chemical composition of pure titanium [Source: ASTM, 2008]

Element	**C**	**N_2**	**O_2**	**H_2**	**Fe**	**Ti**
Max. Weight (%)	0.10	0.03	0.25	0.015	0.30	99.03

Table 4.3 Mechanical properties at room temperature [Source: ASTM, 2008]

Ultimate Tensile Strength (MPa)	**Yield Strength (MPa)**	**Elonga-tion (%) at break**	**Hardness (Rockwell**	**Hardness (Vickers)**	**Modulus of Elasticity (GPa)**	**Fatigue Strength (MPa)**	**Compressive Modulus (GPa)**
345	276	20	80	145	105	300	110

Besides these, there are other process parameters which are not controlled by the machine tool, but, affect machining performance such as, thickness of the work piece, electrical conductivity of work piece, wire type and diameter, dielectric conductivity. Table 4.4 lists controllable process parameters available on the selected WEDM machine and their ranges. These controllable machining parameters are discussed as follows:

Table 4.4 Parameters and their range

S. No	**Name of Parameter**	**Symbol**	**Range**
1.	Pulse on time	T_{on}	105-130 mu
2.	Pulse off time	T_{off}	36-60 mu
3.	Peak current	Ip	40-230A
4.	Spark gap set voltage	SV	5-75V
5.	Wire feed rate	WF	2-12 m/min
6.	Wire Tension	WT	2-12 mu

(i). Pulse on Time (T_{on})

This is the duration of time (μs) during which current is allowed to flow per cycle. The main EDM operation is effectively done during this time. The spark gap is bridged, current is generated and spark is generated. Increased pulse on time allows more heat to sink into the work piece as the discharge energy increases. An increase in discharge energy leads to larger craters thereby reducing surface finish [Tarang, 1995]. Ton range available on selected WEDM machine is 100-131 (machine units), which can be varied in steps of 1. The corresponding actual values of pulse on time are from 0.1μs to 1.65μs in steps of 0.05μs. A conversion table is provided in operation manual of Electronica

Sprintcut-734 machine tool to convert machine units to actual units of Ton and it is given in Appendix I.

(ii). Pulse off Time (T_{off})

This is the duration of time between two successive sparks when the discharge is turned off. Off time is the duration of rest pauses required for reionization of the dielectric. This time also allows the molten material to solidify and to be washed out of the spark gap [Cabannes, 2010]. Pulse off time mainly affects the stability of the cut. When pulse off time is shorter, the number of discharges within a given period becomes more. However, if the pulse off time is too small, the ejected work piece debris will not be flushed away with the flow of dielectric and dielectric fluid will not be deionized. This results into instability of the next spark [Garg et. al, 2010]. The setting range available on the machine tool is 0-63 (machine units) in steps of 1. The corresponding actual values of pulse off time are from 2µs to 52µs in steps of 0.25µs to 2µs. The conversion table in Appendix-I (Table B) shows actual values of pulse off time in micro seconds against machine units.

(iii). Peak Current (Ip)

It represents amount of power used in discharge machining. The current increases until it reaches a preset level during each pulse on time and it is known as peak current. Higher is a peak current, larger the discharge energy. Thus, effects of peak current and pulse on time are similar [Tarang, 1995]. A higher discharge current leads to higher MRR, overcut and larger surface roughness. Further, the depth of recast layer increases and work piece become hardened than parent metal [Hascalyk and Caydas, 2008]. Moreover, very high peak current values lead to frequent wire breakage. Peak current setting available in the selected machine is from 10-230A in steps of 10A.

(iv). Spark Gap Voltage (SV)

This is the reference voltage for actual gap voltage. Higher the servo reference voltage longer is the discharge waiting time. In order to obtain longer discharge waiting time, cutting speed need to be reduced. This will lead to a wider discharge gap. Therefore, discharge conditions become more stable and better surface accuracy results [Tarang, 1995]. A machine setting with smaller value of SV will narrow down the spark gap, which leads to more number of sparks per unit time. It speeds up the machining rate but

the state of machining at the gap become unstable and frequent wire breakage takes place. In selected machine tool SV value can vary from 0 to 99V in step of 1V.

(v). Wire Feed Rate (WF)

This is feed rate at which wire is fed continuously for sparking. In WEDM, wire electrode contributes 70% of the machining cost [Dauw, Beltrami, 1994]. Thus, to achieve economy, lower wire feed rate is recommended. However, frequent wire breakage is observed when the WF is reduced below 5m/min. Higher values of wire feed rate (above 6m/min) are required for working with higher pulse power when the cutting rates are higher [Electronica Sprintcut machine, manual, 2002]. Wire feed setting is available in the range of 1m/min to 15 m/min in step of 1 m/min in the selected machine tool.

(vi). Wire Tension (WT)

The main factors contributing to the geometrical inaccuracy of the WEDM part are the various process forces acting on the wire causing it to depart from the programmed path. These forces include the mechanical forces produced by the pressure from the gas bubbles formed by plasma of the erosion mechanism. Thus, the tension is applied to the wire to keep it straight and un-deflected. WT is the gram equivalent load with which the continuously fed wire is kept under tension so that it remains straight between the wire guides. Wire tension setting is available in the range 1mu to15mu in steps of 1mu. Table C in Appendix–I indicates actual values of wire tension in grams against machine units. A larger value of wire tension (above 10mu) causes frequent wire breakage due to higher tensile forces. Small wire tension (less than 5mu) tends to produce inaccurate parts as the wire become slack [Electronica Sprintcut machine, manual, 2002].

(vii). Flushing Pressure (WP)

The purpose of dielectric is to flush away the debris produced during machining and to keep the wire and work piece cool in addition to aid during machining. Effective flushing may also affect the surface roughness of the work piece as well as influence crack density and recast layer [Wong et al., 1995]. Water pressure can vary from 2 Kg/cm^2 to15 Kg/cm^2 in the step of 1 Kg/cm^2 in selected WEDM machine. Higher input water pressure is recommended for cutting with higher pulse power and jobs of larger thickness [Electronica Sprintcut machine, manual, 2002]. Low input pressure is used for thin jobs and in making trim cuts.

Above discussion reveals that a large number of controllable parameters decide performance of the machine tool in terms of productivity objectives such as cutting rate as well as MRR and quality aspect i.e. surface roughness. The effect of these parameters is different on different materials owing to their different electrical and thermal conductivities, melting points and diverse mechanical properties. Literature review reveals that wrong settings of different parameters may cause abnormal discharge conditions that lead to wire breakage. This imposes a serious constraint on the achievement of high productivity in the subsequent machining of the material. It is, therefore, imperative to study the effect of each controllable process parameter on the desired performance criteria, in order to isolate the process parameters actually affecting the performance measures. It is also necessary to limit the range of the selected process parameters, so that abnormal discharge conditions can be avoided and wire breakage is not experienced in the subsequent machining for the particular material. This necessitates carrying out preliminary investigation following one-factor-at-a-time approach and it is described in the following sections.

4.4 PILOT EXPERIMENTATION

Pilot experimentation is carried out by conducting experiments which are planned using one-factor-at–a–time approach (OFTA). According to this, one process parameter is incremented while values of other parameters are kept at the central levels of their available ranges. This approach is beneficial for studying the effect of individual parameter on the response functions and is used widely in the literature [Rao Paramsewar et al., 2010; Tarang et al., 1995].

The experiments are performed on Electronica Sprintcut-734 WEDM machine from Electronica India Pvt. Ltd. The various input parameters are varied during the experimentation viz. T_{on}, T_{off}, IP, SV, WF and WT, so as to study their effects on cutting rate and surface roughness. There are other parameters which are kept fixed throughout the experimentation as shown in Table 4.5.

Table 4.5 Fixed parameters

S.No.	Machining Parameters	Units	Fixed operating conditions
1.	Electrode material	-	Brass(Ø 0.25mm)
2.	Electrode polarity	-	Negative
3.	Work material	-	Pure titanium
4.	Work material size	mm	148 × 148 × 26
5.	Dielectric fluid	-	deionized water
6.	Dielectric pressure	Kg/cm^2	7
7.	Conductivity of dielectric	mho	±20-24
8.	Working temperature	°C	25

4.4.1 Procedure for Pilot Experimentation

Experiments are conducted on pure titanium (ASTM-grade 2) plate by using one factor at a time approach. The following steps are followed:

(i). The work piece is clamped on x-y table of the machine tool and checked using dial indicator for any perpendicularity errors.

(ii). The wire is made vertical using a verticality block.

(iii). To set the working coordinate system (WCS), a reference point on the ground edge of the work piece is selected.

(iv). Tool path for movement of wire is designated by developing a computer program using ELAPT software supplied by Electronica machine tool manufacturer.

(v). Machine is manually jogged to the point where cutting should begin. A zero is set at the point where initial sparking starts.

(vi). Process parameters are set at the specified levels and a straight cut of 10 mm length is made on a rectangular plate of pure titanium (ASTM-grade 2), as shown in Figure.4.2. This cut length of 10 mm is utilized for recording of cutting rate data and measurement of surface roughness. The cut section of length 4 mm separates the two consecutive experiments. Figure 4.3 indicates view of pure titanium (ASTM-grade 2) plate after performing all preliminary experiments.

(vii). Cutting rate data displayed on the monitor of the machine tool is noted down during cutting and surface roughness of the cut sections is measured after all the experiments are performed. Cutting rate data is directly displayed on the monitor of machine and it is noted at distances of 2.5mm, 5mm and 7.5mm from the initialization of cut, once cutting is stabilized properly. The average of the above

three readings is taken as cutting rate. The center line average (CLA) surface roughness parameter (R_a) is used to quantify surface roughness of the machined surface. It is defined as the arithmetic average of all departures from the roughness profile from the central line of evaluation length. R_a is measured using a contact type stylus based surface roughness tester, Mitutoyo Surftest SJ -301, having a least count of 0.001 µm. The cut-off length is 0.8 mm and evaluation length is 4 mm. R_a is measured at three places perpendicular to the direction of cut and mean of the three readings denotes average surface roughness. Figure 4.4 shows the set up for measurement of surface roughness.

It is important to mention that during experimentation, if wire breakage occurs, the experiment is repeated thrice in order to ascertain the cause of wire breakages due to abnormal discharge conditions. If in all the three experiments, the wire breakage occurs, then the set of parameter values are noted down with remark 'Wire Breakage'. The above procedure outlined from (vi) to (vii) is followed for assessing the effect of each input parameter. The following section describes effect of each input parameter on cutting rate and surface roughness.

4.4.2 Effect of Process Parameters on Cutting Rate and Surface Roughness

The effect of individual process parameter on cutting rate, surface roughness and wire breakage is discussed, which is as follows:

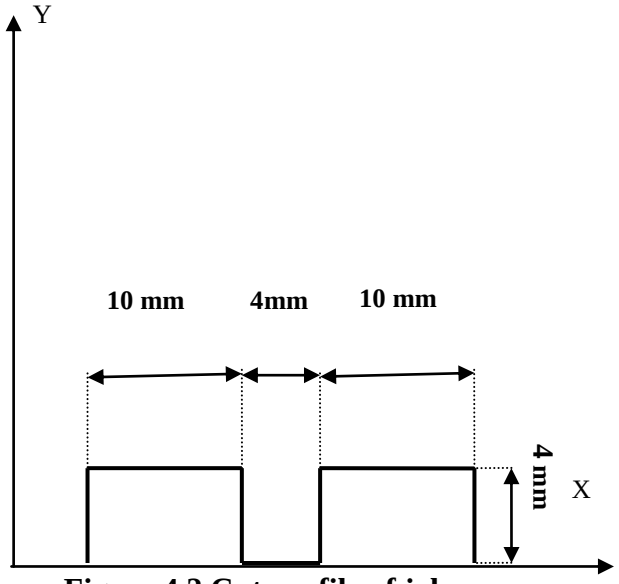

Figure 4.2 Cut profile of job

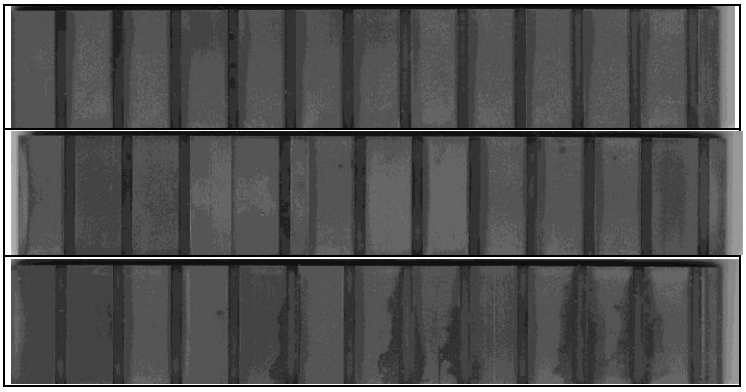

Figure 4.3 Pure titanium (ASTM-grade 2) plate after pilot experiments

Figure 4.4 Set up for surface roughness measurement [Model SJ-301, Source: Central Tool Room Ludhiana]

4.4.2.1 Effect of Pulse on Time (T_{on})

Ton is increased from 105mu to 130mu keeping all other parameters at their mid values (T_{off} =55mu; IP=160A; WF=8m/min; WT=8mu; SV=45Volt; SF=2050). Figure 4.5 (a, b) shows the scatter plots of pulse on time versus response characteristics. The cutting rate increases with the increase in the pulse on time in a practically straight line fashion as shown in Figure. 3a. It was not possible to perform cutting beyond T_{on} >130 mu because of the frequent wire breakage. Figure.4.5 (a) clearly reveals that average cutting rate increased from 0.18 mm/min to 1.26 mm/min. This is attributed to the fact that with higher T_{on}, larger discharge energy is available at the cutting zone, which causes faster erosion of

material. The surface roughness increased from 1.57 µm to 3.25µm as shown in Figure 4.5 (b). This is attributed to the fact that with higher T_{on}, deep craters are formed on work piece surface due to intense heating effect, thereby increasing the surface roughness.

4.4.2.2 Effect of Pulse off Time (T_{off})

T_{off} is increased from 36mu to 60mu keeping all other parameters at their mid values (T_{on}=115 mu; IP= 160A; WF =8m/min; WT= 8mu; SV= 45Volt; SF=2050). Figure 4.6(a,b) shows that the scatter plots of pulse off time versus response characteristics. It reveals that with increase in T_{off} from 36mu to 60mu, average cutting rate decreases from 1.34 mm/min to 0.38 mm/min. With a lower value of T_{off} at 36mu, the cutting rate increases with more number of discharges and increase in the sparking efficiency. Average surface roughness decreases from 2.32µm to 1.95µm. With a large value of T_{off}, the machining stability is improved and the arcing is controlled, resulting in formation of shallow crates on work piece surface. As a result, the surface roughness decreases. Frequent wire breakage occurred for T_{off} values less than 36mu owing to unstable cutting conditions as the dielectric is not deionized properly at the inadequate value of pulse off time.

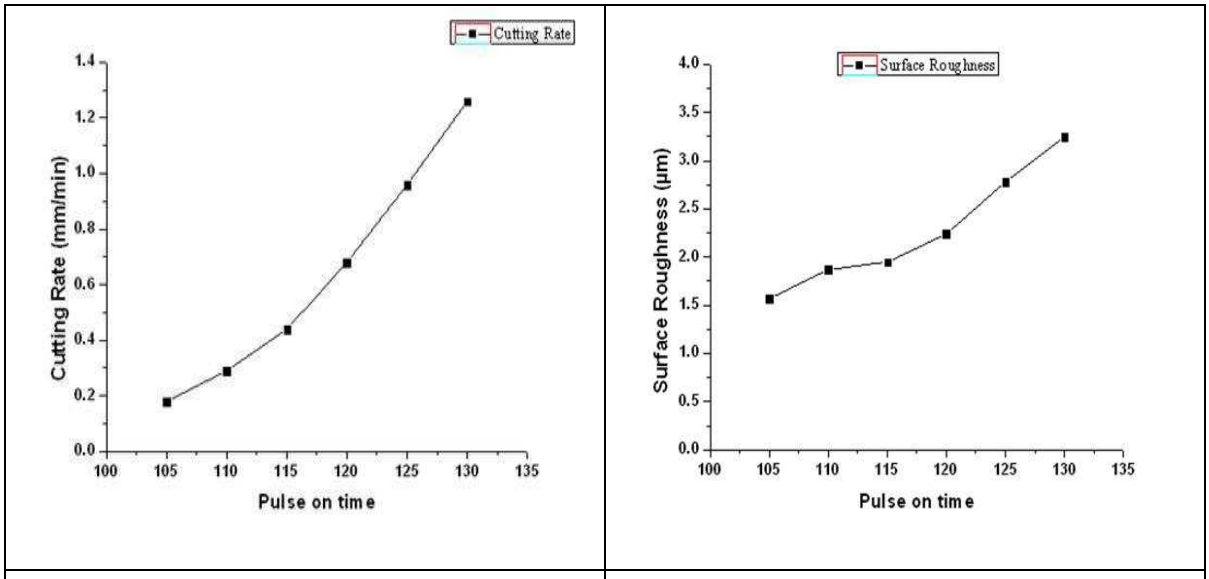

(a) **(b)**

Figure 4.5 (a, b) Effect of pulse on time (T_{on}) on cutting rate and surface roughness (Toff= 55mu, IP= 160A, WP= 8 kg/cm^2, WF= 8 m/min, WT= 8mu, SV=45V)

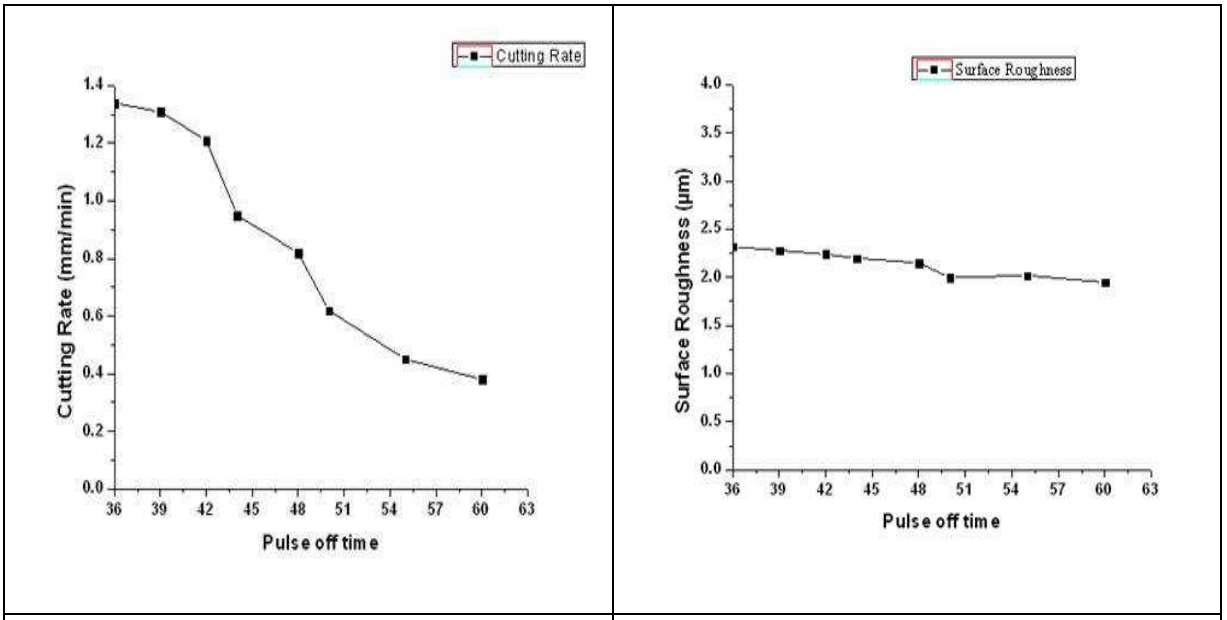

(a) **(b)**

Figure 4.6 (a, b) Effect of pulse off time (T_{off}) on cutting rate and surface roughness (Ton=115 mu; IP= 160A; WF =8m/min; WT= 8mu; SV= 45Volt; SF=2050)

4.4.2.3 Effect of Peak Current (Ip)

IP is increased from 40A to 230A, while other parameters are set at (T_{on}=115 mu; T_{off}= 55mu; WF =8m/min; WT= 8mu; SV= 45Volt; SF=2050). Figure.4.7 (a, b) shows that the scatter plots of peak current versus response characteristics. It clearly indicates that cutting rate improves from 0.22 mm/min to 0.50 mm/min as the Ip is increased from 40A to 230A respectively. This is because; an increase in IP lead to increase in pulse discharge energy which in turn improves cutting rate as well as deteriorates the surface finish. Figure 4.7 (b) depicts the effect of Ip on surface roughness. It shows that as Ip is increased from 40A to 230A, surface roughness increases from 1.58µm to 2.62µm. Further, there is no indication of wire breakage as Ip is increased in the selected range.

4.4.2.4 Effect of Spark Gap Set Voltage

To ascertain the effect of SV on cutting rate and surface roughness, SV is increased from 5V to 75V and other parameters are set at (T_{on}=115 mu; T_{off}= 55mu; Ip = 160 A; WF =8m/min; WT= 8mu; SF=2050). Figure.4.8 (a, b) shows that the scatter plots of spark gap voltage versus response characteristics. Figure 4.8 (a) reveals that as SV is increased from 5V to 75V, a decreasing trend in cutting rate is observed from 0.83 mm/min to 0.23 mm/min respectively. On the contrary, as SV is incremented from 5V to 75V, a trend of

reduction in surface roughness is observed varying from 2.23µm to 1.95µm as shown in Figure.4.8 (b). Due to increase of SV widens the gap between two consecutive sparks which results, less discharge energy is produced per unit time.

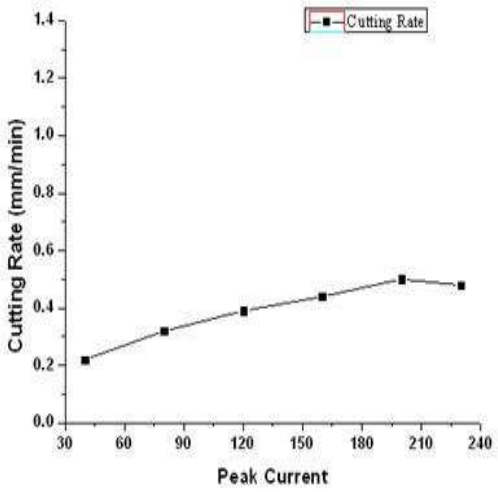

(a)

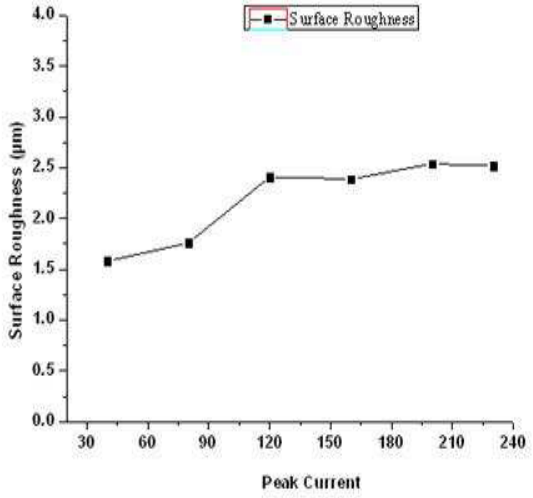

(b)

Figure 4.7(a, b) Effect of peak current on cutting rate and surface roughness (T_{on}=115 mu; T_{off}= 55mu; WF =8m/min; WT= 8mu; SV= 45Volt; SF=2050)

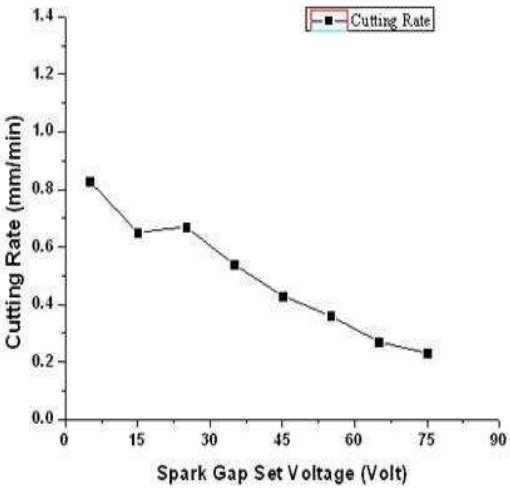

(a)

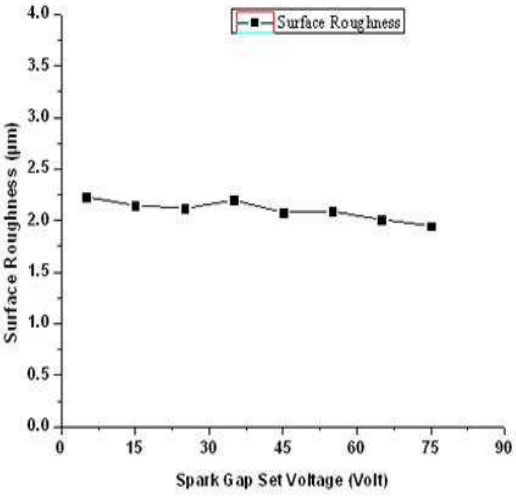

(b)

Figure 4.8 (a, b) Effect of spark gap voltage on cutting rate and surface roughness (T_{on}=115 mu; T_{off}= 55mu; Ip = 160 A; WF =8m/min; WT= 8mu; SF=2050)

4.4.2.5 Effect of Wire Tension (WT)

WT is increased from 2-12 mu and other parameters are kept at (T_{on}=115 mu; T_{off}= 55mu; Ip = 160 A; WF =8m/min; SV= 45Volt; SF=2050). Figure 4.9 (a, b) illustrates the effect of WT on cutting rate. It depicts that WT has negligible effect on the cutting rate and surface roughness when it is increased from 2-12mu. The cutting rate and surface roughness remain practically constant with the increase in wire tension.

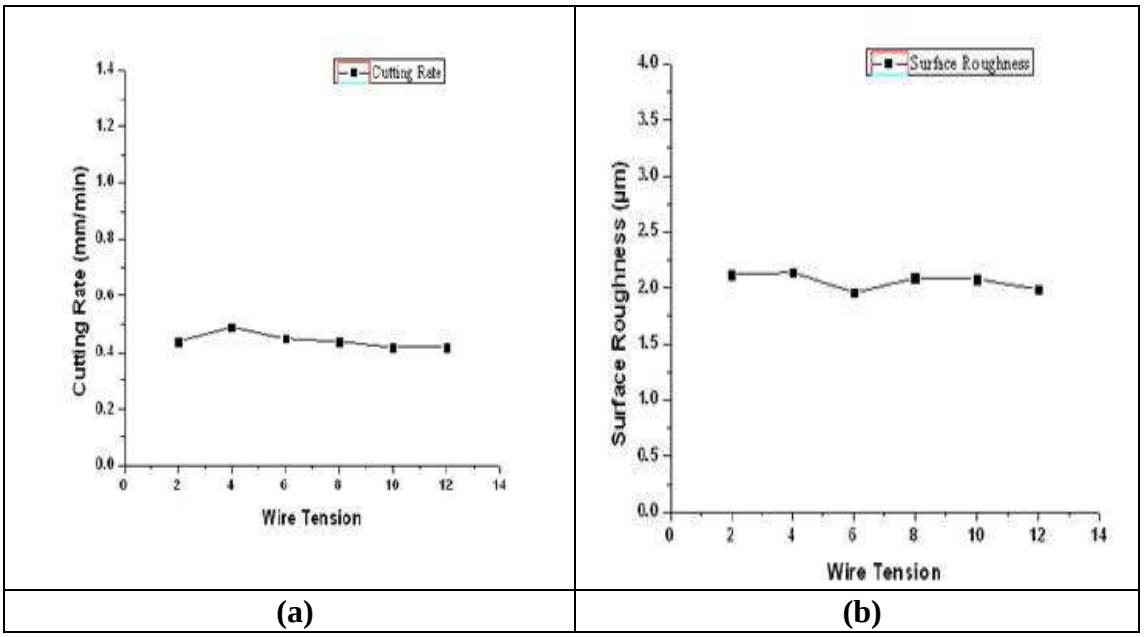

(a) **(b)**

Figure 4.9 (a, b) Effect of wire tension (WT) on cutting rate and surface roughness (T_{on}=115 mu; T_{off}= 55mu; Ip = 160 A; WF =8m/min; SV =45Volts; SF=2050)

4.4.2.6 Effect of Wire Feed rate (WF)

WF is increased from 2 to12 m/min while the other parameters are set at the levels as stated in section 4.4.2.5. Figure 4.10 (a) shows the effect of WF on cutting rate and effect of WF on surface roughness is presented in Figure 4.10 (b). Figure 4.10 (a) reveals that there is negligible effect of WF on cutting rate. Whereas surface roughness is varied from 2.20 µm to 2.31 µm when the wire feed is increased from 2m/min to 12m/min.

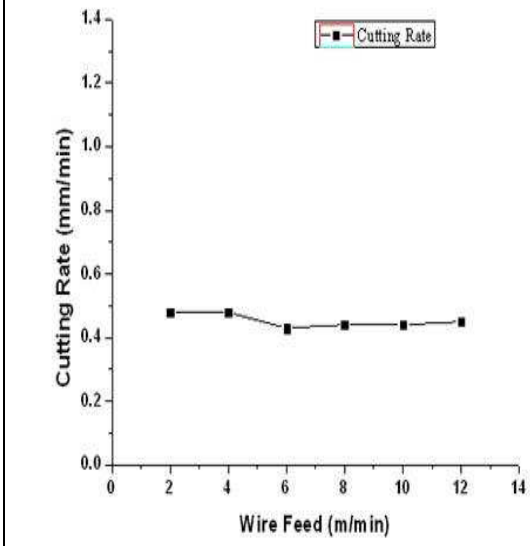

(a)

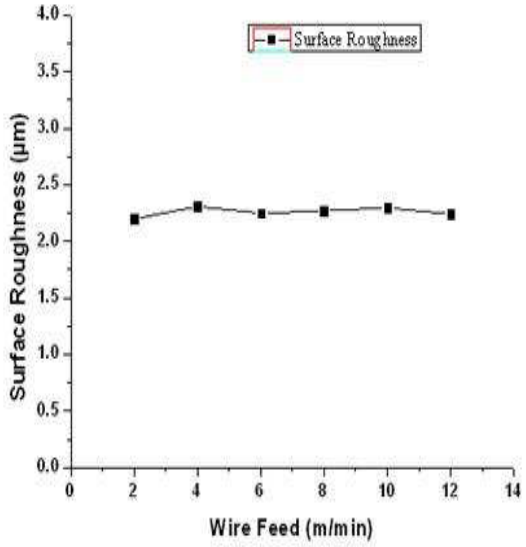

(b)

Figure 4.10 (a, b) Effect of wire feed rate (WF) on cutting rate and surface roughness (T_{on}=115 mu; T_{off}= 55mu; Ip = 160A; WT =8mu; SV =45Volts; SF=2050)

It is observed from Figures 3.5-3.10 that, cutting rate as well as surface roughness in WEDM of pure titanium (grade-2) is mainly affected by pulse on time, pulse off time, peak current and spark gap voltage. Wire tension and wire feed feebly effects on cutting rate, whereas a moderate influence of these on surface roughness was observed.

4.5 EFFECT OF PROCESS PARAMETERS ON WIRE BREAKAGE FREQUENCY

Figure 4.11(a) shows the effect of pulse on time on the wire breaking frequency indicating that the wire breakage frequency continuously increases with an increase in pulse on time. When the value of pulse on time is minimum then there is no wire breakage during the WEDM of pure titanium, but as the pulse on time increases, the probability of wire breakage starts increasing due to increase of discharge rate. Due to increase of pulse on time the rate of discharge energy increases which may significant effect on wire breakage frequency. To have a long duration of electric discharge, it may be possible to select the great value for the pulse on time; however, it may cause a short circuit to occur, resulting in wire breakage. Figure 4.11(b) shows the effect of pulse off time on the wire breakage frequency indicating that the wire breakage frequency increases continuously with decrease in pulse off time. At a maximum value of pulse off

time, the value of wire breakage frequency was zero, but as the pulse off time decreases, it reaches up to its maximum value due to have long duration of each spark. At the minimum value of pulse off time the spark takes longer time to produce the discharge may result to increase the wire breakage frequency. Figure 4.11(c) shows the effect of peak current on wire breakage frequency. This figure indicates that the wire breakage frequency is less at a low value of peak current, but there is a continuous increment in the wire breakage frequency as the peak current increases. This result has been attributed to increase in peak current which leads to the increase in the rate of the heat energy and hence in the rate of melting and evaporization of wire. Figure 4.11(d) shows the effect of spark gap voltage (SV) on the wire breaking frequency indicating that the wire breakage frequency continuously increases with decrease in spark gap voltage. When the value of spark gap voltage is higher, then there is no wire breakage frequency. Parameter servo voltage (SV) is used for controlling advances and retracts of the wire. During machining, the mean machining voltage varies depending on the state of the machining between the workpiece and the electrode. SV established the reference voltage for controlling advances and retracts of the wire. If the mean machining voltage is higher than the set voltage level, the wire advances, and if it is lower, the wire retracts (to be precise, the work table advances or retracts instead of wire).

Therefore, a higher the value for SV, the wider the gap between the work piece and the electrode becomes. Higher values for SV also decrease the number of electric sparks, stabilizing electric discharge, although the machining rate is slowed down. When a smaller value is set for SV, the mean gap becomes narrower, which leads to an increase in number of electric sparks. It can speed up the machining rate; however, the state of machining at the gap may become unstable, resulting in wire breakage. Figure 4.11(e) shows the effect of wire feed (WF) on wire breakage frequency. From this graph, it is evident that the wire breakage frequency decreases with an increase in wire feed (WF). Wire feed is another important parameter in WEDM that show the speed of wire in WEDM. As the wire feed increase the wire consumption and in result the cost of machining will increase while low wire feed can cause to wire breakage in high cutting speed. Figure 4.11(f) shows the effect of wire tension (WT) on wire breakage frequency. From this graph, it is evident that the wire breakage frequency increases with an increase in wire tension (WT). Wire tension is the factor that can control the tension of wire in WEDM. If the wire tension is high enough the wire stays straight otherwise wire drags behind. Graphical analysis of Figures 4.11(a-f) indicates that the wire breakage frequency

is maximum for the parameters i.e. pulse on time (>125mu), pulse off time (<20mu), peak current (>200A), spark gap voltage (<40V), wire feed (>4m/min) and wire tension (<8gram). After deciding the ranges of input process parameters (as given in Table.4.6) in which the wire breakage frequency is minimum, experiments were conducted within this range to determine the effects of input process parameters on performance measures i.e. machining rate, surface roughness, material removal rate (MRR), overcut, dimensional deviation, wire wear ratio, surface crack size density and recast layer thickness.

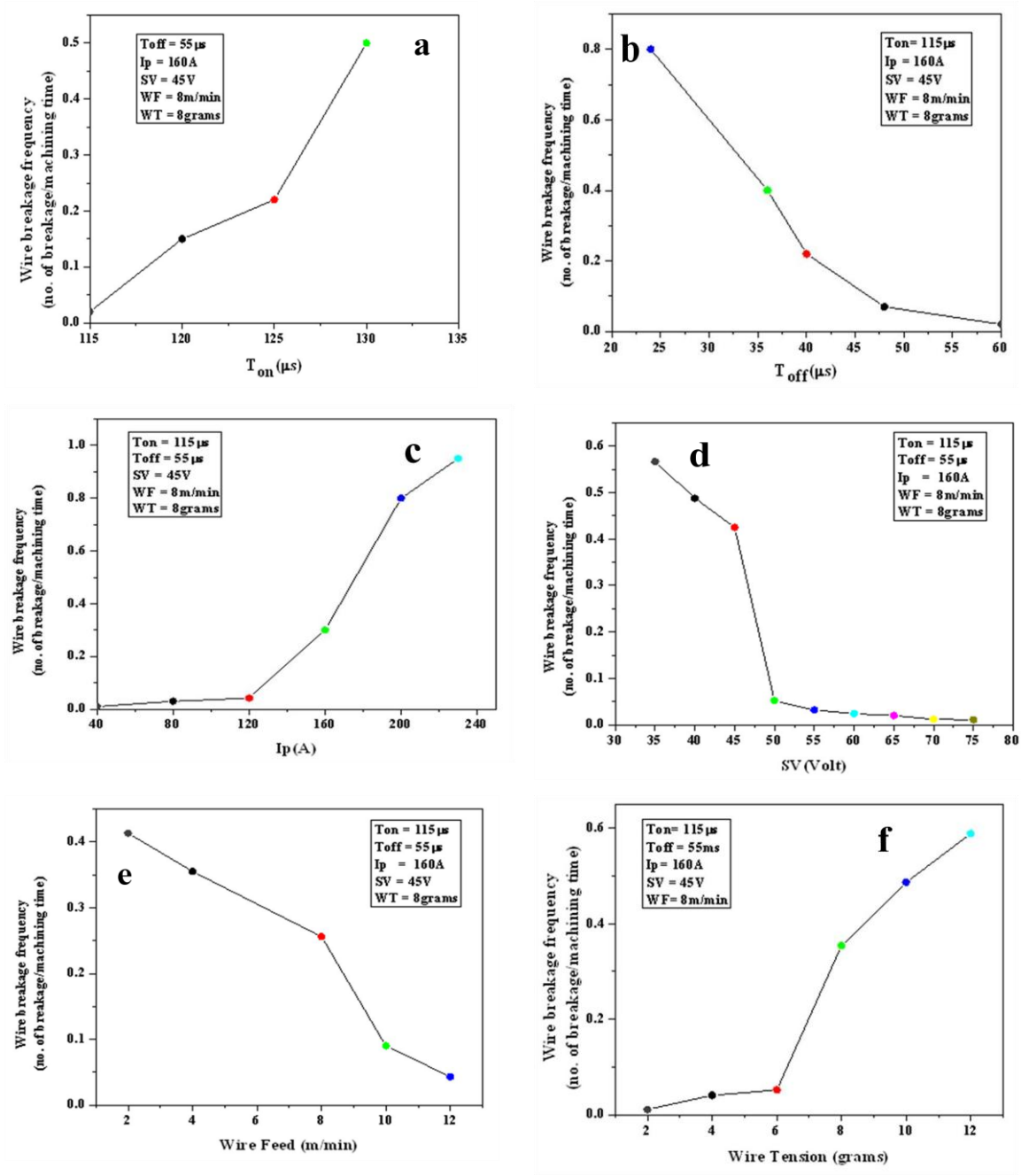

Figure 4.11 Effect of process parameters on wire breakage frequency (a) T_{on}, (b)T_{off}, (c) Ip, (d) SV, (e) WF, (f) WT

The above discussion reveals that Ton, Toff, IP, SV, WF and WT effect cutting rate and surface roughness. Thus, the parameters that effect on cutting rate and surface roughness i.e. T_{on}, T_{off}, Ip, SV, WF and WT are selected to carry out further investigation on WEDM of pure titanium (grade-2). Table 4.6 lists these parameters and their selected ranges.

Table 4.6 Process parameters and their ranges

S. No.	Process Parameters	Symbol	Range (Machine Units)	Range (Actual Units)
1.	Pulse on time	T_{on}	112-120	0.7µs -1.1µs
2.	Pulse off time	T_{off}	44-56	17µs- 38µs
3.	Peak current	Ip	160-200	A
4.	Spark gap voltage	SV	40-60	V
5.	Wire feed	WF	4-10	m/min
6.	Wire tension	WT	4-10	500 - 1400 gram

4.6 MAIN EXPERIMENTAL PLAN

In the present study, experiments are planned by Box- Behnken design (BBD) approach using design expert 6.0® software. In the present work, as there are six control factors as shown in Table 4.6, the construction of BBD for six control factors is based upon partially balanced incomplete block designs. The factorial structure for BBD is 2^3 factorials involving two levels. Table 3.7 shows the design matrix of BBD for six control factors at three levels. Each row of the design matrix (DX) in Table 4.7 involves eight design points in addition to a row of all factors at central levels. Thus, in total 54 design points are generated [Myers and Montgomery, 2002]. Here A, B, C, D, E and F refer to six control factors and +1, -1 and 0 depict high, low and zero level of control factors respectively. The six control factors selected on the basis of preliminary study as shown in Table 4.6 are used in design matrix as input parameters and are varied at three levels (-1,0,+1). Table 4.8 indicates various parameter combinations for different runs of main experimentation. It is planned to carry out experiments with one replication. Thus, in total, 108 experiments are planned to be carried out.

Table 4.7 Design matrix of Box- Behnken design for six factors at three levels

$$D(X)=\begin{bmatrix} A & B & C & D & E & F \\ \pm1 & \pm1 & 0 & \pm1 & 0 & 0 \\ 0 & \pm1 & \pm1 & 0 & \pm1 & 0 \\ 0 & 0 & \pm1 & \pm1 & 0 & \pm1 \\ \pm1 & 0 & 0 & \pm1 & \pm1 & 0 \\ 0 & \pm1 & 0 & 0 & \pm1 & \pm1 \\ \pm1 & 0 & \pm1 & 0 & 0 & \pm1 \\ 0 & 0 & 0 & 0 & 0 & 0 \end{bmatrix}$$

Legend: A, B, C, D, E, F= Control Factors, +1= high level, -1= low level, 0= zero level

4.7 MAIN EXPERIMENTATION

Experiments are performed on a 4- axis Electronica Sprintcut-734 CNC Wire cut machine manufactured by Electronica India Limited, Pune (India) according to the BBD as illustrated in Table 4.8. Table 4.5 provides detail of parameters and their values/ range/type that are kept at as fixed during main experimentation. A rectangular plate of pure titanium with 148mm x 148mm x 26mm size is taken as work piece. The plate is fixed on the machine table and machine setting is done as discussed in section 4.4.1. A 10mm x 10mm rectangular cut is taken on the work piece. Figure 4.12 shows path followed by wire. Wire enters the work piece at point O (5, 0). It moves along OABCDO and exits the work piece from O (5, 0). CNC code for cutting is generated using ELAPT software supplied by the manufacturer. It is important to mention that wire offset is set at zero during cutting.

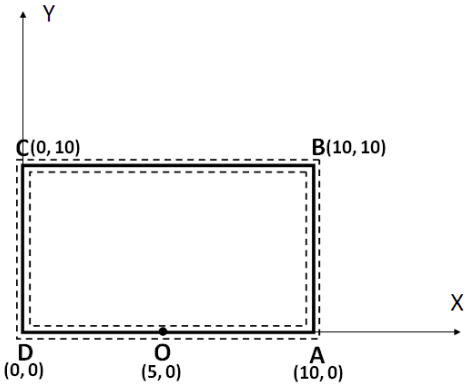

Figure 4.12 Work piece Profile

In order to compute average cutting rate, instantaneous cutting speed is noted at a distance of 2.5mm, 5mm and 7.5mm from the initiation of cut along a particular axis along AB, BC and CD. Thus, on side DA, it is noted at a distance of 2.5mm and 7.5mm from D. This is done to ensure that readings are noted only when cutting is stabilized properly. Average of the readings obtained so provide average cutting rate. Surface roughness of the piece that is cut from the work piece plate is measured using portable Mitutoya Surface Roughness Tester SJ-301 as discussed in section 4.4.1. Six readings of surface roughness (R_a) perpendicular to direction of cut are taken along OABCDO and mean of these readings gives average surface roughness.

MRR determines economics of machining and rate of production. It is calculated using the following relation [Manna and Bhattacharya, 2006].

$$\text{MRR } (mm^3/min) = \text{Average machining rate} \times \text{thickness of plate} \times \text{width of cut} \quad (4.1)$$

Width of cut = (D-A)

D = Desired size of work piece = 10 mm, A = Actual size of the work piece obtained after cutting, which is measured using Mitutoya digital Vernier calliper with a least count of one micron. It is measured at two random places on sides AB, BC and CD and average of these six values represent actual size of work piece (A). Dimensional deviation is an important measure of performance, knowledge of which is very much essential to achieve a close dimensional control in WEDM. Dimensional Deviation is calculated using the following relation [Sarkar et al., 2006]:

$$\text{Dimensional deviation} = 0.5 \times (\text{width of cut}) \quad (4.2)$$

The profile traced by wire and the job are not same. The perpendicular distance between the actual profile and the profile traced by the wire is equal to half of the width of the cut. Thus, the actual job produced is either undersized or oversized depending upon the job is punch or die. In the present study, the job has been considered as a square punch. The dimensional deviation of square punch is equal to the half the width of the cut. The dimensional deviation is measured using a digimatic caliper (Mitutoyo) having least count 0.001mm. The overcut as shown in Figure 3.13 was determined as:

$$\text{Overcut } (\delta) = \text{dimensional deviation (DD)} - 0.5 \times \text{wire diameter (d)} \quad (4.3)$$

$$DD = 0.5(W_P - W_a)$$

Where, W_p = Programmed path, W_a = Actual job profile.

The term wire wear ratio is defined as loss of wire weight after machining. The wire wear ratio is calculated using by following method:

$$\omega_R = \omega_L/\omega i \quad (4.4)$$

Where, ω_R = Wire wear ratio, ω_L = Wire wear loss, ωi = Initial wire weight/unit length. The precision (Make SHIMADZU, Japan and model no. AUX220) balance with 0.001gram accuracy was used for the weight measurements. The average of three repeated measurements was taken to minimize the impact of measurement error. The initial wire was weighted as 6.293 gram for its 25 meter length. At the each end of experiment the 25meter length of used wire is weighted and the loss of the weight was calculated. The loss of wire weight is due to the erosion and crater formed on the surface of wire.

Surface crack density and recast layer thickness measurements were made by importing the SEM micrographs into Carl Zesis Axio-vision Rel.4.8 software. To observe the machined surfaces by taking micrographs of four sides at different magnifications from 500X to 3000X. Therefore, five SEM micrographs were taken on four sides of work sample. Further, knowing the length of crack, surface crack density and recast layer thickness is calculated by following formulae:

$$SCD_i = LC_i / Ai \quad (4.5)$$

Where,

SCD_i = Surface crack density

LC_i = Total length of crack (μm)

A_i = Unit area of micrograph (μm^2)

$$RCL_t = RCL_{Ai} / RC_{Li} \quad (4.6)$$

Where,

RCL_t = Recast layer thickness (μm)

RCL_{Ai} = Area of recast layer (μm^2)

RC_{Li} = Length of recast layer (μm)

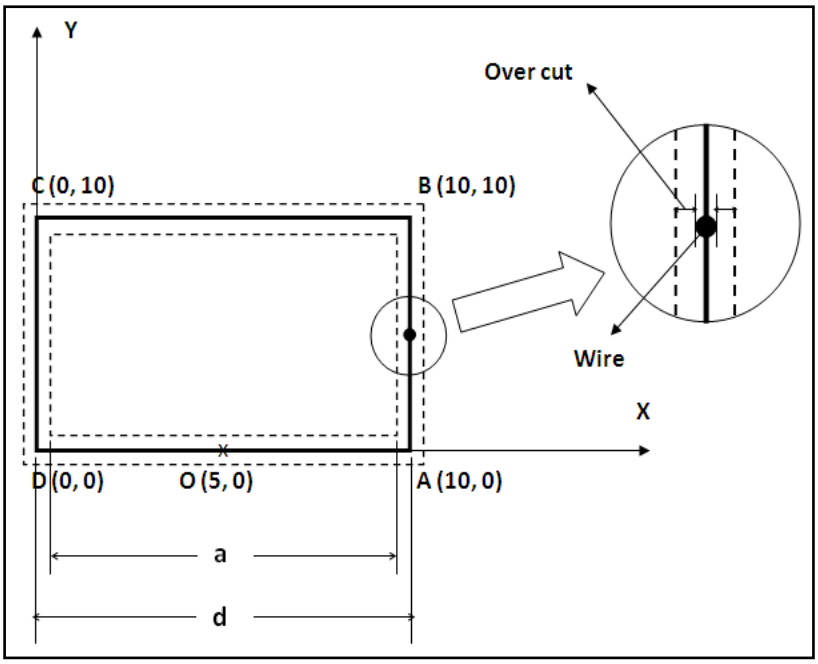

Figure 4.13 Overcut profile

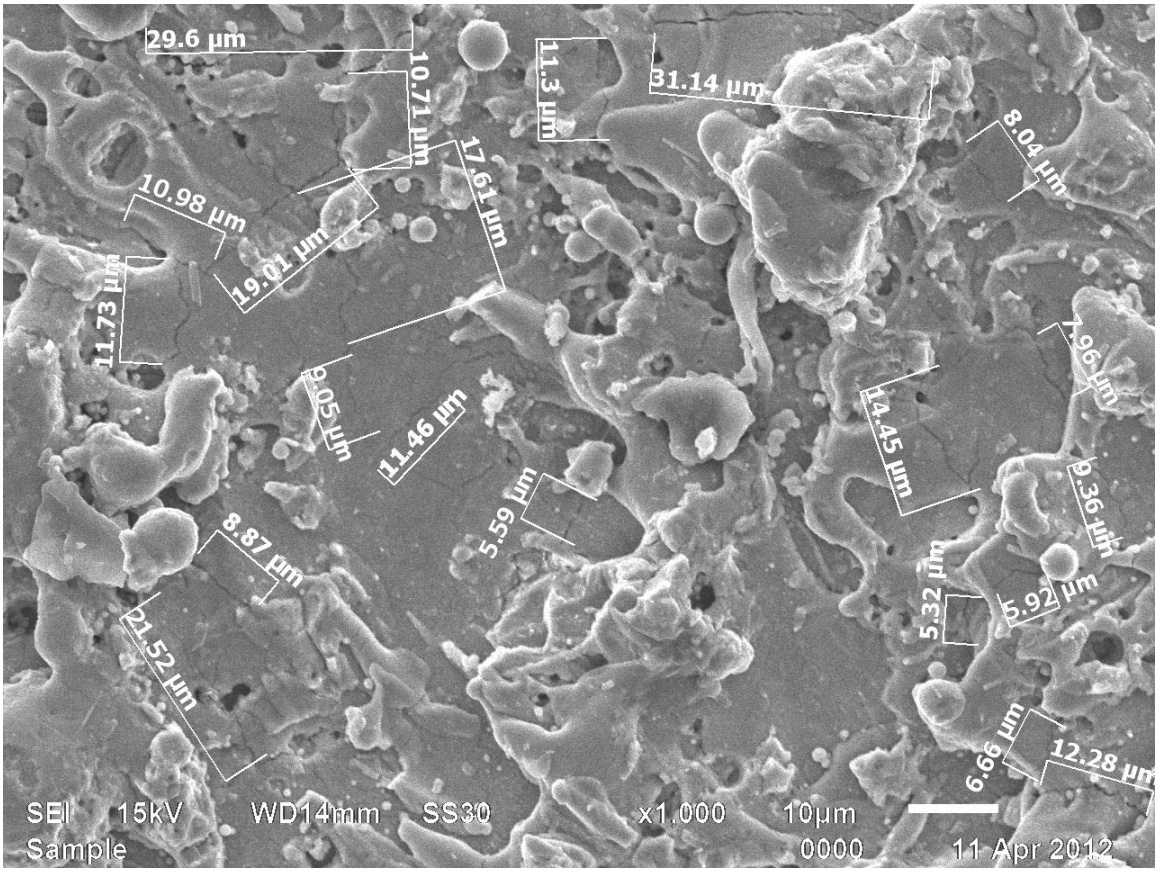

(a)

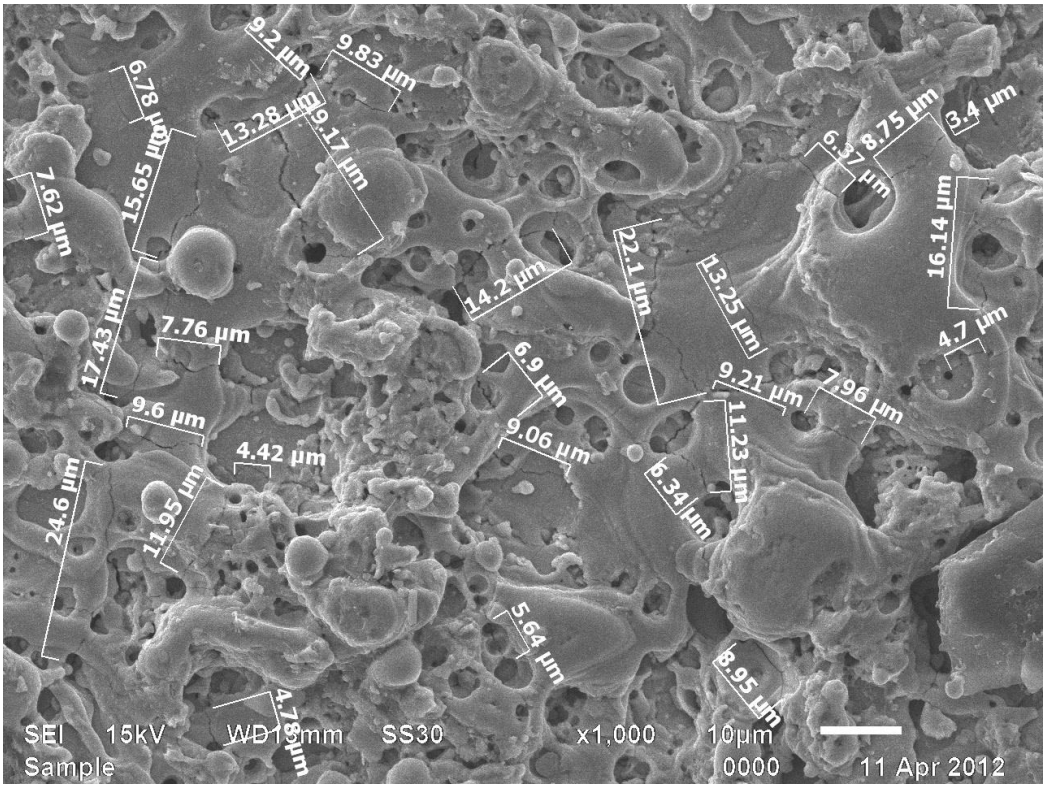

(b)

Figure 4.14 Demonstration of micro-cracks at different parametric condition (a) Exp. 4, LC_i = 187.70µm, NC_i = 20, SCD_i = 0.009µm/µm^2 (b) Exp. 29, LC_i = 157.57µm, NC_i = 18, SCD_i = 0.011µm/µm^2

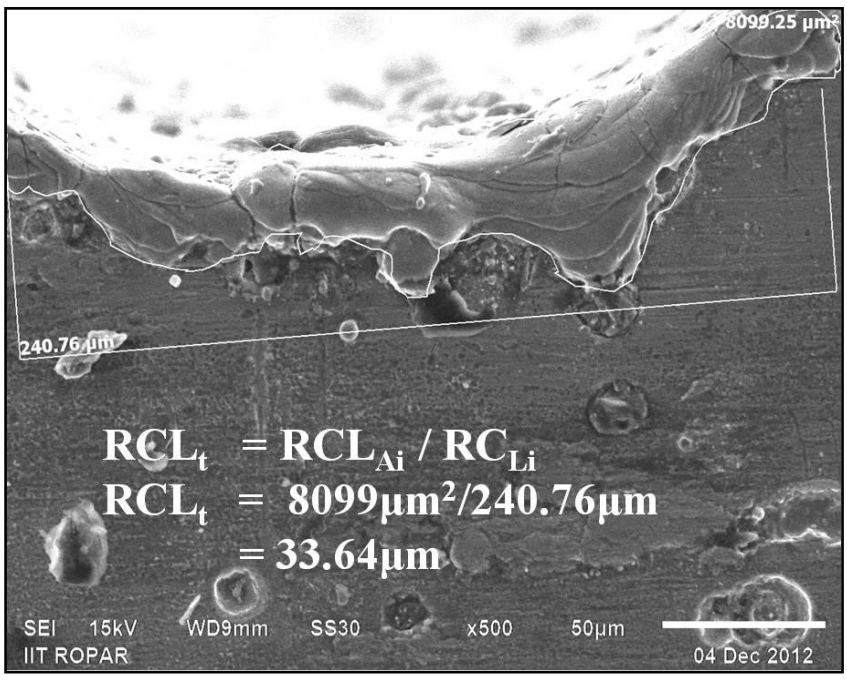

Figure 4.15 Demonstration of Recast Layer Thickness at Exp. No.52

The WEDM surface representing the assessment of length of crack, number of cracks and surface crack density as shown in Figure 4.14.Since it is not easy to compute the cracking in terms of a judgment of the width, length or the depth of crack, or even by the amount of cracking, this research defines a "surface crack size density", i.e. the total length of cracks (μm) in unit area (μm^2) to evaluate the severity of cracking. The unit area for all micrographs has been fixed and it will consider as 12400μm/μm^2. Due to the variable nature of the recast layer observed, an average must be taken. The average recast layer thickness was calculated by measuring the area of the recast material and dividing by the length of the recast layer. Area and length measurements were made by importing the micrographs into Axio-vision Rel.4.8 software. The evaluation of average thickness of recast layer is as shown in Figure 4.15.

Each time, an experiment is performed; a particular set of parameter combination is chosen and work piece is cut as per Figure 4.12. Table 4.9 and Table 4.10 summarize the results obtained for 54 experiments with one replication.

4.8 Experimental set-up

The work material in the form of square plate having dimensions 148 mm × 148 mm × 26 mm was taken for the experimentation work. Figure 4.16 (a-c) shows the machine tool, work material and wire path profile during machining. Figure 4.17 shows the complete job after WEDM.

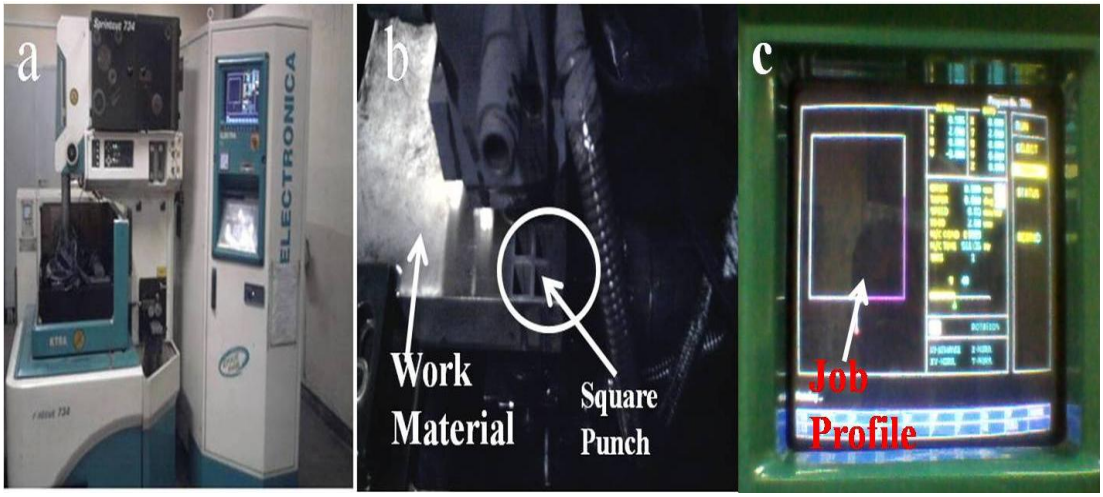

Figure 4.16 Job profile and experimental setup of WEDM machine tool. (a) 4-Axis WEDM CNC type, Electronica Sprintcut-734 machine tool (b) Square punch produced after WEDM (c) Job profile during machining

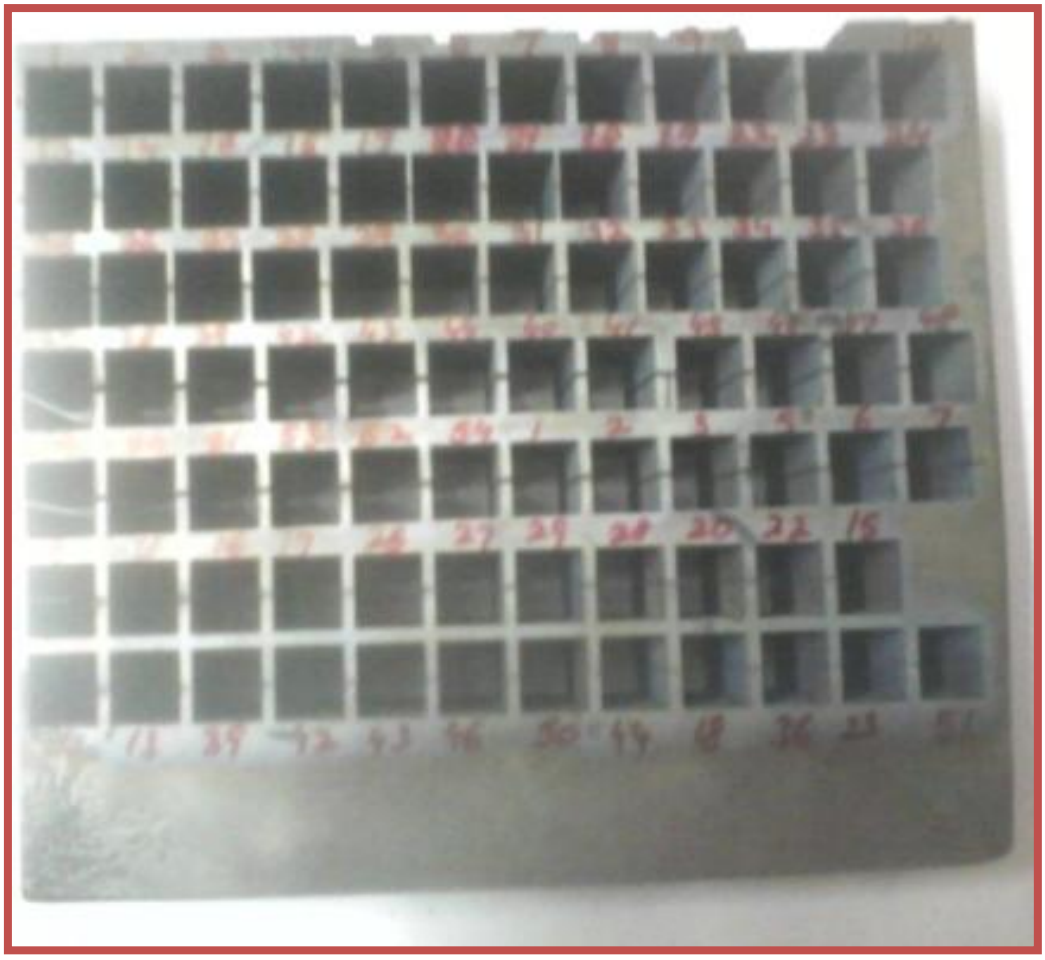

Figure 4.17 Complete job profile after WEDM

Table 4.8 Design matrix for main experimentation

Run Order	Standard Order	Control Factors					
		T_{on}	T_{off}	Ip	SV	WF	WT
1	7	-1	+1	0	+1	0	0
2	50	0	0	0	0	0	0
3	36	0	+1	0	0	+1	-1
4	51	0	0	0	0	0	0
5	29	-1	0	0	-1	+1	0
6	41	-1	0	-1	0	0	-1
7	40	0	+1	0	0	+1	+1
8	2	+1	-1	0	-1	0	0
9	23	0	0	-1	+1	0	+1
10	48	+1	0	+1	0	0	+1
11	12	0	+1	+1	0	-1	0
12	49	0	0	0	0	0	0
13	32	+1	0	0	+1	+1	0
14	30	+1	0	0	-1	+1	0
15	39	0	-1	0	0	+1	+1
16	25	-1	0	0	-1	-1	0
17	31	-1	0	-1	+1	+1	0
18	9	0	-1	-1	0	-1	0
19	4	+1	+1	0	-1	0	0
20	13	0	-1	-1	0	+1	0
21	45	-1	0	-1	0	0	+1
22	17	0	0	-1	-1	0	-1
23	19	0	0	-1	+1	0	-1
24	24	0	0	+1	+1	0	+1
25	8	+1	+1	0	+1	0	0
26	47	-1	0	+1	0	0	+1
27	38	0	+1	0	0	-1	+1
28	14	0	+1	-1	0	+1	0
29	46	+1	0	-1	0	0	+1
30	21	0	0	-1	-1	0	+1
31	43	-1	0	+1	0	0	-1
32	16	0	+1	+1	0	+1	0
33	6	+1	-1	0	+1	0	0
34	34	0	+1	0	0	-1	-1
35	44	+1	0	+1	0	0	-1
36	28	+1	0	0	+1	-1	0
37	20	0	0	+1	+1	0	-1
38	3	-1	+1	0	-1	0	0
39	27	-1	0	0	+1	-1	0
40	37	0	-1	0	0	-1	+1
41	42	+1	0	-1	0	0	-1
42	15	0	-1	+1	0	+1	0
43	5	-1	-1	0	+1	0	0
44	53	0	0	0	0	0	0
45	22	0	0	+1	-1	0	+1
46	52	0	0	0	0	0	0
47	35	0	-1	0	0	+1	-1
48	33	0	-1	0	0	-1	-1
49	54	0	0	0	0	0	0
50	26	+1	0	0	-1	-1	0
51	1	-1	-1	0	-1	0	0
52	10	0	+1	-1	0	-1	0
53	11	0	-1	+1	0	-1	0
54	18	0	0	+1	-1	0	-1

Legend: T_{on}- Pulse on time, T_{off}- Pulse off time, Ip- Peak current, SV- Spark gap voltage, WF- wire feed rate, WT- Wire tension

Table 4.9 Design matrix and output responses-I

Standard Run no.	Pulse on time T_{on} (µs)	Pulse off time T_{off} (µs)	Peak current Ip (A)	Spark gap voltage SV (Volt)	Wire Feed WF (m/min)	Wire Tension WT (grams)	Machining rate (mm/min)	Surface Roughness (µm)	Dimensional Deviation (µm)	Wire wear ratio (WWR)	MRR (mm^3/min)	Overcut (µm)
1	1.1	28	200	50	7	500	1.14	3.22	160	0.095	9.6	40
2	0.9	38	160	50	4	500	0.576	2.48	150	0.063	4.92	26
3	0.7	28	160	60	4	950	0.42	2.23	145	0.079	3.39	22
4	0.9	17	120	50	10	950	0.954	2.75	159	0.086	8.29	38
5	0.9	28	120	60	7	500	0.544	2.47	152	0.061	4.45	31
6	1.1	28	160	40	4	950	1.075	2.93	162	0.088	9.2	33
7	0.9	38	160	50	10	1400	0.586	2.48	150	0.063	4.77	25
8	0.9	28	160	50	7	950	0.695	2.65	152	0.080	5.19	30
9	0.9	17	160	50	4	500	1.014	2.81	160	0.089	8.81	33
10	1.1	28	160	40	10	950	1.075	2.94	160	0.088	8.59	33
11	1.1	38	160	40	7	950	0.995	2.91	160	0.087	8.3	32
12	1.1	28	160	60	4	950	0.809	2.83	159	0.079	7.03	35
13	0.9	17	160	50	10	500	1.012	2.79	160	0.076	8.19	32
14	0.9	28	160	50	7	950	0.573	2.61	150	0.064	4.67	30
15	0.7	28	120	50	7	500	0.406	2.49	145	0.048	3.28	25
16	0.9	28	160	50	7	950	0.697	2.68	152	0.082	5.51	31
17	0.9	28	120	60	7	1400	0.538	2.49	150	0.059	4.66	28
18	0.7	38	160	40	7	950	0.48	2.32	145	0.060	3.65	28
19	0.9	38	120	50	10	950	0.535	2.31	151	0.056	4.37	26
20	0.9	28	200	40	7	1400	0.825	2.89	152	0.079	6.72	38
21	0.9	28	200	60	7	500	0.773	2.69	152	0.072	6.67	32
22	0.9	38	200	50	10	950	0.792	2.57	153	0.074	6.54	35
23	0.9	28	120	40	7	1400	0.625	2.71	152	0.068	5.07	29
24	0.7	28	120	50	7	1400	0.425	2.51	145	0.054	3.3	24
25	0.9	38	200	50	4	950	0.799	2.56	155	0.078	7.07	35
26	1.1	28	160	60	10	950	0.81	2.82	153	0.081	6.77	37
27	1.1	28	120	50	7	500	0.83	2.77	158	0.074	7.1	33
28	0.7	28	160	40	10	950	0.521	2.35	150	0.085	4.27	30
29	0.7	28	200	50	7	500	0.535	2.48	150	0.083	4.49	31
30	0.7	17	160	40	7	950	0.858	2.70	153	0.089	6.9	33
31	0.7	28	200	50	7	1400	0.54	2.51	150	0.082	4.44	33
32	0.9	28	160	50	7	950	0.658	2.65	150	0.081	4.7	31
33	0.9	17	200	50	4	950	1.02	2.88	159	0.092	8.06	42
34	0.9	28	160	50	7	950	0.656	2.65	152	0.081	5.61	33
35	1.1	17	160	40	7	950	1.28	3.28	165	0.107	11.16	43
36	0.9	17	200	50	10	950	1.03	2.98	160	0.095	8.28	37
37	0.9	28	200	40	7	500	0.829	2.84	155	0.079	7.07	35
38	0.7	28	160	40	4	950	0.529	2.33	150	0.081	4.41	30
39	0.9	38	160	50	10	500	0.589	2.50	150	0.064	4.96	25
40	0.9	28	160	50	7	950	0.659	2.69	152	0.081	5.65	32
41	1.1	38	160	60	7	950	0.792	2.66	153	0.070	6.77	33
42	0.7	17	160	60	7	950	0.495	2.60	150	0.081	4.14	30
43	0.9	28	200	60	7	1400	0.778	2.68	155	0.072	6.57	32
44	0.9	17	120	50	4	950	0.959	2.75	155	0.086	7.61	35
45	0.7	28	160	60	10	950	0.429	2.28	145	0.079	3.75	25
46	1.1	28	120	50	7	1400	0.823	2.75	158	0.074	7.11	35
47	0.7	38	160	60	7	950	0.395	2.15	140	0.064	3.28	24
48	0.9	17	160	50	4	1400	0.981	2.85	159	0.088	8.15	31
49	0.9	28	120	40	7	500	0.635	2.78	158	0.068	5.36	31
50	1.1	17	160	60	7	950	1.00	3.00	159	0.085	8.45	40
51	0.9	38	120	50	4	950	0.541	2.29	150	0.060	4.55	25
52	1.1	28	200	50	7	1400	1.052	3.12	159	0.091	8.37	35
53	0.9	17	160	50	10	1400	0.962	2.82	155	0.088	7.53	37
54	0.9	38	160	50	4	1400	0.592	2.49	150	0.060	4.92	25

Table 4.10 Design matrix and output responses-II

Standard Run no.	Pulse on time T_{on} (µs)	Pulse off time T_{off} (µs)	Peak Current Ip (A)	Spark gap Voltage (Volt)	Wire Feed (m/min)	Wire Tension (gram)	Surface Crack Density SCD_i (µm/µm^2)	Recast Layer Thickness RCL_t (µm)
1	1.1	28	200	50	7	500	0.025	58.63
2	0.9	38	160	50	4	500	0.005	46.47
3	0.7	28	160	60	4	950	0.008	31.01
4	0.9	17	120	50	10	950	0.009	49.35
5	0.9	28	120	60	7	500	0.007	44.48
6	1.1	28	160	40	4	950	0.014	49.35
7	0.9	38	160	50	10	1400	0.005	44.42
8	0.9	28	160	50	7	950	0.007	47.32
9	0.9	17	160	50	4	500	0.010	46.37
10	1.1	28	160	40	10	950	0.016	53.63
11	1.1	38	160	40	7	950	0.014	49.80
12	1.1	28	160	60	4	950	0.015	46.54
13	0.9	17	160	50	10	500	0.009	47.25
14	0.9	28	160	50	7	950	0.007	45.24
15	0.7	28	120	50	7	500	0.006	33.28
16	0.9	28	160	50	7	950	0.007	44.52
17	0.9	28	120	60	7	1400	0.007	44.45
18	0.7	38	160	40	7	950	0.007	32.75
19	0.9	38	120	50	10	950	0.006	44.21
20	0.9	28	200	40	7	1400	0.021	49.41
21	0.9	28	200	60	7	500	0.019	47.88
22	0.9	38	200	50	10	950	0.017	44.31
23	0.9	28	120	40	7	1400	0.009	48.32
24	0.7	28	120	50	7	1400	0.007	30.36
25	0.9	38	200	50	4	950	0.020	44.94
26	1.1	28	160	60	10	950	0.012	49.60
27	1.1	28	120	50	7	500	0.009	43.36
28	0.7	28	160	40	10	950	0.008	39.13
29	0.7	28	200	50	7	500	0.011	41.19
30	0.7	17	160	40	7	950	0.013	41.31
31	0.7	28	200	50	7	1400	0.012	31.21
32	0.9	28	160	50	7	950	0.007	45.16
33	0.9	17	200	50	4	950	0.017	53.94
34	0.9	28	160	50	7	950	0.008	44.27
35	1.1	17	160	40	7	950	0.023	56.13
36	0.9	17	200	50	10	950	0.013	52.36
37	0.9	28	200	40	7	500	0.021	54.13
38	0.7	28	160	40	4	950	0.012	32.10
39	0.9	38	160	50	10	500	0.008	44.75
40	0.9	28	160	50	7	950	0.004	49.23
41	1.1	38	160	60	7	950	0.014	44.42
42	0.7	17	160	60	7	950	0.010	32.54
43	0.9	28	200	60	7	1400	0.020	46.21
44	0.9	17	120	50	4	950	0.015	42.64
45	0.7	28	160	60	10	950	0.008	33.72
46	1.1	28	120	50	7	1400	0.014	42.15
47	0.7	38	160	60	7	950	0.010	29.35
48	0.9	17	160	50	4	1400	0.014	44.36
49	0.9	28	120	40	7	500	0.013	42.39
50	1.1	17	160	60	7	950	0.019	46.56
51	0.9	38	120	50	4	950	0.004	43.98
52	1.1	28	200	50	7	1400	0.017	33.64
53	0.9	17	160	50	10	1400	0.012	46.28
54	0.9	38	160	50	4	1400	0.007	44.50

CHAPTER 5
RESULTS AND DISCUSSION

The previous focused on carrying out preliminary investigation to sort out the significant process parameters affecting the responses and to identify the range of these in order to isolate the levels of process parameters at which wire breakage occurs. These results are utilized in planning the main experimentation and the experiments are conducted as per the design matrix suggested by (Box Bhenken Design) as shown in Table 4.8. Table 4.9-4.10 indicated the different runs and the corresponding values of the responses obtained. This chapter concentrates on analysis of results of main experimentation, in order to identify individual as well as interaction effects of process parameters on various responses i.e. machining rate, surface roughness, material removal rate (MRR), overcut, dimensional deviation wire wear ratio, surface crack size density and recast layer thickness. Design Expert 6.0.7® software is used to check adequacy of fitted model and carry out regression and graphical analysis using ANOVA. Also the multi-response optimization of process parameters was done using desirability approach. The predictions from this model were validated by conducting experiments. Figure 5.1 shows the flow chart of the various steps involved in the analysis of results and optimization. These steps are discussed in the following sections and sub sections.

5.1 ASSESSMENT OF THE ADEQUACY OF MODEL FITTING

To assess for adequacy of the model, three different tests viz. sequential model sum of squares, lack of fit test and model summary statistics have been performed for machining rate, surface roughness, material removal rate (MRR), overcut, dimensional deviation wire wear ratio, surface crack size density and recast layer thickness responses. The *sequential sum of squares* shows contribution of the terms of increasing complexity to the model. This test selects the highest order polynomial where the terms are not aliased. Generally, a model with highest F-value and lower p- value is selected [Montgomery, 2002]. The *lack of fit test* is a measure of the failure of the model to represent data in the experimental domain at which points are not included in the regression and variations are observed in the model that cannot be accounted by random error [Montgomery, 2002]. For the model to be fit, this test should indicate insignificant lack of fit. A p-value, greater

than 0.05 nullifies the lack of fit of the model to the response data and the model can be utilized for prediction of response parameter for 95% of confidence interval.

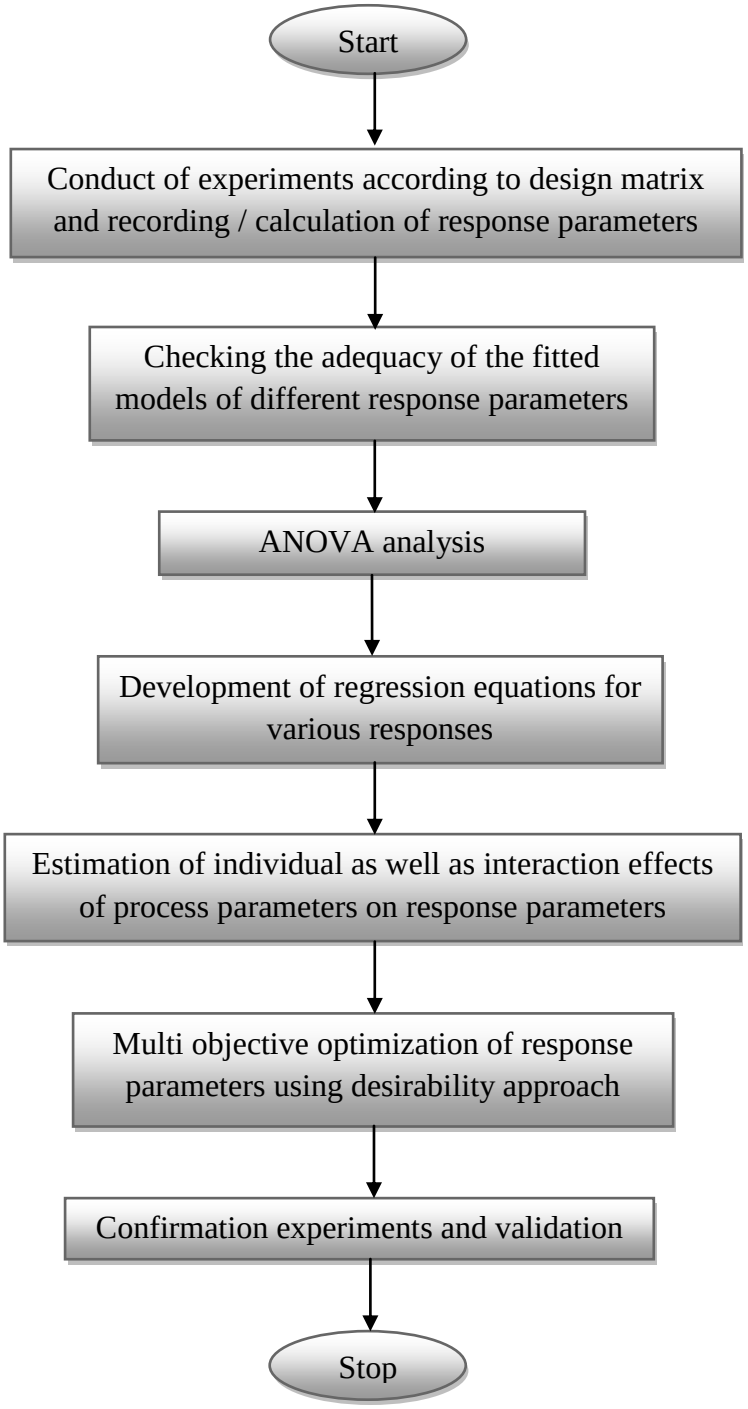

Figure 5.1 Methodology of the experimentation and analysis of results

Model summary statistics gives details about standard deviation, R^2, Predicted R^2 and Prediction error sum of squares (PRESS) of the model. Generally, a model with lesser standard deviation, R^2 closer to 1 and smaller value of PRESS is selected [Montgomery, 2002].

Tables 5.1-5.8 show the data related to sequential model sum of squares, lack of fit test and model summary statistics for machining rate, surface roughness, material removal rate (MRR), overcut, dimensional deviation, wire wear ratio, surface crack size density and recast layer thickness respectively. Quadratic models are recommended for machining rate, surface roughness, material removal rate (MRR), overcut, dimensional deviation wire wear ratio, surface crack density and recast layer thickness, by the Design Expert® software after performing above mentioned three tests.

5.2 ANALYSIS OF VARIANCE AND MATHEMATICAL MODELS OF RESPONSE CHARACTERISTICS

Analysis of variance is carried out to statistically analyze the results. ANOVA checks the values of R^2 as it explains the ratio of the variability explained by the model to the total variability inherent in the observation data of experiments. It also shows *adequate precision* which measures signal to noise ratios. A ratio greater than 4 indicates the model to be fit. Process variables having p-value < 0.05 are considered significant terms for the given response parameters. The backward elimination process eliminates the insignificant terms to adjust the fitted quadratic models and in the present work backward elimination process with α to exit=0.05 is used to eliminate the insignificant terms.

The hierarchy of different models is preserved to develop the mathematical models as it is observed that only hierarchical models are invariant under linear transformations [Piexto, 1987]. Principle of Hierarchy explains that although a factor as a main effect is found to be insignificant as regards to its contribution towards the response parameter, but; if its higher order terms viz. interaction or quadratic terms are significant, main effect will be included in the analysis as a term of significance.

The results and analysis for different responses from the application of ANOVA test are discussed in following sections.

Table 5.1 Adequacy checking of model of machining rate

Sequential Model Sum of Squares						
Source	**Sum of Squares**	**Degrees of Freedom**	**Mean Square**	**F-Value**	**Prob.> F (p-value)**	**Remarks**
Mean	29.84	1	29.84			
Linear	2.34	6	0.39	59.56	< 0.0001	
2FI	0.057	15	0.003807	0.49	0.9303	
Quadratic	0.17	6	0.028	9.16	< 0.0001	Suggested
Cubic	0.064	18	0.003555	1.73	0.2178	
Residual	0.016	8	0.002057			
Total	32.49	54	0.60			
Lack of Fit Tests						
Source	**Sum of Squares**	**Degrees of Freedom**	**Mean Square**	**F-Value**	**Prob.> F (p-value)**	**Remarks**
Linear	0.30	42	0.007084	3.51	0.0814	
2FI	0.24	27	0.008905	4.41	0.0524	
Quadratic	0.070	21	0.003350	1.66	0.3019	Suggested
Cubic	0.006355	3	0.002118	1.05	0.4478	
Pure Error	0.010	5	0.002021			
Model Summary Statistics						
Source	**Standard Deviation**	**R-Squared**	**Adjusted R-Squared**	**Predicted R-Squared**	**PRESS**	**Remarks**
Linear	0.081	0.8838	0.8689	0.8484	0.40	
2FI	0.088	0.9053	0.8432	0.7292	0.72	
Quadratic	0.056	0.9696	0.9380	0.8557	0.38	Suggested
Cubic	0.045	0.9938	0.9588	0.3798	1.64	

Table 5.2 Adequacy checking of model of material removal rate (MRR)

Sequential Model Sum of Squares						
Source	**Sum of Squares**	**Degrees of Freedom**	**Mean Square**	**F-Value**	**Prob.> F (p-value)**	**Remarks**
Mean	2049.43	1	2049.43			
Linear	166.21	6	27.70	51.85	< 0.0001	
2FI	5.91	15	0.39	0.66	0.8049	
Quadratic	13.24	6	2.21	9.64	< 0.0001	Suggested
Cubic	4.32	18	0.24	1.18	0.4263	
Residual	1.63	8	0.20			
Total	2240.76	54	41.50			
Lack of Fit Tests						
Source	**Sum of Squares**	**Degrees of Freedom**	**Mean Square**	**F-Value**	**Prob.> F (p-value)**	**Remarks**
Linear	24.12	42	0.57	2.89	0.1184	
2FI	18.20	27	0.67	3.39	0.0886	
Quadratic	4.96	21	0.24	1.19	0.4652	Suggested
Cubic	0.64	3	0.21	1.07	0.4416	
Pure Error	0.99	5	0.20			
Model Summary Statistics						
Source	**Standard Deviation**	**R-Squared**	**Adjusted R-Squared**	**Predicted R-Squared**	**PRESS**	**Remarks**
Linear	0.73	0.8688	0.8520	0.8318	32.19	
2FI	0.77	0.8997	0.8338	0.7378	50.16	
Quadratic	0.48	0.9689	0.9366	0.8571	27.34	Suggested
Cubic	0.45	0.9915	0.9435	0.1406	164.42	

Table 5.3 Adequacy checking of model of surface roughness

Sequential Model Sum of Squares						
Source	**Sum of Squares**	**Degrees of Freedom**	**Mean Square**	**F-Value**	**Prob.> F (p-value)**	**Remarks**
Mean	383.84	1	383.84			
Linear	2.89	16	0.48	82.17	< 0.0001	
2FI	0.11	15	0.007183	1.37	0.2227	
Quadratic	0.11	6	0.018	7.75	< 0.0001	Suggested
Cubic	0.051	18	0.002832	2.42	0.1019	
Residual	0.009362	8	0.001170			
Total	387.01	54	7.17			
Lack of Fit Tests						
Source	**Sum of Squares**	**Degrees of Freedom**	**Mean Square**	**F-Value**	**Prob.> F (p-value)**	**Remarks**
Linear	0.27	42	0.006476	8.20	0.0133	
2FI	0.16	27	0.006084	7.70	0.0158	
Quadratic	0.056	21	0.002685	3.40	0.0893	Suggested
Cubic	0.005412	3	0.001804	2.28	0.1965	
Pure Error	0.003950	5	0.00079			
Model Summary Statistics						
Source	**Standard Deviation**	**R-Squared**	**Adjusted R-Squared**	**Predicted R-Squared**	**PRESS**	**Remarks**
Linear	0.077	0.9130	0.9019	0.8818	0.37	
2FI	0.073	0.9469	0.9121	0.8242	0.56	
Quadratic	0.048	0.9810	0.9612	0.9053	0.30	Suggested
Cubic	0.034	0.9970	0.9804	0.5612	1.39	

Table 5.4 Adequacy checking of model of dimensional deviation

Sequential Model Sum of Squares						
Source	**Sum of Squares**	**Degrees of Freedom**	**Mean Square**	**F-Value**	**Prob.> F (p-value)**	**Remarks**
Mean	0.000001271	1	0.000001271			
Linear	1251.33	6	208.56	52.22	< 0.0001	
2FI	60.38	15	4.03	1.01	0.4684	
Quadratic	61.45	6	10.24	4.04	0.0054	Suggested
Cubic	47.67	18	2.65	1.16	0.4339	
Residual	18.21	8	2.28			
Total	0.000001272	54	23560.48			
Lack of Fit Tests						
Source	**Sum of Squares**	**Degrees of Freedom**	**Mean Square**	**F-Value**	**Prob.> F (p-value)**	**Remarks**
Linear	182.37	42	4.34	4.07	0.0603	
2FI	122.00	27	4.52	4.24	0.0569	
Quadratic	60.54	21	2.88	2.70	0.1366	Suggested
Cubic	12.87	3	4.29	4.02	0.0841	
Pure Error	5.33	5	1.07			
Model Summary Statistics						
Source	**Standard Deviation**	**R-Squared**	**Adjusted R-Squared**	**Predicted R-Squared**	**PRESS**	**Remarks**
Linear	2.00	0.8696	0.8529	0.8292	245.75	
2FI	1.99	0.9115	0.8535	0.7517	357.37	
Quadratic	1.59	0.9542	0.9067	0.7749	323.98	Suggested
Cubic	1.51	0.9873	0.9162	1.2958	3303.68	

Table 5.5 Adequacy checking of model of overcut

Sequential Model Sum of Squares						
Source	**Sum of Squares**	**Degrees of Freedom**	**Mean Square**	**F-Value**	**Prob.> F (p-value)**	**Remarks**
Mean	54403.63	1	54403.63			
Linear	927.88	6	154.65	24.51	< 0.0001	
2FI	109.31	15	7.29	1.25	0.2908	
Quadratic	118.41	6	19.74	7.46	0.0001	Suggested
Cubic	35.62	18	1.98	0.48	0.9080	
Residual	33.15	8	4.14			
Total	55628.00	54	1030.15			
Lack of Fit Tests						
Source	**Sum of Squares**	**Degrees of Freedom**	**Mean Square**	**F-Value**	**Prob.> F (p-value)**	**Remarks**
Linear	289.66	42	6.90	5.05	0.0386	
2FI	180.35	27	6.68	4.89	0.0423	
Quadratic	61.94	21	2.95	2.16	0.2010	Suggested
Cubic	26.31	3	8.77	6.42	0.0363	
Pure Error	6.83	5	1.37			
Model Summary Statistics						
Source	**Standard Deviation**	**R-Squared**	**Adjusted R-Squared**	**Predicted R-Squared**	**PRESS**	**Remarks**
Linear	2.51	0.7578	0.7269	0.6722	401.32	
2FI	2.42	0.8471	0.7468	0.5002	611.93	
Quadratic	1.63	0.9438	0.8855	0.7277	333.43	Suggested
Cubic	2.04	0.9729	0.8206	4.5096	6745.84	

Table 5.6 Adequacy checking of model of wire wear ratio

Sequential Model Sum of Squares						
Source	**Sum of Squares**	**Degrees of Freedom**	**Mean Square**	**F-Value**	**Prob.> F (p-value)**	**Remarks**
Mean	0.32	1	0.32			
Linear	0.005660	6	0.0009433	20.84	< 0.0001	
2FI	0.0003769	15	0.0000251	0.46	0.9443	
Quadratic	0.0008817	6	0.0001469	4.40	0.0034	Suggested
Cubic	0.0005211	18	0.0000289	0.67	0.7755	
Residual	0.0003480	8	0.0000434			
Total	0.33	54	0.006048			
Lack of Fit Tests						
Source	**Sum of Squares**	**Degrees of Freedom**	**Mean Square**	**F-Value**	**Prob.> F (p-value)**	**Remarks**
Linear	0.001885	42	0.00004488	0.92	0.6159	
2FI	0.001508	27	0.00005585	1.15	0.4857	
Quadratic	0.0006262	21	0.00002982	0.61	0.8039	Suggested
Cubic	0.0001051	3	0.00003504	0.72	0.5809	
Pure Error	0.0002428	5	0.00004857			
Model Summary Statistics						
Source	**Standard Deviation**	**R-Squared**	**Adjusted R-Squared**	**Predicted R-Squared**	**PRESS**	**Remarks**
Linear	0.006728	0.7268	0.6919	0.6381	0.002818	
2FI	0.007397	0.7752	0.6277	0.3165	0.005323	
Quadratic	0.005781	0.8884	0.7725	0.5350	0.003621	Suggested
Cubic	0.006595	0.9553	0.7040	2.5007	0.027	

Table 5.7 Adequacy checking of model of surface crack density

Sequential Model Sum of Squares						
Source	**Sum of Squares**	**Degrees of Freedom**	**Mean Square**	**F-Value**	**Prob.> F (p-value)**	**Remarks**
Mean	0.007397	1	0.007397			
Linear	0.0008696	6	0.0001449	11.59	< 0.0001	
2FI	0.0001251	15	0.000008342	0.58	0.8707	
Quadratic	0.0003374	6	0.00005624	11.69	< 0.0001	Suggested
Cubic	0.00009242	18	0.000005134	1.26	0.3868	
Residual	0.000009333	8	0.000001867		0.0790	
Total	0.008854	54	0.0001640			
Lack of Fit Tests						
Source	**Sum of Squares**	**Degrees of Freedom**	**Mean Square**	**F-Value**	**Prob.> F (p-value)**	**Remarks**
Linear	0.0005783	42	0.00001377	7.38	0.0168	
2FI	0.0004532	27	0.00001679	8.99	0.0111	
Quadratic	0.0001158	21	0.000005514	2.95	0.1162	Suggested
Cubic	0.00002337	3	0.000007792	4.17	0.0790	
Pure Error	0.000009333	5	0.000001867			
Model Summary Statistics						
Source	**Standard Deviation**	**R-Squared**	**Adjusted R-Squared**	**Predicted R-Squared**	**PRESS**	**Remarks**
Linear	0.003536	0.5967	0.5452	0.4863	0.0007486	
2FI	0.003802	0.6826	0.4743	0.1869	0.001185	
Quadratic	0.002194	0.9141	0.8250	0.5756	0.0006184	Suggested
Cubic	0.002022	0.9776	0.8513	3.1156	0.005997	

0.9321

Table 5.8 Adequacy checking of model of recast layer thickness

Sequential Model Sum of Squares						
Source	**Sum of Squares**	**Degrees of Freedom**	**Mean Square**	**F-Value**	**Prob.> F (p-value)**	**Remarks**
Mean	105600	1	105600			
Linear	1711.36	6	285.23	20.08	< 0.0001	
2FI	138.53	15	9.24	0.56	0.8843	
Quadratic	353.53	6	58.92	8.73	< 0.0001	Suggested
Cubic	154.27	18	8.57	3.22	0.0480	
Residual	18.63	8	3.73			
Total	107900	54	1998.79			
Lack of Fit Tests						
Source	**Sum of Squares**	**Degrees of Freedom**	**Mean Square**	**F-Value**	**Prob.> F (p-value)**	**Remarks**
Linear	648.99	42	15.45	4.15	0.0581	
2FI	510.46	27	18.91	5.07	0.0391	
Quadratic	156.93	21	7.47	2.01	0.2262	Suggested
Cubic	2.66	3	0.89	0.24	0.8665	
Pure Error	18.63	5	3.73			
Model Summary Statistics						
Source	**Standard Deviation**	**R-Squared**	**Adjusted R-Squared**	**Predicted R-Squared**	**PRESS**	**Remarks**
Linear	3.77	0.7194	0.6835	0.6225	898.12	
2FI	4.07	0.7776	0.6316	0.2847	1701.63	
Quadratic	2.60	0.9262	0.8496	0.6441	846.73	Suggested
Cubic	1.63	0.9911	0.9407	0.7024	708.09	

5.2.1 Analysis of variance and mathematical model for machining rate

As discussed in section 5.1, quadratic model for machining rate is recommended by Design expert 6.0.7® software. Table 5.9 shows ANOVA for the quadratic model at 95% confidence level. It indicates that F-value of model is 115.61 and coresponding p-value is less than 0.001. It implies that there is only a 0.01% chance that such large F- value of model can occur due to noise. Moreover, lack of fit of 0.450 implies that it is not significant relative to pure error. Thus, quadratic model is significant at 95% confidence level. The other important coefficient R^2, which is called determination coefficient, is defined as the ratio of the explained variation to the total variation and is a measure of the degree of fit. When R^2 approaches to unity, the response model fits better to the actual data and shows less difference between the predicted and actual values. The obtained values are predicted R^2 of 0.9384 is in reasonable agreement with the adjusted R^2 of 0.9511. Figure 5.2 shows normal probability plot of residuals for machining rate. It clearly shows that errors are normally distributed as most of the residuals are clustered around straight line. It is observed that, regression model is fairly well fitted with observed values. As adequate precision is 45.01 as shown in Table 5.9, thus the quadratic model can be used to navigate in the design space.

Based on the proposed second-order polynomial model, the effects of the process variables on the machining rate have been determined by using Design expert 6.0 software and the relevant data from Table 3.10. The mathematical relationship for correlating the machining rate and the considered process variables is obtained as follows:

$$\text{Machining rate} = 3.02557 + 0.43917 \times T_{on} - 0.10969 \times Toff - 0.010581 \times Ip - 0.019722 \times SV + 1.00203 \times T_{off}^2 + 1.79134 \times Ip^2 + 4.60937 \times T_{on} \times Ip + 1.125 \times T_{off} \times Ip + 4.22619 \times T_{off} \times SV \quad (5.1)$$

The quadratic functions of pulse off time and peak current have significant effects on machining rate and can be used to predict machining rate within the limits of control factors. All the sources having probability (Prob>F) less than 0.05, represent factors of statistical significance for the response under question. In addition to all of the individual factor effects, two-factor interactions are also found to be significant (Table 5.9). Figure 5.3 shows plot of experimental and predicted data for machining rate. It depicts that Equation 5.1 is adequate to represent the actual relationship between process parameters and responses [Taweel, 2009].

Table 5.9 ANOVA for response surface of reduced quadratic model of machining rate

Source	Sum of Squares	Degrees of Freedom	Mean Square	F- Value	Prob. > F (p-value)	Remarks	% Contribution
Model	2.54	9	0.28	115.61	<0.0001	significant	
A	1.33	1	1.33	544.58	<0.0001	significant	50.18
B	0.63	1	0.63	258.73	<0.0001	significant	23.77
C	0.22	1	0.22	90.15	<0.0001	significant	8.30
D	0.16	1	0.16	64.52	<0.0001	significant	6.03
B^2	0.16	1	0.16	64.01	<0.0001	significant	6.03
C^2	0.011	1	0.011	4.31	0.0438	significant	0.41
A×C	0.011	1	0.011	4.46	0.0405	significant	0.41
B×C	0.018	1	0.018	7.32	0.0097	significant	0.67
B×D	0.016	1	0.016	6.45	0.0147	significant	0.60
Residual	0.11	44	0.002441				
Lack of Fit	0.097	39	0.002495	1.23	0.4503	Not Significant	
Pure Error	0.010	5	0.002021				
Corrected Total	2.65	53					

Standard Deviation	0.049	R^2	0.9594
Mean	0.74	Adjusted R^2	0.9511
Coefficient of variation	6.65	Predicted R^2	0.9384
PRESS	0.16	Adequate Precision	45.018

Legend: A- Pulse on time, B- Pulse off time, C- Peak current, D- Spark gap set voltage, E-Wire feed rate, F- Wire tension

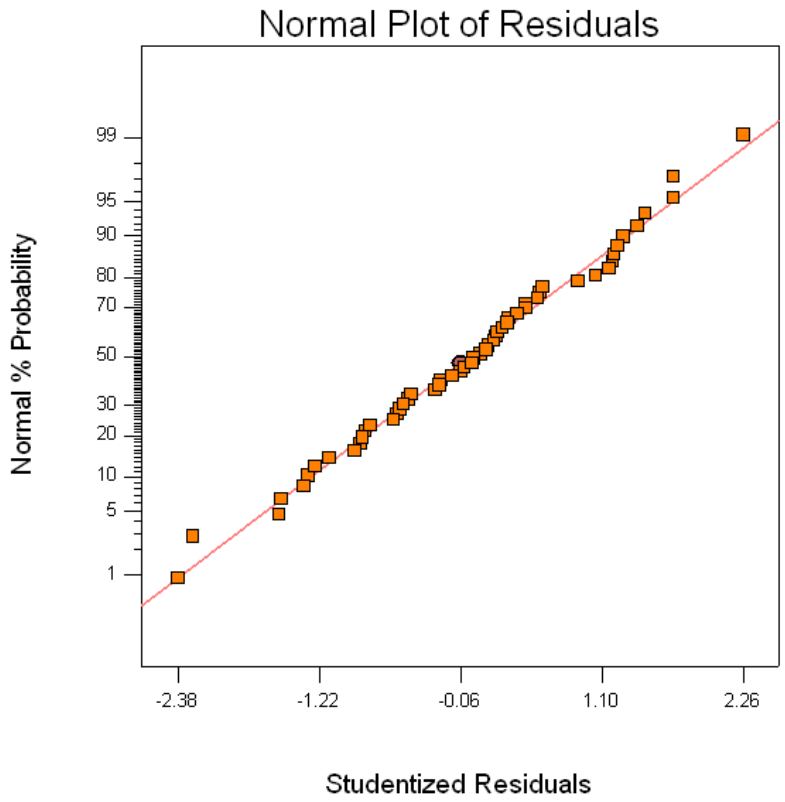

Figure 5.2 Normal probability plots of residuals for machining rate

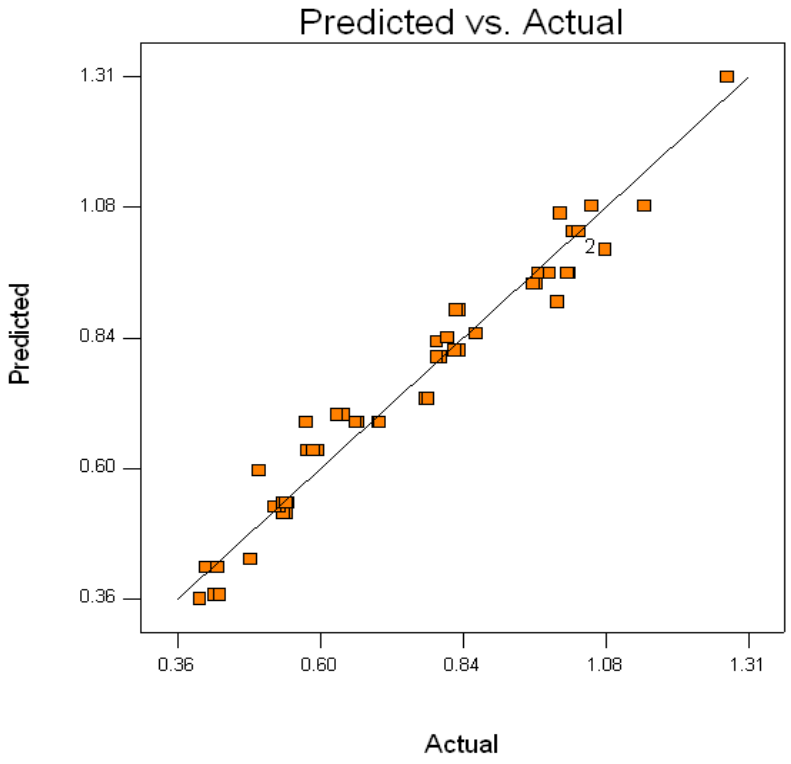

Figure 5.3 Plot of actual versus predicted of machining rate data

5.2.2 Analysis of variance and mathematical model for material removal rate (MRR)

Quadratic model for MRR is proposed by the Design expert 6.0® software. Adequacy of the model is checked using ANOVA as discussed in section 5.1 at 95 % confidence level and presented in Table 5.10. It indicates that F-value of the model is 97.91 and coresponding p-value is less than 0.0001. Thus, quadratic model is significant at 95% confidence level. The p-value of lack of fit is greater than 0.05. Thus, lack of fit is insignificant. Further, lack of fit value of 0.475 implies that it is not significant relative to pure error. Moreover, R^2 value of 0.9457 shows that 94.57% of the variation of MRR is attributed to control factors. This confirms that accuracy and general ability of polynomial model is good. Further, predicted R^2 of 0.9228 is in reasonable agreement with adjusted R^2 of 0.9360 and it indicates a high correlation between observed values and predicted values. Figure 5.4 shows normal probability plot of residuals for MRR. It clearly shows that errors are normally distributed as most of the residuals are clustered around the straight line. The plot of observed versus predicted values as presented in Figure 5.5 indicate that observed response are closer to the predicted values and model can define actual relationship between process parameters and output. Adequate precision value is 40.903 and it suggests that quadratic model can be used to navigate in the design space.

It was observed from the F and P values that the factors A (T_{on}) and B (T_{off}) are most significant for MRR. This can also be observed from the values of percent contribution obtained for each source, which quantifies the contribution of a parameter towards the variation in response (MRR). Almost 74% of the total variation in the response data could be contributed to factors A (T_{on}) and B (T_{off}). In this case A, B, C, D, BC, BD, B^2 and C^2 are significant model terms.

$$\text{Material removal rate (MRR)} = 22.08597 + 10.23958 \times T_{on} - 1.00948 \times T_{off} - 0.070586 \times Ip - 0.17842 \times SV + 0.00854025 \times T_{off}^2 + 0.000172852 \times Ip^2 + 0.00126488 \times T_{off} \times Ip + 0.00425 \times T_{off} \times SV \quad (5.2)$$

Table 5.10 ANOVA for response surface of reduced quadratic model of material removal rate (MRR)

Source	Sum of Squares	Degrees of Freedom	Mean Square	F-Value	Prob. > F (p-value)	Remarks	% Contribution
Model	180.93	8	22.62	97.91	<0.0001	significant	
A	100.66	1	100.66	435.74	<0.0001	significant	52.61
B	41.27	1	41.27	178.64	<0.0001	significant	21.57
C	14.62	1	14.62	63.28	<0.0001	significant	7.64
D	9.09	1	9.09	39.35	<0.0001	significant	4.75
B^2	11.35	1	11.35	49.12	<0.0001	significant	5.93
C^2	0.98	1	0.98	4.24	0.0453	significant	0.512
B×C	2.26	1	2.26	9.77	0.0031	significant	1.18
B×D	1.59	1	1.59	6.90	0.0118	significant	0.83
Residual	10.39	45	0.23				
Lack of Fit	9.40	40	0.24	1.18	0.4750	Not significant	
Pure Error	0.99	5	0.20				
Corrected Total	191.32	53					

Standard Deviation	0.48	R^2	0.9457
Mean	6.16	Adjusted R^2	0.9360
Cofficient of Variation	7.80	Predicted R^2	0.9228
PRESS	14.77	Adequate Precision	40.903

Legend: A- Pulse on time, B- Pulse off time, C- Peak current, D- Spark gap set voltage, E-Wire feed rate, F- Wire tension

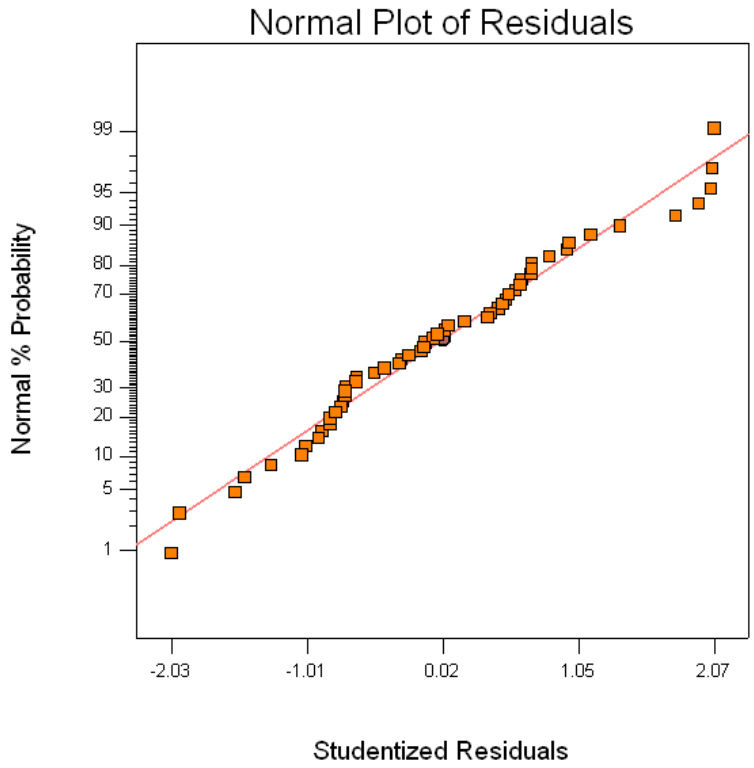

Figure 5.4 Normal probability plots of residuals for metal removal rate

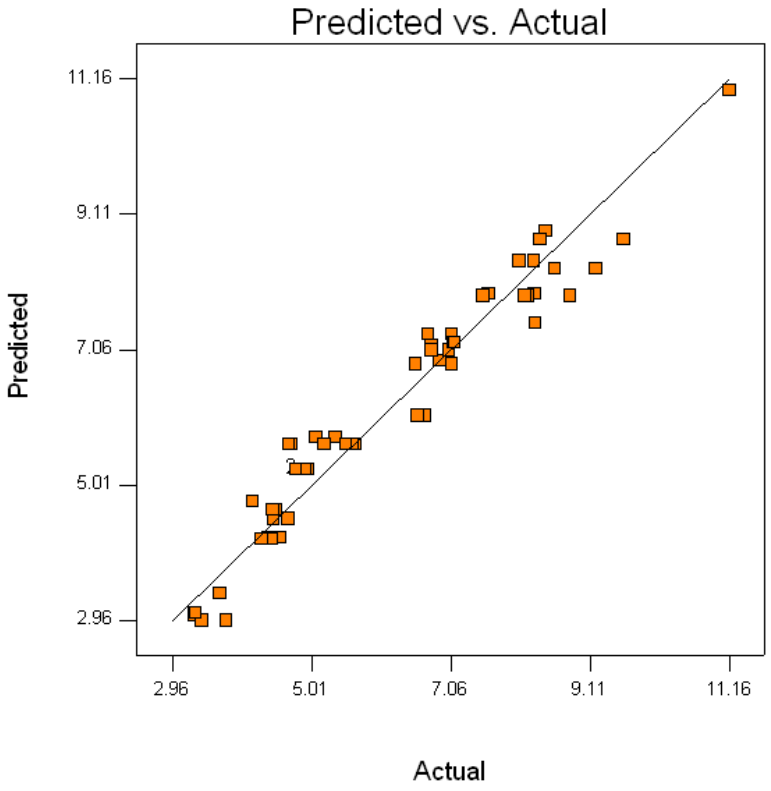

Figure 5.5 Plot of actual versus predicted of metal removal rate

5.2.3 Analysis of variance and mathematical model for surface roughness

Surface roughness is an important process criterion, which dictates the condition of the surface component which has to be machined. If the surface finish of the machined work material is the decisive factor due to its application requirements, then the work material must be machined with low material removal rate. Based on analysis of variance as shown in Table 5.11 the T_{on}, T_{off}, Ip, SV and one interaction (T_{on} × Ip) is significant to surface roughness. During preparation of model, non-significant terms are eliminated by backward elimination. The Values of 'Prob.> F' less than 0.05 indicates that model terms are significant at 95% confidence level. In addition to this normal plot of residuals and residual versus predicted plots has also been drawn as shown in Figure 5.6-5.7. The data is normally distributed. Most of residuals are falling on the straight line, implying that errors are normally distributed. It also indicates that regression model is fairly well fitted with observed values. The plot of predicted and observed values explains that analysis is adequate to define the true functional relationship between input process parameters and surface roughness. F-value of model is 145.26 and the associated p-value is lower than 0.05 and it indicates that the model is significant. Further, it implies that there is only 0.01% chance that a model F- value such large could occur due to noise. To fit the quadratic model for surface roughness appropriate, the non significant terms are eliminated by backward elimination. The *p*-value for lack of fit is 0.1173 suggesting that this model adequately fits the data. The "Pred R-Squared" of 0.9527 is in reasonable agreement with the " Adj R-Squared" of 0.9646.

From ANOVA results, it could be observed that factors A (Ton), B (Toff), C (peak current), D (spark gap voltage) are significant, in addition to one two-factor interaction (AC) and three higher order terms (B^2,E^2, F^2). As observed in the case of MRR, here also the factors A and B contribute almost 83% of the total variation in the response data, and thus are most significant. Following response surface equation represents the defining relation between surface roughness and process parameters. Following response surface equation defining relation between surface roughness and process parameters in actual factors is obtained.

$$\text{Surface Roughness} = 3.86021 - 0.76667 \times T_{on} - 0.035278 \times T_{off} - 0.00922396 \times Ip - 0.00866667 \times SV + 0.1247WF - 0.000365432 \times WT + 0.00031746 \times T_{off}^2 - 0.00875 \times WF^2 + 0.000000191358 \times WT^2 + 0.012969 \times Ton \times Ip \quad (5.3)$$

Table 5.11 ANOVA for response surface of reduced quadratic model of surface roughness

Source	Sum of Squares	Degrees of Freedom	Mean Square	F-Value	Prob. > F (p-value)	Remarks	% Contribution
Model	3.08	10	0.31	145.26	<0.0001	significant	
A	1.64	1	1.64	775.10	<0.0001	significant	55.0
B	0.84	1	0.84	396.22	<0.0001	significant	28.0
C	0.23	1	0.23	108.54	<0.0001	significant	8.0
D	0.18	1	0.18	85.03	<0.0001	significant	6.0
B^2	0.013	1	0.013	6.36	0.0155	significant	0.41
E^2	0.068	1	0.068	32.18	<0.0001	significant	2.15
F^2	0.019	1	0.019	8.90	0.0047	significant	0.6
A×C	0.086	1	0.086	40.62	<0.0001	significant	2.71
Residual	0.091	43	0.002120				
Lack of Fit	0.087	38	0.002295	2.91	0.1173	Not Significant	
Pure Error	0.003950	5	0.000790				
Corrected Total	3.17	53					
Standard Deviation		0.046		R^2		0.9712	
Mean		2.67		Adjusted R^2		0.9646	
Coefficient of variation		1.73		Predicted R^2		0.9527	
PRESS		0.15		Adequate Precision		51.529	

Legend: A- Pulse on time, B- Pulse off time, C- Peak current, D- Spark gap set voltage, E-Wire feed rate, F- Wire tension

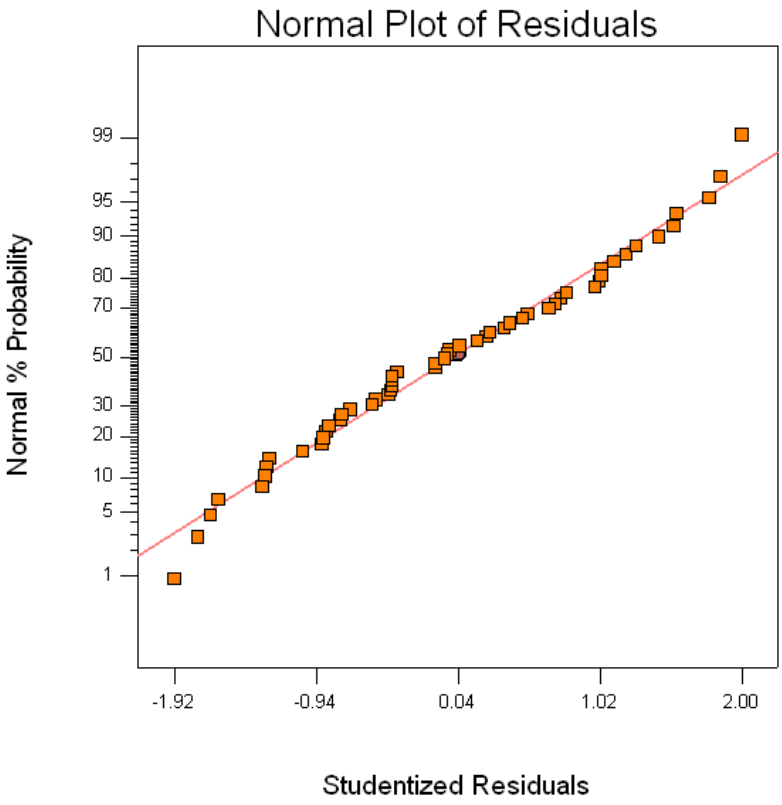

Figure 5.6 Normal probability plots of residuals for surface roughness

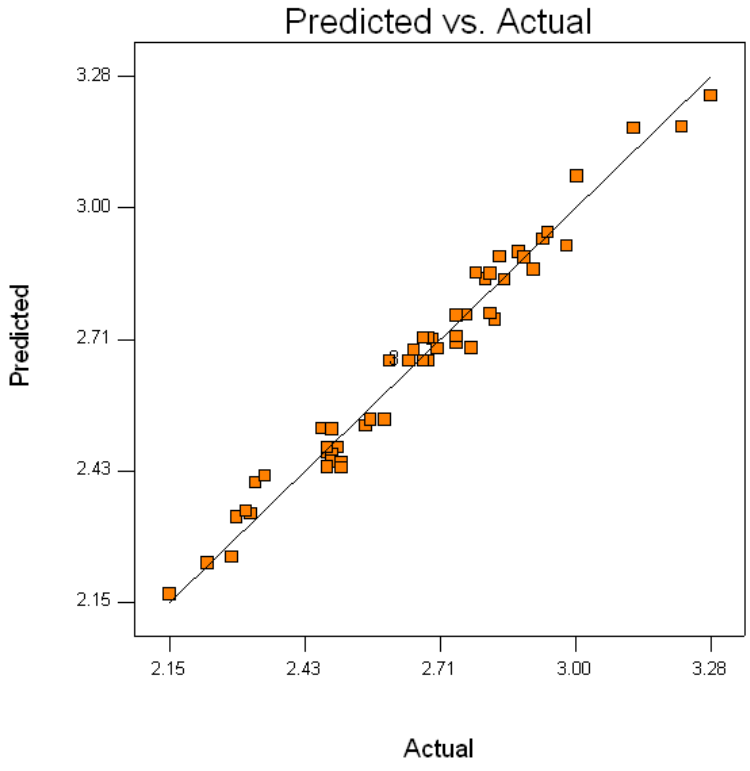

Figure 5.7 Plot of actual versus predicted of surface roughness

5.2.4 Analysis of variance and mathematical model for dimensional deviation

The term "dimensional deviation" is defined as the profile traced by wire and the job profile are not similar. The perpendicular distance between the actual profile and the profile traced by the wire is equal to half of the width of the cut [Sarkar et al., 2005]. Thus, the actual job produced is either undersized or oversized depending upon the job is punch or die. In the present study, the job has been considered as a square punch as shown in Figure 4.17. The dimensional deviation of square punch is equal to the half the width of the cut. The term "dimensional deviation" has been used as response parameter during rough cutting operation with zero wire offset. The dimensional deviation was measured using a digimatic caliper (Mitutoyo) having least count 0.001mm. Table 5.8 shows analysis of variance (ANOVA) for the quadratic model at 95% confidence level which is obtained by eliminating non significant terms by backward elimination. It shows that F-value of the model is 49.16 and coresponding p-value is less than 0.001, indicating that quadratic model is significant at 95% confidence level. Lack of fit of 0.1321 with p-value 2.72 implies that it is not significant relative to pure error. Moreover, predicted R^2 of 0.9196 is in reasonable agreement with adjusted R^2 of 0.9009, which indicates a high correlation between observed and predicted values.

Figure 5.8-5.9 shows normal probability plot of residuals for dimensional deviation. A check on the plot reveals that residuals are clustered near to straight line, which means that errors are normally distributed and regression model is fairly well fitted with observed values. Plot of observed responses and predicted values reveals that there is slight deviation of predicted values around the plot of observed response. The adequate precision is 25.323; it suggests that quadratic model can be used to navigate in the design space.

Table 5.12 reveals that main effects of T_{on}, T_{off}, Ip, SV; interaction effects between SV and WT are found to be statistically significant for dimensional deviation.

The regression equation for the dimensional deviation has been modeled as follows:

$$\text{Dimensional deviation} = 192.21845 + 28.75000 \times T_{on} - 0.97071 \times T_{off} - 0.23551 \times Ip - 0.46806 \times SV - 1.86700 \times WF - 0.015278 \times WT + 0.011372 \times T_{off^2} + 0.00082386 \times Ip^2 + 0.12542\ WF^2 + 0.000277778 \times SV \times WT \quad (5.4)$$

Table 5.12 ANOVA for response surface of reduced quadratic model of dimensional deviation

Source	Sum of Squares	Degrees of Freedom	Mean Square	F-Value	Prob. > F (p-value)	Remarks	% Contribution
Model	1323.30	10	132.33	49.16	<0.0001	significant	
A	793.50	1	793.50	294.80	<0.0001	significant	55.14
B	315.38	1	315.38	117.17	<0.0001	significant	21.91
C	30.38	1	30.38	11.28	0.0016	significant	2.11
D	100.04	1	100.04	37.17	<0.0001	significant	6.95
F	9.38	1	9.38	3.48	0.0688	significant	0.65
B^2	17.29	1	17.29	6.42	0.0150	significant	1.20
C^2	21.84	1	21.84	8.12	0.0067	significant	1.51
E^2	14.02	1	14.02	5.21	0.0275	significant	0.97
D×F	12.50	1	12.50	4.64	0.0368	significant	0.86
Residual	115.74	43	2.69				
Lack of Fit	110.41	38	2.91	2.72	0.1321	Not significant	
Pure Error	5.33	5	1.07				
Corrected Total	1439.04	53					

Standard Deviation	1.64	R^2	0.9196
Mean	153.41	Adjusted R^2	0.9009
Cofficient of Variation	1.07	Predicted R^2	0.8631
PRESS	196.99	Adequate Precision	30.836

Legend: A- Pulse on time, B- Pulse off time, C- Peak current, D- Spark gap set voltage, E-Wire feed rate, F- Wire tension

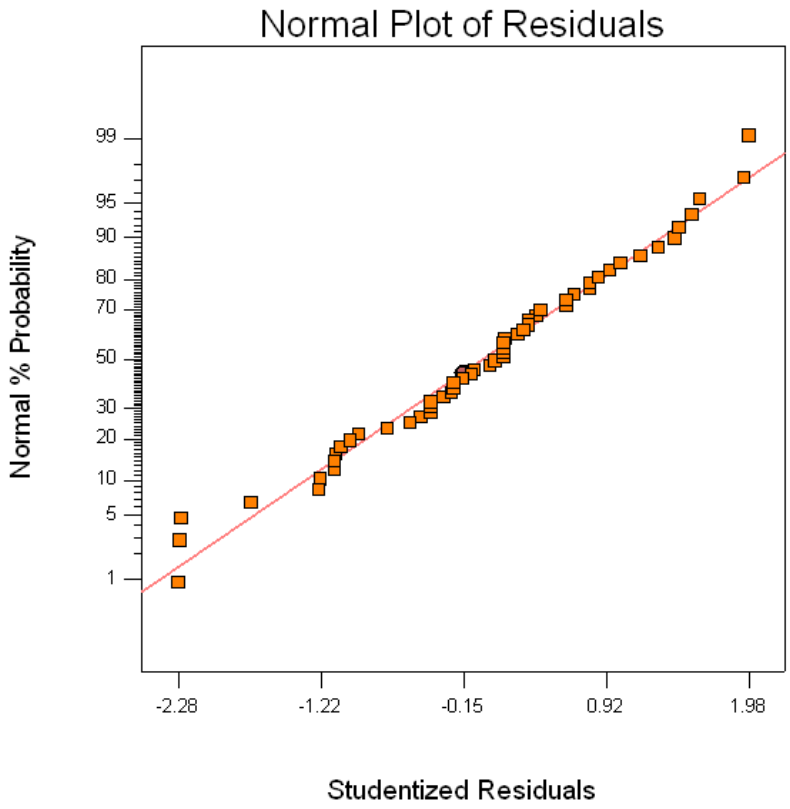

Figure 5.8 Normal probability plots of residuals for dimensional deviation

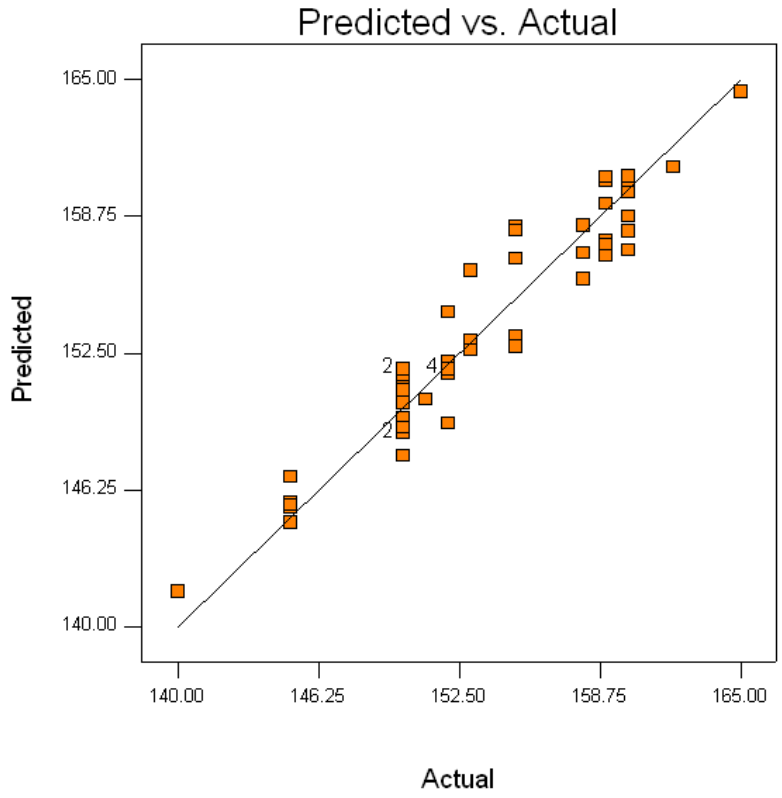

Figure 5.9 Plot of actual versus predicted of dimensional deviation

5.2.5 Analysis of variance and mathematical model for overcut

Adequacy of the model is checked using ANOVA as shown in Table 5.13. It indicates that F-value of the model is 30.71 and coresponding p-value is less than 0.0001. Thus, quadratic model is significant at 95% confidence level. The p-value of lack of fit is greater than 0.05. Thus, lack of fit is insignificant. Further, lack of fit value of 0.1719 implies that it is not significant relative to pure error. Moreover, R^2 value of 0.8999 shows that 90% of the variation of overcut is attributed to control factors. This confirms that accuracy and general ability of polynomial model is good. Further, predicted R^2 of 0.8191 is in reasonable agreement with adjusted R^2 of 0.8706 and it indicates a high correlation between observed values and predicted values. Figure 5.10 shows normal probability plot of residuals for overcut. It clearly shows that errors are normally distributed as most of the residuals are clustered around the straight line. The plot of observed versus predicted values as presented in Figure 5.11 indicate that observed response are closer to the predicted values and model can define actual relationship between process parameters and output. Adequate precision value is 21.808 and it suggests that quadratic model can be used to navigate in the design space.

Factors A and B (T_{on}, T_{off}) are found to be most significant with a contribution of 30.07% and 28.76% respectively in the variation of overcut data. The values of "Prob>F" less than 0.05, indicate that the model terms are significant. In this case A, B, C, D, B^2, C^2, E^2, F^2, AD, BC are significant model terms. The regression model for overcut is given as :

$$\text{Overcut} = 102.82449 - 17.91667 \times T_{on} - 1.55367 \times T_{off} - 0.56702 \times Ip - 0.78333 \times SV + 1.83519 \times WF + 0.020770 \times WT + 0.010355 \times T_{off^2} + 0.00165104 \times Ip^2 - 0.12315 \times WF^2 - 0.0000110288 \times WT^2 + 0.75000 \times T_{on} \times SV + 0.00386905 \times T_{off} \times Ip \qquad (5.5)$$

Table 5.13 ANOVA for response surface of reduced quadratic model of overcut

Source	Sum of Squares	Degrees of Freedom	Mean Square	F-Value	Prob. > F (p-value)	Remarks	% Contribution
Model	1101.81	12	91.82	30.71	<0.0001	significant	
A	368.17	1	368.17	123.16	<0.0001	significant	30.07
B	352.67	1	352.17	117.97	<0.0001	significant	28.76
C	176.04	1	176.04	58.89	<0.0001	significant	14.37
D	28.17	1	28.17	9.42	<0.0038	significant	2.30
B^2	14.22	1	14.22	4.76	0.0350	significant	1.16
C^2	76.13	1	76.13	25.47	<0.0001	significant	6.21
E^2	13.40	1	13.40	4.48	0.0403	significant	1.09
F^2	54.41	1	54.41	18.20	<0.0001	significant	4.44
A×D	36.00	1	36.00	12.04	0.0012	significant	2.94
B×C	21.13	1	21.13	7.07	0.0111	significant	1.72
Residual	122.56	41	2.99				
Lack of Fit	115.73	36	3.21		0.1719	not significant	
Pure Error	6.83	5	1.37				
Corrected Total	1224.37	53					

Standard Deviation	1.73	R^2	0.8999
Mean	31.74	Adjusted R^2	0.8706
Cofficient of Variation	5.45	Predicted R^2	0.8191
PRESS	221.51	Adequate Precision	21.808

Legend: A- Pulse on time, B- Pulse off time, C- Peak current, D- Spark gap set voltage, E-Wire feed rate, F- Wire tension

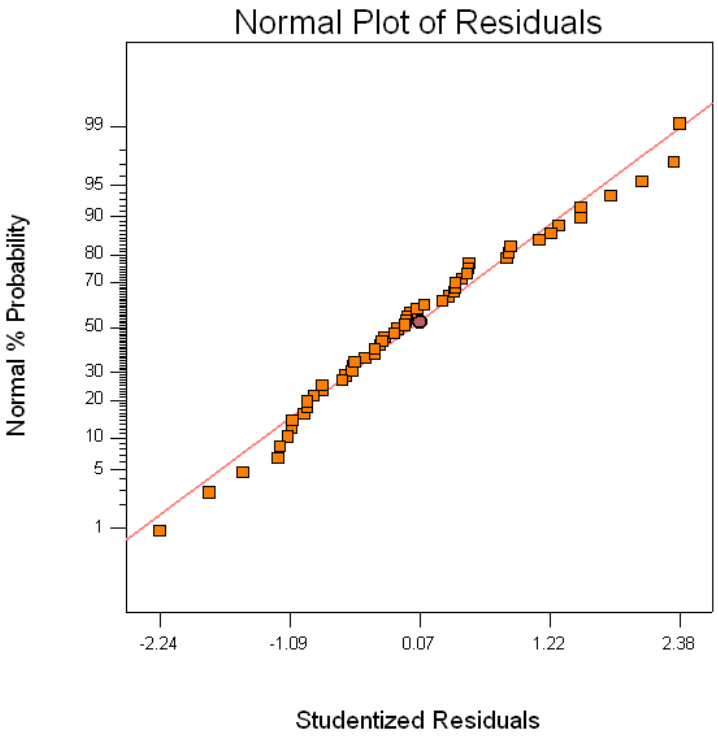

Figure 5.10 Normal probability plots of residuals for overcut

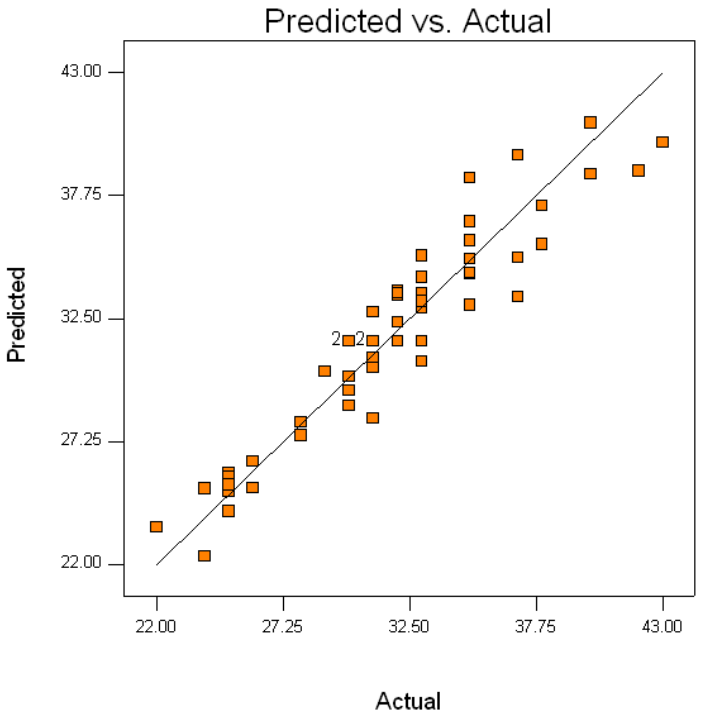

Figure 5.11 Plot of actual versus predicted of overcut

5.2.6 Analysis of variance and mathematical model for wire wear ratio

Based on ANOVA as shown in Table 5.14, factors T_{on}, T_{off}, I_P , SV and an interaction ($T_{on} \times SV$) are found to be the significant parameters at 95% level. The data is normally distributed. It is observed that all the experimental results are approximately very close to the predicted values (Figures 5.12-5.13). The model F-value 30.30 implies that model is significant. There is only a 0.01% chance that a "Model F-Value" this large could occur due to noise. The "Lack of fit F-value" of 0.50 implies that lack of fit is not significant relative to the pure error. The "Pred R-Squared" of 0.7755 is in reasonable agreement with the " Adj R-Squared" of 0.8156. "Adeq Precision" measures the signal to noise ratio. A ratio greater than 4 is desirable. The ratio is 21.504 indicates an adequate signal and it suggests that quadratic model can be used to navigate in the design space. The regression equation for the wire wear ratio was modeled as follows:

$$\text{Wire wear ratio (WWR)} = + 0.044666 - 0.049740 \times T_{on} - 0.00104365 \times T_{off} + 0.00020625 \times Ip + 0.000805208 \times SV + 0.00606636 \times WT + 0.080469 \times T_{on2} - 0.0000000316358 \times WT^2 - 0.00134375 \times T_{on} \times SV \quad (5.6)$$

Based on the results of ANOVA test, it could be observed that factor T_{off} is most significant, followed by peak current (IP). Together, these two factors contribute more than 57% towards the variation in wire wear ratio data. Two of the higher order terms (A^2, F^2) are also significant. Figure 5.13 indiacates that the predicted values have slight variation around the central line, however, except two data points, the plot could justify the ability of the model to predict the respponse with reasonable accuracy.

Table 5.14 ANOVA for response surface of reduced quadratic model of wire wear ratio

Source	Sum of Squares	Degrees of Freedom	Mean Square	F-Value	Prob. > F (p-value)	Remarks	% Contribution
Model	0.006568	8	0.000821	30.30	<0.0001	significant	
A	0.000748	1	0.000748	27.61	<0.0001	significant	9.60
B	0.002882	1	0.002882	106.36	<0.0001	significant	37.0
C	0.001634	1	0.001634	60.28	<0.0001	significant	20.98
D	0.000392	1	0.000392	14.47	<0.0004	significant	5.03
F	0.0000015	1	0.0000015	0.055	0.8151	Not significant	0.019
A^2	0.0001326	1	0.0001326	4.89	0.0321	significant	1.70
F^2	0.0005253	1	0.0005253	19.39	<0.0001	significant	6.74
A×D	0.0001156	1	0.0001156	4.26	0.0447	significant	1.48
Residual	0.001219	45	0.00002710				
Lack of Fit	0.0009765	40	0.00002441	0.50	0.8989	Not significant	
Pure Error	0.0002428	5	0.00004857				
Corrected Total	0.007788	53					

Standard Deviation	0.005205	R^2	0.8434
Mean	0.077	Adjusted R^2	0.8156
Cofficient of Variation	6.78	Predicted R^2	0.7753
PRESS	0.001750	Adequate Precision	21.504

Legend: A- Pulse on time, B- Pulse off time, C- Peak current, D- Spark gap set voltage, E-Wire feed rate, F- Wire tension

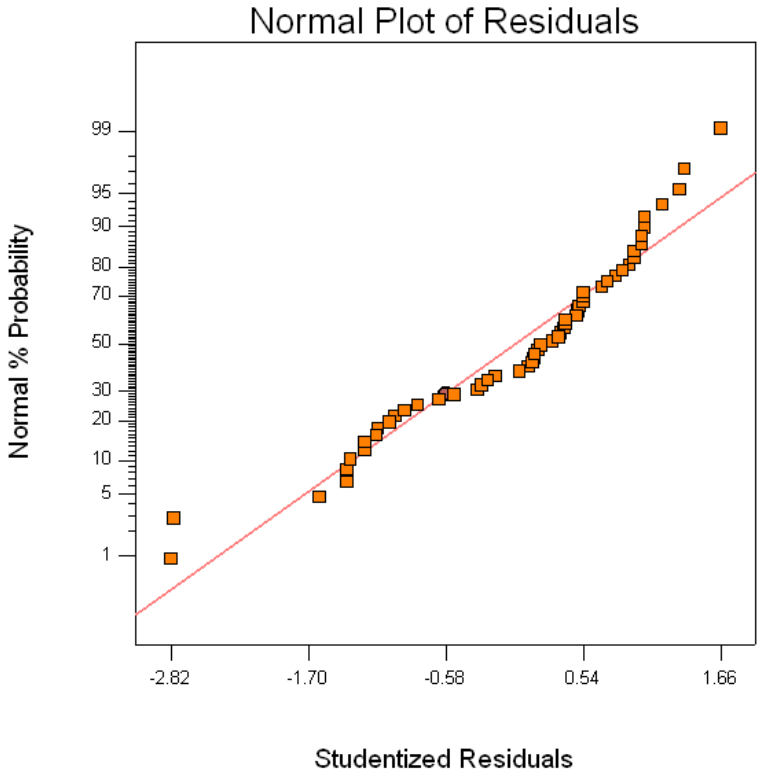

Figure 5.12 Normal probability plots of residuals for wire wear ratio

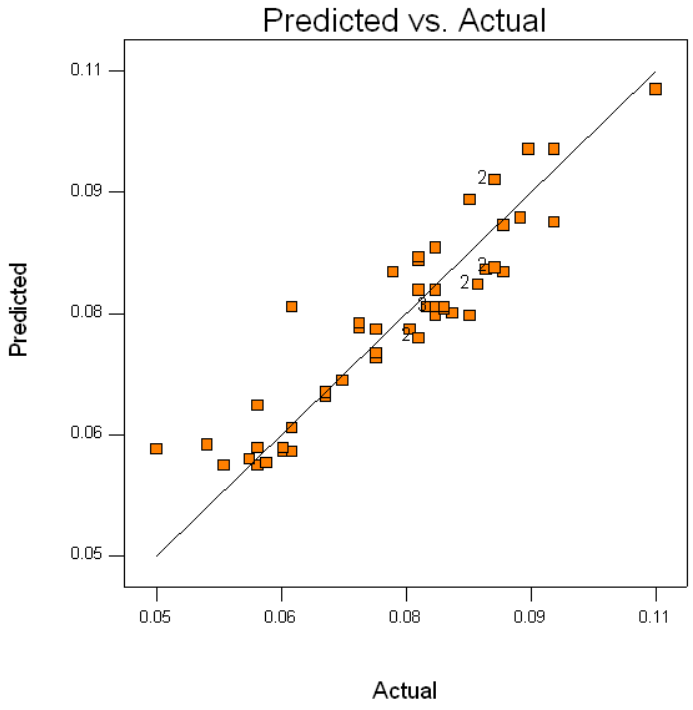

Figure 5.13 Plot of actual versus predicted of wire wear ratio

5.2.7 Analysis of variance and mathematical model for surface crack size density

In order to ensure a good model, test for significance of regression model, test for significance on individual model coefficients and test for lack of fit need to be performed. Adequacy of the model is checked using ANOVA as shown in Table 5.15. It indicates that F-value of the model is 26.14 and coresponding p-value is less than 0.0001. Thus, quadratic model is significant at 95% confidence level. The p-value of lack of fit is greater than 0.05. Thus, lack of fit is insignificant. Further, lack of fit value of 0.1514 implies that it is not significant relative to pure error. Moreover, R^2 value of 0.8738 signifies that 87.38% of the variation of surface crack density is attributed to control factors. This confirms that accuracy and general ability of polynomial model is good. Further, predicted R^2 of 0.7862 is in reasonable agreement with adjusted R^2 of 0.8408 and it indicates a high correlation between observed values and predicted values.

Figure 5.14 shows normal probability plot of residuals for surface crack density. It clearly shows that errors are normally distributed as most of the residuals are clustered around the straight line. The plot of observed versus predicted values as presented in Figure 5.15 indicate that observed response are closer to the predicted values and model can define actual relationship between process parameters and output. Adequate precision value is 17.555 and it suggests that quadratic model can be used to navigate in the design space. In this case A, B, C, D, A^2, B^2, C^2, D^2, BC and BD are significant model terms.

The regression equation for the surface crack density was modeled as follows:

$$\text{Surface Crack Density (SCDi)} = 0.22984 - 0.052708 \times T_{on} - 0.00271712 \times T_{off} - 0.000910417 \times Ip - 0.00396071 \times SV - 0.00025 \times WF + 0.038542 \times T_{on2} + 0.0000170068 \times T_{off}^2 + 0.00000265625 \times Ip^2 + 0.0000354167 \times SV^2 + 0.00000625 \times T_{off} \times Ip + 0.0000119048 \times T_{off} \times SV \quad (5.8)$$

A look at the ANOVA results concludes that factors peak current (IP) and pulse on time (Ton) are highly significant as more than 50% of the total variation is caused by these factors. The higher order term C^2 follows these factors in the ordr of significance, with 14% contribution to the variance. The crack formation was usually associated with the development of high thermal stresses which exceeding the fracture strength, as well as with plastic deformation. In addition, the formation of micro-cracks not only influenced by the setting of machining parameters but also depended on several materials properties.

Table 5.15 ANOVA for response surface of reduced quadratic model of surface crack density

Source	Sum of Squares	Degrees of Freedom	Mean Square	F-Value	Prob. > F (p-value)	Remarks	% Contribution
Model	0.001273	11	0.0001158	26.44	< 0.0001	significant	
A	0.0002667	1	0.0002667	60.91	< 0.0001	significant	18.30
B	0.00009204	1	0.00009204	21.02	< 0.0001	significant	6.31
C	0.000477	1	0.000477	108.96	< 0.0001	significant	32.73
D	0.00002017	1	0.00002017	4.61	0.0377	significant	1.38
E	0.0000135	1	0.0000135	3.08	0.0864	significant	0.92
A^2	0.00002535	1	0.00002535	5.79	0.0206	significant	2.80
B^2	0.00004091	1	0.00004091	9.34	0.0039	significant	2.80
C^2	0.0002102	1	0.0002102	48.01	< 0.0001	significant	14.42
D^2	0.0001338	1	0.0001338	30.56	< 0.0001	significant	9.18
B×C	0.00005513	1	0.00005513	12.59	0.0010	significant	3.78
B×D	0.0000125	1	0.0000125	2.85	0.0985	significant	0.85
Residual	0.0001839	42	0.000004378				
Lack of Fit	0.0001746	37	0.000004718	2.53	0.1514	Not significant	
Pure Error	0.000009333	5	0.000001867				
Corrected Total	0.001457	53					

Standard Deviation	0.002184	R^2	0.9560
Mean	0.012	Adjusted R^2	0.9265
Cofficient of Variation	18.66	Predicted R^2	0.7709
PRESS	0.0003338	Adequate Precision	17.555

Legend: A- Pulse on time, B- Pulse off time, C- Peak current, D- Spark gap set voltage, E-Wire feed rate, F- Wire tension

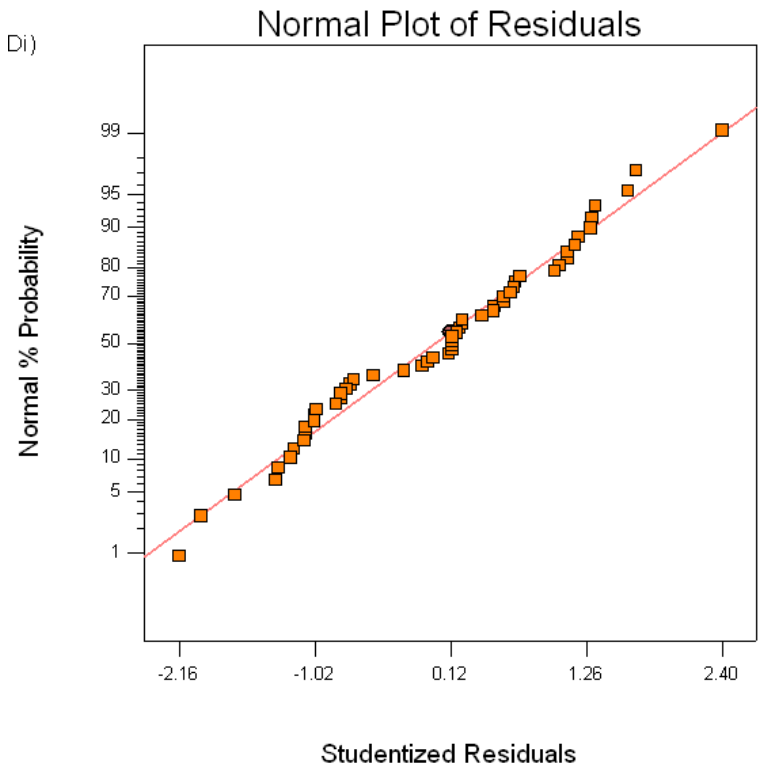

Figure 5.14 Normal probability plots of residuals for surface crack density

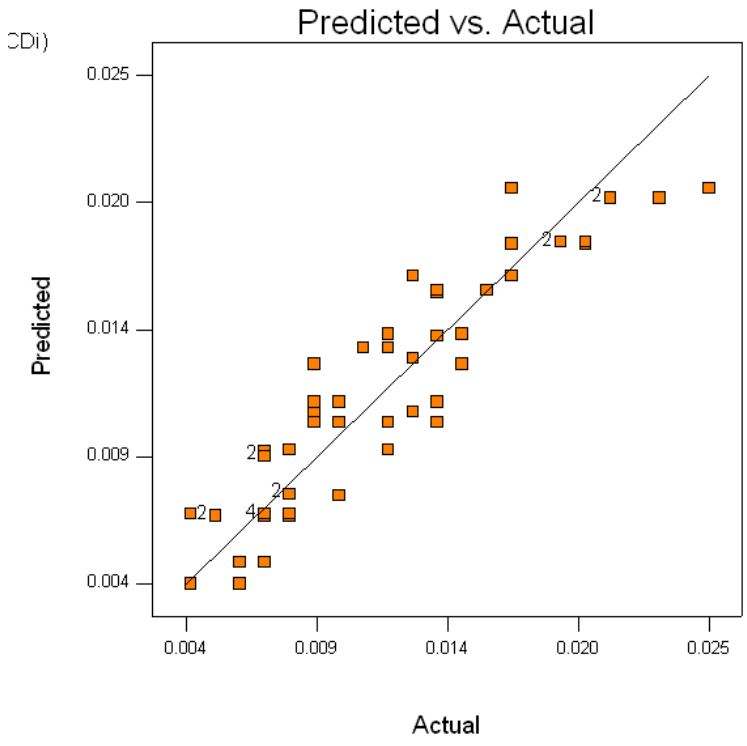

Figure 5.15 Plot of actual versus predicted of surface crack density

5.2.8 Analysis of variance and mathematical model for recast layer thickness

Adequacy of the model is checked using ANOVA as shown in Table 5.16. It indicates that F-value of the model is 41.09 and coresponding p-value is less than 0.0001. Thus, quadratic model is significant at 95% confidence level. The p-value of lack of fit is greater than 0.05. Thus, lack of fit is insignificant. Further, lack of fit value of 0.3148 implies that it is not significant relative to pure error. Moreover, R^2 value of 0.8937 shows that 89.37% of the variation of recast layer thickness is attributed to control factors. This confirms that accuracy and general ability of polynomial model is good. Further, predicted R^2 value (0.8328) is in reasonable agreement with adjusted R^2 (0.8719) and it indicates a high correlation between observed values and predicted values.

Figure 5.16 shows normal probability plot of residuals for recast layer thickness. It clearly shows that errors are normally distributed as most of the residuals are clustered around the straight line. The plot of observed versus predicted values (as presented in Figure 5.17) indicates that observed response values are closer to the predicted values and model can define actual relationship between process parameters and output. Adequate precision value is 25.125 and it suggests that quadratic model can be used to navigate in the design space. In this case A, B, C, D, E, F, A^2, BC and CF are significant model terms.

$$\text{Recast Layer Thickness } (RCL_t) = -114.93491 + 262.09750 \times T_{on} + 0.45163 \times T_{off} + 0.27118 \times Ip - 0.21537 \times SV + 0.31681 \times WF + 0.013802 \times WT - 125.18958 \times T_{on}^2 - 0.00394345 \times T_{off} \times Ip - 0.000106111 \times Ip \times WT \quad (5.9)$$

The recast layer was observed at the cross section of the wire cut EDM surface. The recast layer is defined as the material melted by electrical discharge and re-solidified on the work surface without being ejected nor removed by dielectric fluid [Lee, 2003]. It is very difficult to remove and its appearance is observed through a scanning electron microscope at different levels of magnification. The recast layer thickness was changed due to superficial hardening of the work material by the discharge heat of electrical spark. The intensity of spark depends on peak current, pulse on time and pulse off time.

Table 5.16 ANOVA for response surface of reduced quadratic model of recast layer thickness

Source	Sum of Squares	Degrees of Freedom	Mean Square	F-Value	Prob. > F (p-value)	Remarks	% Contribution
Model	2126.02	9	236.22	41.09	< 0.0001	significant	
A	1296.98	1	1296.98	225.60	< 0.0001	significant	18.30
B	85.09	1	85.09	14.80	0.0004	significant	6.31
C	147.26	1	147.26	25.61	< 0.0001	significant	32.73
D	111.33	1	111.33	19.36	< 0.0001	significant	1.38
E	21.68	1	21.68	3.77	0.0586	significant	0.92
F	49.02	1	49.02	8.53	0.0055	significant	2.80
A^2	334.35	1	334.35	58.16	< 0.0001	significant	2.80
B×C	21.95	1	21.95	3.82	0.0571	significant	3.78
C×F	58.37	1	58.37	10.15	0.0027	significant	0.85
Residual	252.96	44	5.75				
Lack of Fit	234.33	39	6.01	1.61	0.3148	Not significant	
Pure Error	18.63	5	3.73				
Corrected Total	2378.98	53					

Standard Deviation	2.54	R^2	0.9753
Mean	44.21	Adjusted R^2	0.9564
Cofficient of Variation	5.74	Predicted R^2	0.8210
PRESS	425.85	Adequate Precision	25.125

Legend: A- Pulse on time, B- Pulse off time, C- Peak current, D- Spark gap set voltage, E-Wire feed rate, F- Wire tension

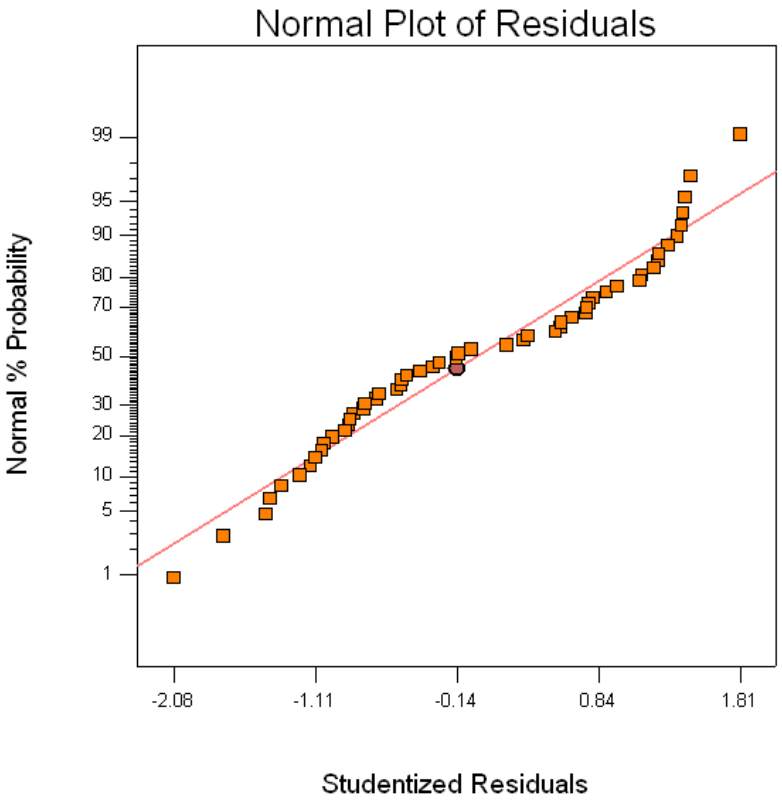

Figure 5.16 Normal probability plots of residuals for recast layer thickness

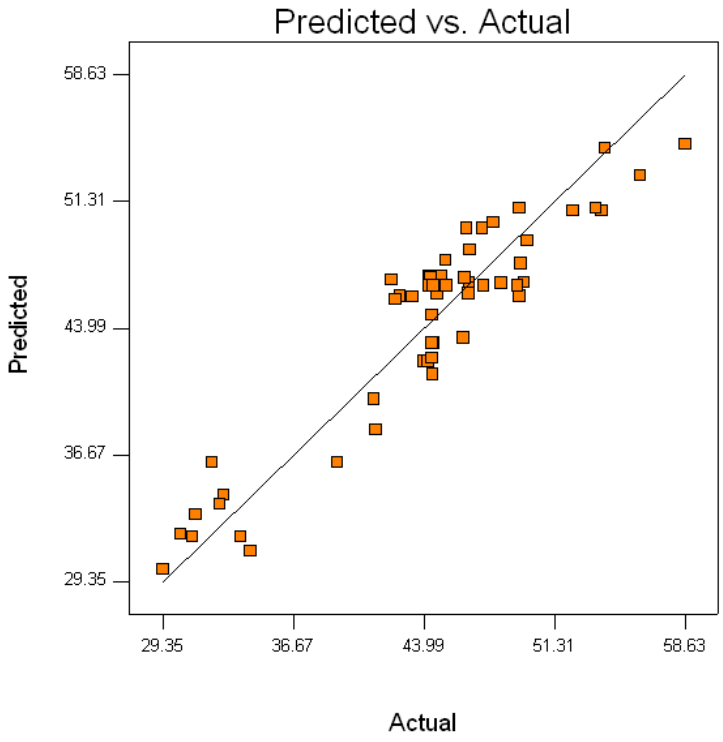

Figure 5.17 Plot of actual versus predicted of recast layer thickness

5.3 EFFECT OF PROCESS PARAMETERS ON RESPONSE CHARACTERISTICS

This section presents the effect of process parameters on response characteristics i.e. machining rate, surface roughness, material removal rate (MRR), overcut, dimensional deviation wire wear ratio, surface crack size density and recast layer thickness. It discusses individual as well as the interaction effects of various parameters on considered response characteristics. The effect of various parameters on different response characteristics is given in following sub sections.

5.3.1 Effect of process parameters on machining rate

Based on main effect plots as shown in Figures from 5.18 to 5.21, the machining rate was mainly affected by T_{on}, T_{off}, Ip and SV. Machining rate is increased significantly from 0.446 to 0.916 mm/min as pulse on time was increased by 0.7µs to 1.1µs. This is due to the fact that higher value of pulse on time increases the duration of discharge energy and it leads to rapid melting and evaporation of material. Thus, large chunks of material are removed and hence, increase in cutting rate is obtained. The present result is in line with the result obtained in earlier studies [Tarang et al. 1995; Sarkar et al. 2006]. As for peak current a slight increment of machining rate was occurred when peak current was increased from 120 to 200 A with value of 0.614 to 0.805mm/min. Increase in machining rate with peak current is due to higher discharge energy resulting into increased heat density within the work piece electrode gap. Higher heat accelerates the process of melting and evaporation of the material leading to faster erosion of material and hence, machining rate increases. This is in agreement with the findings of [Tarang et al. 1995], [Yan et al., 2005] and [Patil and Brahmakar, 2006].

Meanwhile, by decreasing the pulse off time and spark gap voltage, the machining rate significantly improved (assessed as 0.629 to 0.954 mm/min and 0.600 to 0.762 mm/min respectively). Increased duration of pulse off time decreases the number of discharges within a given period. Thus, less discharge energy is impinged on the work piece in a given time that reduces the rate of metal erosion, thereby reducing the cutting rate [Saha et al. 2009]. Since pulse on time and pulse off time showed the higher percentage contribution as compared to the other two factors (peak current and spark gap voltage), they can be considered most significant to the machining rate. Each cycle has an on-time and off-time that is expressed in µs. Based on the trends of influence (Figures 5.18-5.21),

maximum machining rate can be obtained when the parameters are set at; T_{on}= 1.1 µs, T_{off} = 17 µs, Ip = 200A, SV= 40V, WF = 7m/min and WT = 980 grams. The percentage contribution of significant parameters is; T_{on}: 54%, T_{off}: 26%, Ip: 9%, SV: 7% and error: 4%.

Based on Table 5.5, three interactions have been found to be significant (T_{on} ×Ip, T_{off}×Ip and T_{off}×SV) as shown in Figures from 5.22 to 5.24. The "Prob>F" value of T_{on}×Ip, T_{off}×Ip and T_{off}×SV interactions are 0.0405, 0.0097 and 0.0147 respectively. When peak current was set at 120A and pulse on time was varied from 0.7 to 1.1µs, machining rate was increased significantly, from 0.415 to 0.812 mm/min. Also, machining rate increased significantly when peak current was set at the higher level (200A) with pulse on time remains unchanged. When pulse off time was varied from 17 to 38µs, at constant peak current of 120A, the machining rate was observed to decrease from 0.934mm/min to 0.515mm/min. When pulse off time was decreased from 38 to 17µs, increment in the machining rate was observed (0.593 to 0.828 mm/min), at constant spark gap voltage of 60V.

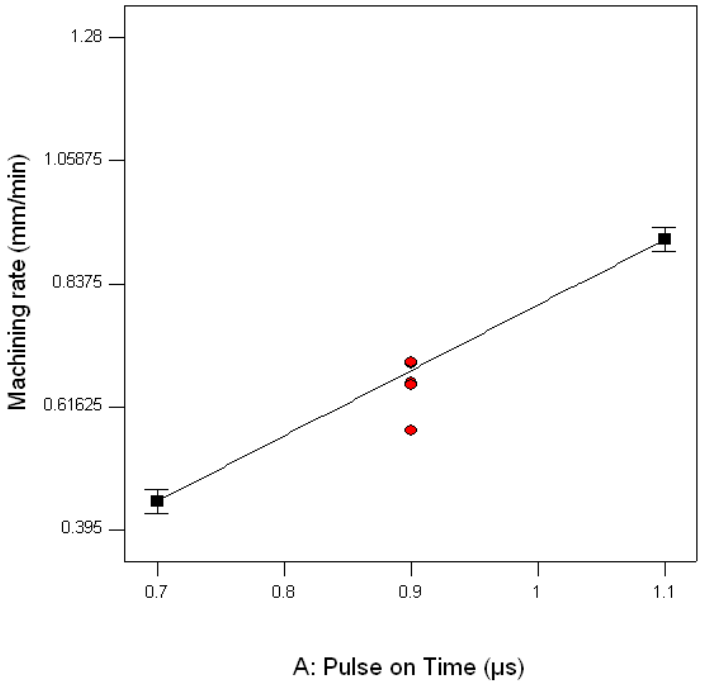

Figure 5.18 Effect of pulse on time on machining rate

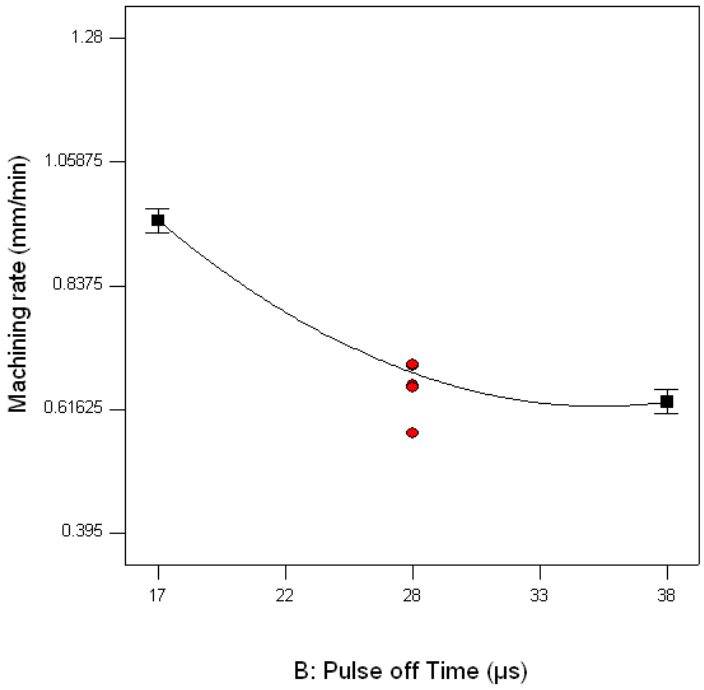

Figure 5.19 Effect of pulse off time on machining rate

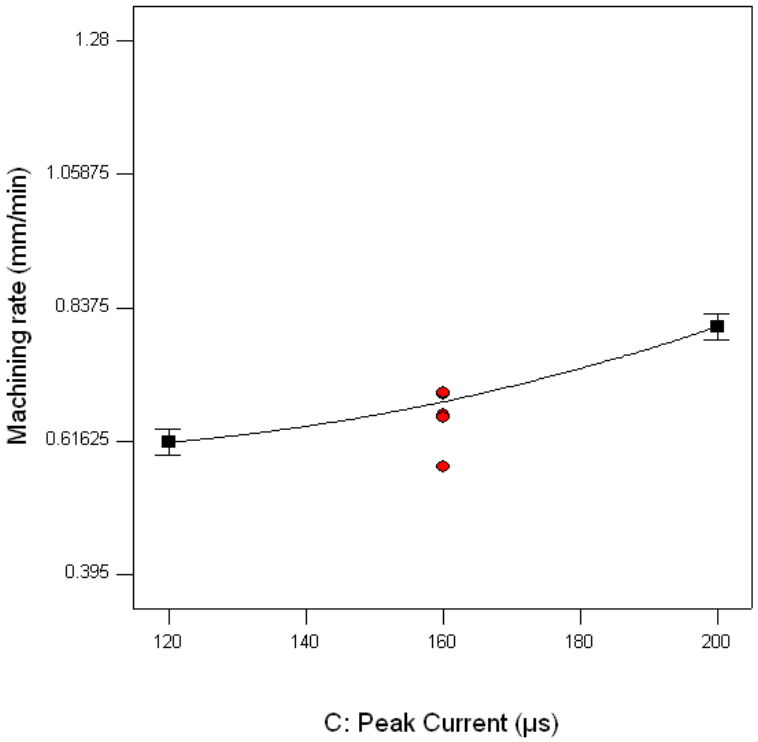

Figure 5.20 Effect of peak current on machining rate

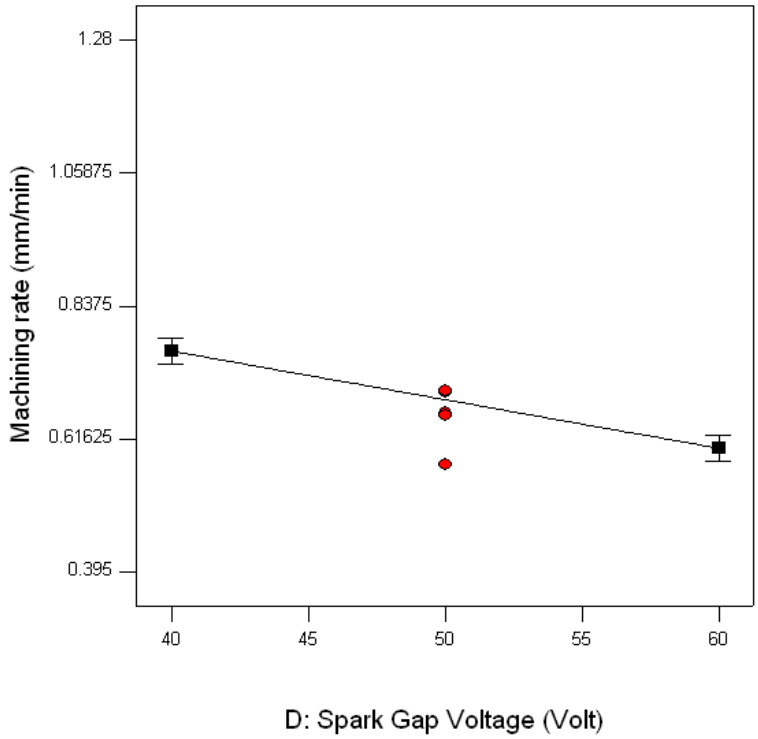

Figure 5.21 Effect of spark gap voltage on machining rate

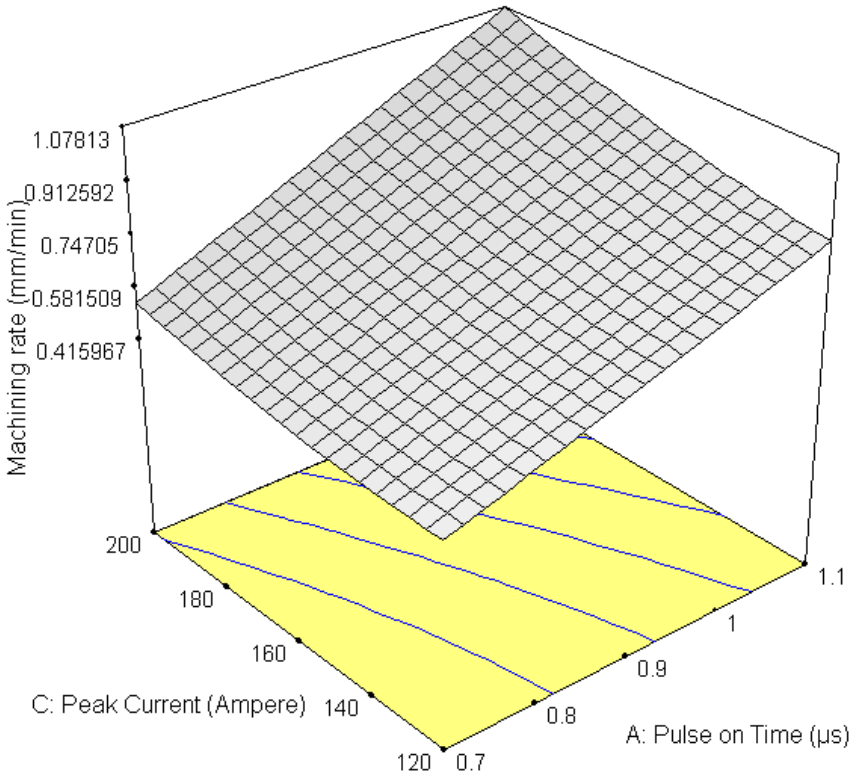

Figure 5.22 Interaction plot between pulse on time and peak current for machining rate

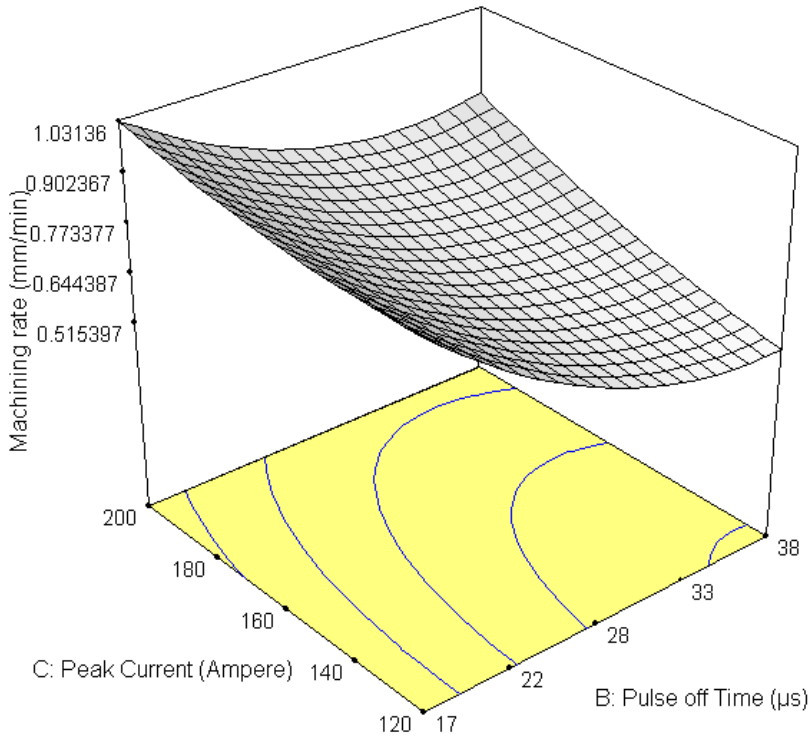

Figure 5.23 Interaction plot between pulse off time and peak current for machining rate

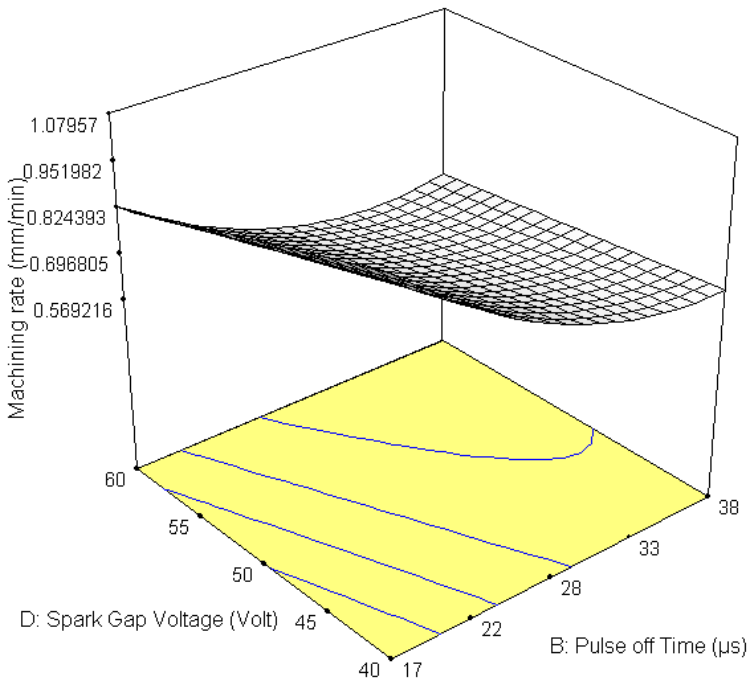

Figure 5.24 Interaction plot between pulse off time and spark gap voltage for machining rate

5.3.2 Effect of process parameters on material removal rate (MRR)

The individual (main) effects plots and interaction plots were considered only for those factors that were found significant from ANOVA test (Table 5.10). Main effect plots of T_{on}, T_{off}, Ip, SV on MRR are shown in Figure 5.25 to 5.28 respectively. Figures 5.29 and 5.30 represent the interaction effect between T_{off} × Ip, T_{off} × SV on MRR respectively.

From figures 5.25-5.29, it could be observed that higher MRR could be obtained at increased values of pulse on time, peak current. On the other hand, a reduction in pulse off time and spark gap voltage is found to improve the MRR. It was observed from Figure 5.29, that MRR increased from 4.91mm^3/min to 7.70mm^3/min, with the increase in peak current from 120- 200amp and simultaneous decrease of pulse off time from 38 to 17µs. Due to increase in peak current and decrease of pulse off time, the rate of discharge energy increases, together with an improvement in the discharge frequency. The concentration of discharge energy in the spark gap leads to melting and vaporization of molten metal and floating metal suspended in the electrical discharge which leads to increase of MRR. It was observed from Figure 5.30 that MRR increased significantly from 6.81mm^3/min to 8.93mm^3/min, with the decrease of pulse off time and spark gap voltage. This may be attributed to the reduced gap between the work and wire electrode during the spark, when the spark gap voltage is set at a lower value. The reduced gap results in higher sparking frequency and thus, the machining speed is improved.

The present study revealed that higher MRR can be achieved at the lower spark gap voltage and pulse off time coupled with higher peak current. An increase in discharge energy causes a pool of molten metal to be formed and overheated. The overheated molten metal evaporates, forming gas bubbles that explode when the discharge ceases, taking molten metal material away. The result is the formation of a crater. It has been observed that increasing the pulse on time and peak current results in formation of deeper and wider craters, thus improving the MRR. Based on experimental results (as shown in Table 4.9), maximum MRR (11.16 mm^3/min) was obtained when the parameters were set at pulse on time = 1.1µs, pulse off time = 17µs, peak current = 160A, spark gap voltage= 40V, wire feed = 7m/min and wire tension = 950 grams. From the previous studies that some of the molten material was not flushed away from the gap by dielectric fluid and remained in the electrical discharge. This material re-solidifies on the surface of machined samples that is known as recast layer [Lee and Li, 2003].

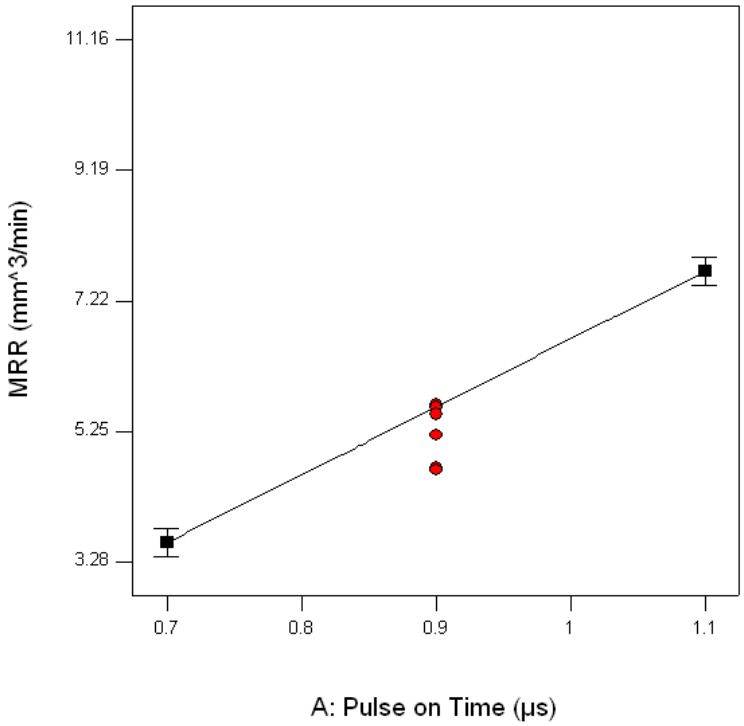

Figure 5.25 Effect of pulse on time on material removal rate (MRR)

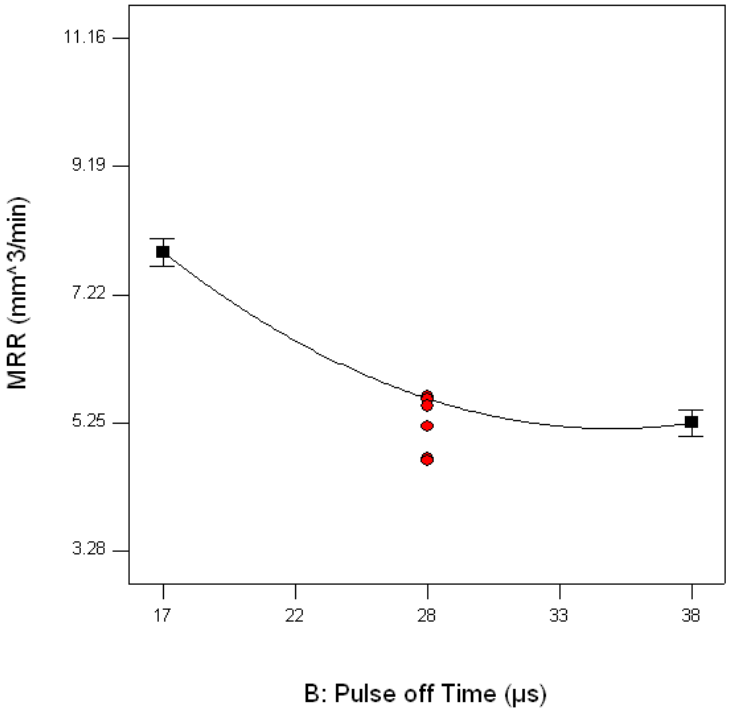

Figure 5.26 Effect of pulse off time on material removal rate (MRR)

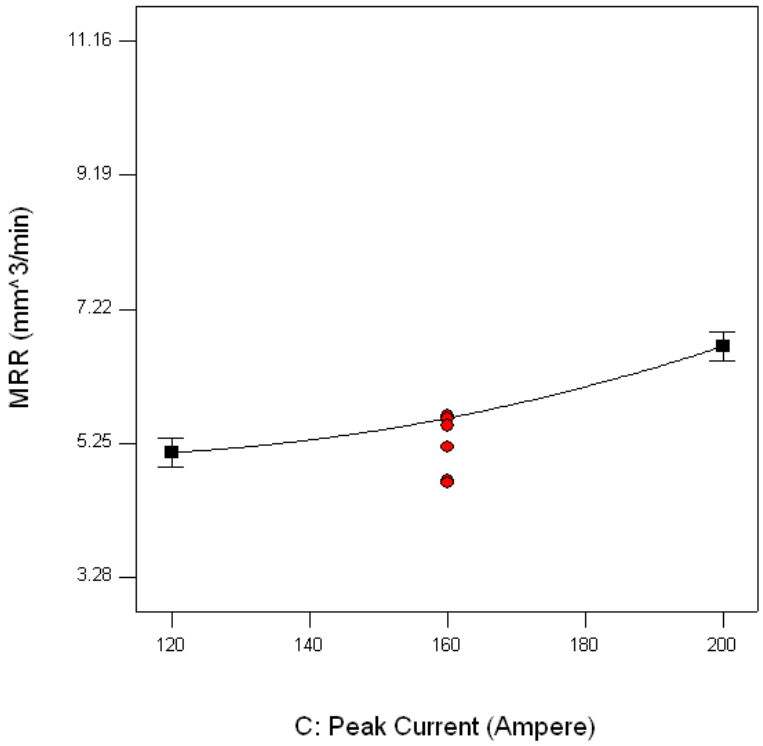

Figure 5.27 Effect of peak current on material removal rate (MRR)

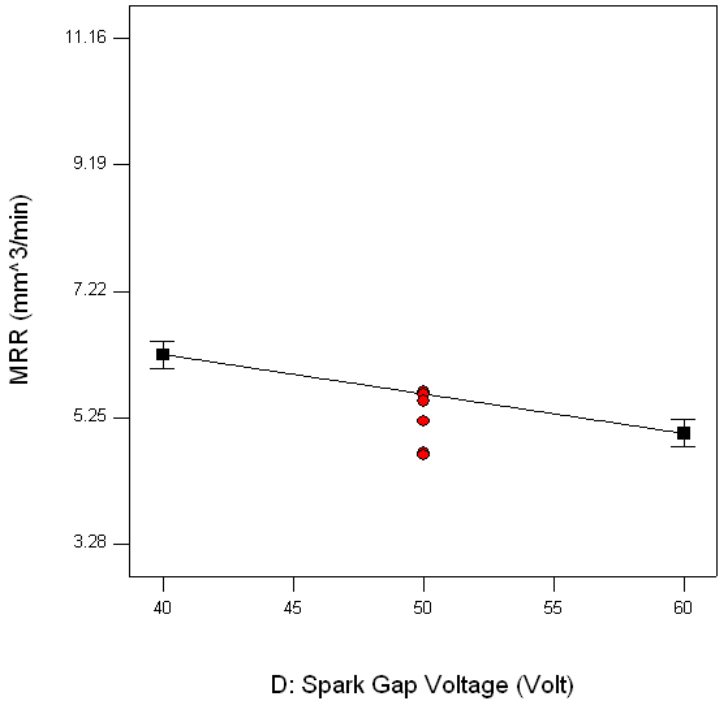

Figure 5.28 Effect of spark gap voltage on material removal rate (MRR)

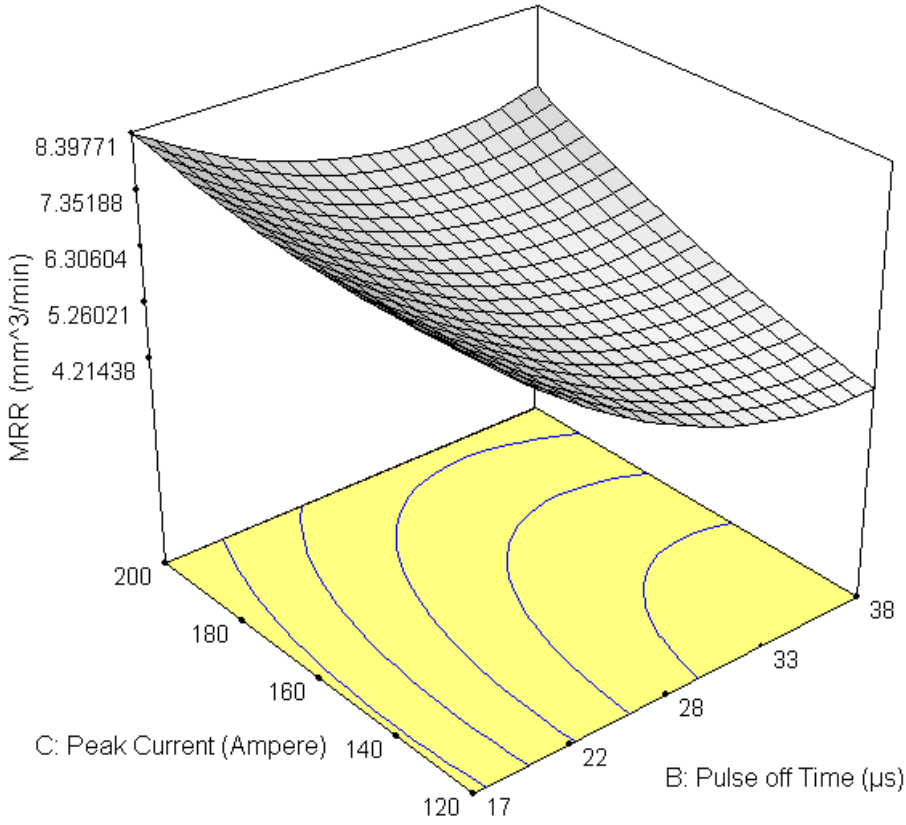

Figure 5.29 Interaction plot between pulse off time and peak current for material removal rate

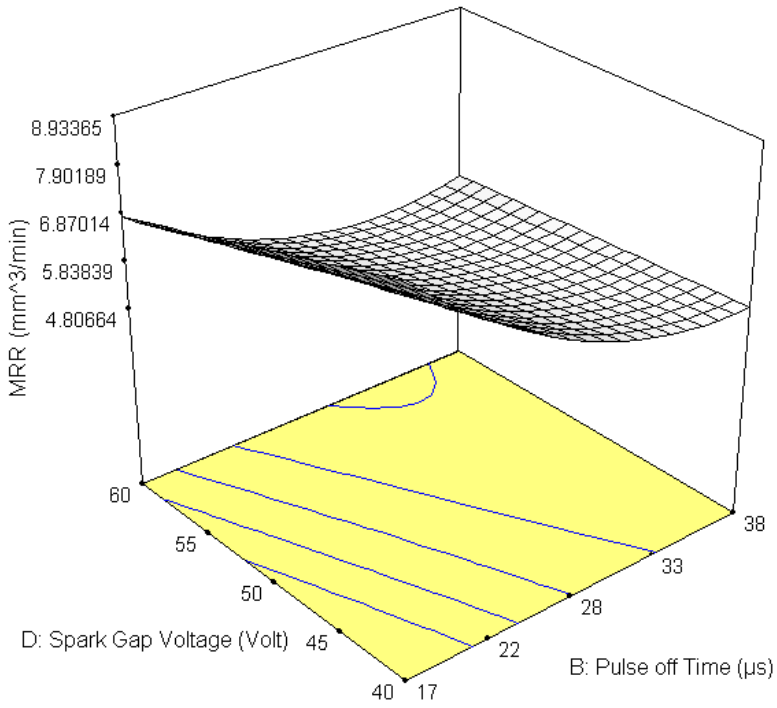

Figure 5.30 Interaction plot between pulse off time and spark gap voltage for material removal rate

5.3.3 Effect of process parameters on surface roughness

Based on analysis of variance (Table 5.7), T_{on}, T_{off}, Ip, SV and one interaction (T_{on}×Ip) is significant for surface roughness. From the main effect plots, figures from 5.31 to 5.34, it was observed that as the pulse on time is increased the surface roughness increased significantly with value of 2.40 to 2.93µm. During pulse on time, the spark gap is bridged, current is generated and the work is accomplished. The longer the spark is sustained, more is the material removal. Consequently the resulting craters will be broader and deeper; therefore surface roughness increases. It is also observed that surface roughness increases slightly with increase in the peak current. The higher is the peak current setting, the larger is the discharge energy. This leads to increase in surface roughness. In order to obtain better surface roughness during WEDM of pure titanium, the optimum parameter combination obtained is; pulse on time = 0.7µs, pulse off time=38µs, peak current=120A, spark gap voltage= 60V, wire feed = 7m/min and wire tension = 980 grams. The percentage contributions of significant parameters are; pulse on time- 55%, pulse off time- 28%, peak current- 8%, spark gap voltage- 6% and error- 3%.

When pulse on time was increased from 0.7 to 1.1µs, keeping peak current constant at 120A, the surface roughness increased from 2.41 to2.72µm (Figure 5.35). When pulse on time was varied from 0.7 to 1.1µs at constant peak current of 200A, the surface roughness increased from 2.40 to 3.13µm. The surface roughness increased when pulse on time and peak current were increased due to the longer time for machining which lead to the higher possibility of "double sparking" and localized sparking to occur. In the other words, double sparking or re-sparking can cause poor surface finish since only the initial phase sparks contribute to the material removal, while the following sparks are poorly distributed along the surface, debris and removed particles. The surface roughness is most affected by the amount of discharge energy which increases with increase in pulse on time. The surface roughness depends on the size of spark crater. A shallow crater together with a larger diameter leads to a better workpiece surface roughness. To obtain a flat crater, it is important to control the electrical discharging energy at a smaller level by setting a small pulse on time. A large discharging energy will cause violent sparks resulting in a deeper erosion crater on the surface. Accompanying the cooling process after the spilling of molten metal, residues remain at the periphery of the crater to form a rough surface. The surface roughness increased when pulse on time and peak current increased due to the longer time for machining which lead to the higher possibility of

"double sparking" and localized sparking to occur [Kumar et al., 2012]. In the other words, double sparking or re-sparking can cause poor surface finish since only the initial phase sparks contributed to the material removal, while the following sparks were poorly distributed along the surface, debris and removed particles [Liao and Yu, 2003; Liu et al., 2009].

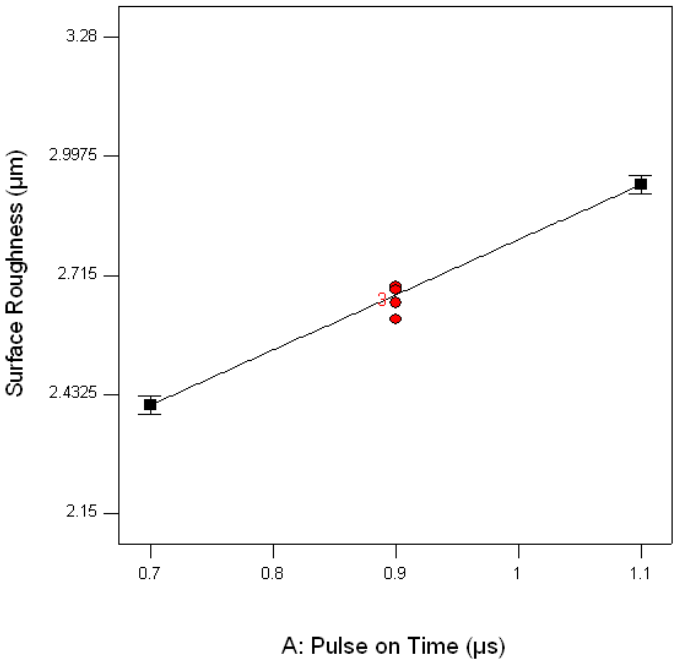

Figure 5.31 Effect of pulse on time on surface roughness

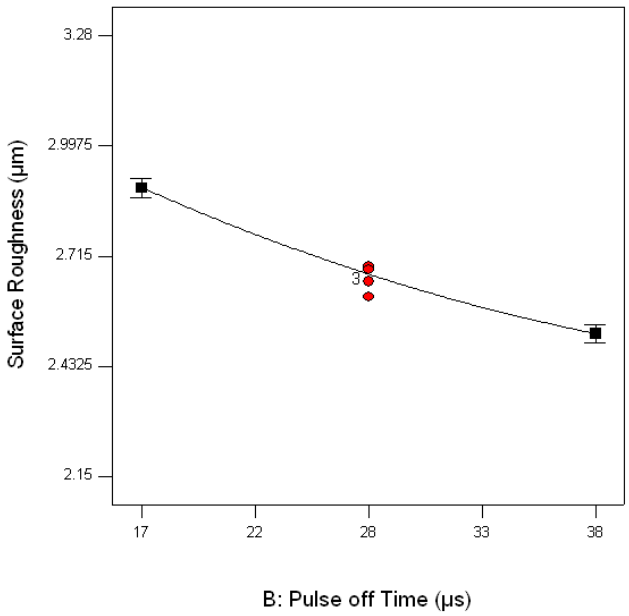

Figure 5.32 Effect of pulse off time on surface roughness

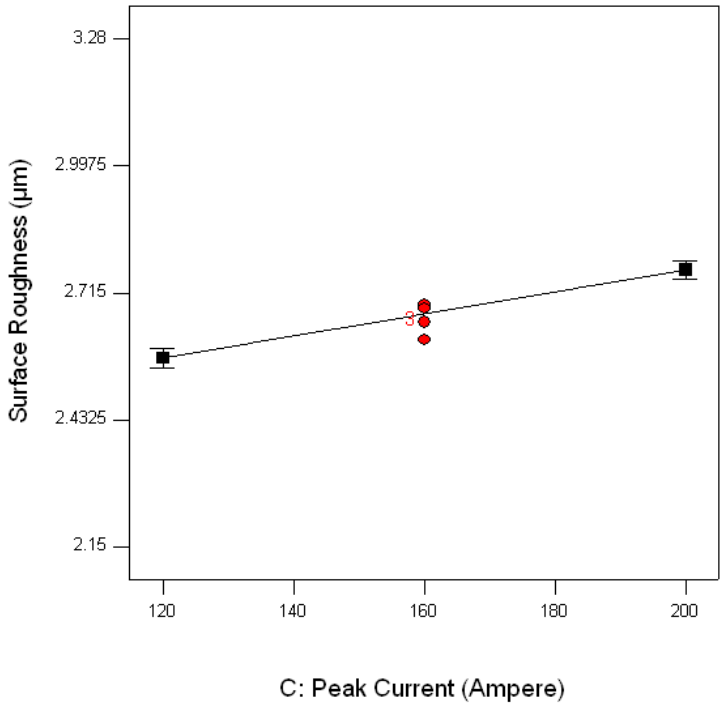

Figure 5.33 Effect of peak current on surface roughness

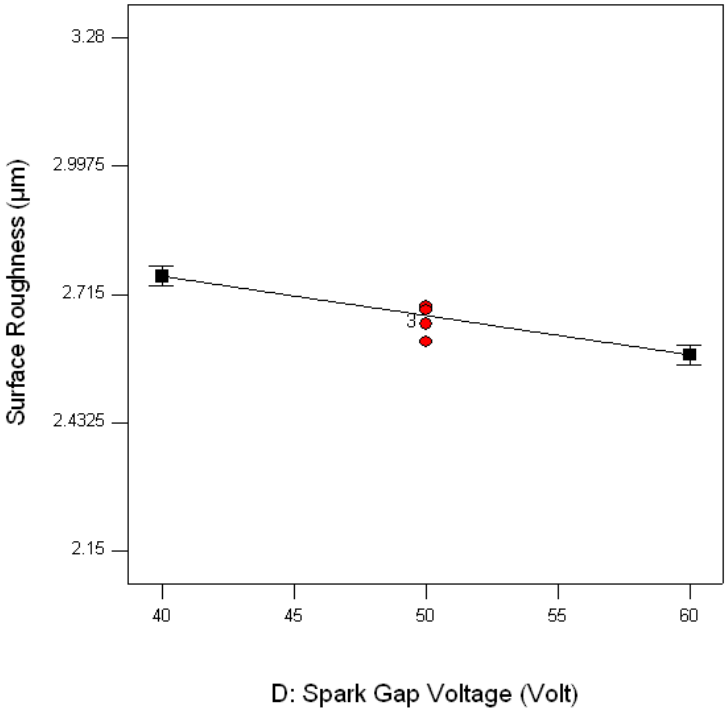

Figure 5.34 Effect of spark gap voltage on surface roughness

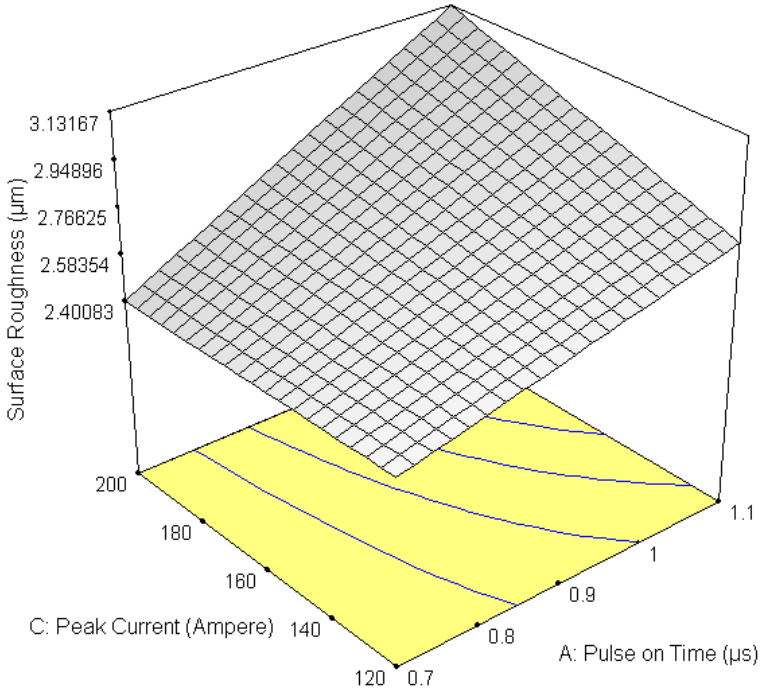

Figure 5.35 Interaction plot between pulse on time and peak current for surface roughness

5.3.4 Effect of process parameters on dimensional deviation

The effects of significant process parameters obtained from ANOVA (Table 5.12) i.e. T_{on}, T_{off}, Ip, SV and one interaction (SV× WT) for dimensional deviation are presented in this section. From the main effect plots based on the figures from 5.36 to 5.39, it is observed that when pulse on time increased, the value of dimensional deviation also increased significantly. The dimensional deviation is decreased from 153.80µm to 149.32 µm on increasing the spark gap voltage from 40 volt to 60 volt. When peak current increased from 120 to 200A, a less significant effect on dimensional deviation (i.e. 151 to 154µm) is observed. The dimensional deviation is found to be significantly affected by pulse on time and pulse off time factors. A probable reason for it may be that with increase in pulse on time, discharge energy increases. During every individual spark discharge, the wire experiences an impact that acts in the reverse direction of the discharge occurrence so that dimensional deviation increases. The percentage contributions of significant parameters are pulse on time: 59%, pulse off time: 23%, peak current: 2%, spark gap voltage: 7% and error: 9%.

It is observed from Figure 5.40 that dimensional deviation decreases with higher spark gap voltage. The dimensional deviation gradually increases with the increase in the wire

tension. When spark gap voltage was increased from 40 to 60V, the dimensional deviation decreased from 155 to 149µm. Due to increase of the wire tension, the wire bending is controlled which leads to a dynamic stable condition of the diameter and the depth of the crater leading to higher dimensional deviation. Wire tension is main significant factor for dimensional deviation. The wire is very thin (Ø0.25mm) and flexible. It deforms due to various forces acting during the discharge and deflects opposite to the cutting direction. The actual wire position is always behind the wire guide. Gap force develops mainly due to reaction of explosive force from gas bubbles. Hydraulic force, electromagnetic force, electrostatic force etc. are other contributing forces. Primarily due to unstable nature of the plasma channel and stochastic nature of sparking, the force exerted on the wire is not constant; instead it fluctuates with respect to time which in turn promotes continuous vibration in the wire. This vibration is one major source of dimensional deviation in WEDM [Wang and Ravani, 2003].

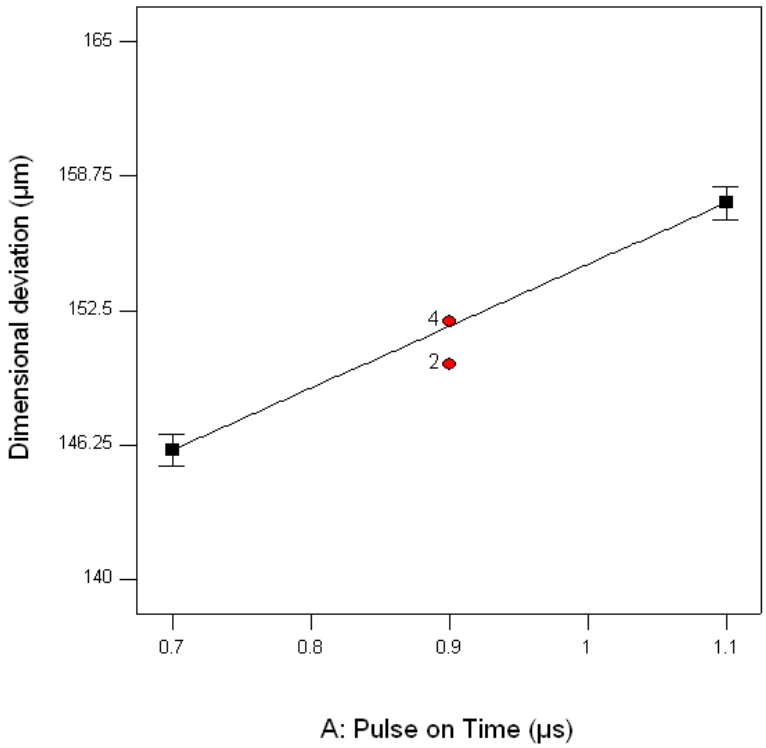

Figure 5.36 Effect of pulse on time on dimensional deviation

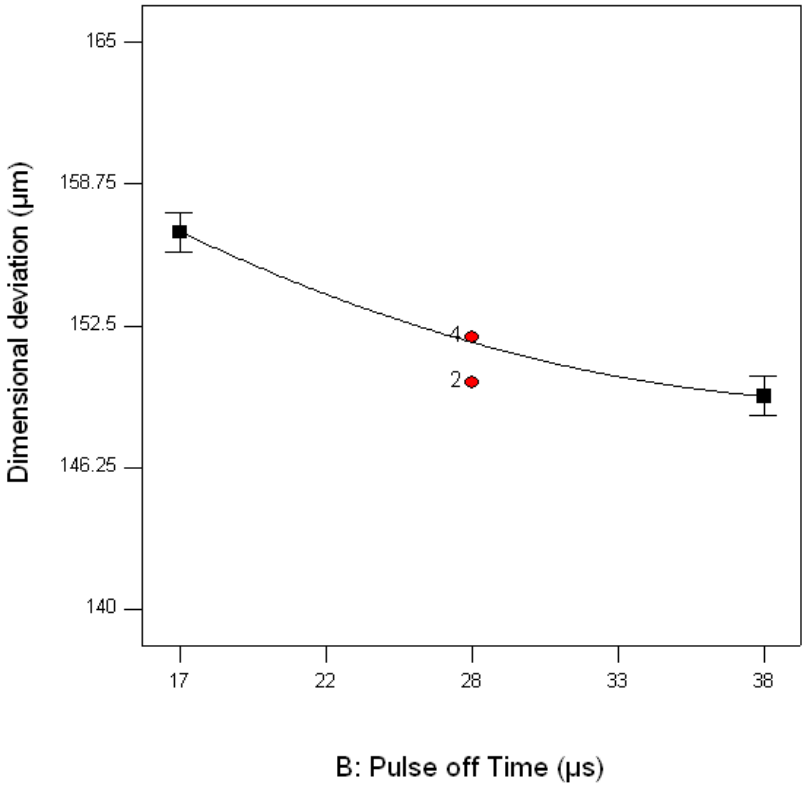

Figure 5.37 Effect of pulse off time on dimensional deviation

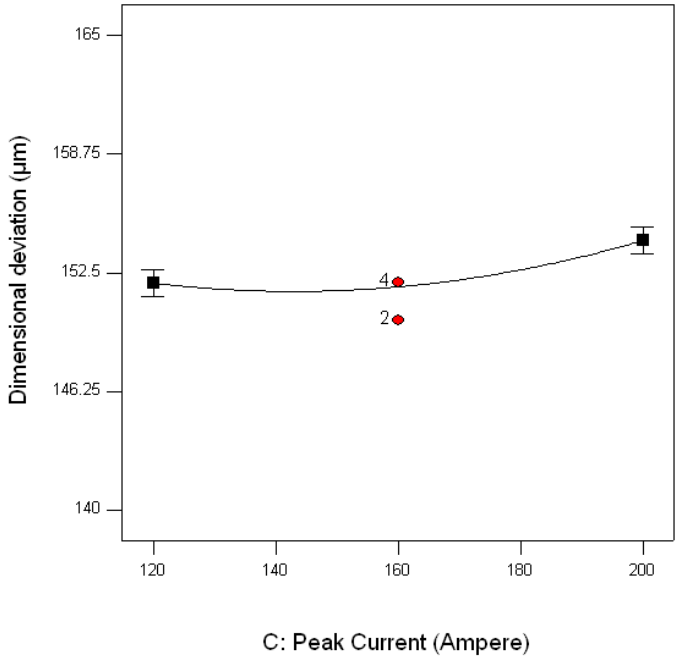

Figure 5.38 Effect of peak current on dimensional deviation

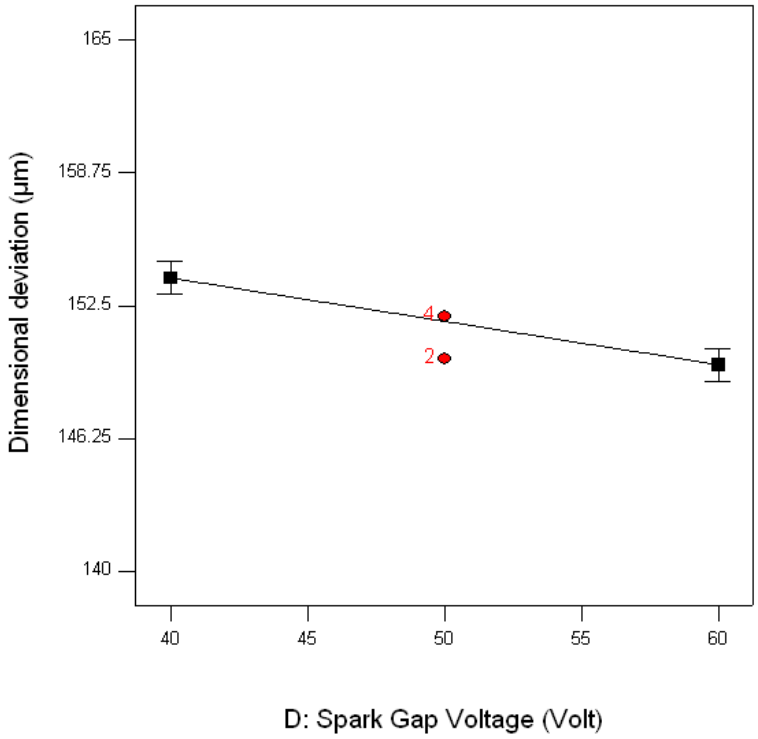

Figure 5.39 Effect of spark gap voltage on dimensional deviation

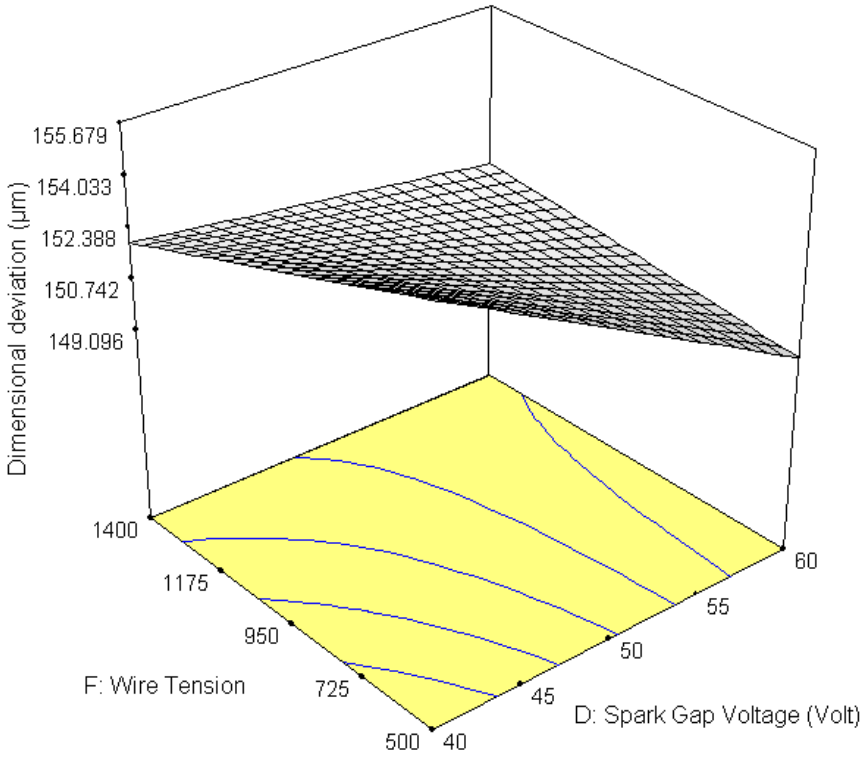

Figure 5.40 Interaction plot between spark gap voltage and wire tension for dimensional deviation

5.3.5 Effect of process parameters on overcut

The ANOVA (Table 5.13) test summarizes the effects of process variables and the interactions for second order quadratic model for overcut. By checking F and P values, it is seen that the factors A (pulse on time) and B (pulse off time) have most significant effect on Overcut. The value of "Prob>F" (less than 0.05) indicates that the model terms A,B,C,D,B^2,C^2,E^2,F^2,AD,BC are significant. From the main effect plots based on the Figures from 5.41 to 5.44, it has been observed that while pulse on time is increased from 0.7µs to 1.1µs, the value of overcut increased significantly. The increment of overcut was observed as 27.62µm to 35.46µm. Meanwhile, when pulse off time decreased from 38 to 17µs and Ip increased from 120 to 200A, the most significant effect on overcut (i.e. 36.51µm to 28.85µm and 31.47µm to 36.89µm) is realized. While spark gap voltage is varied from 40V to 60V, the overcut was decreased from 32.62µm to 30.46µm.

In order to obtain the optimal value of overcut, the parameter combination obtained is; pulse on time = 0.7µs, pulse off time = 36µs, peak current =160A, spark gap voltage = 50V, wire feed = 7m/min and wire tension = 950 gram. Figure 5.45 shows the three-dimensional response surface for overcut in terms of process parameters pulse on time and spark gap voltage. Increase in pulse on time results in higher spark energy which produces larger craters on the machined surface. Therefore, this results in higher overcut. At higher level of spark gap voltage (of 50V to 60V), the spark energy per pulse is greater. This high spark energy produces larger amount of debris. The debris are trapped in the spark gap and may cause unwanted spark. The unwanted sparks result in wire erosion, which results in less material removal, as the significant amount of spark energy is employed in sparking with debris, leading to reduced overcut values.

Figure 5.46 shows the three-dimensional response surface in terms of process parameters pulse off time and peak current, at a pulse on time of 0.9µs, spark gap voltage of 50V, wire feed of 7 m/min and wire tension of 950gram. It is observed that overcut is decreased by increasing the pulse off time from 17µs to 38µs, with a parallel decrease of peak current from 200A to 120A. On increasing the pulse off time, the machining status becomes stable and the probability of uncontrolled sparking is reduced. Also, the sparking frequency is reduced. All these effects contribute to reduction in the overcut.

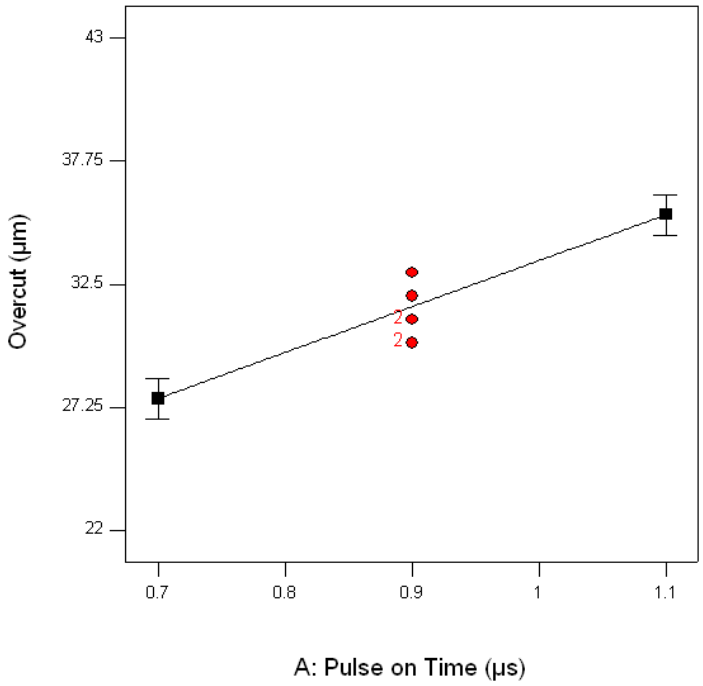

Figure 5.41 Effect of pulse on time on overcut

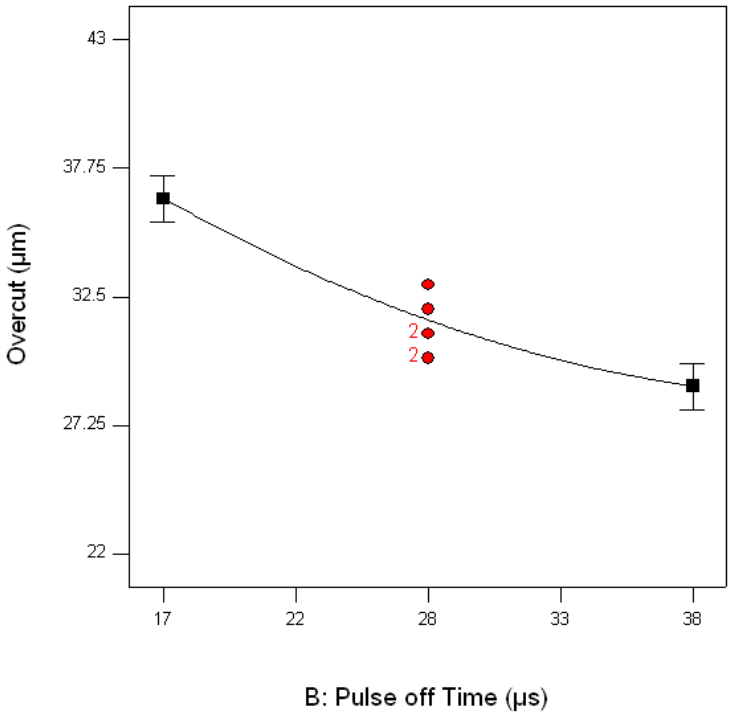

Figure 5.42 Effect of pulse off time on overcut

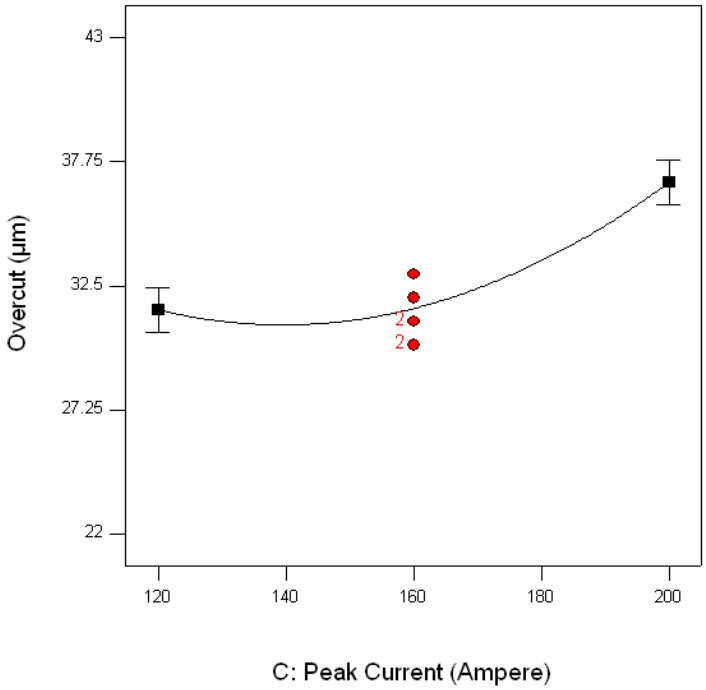

Figure 5.43 Effect of peak current on overcut

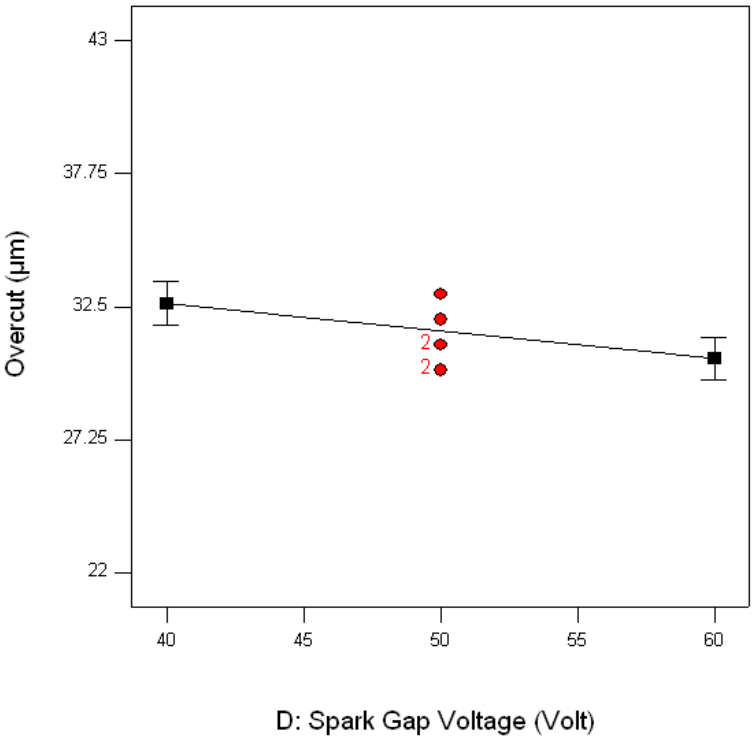

Figure 5.44 Effect of spark gap voltage on overcut

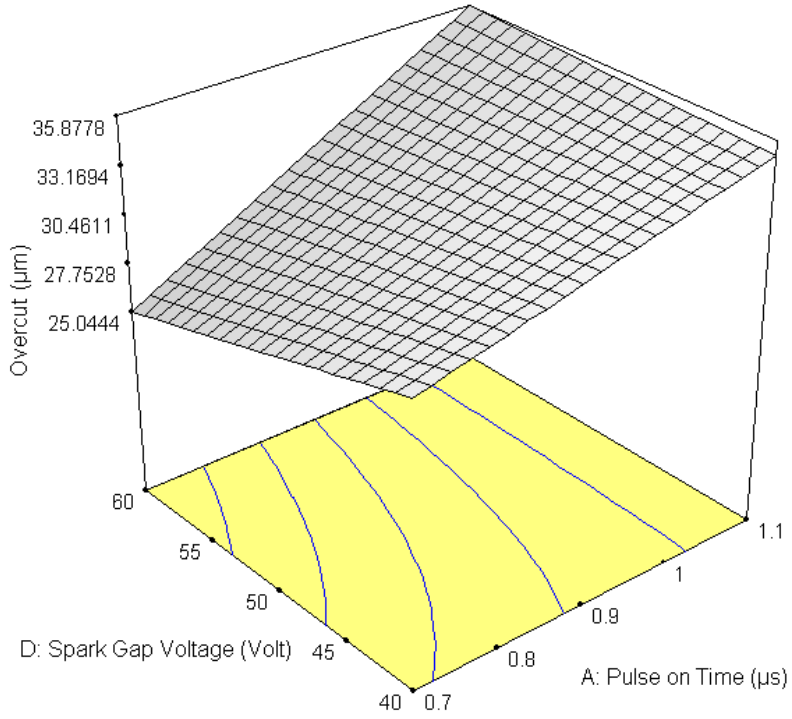

Figure 5.45 Interaction plot between spark gap voltage and pulse on time for overcut

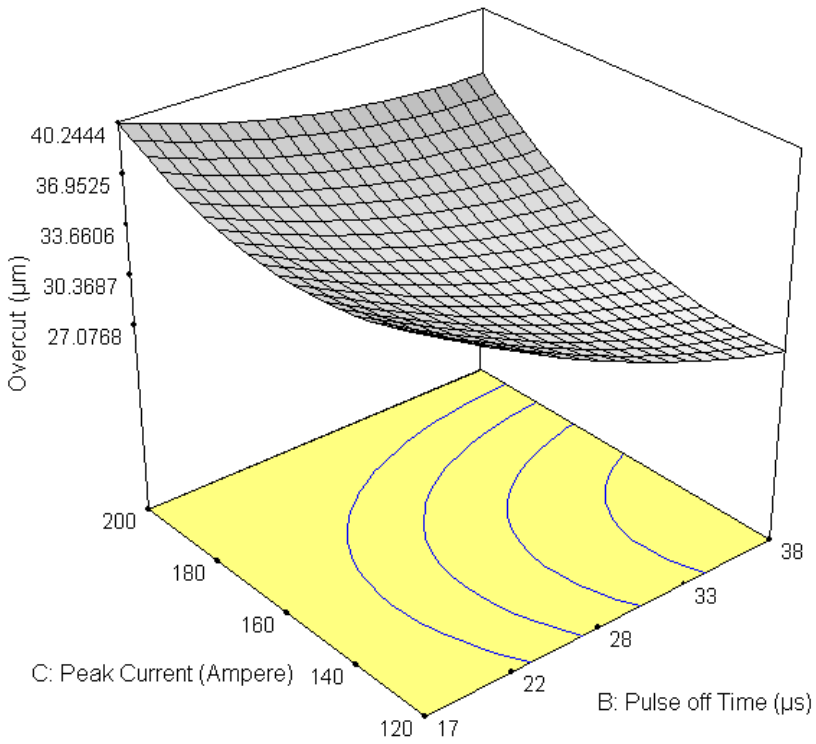

Figure 5.46 Interaction plot between peak current and pulse off time for overcut

5.3.6 Effect of process parameters on wire wear ratio

Based on analysis of variance (Table 5.14), four input factors T_{on}, T_{off}, Ip, SV and one interaction (T_{on}×SV) are significant for wire wear ratio. From the main effect plots as shown in Figures from 5.47 to 5.50, it has been observed that if pulse on time is increased, the value of wire wear ratio is also increased significantly. The increment of wire wear ratio was observed as 0.075 to 0.087. Meanwhile, a reverse result was observed when spark gap voltage was increased from 40V to 60V; the wear ratio is decreased from 0.082 to 0.074.Increment in peak current results in a corresponding increase in wire wear ratio due to intense thermal effect on the wire electrode, which causes severe wear of the wire surface. On the other hand, wire wear ratio decreases rapidly while increasing the pulse off time.

In this case, there was only one interaction involved in affecting the wire wear ratio. It is observed from Figure 5.51, when pulse on time and spark gap voltage are set at the lowest level (0.7μs and 60V respectively), the wire wear ratio reaches its minimum value, which is 0.074. Meanwhile, as the spark gap voltage is set at 40V and pulse on time is increased from 0.7 to 1.1μs, the wire wear ratio increased significantly from 0.077 to 0.093. Based on the graph, it was the highest increment of wire wear ratio. Furthermore, when spark gap voltage is set up at the high level (spark gap voltage= 60V) and pulse on time is set at 1.1μs, the wire wear ratio is recorded as 0.080.

From these results, the optimum setting of the parameters can be adjusted in order to minimize the wire wear ratio, which is identified as; pulse on time at 0.7μs, pulse off time at 38 μs, peak current at 120 A and spark gap voltage at 60V. It is observed experimentally that the increasing of pulse on time results in formation of larger craters on the wire surface and wire electrode wear out more rapidly. The higher wire wear ratio is always accompanied by high peak current and low pulse off time [Tosun et al., 2003a]. The percentage contributions of significant parameters are pulse on time: 9%, pulse off time: 50.94%, peak current: 28.88%, spark gap voltage: 6.92%.

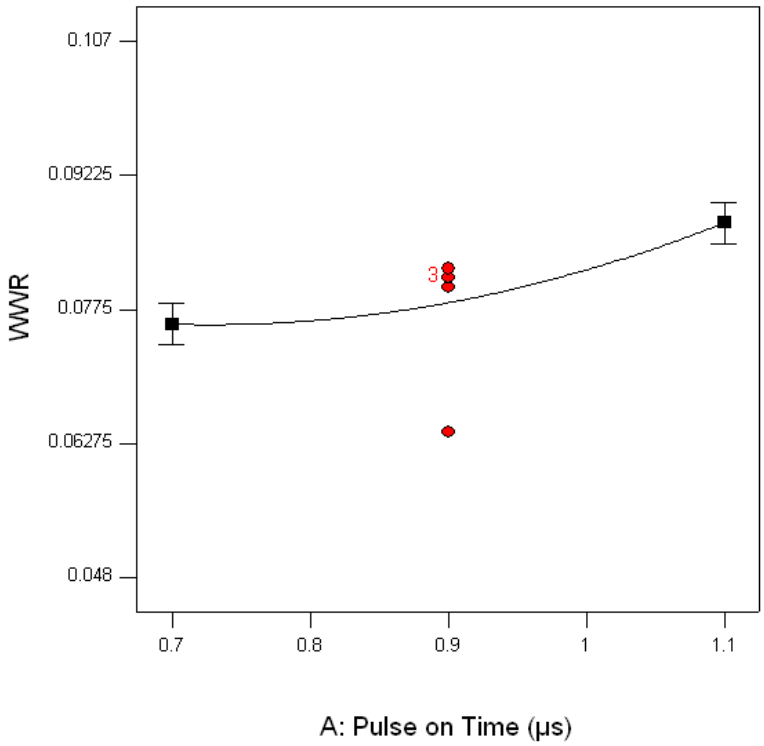

Figure 5.47 Effect of pulse on time on wire wear ratio

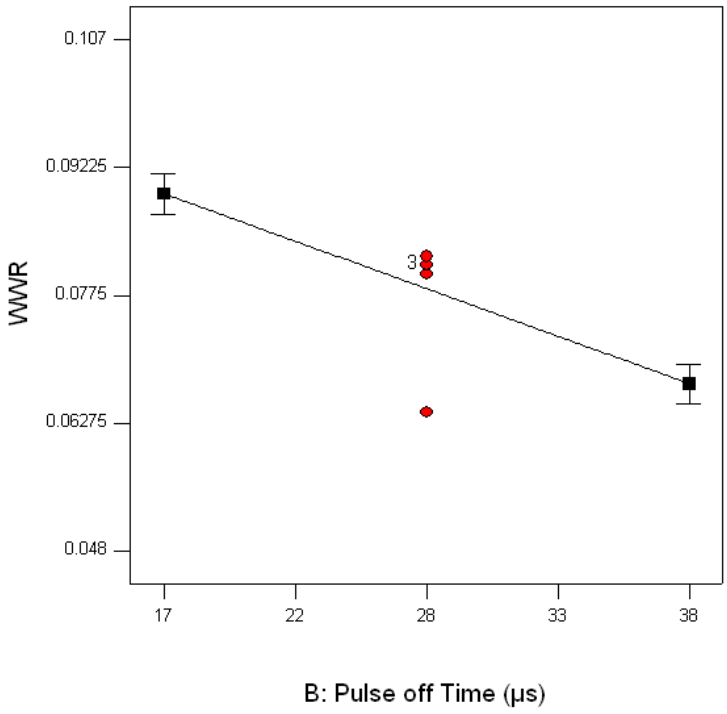

Figure 5.48 Effect of pulse off time on wire wear ratio

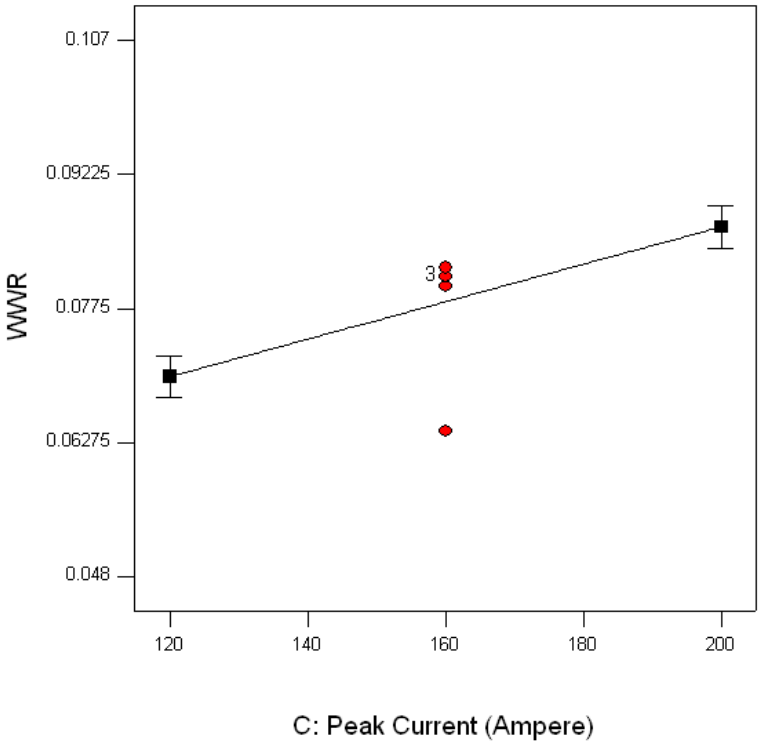

Figure 5.49 Effect of peak current on wire wear ratio

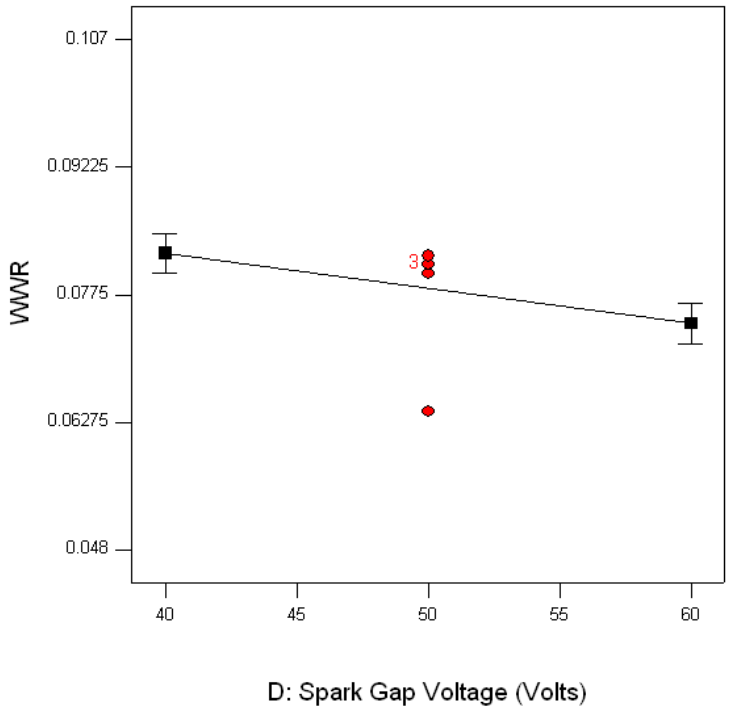

Figure 5.50 Effect of spark gap voltage on wire wear ratio

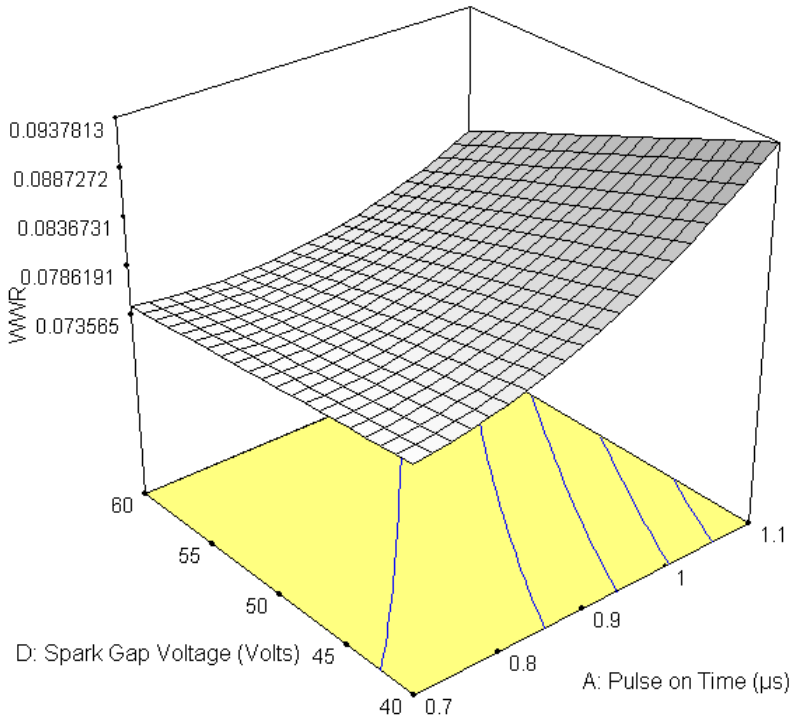

Figure 5.51 Interaction plot between spark gap voltage and pulse on time for wire wear ratio

5.3.7 Effect of process parameters on surface crack size density

WEDM process is very complex due to rapid local heating, quenching and random attack of the spark. At each discharge, the local temperature increases more than the boiling point of the material. The thermal nature of the WEDM process, which involve melting/ vaporization followed by rapid cooling/ quenching, results in surface damage in the form of crack formation coupled with the development of high thermal stresses exceeding the fracture strength of the material, as well as with plastic deformation [Ekmekci et al.; 2009].Cracks typically refer to as micro-cracks, caused by incompatible internal permanent strains due to quick local heating cycle. However, the length and density of cracks depend on the discharge energy and also on the thermal properties of the workpiece material.

The discharge energy is the function of peak current, pulse on time, pulse off time and spark gap voltage. In this case, pulse on time, pulse off time, peak current and spark gap voltage have significant effect on surface crack density. From the main effect plots as shown in Figure 5.52 to 5.55, it was observed that if pulse on time is increased from 0.7µs to 1.1µs, the value of surface crack density gets increased significantly. The increment of

surface crack density was observed from 0.0049μm/μm^2 to 0.0115μm/μm^2. Meanwhile, when pulse off time is decreased from 38 to 17μs and peak current is increased from 120 to 200A; it results in the most significant effect on surface crack density i.e. the crack density increases from 0.0066μm/μm^2 to 0.010μm/μm^2 and 0.0065μm/μm^2 to 0.015μm/μm^2 respectively. When, spark gap voltage is varied from 60V to 40V, the surface crack density increases from 0.0093μm/μm^2 to 0.011μm/μm^2. In order to obtain optimal value of surface crack density, the parameter combination is set at pulse on time = 0.7μs, pulse off time = 38μs, peak current =120A, spark gap voltage = 50V, wire feed = 7m/min and wire tension = 950 gram.

Interaction plots (Figure 5.56) are created by plotting two variables jointly on the same graph. It is obvious that an interaction exists between Pulse off Time × Peak Current and Pulse off Time × Spark Gap Voltage for the surface crack density. It was observed that surface crack density varies from 0.005μm/μm^2 to 0.015μm/μm^2 with the decrease of pulse off time and simultaneously increase of peak current. Pulse off Time × Spark Gap Voltage interaction has also showed a significant effect on surface crack density, which varies from 0.008μm/μm^2 to 0.014μm/μm^2.

The cracks at different settings of peak current, pulse off time and pulse on time were observed on the machined surface as shown in Figure 5.57. The study observed less formation of surface cracks while the machining is carried out according to the conditions pertaining to experiment no.3, 11, 16, 19 as shown in Figure 5.58. The machined surfaces reveal that the surface cracks have three different characteristics. The first type of cracks is called surface cracks. The second type of cracks is known as penetrating cracks that penetrate into the subsurface of the material. The third type of cracks is visualized around globular or irregularly shaped attachments on the crater rim as shown in Figure 5.59. All of the cracks are usually observed when machining is performed in de-ionized water and machined sample is quenched and tempered proceeding to machining. Regarding the surface crack density analysis, the percentage contributions of significant parameters are pulse on time: 18.30%, pulse off time: 6.31%, peak current: 32.73%, spark gap voltage: 1.38%.

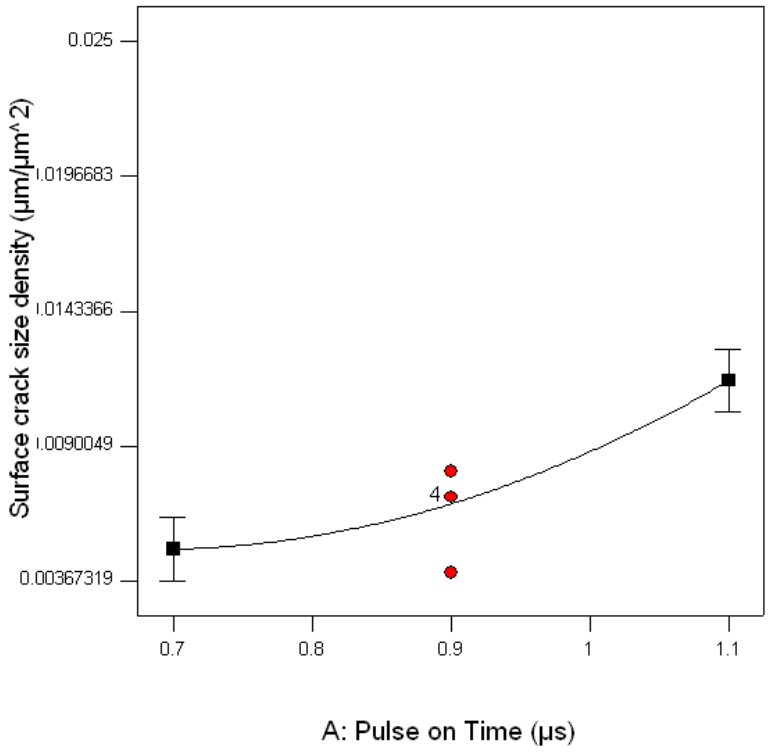

Figure 5.52 Effect of pulse on time on surface crack size density

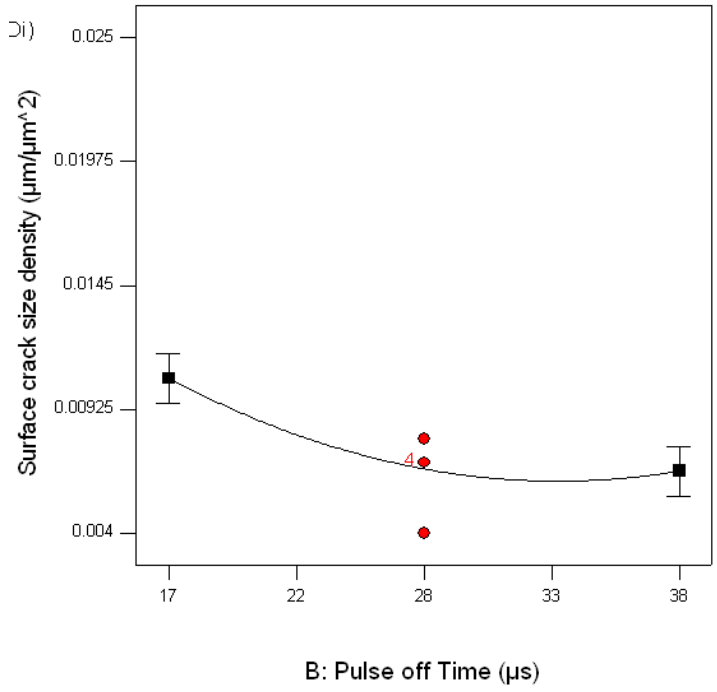

Figure 5.53 Effect of pulse off time on surface crack size density

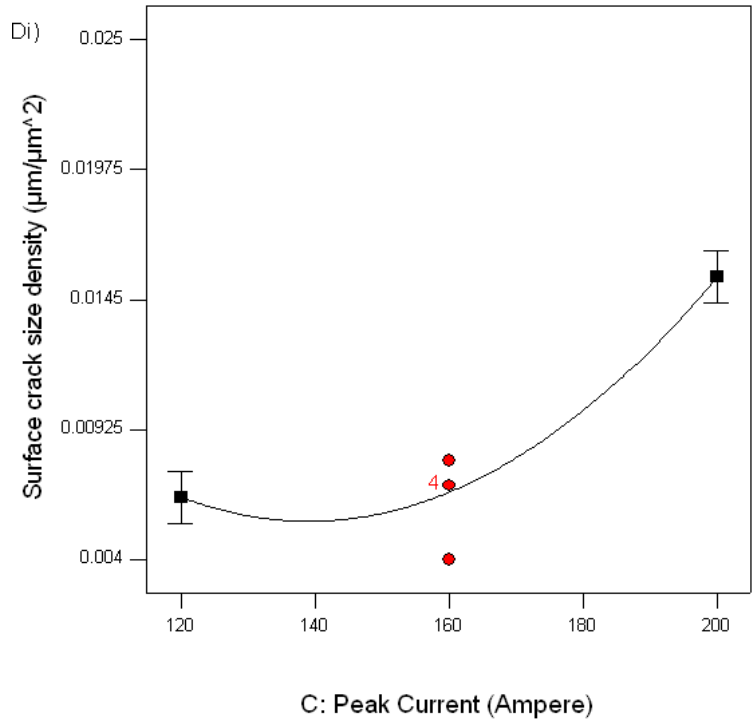

Figure 5.54 Effect of peak current on surface crack size density

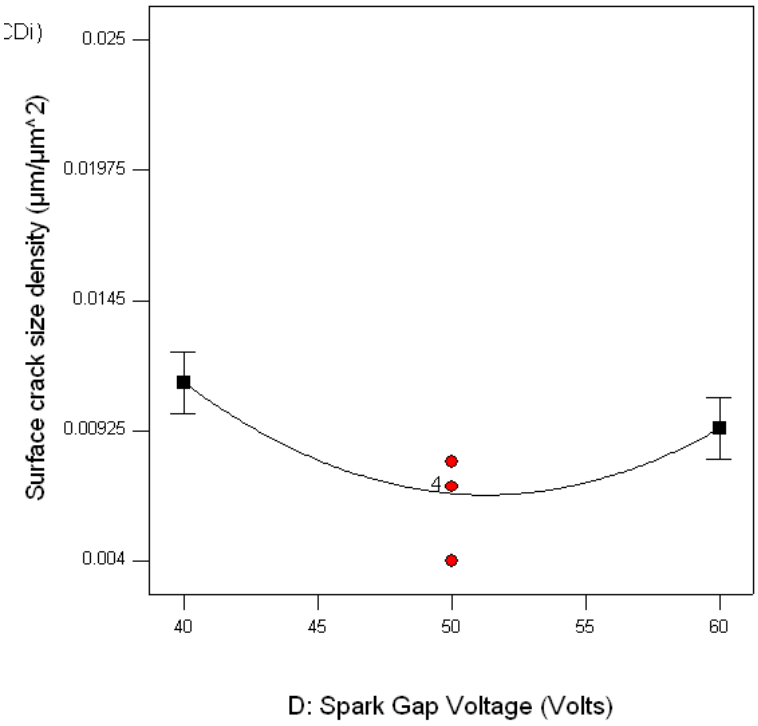

Figure 5.55 Effect of spark gap voltage on surface crack size density

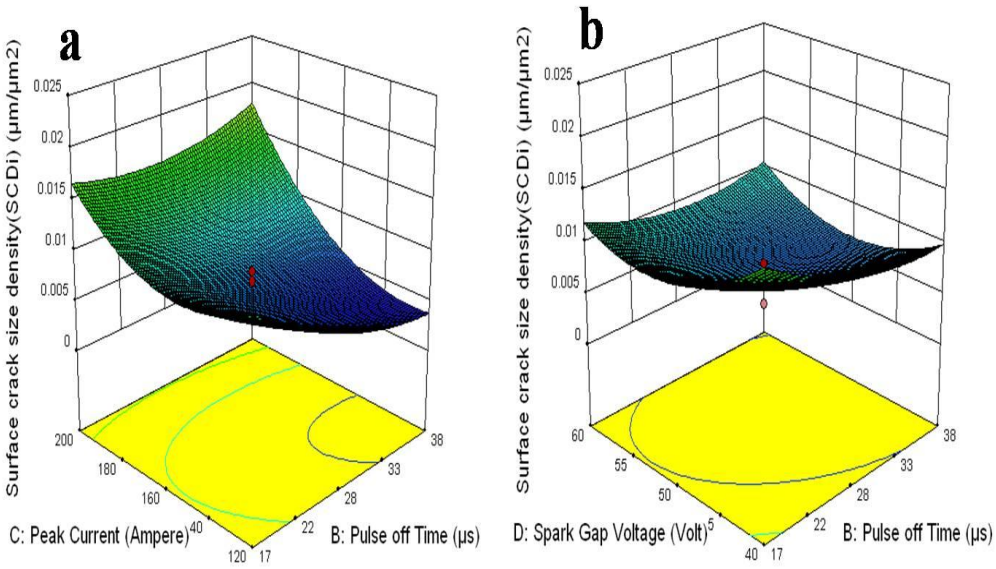

Figure 5.56 Three dimensional interaction plots showing the effects of two parameters on surface crack density (a) pulse off time and peak current, (b) pulse off time and spark gap voltage

5.3.8 Effect of process parameters on recast layer thickness

Due to rapid local heating and quenching and random attack of the spark, a multi layered surface is created on the workpiece. This consists of three layers namely: recast layer on the top of the work surface, the Heat Affected Zone, and the transformed layer, where a change in grain structure from the base structure is apparent [Zhang et al.; 2011]. The formation of these layers depends on the process conditions and workpiece properties like chemical composition and thermal conductivity. The molten material produced during the spark is partly flushed away by the dielectric, and the rest re-solidifies that forms the recast layer at the top. It has altered metallurgical structure after going through the extremely high energy thermal process accompanied by dielectric cooling process. This layer usually differs significantly from the base material and it is typically very fine grained and hard. The recast layer thickness is dependent on heat transfer and the micro-structural change undergone by the workpiece during the WEDM process. The existence of recast layer on WEDM surface is estimated and governed by the efficiency of heat transfer through the rapidly solidifying metal. The heat transfer is a function of the amount of heat supplied by spark energy. The effect of the machining parameters on the recast layer thickness are enlightened distinguishably and established by main effect and three dimensional interaction plots. Figure.5.60-5.63 depicts the plots of the main effects

on recast layer thickness; those can be used to graphically assess the effects of the parameters on the response. It indicates that pulse on time, pulse off time, peak current

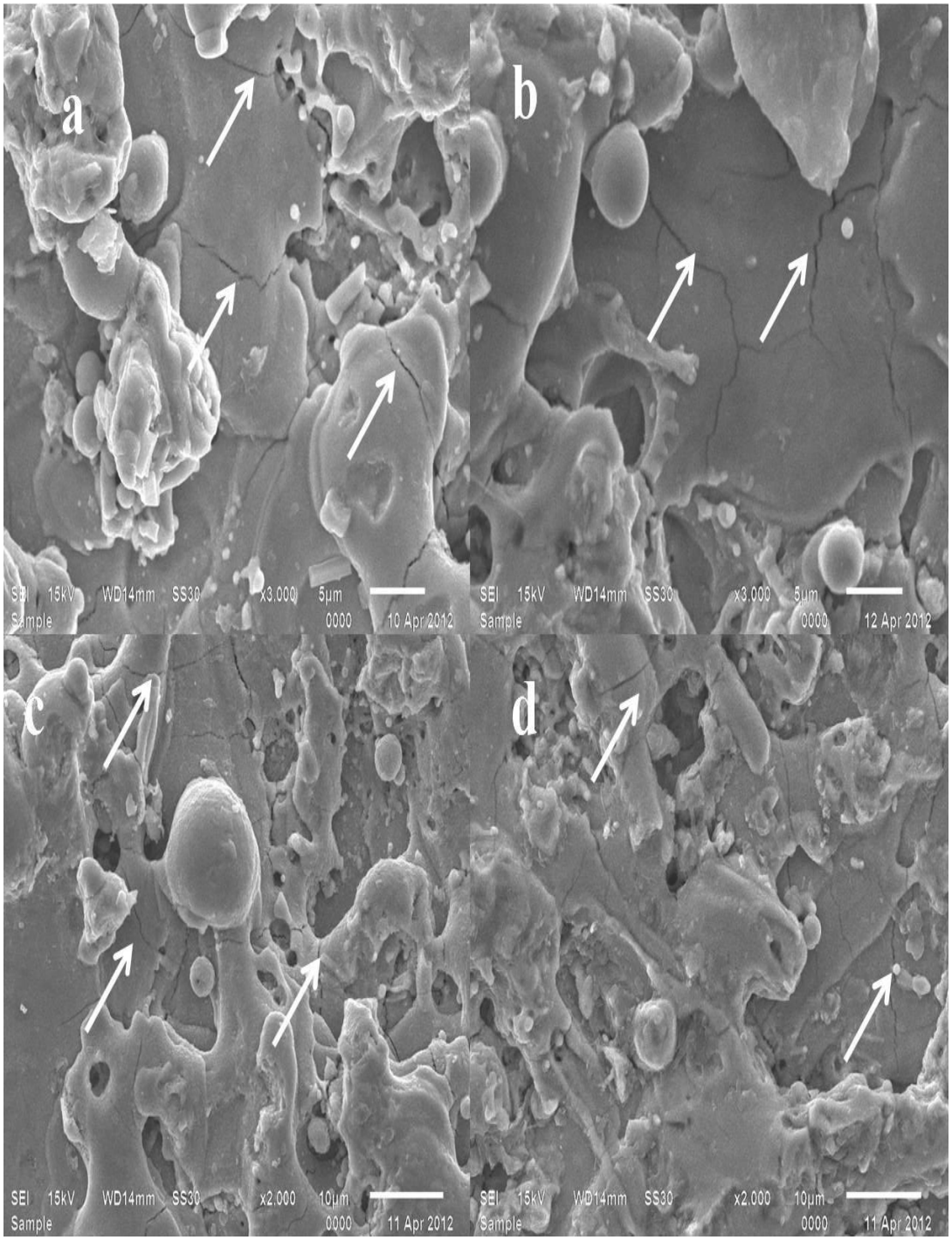

Figure 5.57 SEM micrographs of cracks observed at (a) pulse on time = 0.9µs, pulse off time = 28µs, peak current= 120A, spark gap voltage= 50V (b) pulse on time = 1.1µs, pulse off time = 17µs, peak current= 200A, spark gap voltage= 40V (c) pulse on time = 0.7µs, pulse off time = 28µs, peak current= 120A, spark gap voltage= 60V (d) pulse on time = 0.9µs, pulse off time = 38µs, peak current= 160A, spark gap voltage= 60V

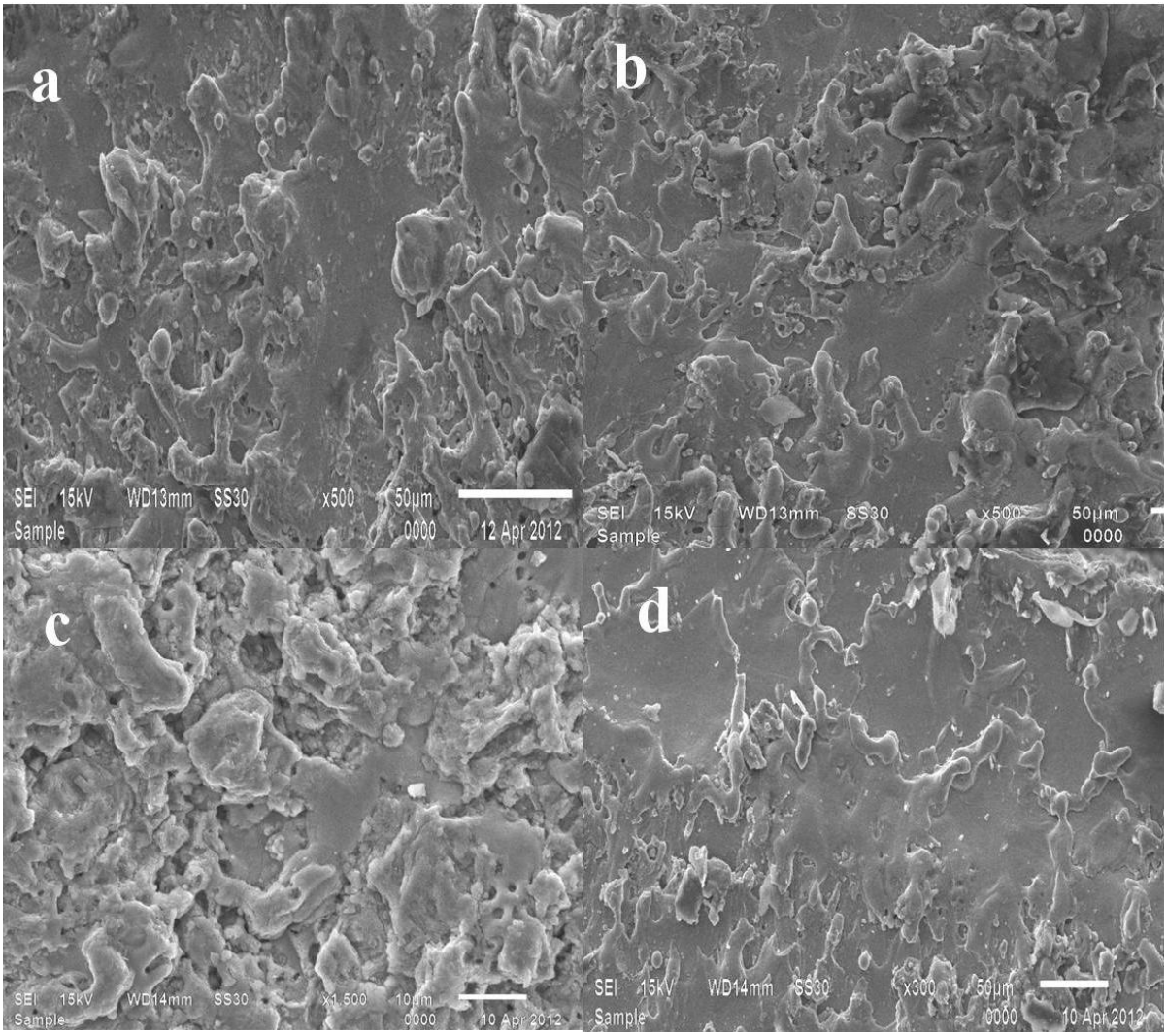

Figure 5.58 SEM micrographs with less number of craters and cracks were observed at Exp. No. 3,15,16,19.

and spark gap voltage have significant effect on recast layer thickness. However, peak current is the most influencing parameter showing a sharp increase of recast layer thickness from 43.96µm to 48.91µm. In addition, recast layer thickness is directly affected by pulse on time, but its main effect is sharply increasing by 34.07µm to 48.78µm. While, pulse off time is also affected to the recast layer thickness and its effect increases by 49.35µm to 48.32µm. The effect of spark gap voltage varied from 60V to 40V the recast layer thickness was increased from 44.28µm to 48.59µm. Figure.5.64 shows that two parameter interactions plot between pulse off Time × peak Current and peak Current × wire tension. Each pair of the parameter is plotted keeping the other parameters constant at the mean level. In each plot, the parameters of interest are varied

from its low level to its medium and medium to high level. It can be seen in the figure that all of them are intersecting each other significantly and hence showing significant interaction at a confidence level of 95%.

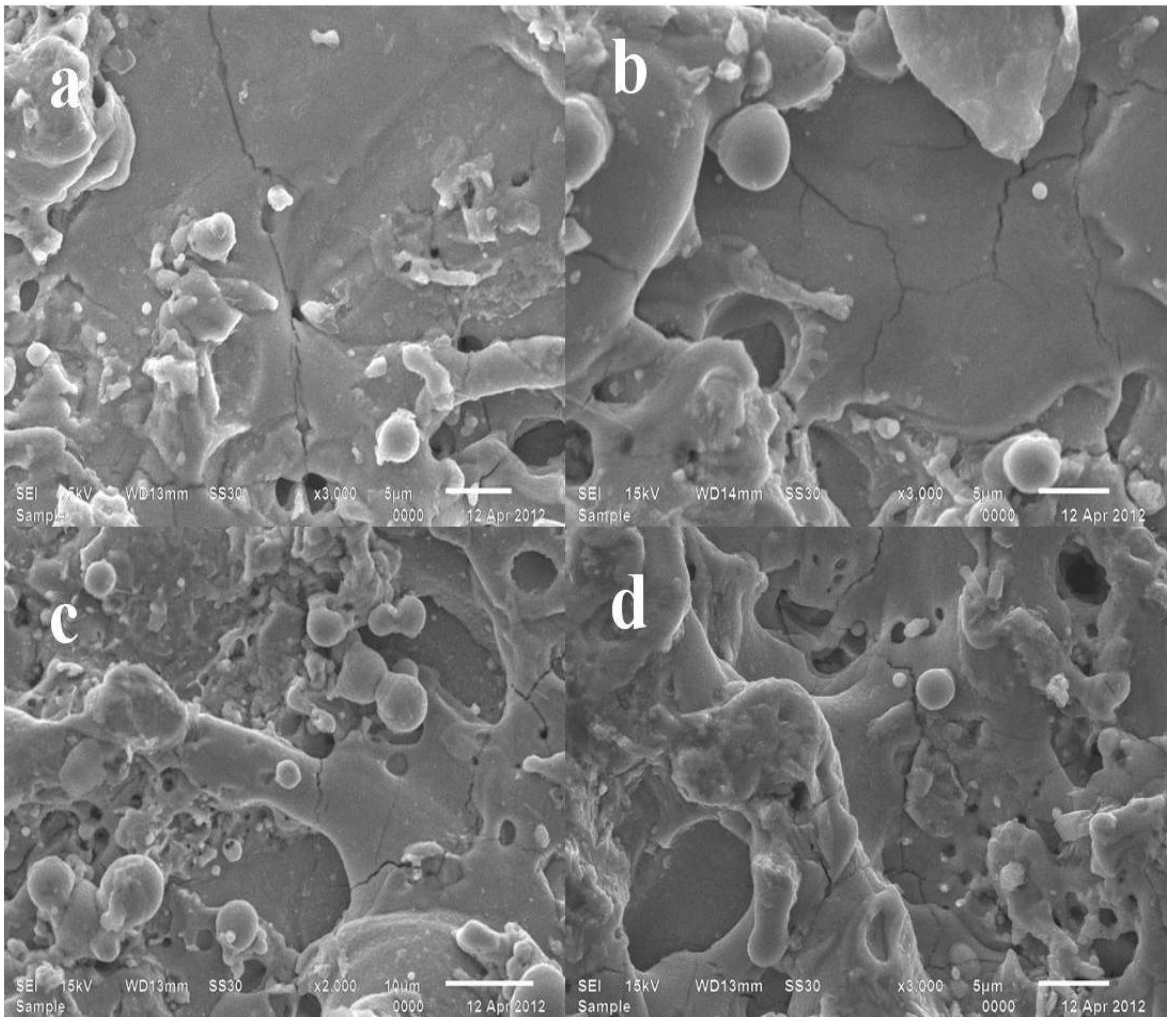

Figure 5.59 SEM micrographs of length of cracking show (a) surface cracks, (b) penetrating cracks, (c, d) cracks is visualized around globular or irregularly shaped attachments on crater rims

It is observed from the plot that, the recast layer thickness tends to increase from 35μm to 50μm significantly with parallel increase of peak current and pulse on time. This can be attributed to the increase in peak current generates stronger sparks causing a higher temperature and there is a formation of more molten material. The dielectric used for flushing is unable to flush away progressively the molten metal, and hence it gets deposited in the parent material. Subsequently, the un-flushed molten metal is quenched, and re-solidifies and thus thicker recast layer thickness is formed [Govindan and Joshi, 2012]. With the longer pulse on time, the produced heat, which is generally very high,

conducted deep into the material, melts more material, and thus after subsequent quenching, deeper recast layer is formed.

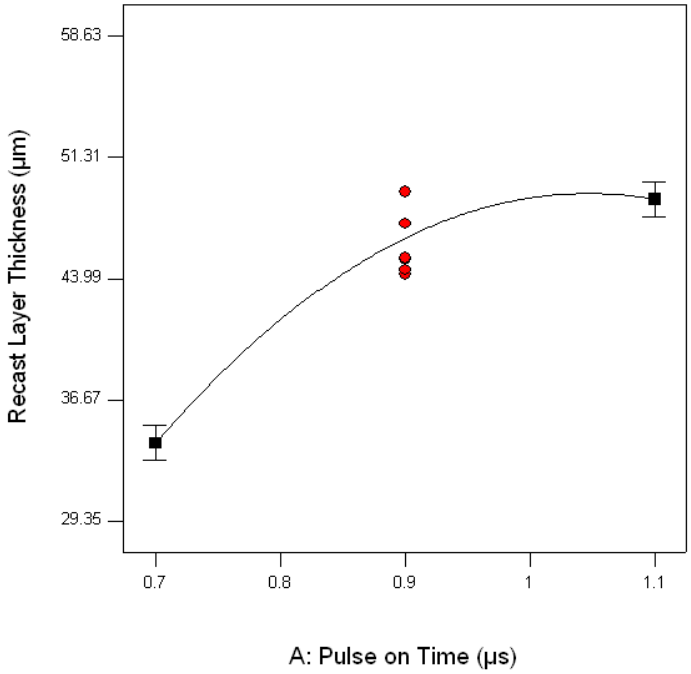

Figure 5.60 Effect of pulse on time on recast layer thickness

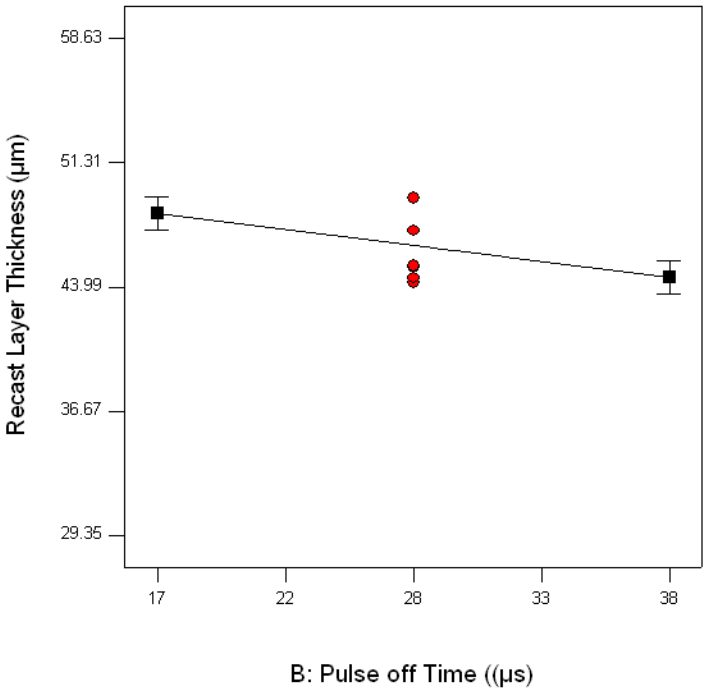

Figure 5.61 Effect of pulse off time on recast layer thickness

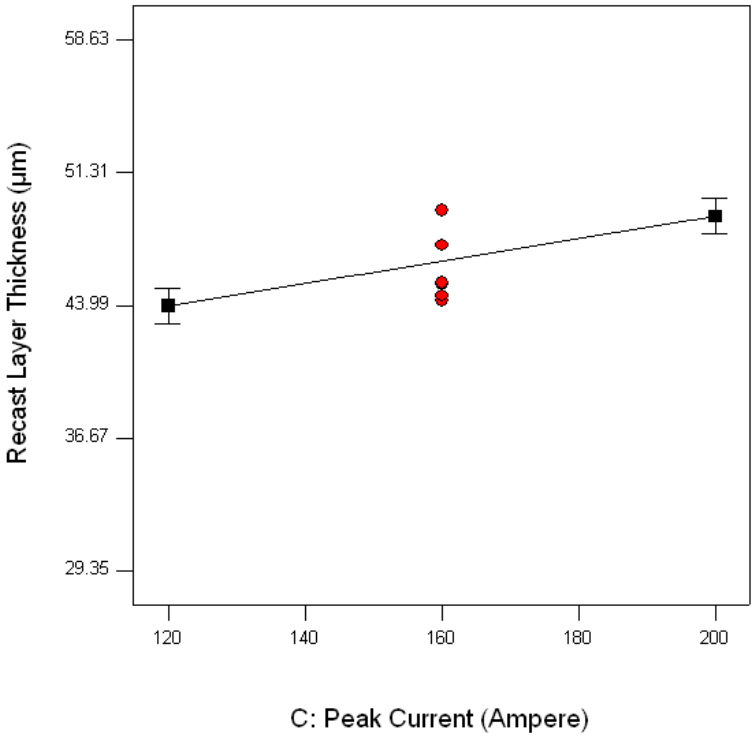

Figure 5.62 Effect of peak current on recast layer thickness

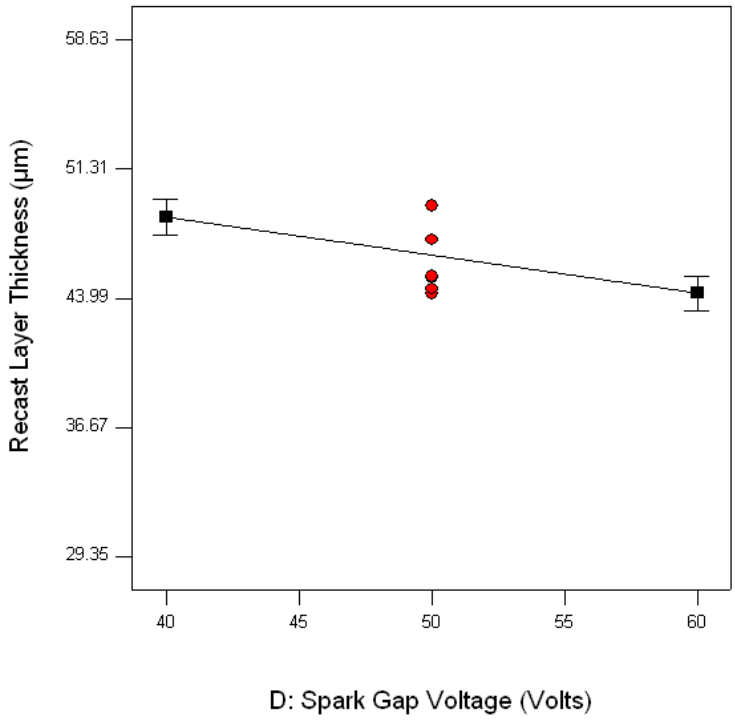

Figure 5.63 Effect of spark gap voltage on recast layer thickness

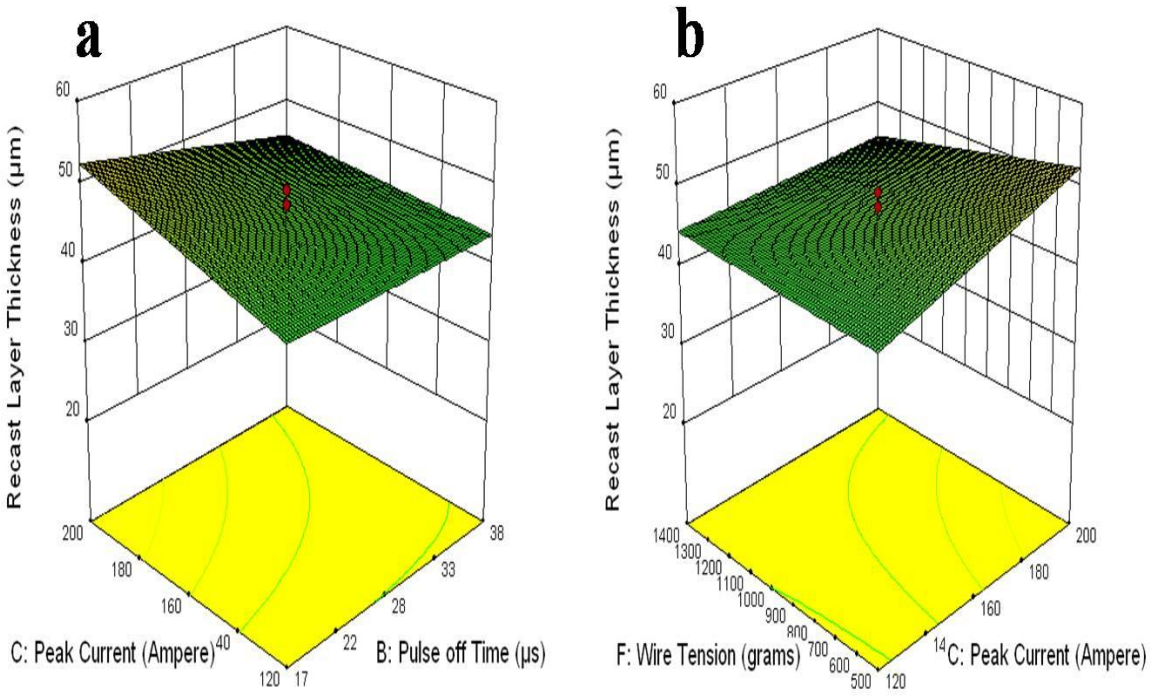

Figure 5.64 Three dimensional interaction plots showing the effects of two parameters on recast layer thickness (a) pulse off time and peak current, (b) peak current and wire tension

5.4 MULTI-RESPONSE OPTIMIZATION USING DESIRABILITY FUNCTION

[Derringer and Suich, 1980] describe a multiple response method called desirability. It is an attractive method for industry for optimization of multiple quality characteristic problems. The method is attractive because it is intuitive and simple. The inputs are mean response estimates, target value, and upper and lower acceptability bounds. The individual desirability is combined using the geometric mean. The desirability of a product characteristic value depends on the lower and upper ranges of product specification. Improper selection of ranges can result in a very different "optimum." The basic idea of the desirability function approach is to transform a multiple response problem into a single response problem by means of mathematical transformations. The desirability function involves transformation of each estimated response variable $\hat{y}$ to a desirability value di, where $0 \leq di \leq 1$. The value of di increases as the "desirability" of the corresponding response increases. The procedure followed in this work for

simultaneous optimization of the three responses is a modification of the method developed by [Montgomery, 2002].

Step-1 Calculate the individual desirability (di) for each response ($\hat{y}$).

Step-2 Combining individual desirabilities to obtain composite desirability (DG) for given weights of material removal rate, wire wear ratio and surface roughness. Composite desirability is the weighted geometric mean of individual desirability for the given responses.

Step-3 Maximizing the composite desirability and identifying the optimal parameter combinations.

$$di = \begin{cases} 0 & \hat{y} < Ai \\ (\hat{y} - Ai/ti - Ai)^{w} & Ai \le \hat{y} \le ti \\ 1 & \hat{y} > ti \end{cases} \quad (5.10)$$

If the target (ti) is to minimize a response, the individual desirability (di) is calculated as

$$di = \begin{cases} 1 & \hat{y} < ti \\ (Bi - \hat{y}/Bi - ti)^{w} & ti \le \hat{y} \le Bi \\ 0 & \hat{y} > Bi \end{cases} \quad (5.11)$$

Where,

Ai = lower limit value of response $\hat{y}$

Bi = upper limit value of response $\hat{y}$

If the object for the response is a target value, then individual desirability (di) is calculated as:

di = $[(\hat{y} - Ai) / (ti - Ai)]^{w}$ $Li \le \hat{y} \le ti$

di = $[(Bi - \hat{y}) / (Bi - ti)]^{w}$ $ti \le \hat{y} \le Bi$

di = 0 if $\hat{y} < Ai$

di = 0 if $\hat{y} > Bi$

If the importance is same for each response, the composite desirability (DG) the geometric mean of all desirability functions and is given by

$$DG=(d_1 \times d_2 \times d_3 \times \ldots\ldots\ldots\ldots\ldots \times d_n)^{1/n} = \left(\prod_{i=1}^{n} di \right)^{1/n} \quad (5.12)$$

Where n = no. of responses=3

It can be extensive to reflect the possible difference in the importance of different responses by giving weights. Where the weight wi satisfies 0<wi<1 and $w_1 + w_2 +$---------$w_n = 1$

$$DG=(d_1^{w1}\times d_2^{w2} \times \ldots\ldots\ldots\ldots.d_n^{wn})^{1/n} \quad (5.13)$$

The factor settings with maximum total desirability are considered to be optimal parameter combination. In the present work, desirability function is utilized to determine the optimum parameter combinations for optimization of machining rate, surface roughness, material removal rate (MRR), overcut, dimensional deviation wire wear ratio, surface crack size density and recast layer thickness.

Table 5.17 illustrates the constraints for carrying out optimization of responses i.e. machining rate, surface roughness, MRR, overcut, dimensional deviation wire wear ratio, surface crack size density and recast layer thickness respectively. Goals to maximize, minimize or to keep the response at a target value and limits for control factors are established for each response individually in order to accurately determine their impact on individual desirability. Weights are assigned to give added emphasis to upper / lower bounds or to emphasize a target value. The default value '1'of weight is assigned to a goal to adjust the shape of its particular desirability function. The default value '3' and '5' taken by design expert® software is used to designate importance of objective function. The ultimate objective of optimization is to find a good set of conditions that will meet all the goals. It is not necessary that the value of desirability is always 1.0 as this value is completely dependent on the manner in which lower and upper limits are set relative to the actual optimum [Aggarwal et al., 2008]. This data is used for carrying out multi-objective optimization of machining rate, surface roughness, material removal rate (MRR), overcut, dimensional deviation, wire wear ratio, surface crack size density and recast layer thickness using design expert® are presented in Table 4.9 and Table 4.10. It shows first twenty five optimal solutions. Solution number 1 is selected as the optimal parameter combination because it is having desirability closer to one. Table 5.18 and Table 5.19 shows the values of 25 levels combinations of process parameters that will give high value of composite desirability (ranged from 0.603 to 0.533), and the predicted values of responses obtained are also given.

Figure 5.65 to 5.67 shows the three dimensional response surface, optimized bar histograms and ramp graphs for overall desirability of all the responses i.e. machining rate, surface roughness, material removal rate (MRR), overcut, dimensional deviation, wire wear ratio, surface crack size density and recast layer thickness. The near-optimal

region was located close to the right hand center region of the plot, which had a composite desirability value greater than 0.603 that gradually reduced as we moved left and upwards.

Table 5.17 Constraints of input parameters and responses

Parameters	Target	Lower limit	Upper limit	Lower weight	Upper weight	Importance
T_{on}	In range	0.7	120	1	1	3
T_{off}	In range	17	38	1	1	3
Ip	In range	120	200	1	1	3
SV	In range	40	60	1	1	3
WF	In range	4	10	1	1	3
WT	In range	500	1400	1	1	3
Machining rate	maximize	0.395	1.28	1	1	5
MRR	maximize	3.28	11.16	1	1	5
Surface roughness	minimum	2.15	3.28	1	1	3
Dimensional deviation	minimum	140	165	1	1	3
Overcut	minimum	22	43	1	1	3
Wire wear ratio	minimum	0.048	0.107	1	1	3
Surface crack size density	minimum	0.004	0.025	1	1	3
Recast layer thickness	minimum	29.35	58.63	1	1	3

Table 5.18 Optimal solutions for machining rate; surface roughness, dimensional deviation and wire wear ratio

Exp. no.	T_{on} (µs)	T_{off} (µs)	Ip (Ampere)	SV (Volt)	WF (m/min)	WT (grams)	Machining rate (mm/min)	Surface Roughness (µm)	Dimensional Deviation (µm)	Wire wear ratio (WWR)	Desirability
1	1.1	38	165	40	4	1400	0.737	2.43	149.67	0.065	0.565
2	1.0	38	160	40	4	500	0.725	2.40	149.63	0.065	0.564
3	1.1	38	151	43	4	500	0.726	2.44	149.35	0.065	0.564
4	1.0	38	166	46	4	500	0.726	2.40	150.15	0.066	0.562
5	1.1	33	173	40	4	500	0.731	2.49	148.74	0.065	0.562
6	1.1	30	154	40	10	1394	0.790	2.53	150.31	0.065	0.561
7	1.1	38	144	40	5	1398	0.719	2.47	148.50	0.065	0.559
8	1.1	26	151	40	10	500	0.741	2.47	149.64	0.066	0.554
9	1.1	31	157	40	10	1393	0.724	2.39	150.36	0.067	0.549
10	1.0	21	130	40	4	1400	0.730	2.47	149.22	0.067	0.548
11	1.0	23	145	40	10	1400	0.662	2.37	147.54	0.067	0.547
12	1.1	24	146	40	10	500	0.721	2.41	150.18	0.061	0.546
13	0.9	21	154	40	4	1400	0.707	2.45	148.75	0.067	0.546
14	1.1	26	137	40	10	500	0.799	2.51	151.40	0.064	0.544
15	1.0	28	154	40	9	505	0.762	2.44	151.38	0.064	0.544
16	1.1	38	138	43	10	1400	0.745	2.43	150.89	0.060	0.540
17	0.9	18	149	40	4	1400	0.708	2.48	148.24	0.064	0.534
18	1.1	25	138	40	9	1400	0.765	2.45	151.37	0.072	0.534
19	0.9	17	162	40	4	1400	0.734	2.45	150.24	0.074	0.531
20	0.9	17	152	40	4	500	0.721	2.43	150.00	0.073	0.530
21	1.1	38	148	41	4	788	0.719	2.43	150.32	0.058	0.525
22	1.1	26	142	48	4	1400	0.759	2.49	150.91	0.074	0.523
23	1.0	38	156	48	4	1100	0.725	2.43	150.56	0.076	0.519
24	1.0	22	148	40	7	500	0.761	2.53	150.60	0.065	0.515
25	1.0	38	176	58	10	500	0.709	2.47	149.41	0.077	0.515

Table 5.19 Optimal solutions for MRR; overcut, surface crack density and recast layer thickness

Exp. no.	T_{on} (µs)	T_{off} (µs)	Ip (Ampere)	SV (Volt)	WF (m/min)	WT (grams)	MRR (mm^3/min)	Overcut (µm)	SCD_i (µm/ $µm^2$)	RCL_t (µm)	Desirability
1	1.1	38	165	40	4	1400	7.63	29.20	0.004	29.336	0.603
2	1.0	38	160	40	4	500	7.46	28.82	0.004	29.321	0.599
3	1.1	38	151	43	4	500	7.14	28.11	0.004	29.045	0.589
4	1.0	38	166	46	4	500	7.53	29.80	0.004	29.337	0.583
5	1.1	33	173	40	4	500	7.98	31.21	0.004	29.288	0.579
6	1.1	30	154	40	10	1394	7.79	30.79	0.004	29.349	0.577
7	1.1	38	144	40	5	1398	7.00	28.15	0.004	29.275	0.577
8	1.1	26	151	40	10	500	8.47	32.40	0.004	29.237	0.577
9	1.1	31	157	40	10	1393	7.79	30.81	0.004	29.326	0.576
10	1.0	21	130	40	4	1400	9.19	33.79	0.004	29.379	0.574
11	1.0	23	145	40	10	1400	8.87	33.28	0.004	29.406	0.573
12	1.1	24	146	40	10	500	8.84	33.23	0.004	29.420	0.573
13	0.9	21	154	40	4	1400	8.38	32.37	0.004	29.444	0.573
14	1.1	26	137	40	10	500	8.16	31.95	0.004	29.551	0.571
15	1.0	28	154	40	9	505	8.08	31.89	0.004	29.586	0.568
16	1.1	38	138	43	10	1400	6.78	27.87	0.004	29.606	0.566
17	0.9	18	149	40	4	1400	8.69	33.27	0.004	29.639	0.564
18	1.1	25	138	40	9	1400	8.41	32.76	0.004	29.667	0.563
19	0.9	17	162	40	4	1400	8.84	33.74	0.004	29.677	0.558
20	0.9	17	152	40	4	500	8.96	34.01	0.004	29.704	0.555
21	1.1	38	148	41	4	788	7.07	29.65	0.004	29.735	0.553
22	1.1	26	142	48	4	1400	7.64	31.45	0.004	29.742	0.552
23	1.0	38	156	48	4	1100	7.20	30.55	0.004	29.795	0.543
24	1.0	22	148	40	7	500	8.55	30.97	0.004	29.431	0.536
25	1.0	38	176	58	10	500	6.94	30.45	0.004	29.831	0.527

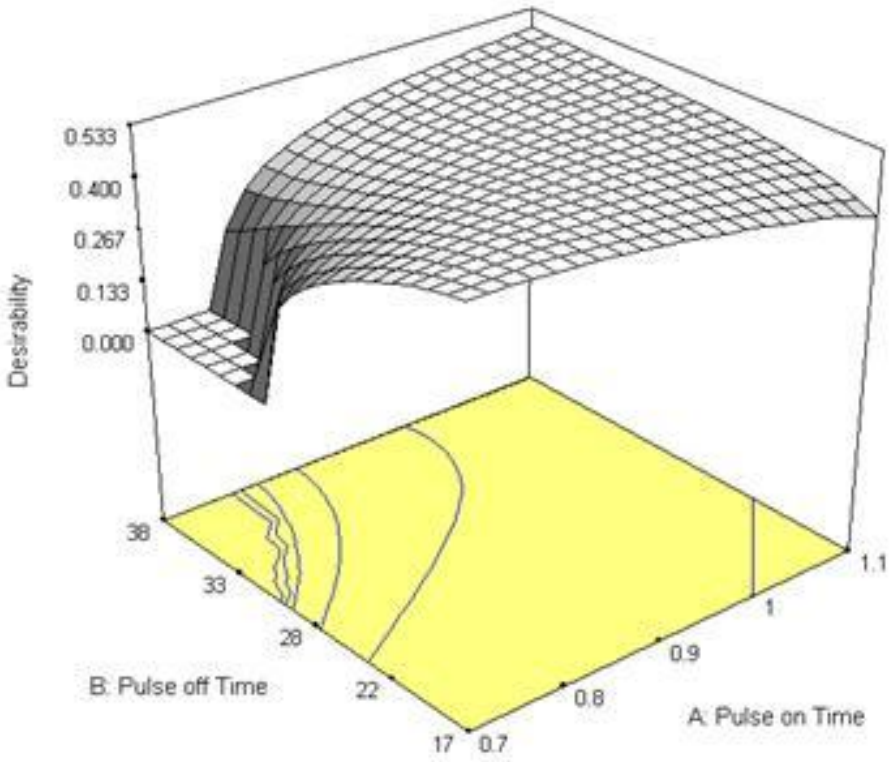

Figure 5.65 3D surface plot of composite desirability for all responses

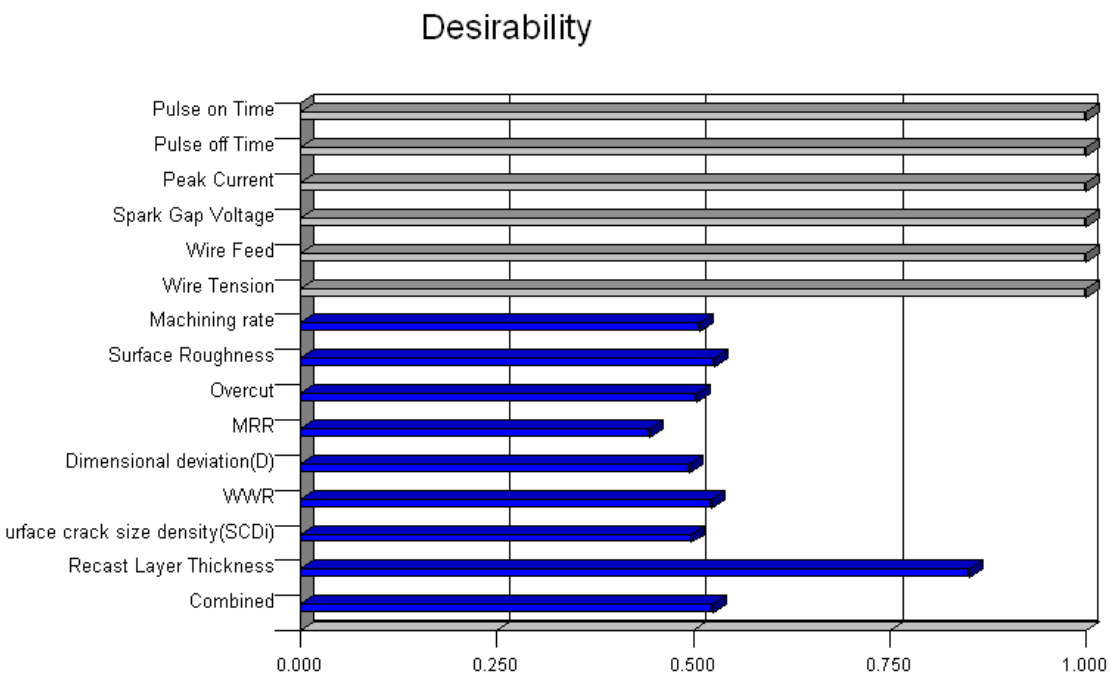

Figure 5.66 Bar histogram plot of composite desirability for all responses

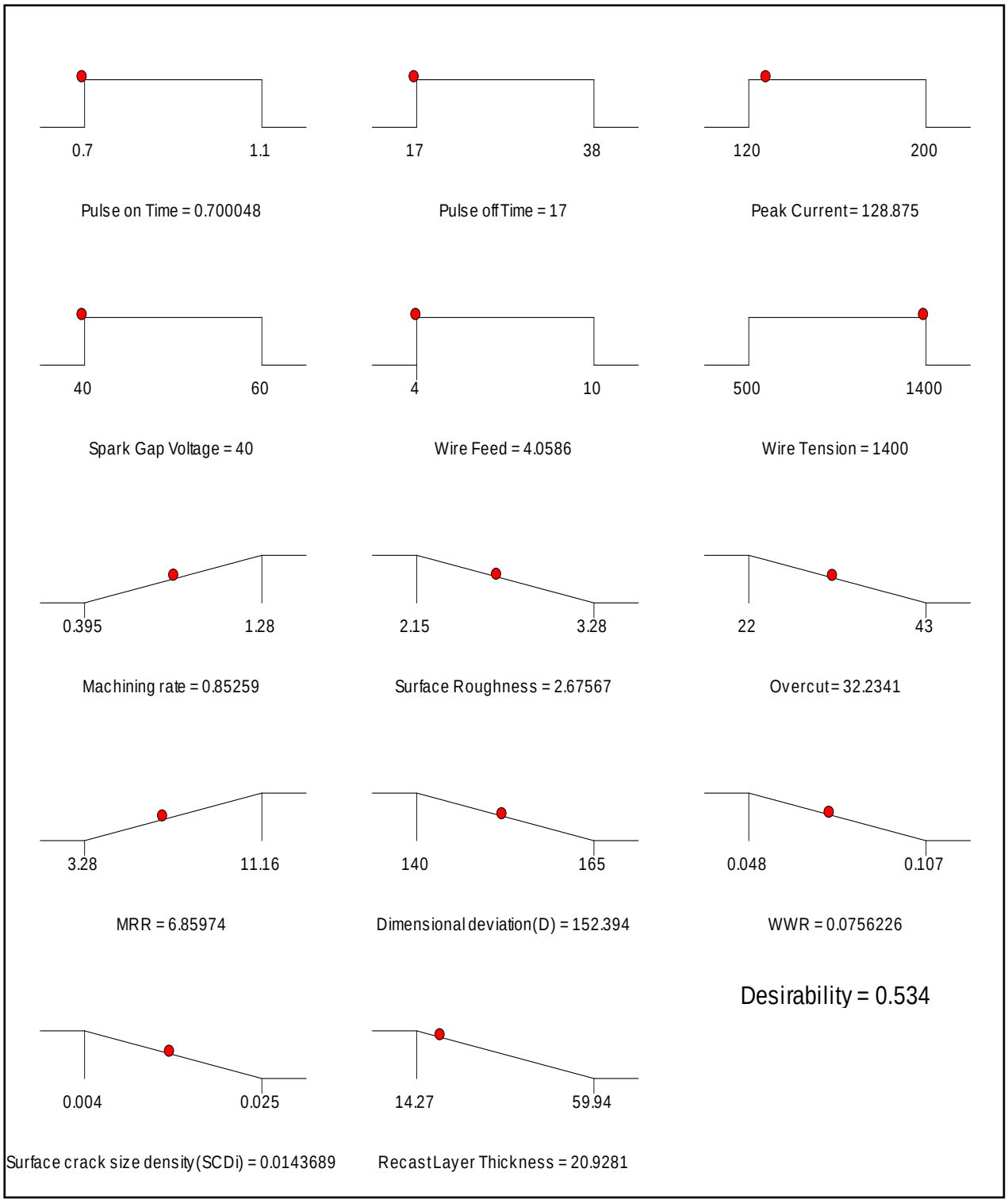

Figure 5.67 Ramp graph of optimal setting for all responses

5.4.1 Confirmatory experiments

Confirmatory experiments are carried out at the optimized value of response characteristics to check the validity of optimization results. Table 5.20 shows the results obtained from confirmatory experiments. The error between the predicted values and the experimental observations lies within ± 5%. Thus, confirmatory experiments confirm excellent reproducibility of the results.

Tables 5.9 to 5.16 can be utilized as technology guidelines to select the machining parameters as per the needs of part drawings.

Table 5.20 Experimental validations of developed models with optimal parameter settings

Responses	Predicted	Experimental	Error (%)	Desirability
Machining Rate (mm/min)	0.8525	0.8912	4.342	0.588
MRR(mm^3/min)	7.63	8.20	6.95	0.588
Surface roughness(μm)	2.64	2.53	4.303	0.562
Dimensional deviation(μm)	151.60	147.63	2.689	0.561
Overcut(μm)	29.20	31.17	6.32	0.573
Wire wear ratio	0.065	0.069	5.79	0.565
Surface crack size density(μm/$μm^2$)	0.0039	0.0041	4.87	0.688
Recast layer thickness(μm)	29.23	30.29	3.49	0.665

5.5 MICROSTRUCTURE AND MATERIAL TRANSFORMATION ANALYSIS OF MACHINED SURFACES

The present research work is mainly focused on the investigation of integrity of the work surface and wire electrode surface after machining with WEDM. Experimental results showed that pulse on time, pulse off time and peak current significantly affected the surface integrity with the formation of deep-wide overlapping craters, pock marks, debris, micro cracks and recast layer. The discharge energy impinged on the work piece during WEDM melts the material and debris are flushed away by dielectric. Thermal action of EDM process affects the surface integrity of a machined component [Yadav et al., 2002]. An extremely fast heating, melting and vaporization is followed by a fast cooling of work material in the sparking zone during the process of metal removal, produce a huge change

in the surface topography of the work piece. Thus, surface integrity analysis is done with a view to analyze the parametric influence on the surface defects i.e. voids, cracks, roughness as well as on the thickness of the recast layer deposited on the machined surface. Both carbides and oxides were formed either in free form and/or in compound form due to decomposition of de-ionized water, machined samples and wire material. WEDM cut parts must often be post-processed to remove the negatively affected material. Furthermore, the surface integrity effects are dependent upon both the WEDM process parameters and the chemical composition of the workpiece. Much work has been devoted to the study of surface integrity in WEDM of common steel alloys, particularly tool and die-steels. However, little research has been reported on the effects of WEDM on the surface characteristics of pure titanium. Specifically, no significant literature has been found relating to surface integrity of pure titanium.

The following subsections investigate the effect of process parameters on microstructure and the thickness of recast layer produced in the machined pure titanium (grade-2) samples.

5.5.1 Material and test condition

During experiments, parameters such as pulse on time, pulse off time, peak current and spark gap voltage were varied to explore their effects on surface integrity of pure titanium. After WEDM, the metallographic investigations of machined samples were made using energy dispersive X-ray analysis (EDX), scanning electron microscope (SEM) and X-ray diffraction (XRD) techniques. In present study, the surface integrity was analyzed by using scanning electron microscope (JEOL, Japan, JSM-6610LV) and an energy-dispersive X-ray spectrometer (EDX). The machined samples were etched with Krolls reagent (2ml Hydrofluoric acid, 10ml nitric acid and 88ml distilled water). Then the samples were also cleaned with acetone $(CH_3)_2CO$. The X-ray diffraction analysis (XRD) was used to investigate the material transfer from dielectric fluid and tool electrode on the machined surface.

5.5.2 Results and discussion on the machined surface topography

The quality of a machined surface is generally characterized by surface topography which includes micro-cracks, heat affected zone, recast layer and phase transformations on the surface and subsurface regions. The surface properties might be altered due to effect of process parameters such as pulse on time, pulse off time, peak current and spark gap

voltage. It was observed from SEM micrographs, (Figure 5.68) that machined surface contained globules of debris, spherical particles, craters, pockmarks and micro-cracks. The pulse on time (1.1μs) and peak current (200A) were observed as the most significant parameters affecting the surface properties. The increase in pulse on time resulted in the formation of deep craters on the machined surface. These deep and overlapping craters were formed due to successive electrical discharge, intense heat transferred to the surface of the sample which caused local melting or evaporization of work material. Some of the molten material produced by the discharge was carried away by the deionized water. The remaining molten material re-solidified to form lumps of debris as observed in Figure 5.68(f). During short pulse on-time, electric sparks produced small craters on work surface as shown in Figure 5.68(d). During WEDM some of titanium particles protruded and completely dislodged from the machined surface as observed in Figure 5.68(e-g) at higher values of pulse on time (1.1μs) and peak current (200A). Also the formation of spherical shape particles was observed and it may be due to surface tension of molten material. Matt surfaces with many fine nodules were also observed in Figure 5.68(b). These nodules may be formed due to solidification of molten or vaporized titanium particles during machining. The machined surface included minor hillocks and valleys as seen in Figure 5.69(a-c) at intermediate magnitudes of pulsed current (160A) and pulse-on duration (0.9μs). The more frequent melt expulsion resulted in the formation of deep and larger craters on the machined surface as shown in Figure 5.68(e).

The main possible reason for deep and big craters is the oxidation reaction, the impulsive force of dielectric pressure concentrated on localized spark gap area. It was observed from Figure 5.68(d-f) that WEDM surfaces may also have macro-ridges as formed by melted material. This melted material was blasted out of the machined surface by the discharge pressure. Then it reached solidification temperature, being cooled by the surrounding dielectric fluid. It was observed from SEM micrographs Figure 5.70(a-f) that fewer craters and no micro-cracks were formed at low peak current (120A) and pulse on time (0.7μs). Due to low peak current and pulse on time, the work surface is impinged with less intensive discharge. High peak current and low pulse off time increased the debris in the spark gap, which lead to abnormal arcing. The abnormal arcing decreases the discharge rate and material removal rate [Sarkar et al.; 2010].

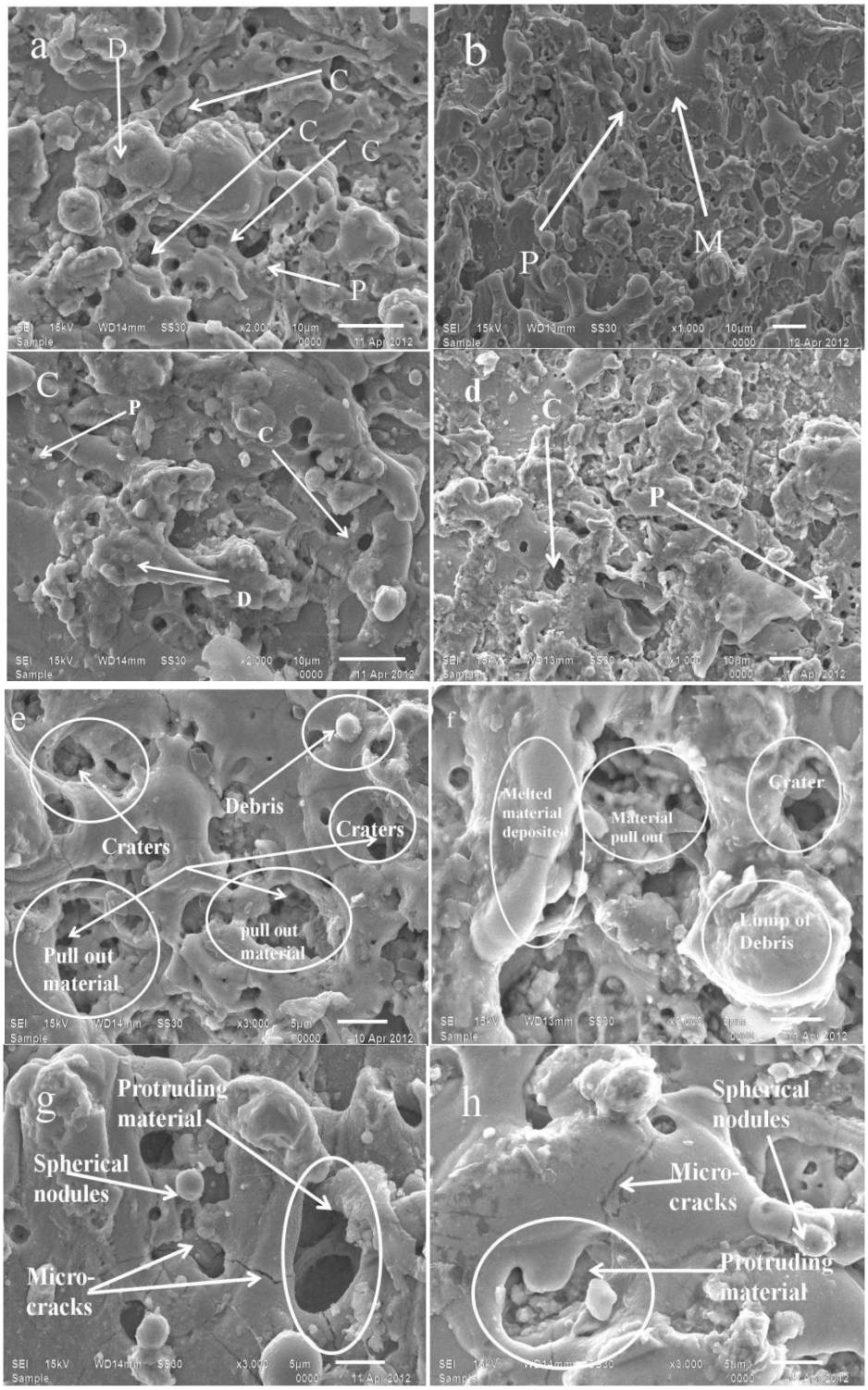

Figure 5.68 SEM micrographs observed with C→Craters, P→Pockmarks, D→Debris, →Matt surface, spherical nodule and protuding material at higher pulse on time =1.1µs, pulse off time = 17µs and peak current=200A Ra= 3.22µm, 2.93µm, 2.68µm, 2.55µm.

The percent contributions of various factors have been shown in Fig. 5.90(a). The percentage contribution of pulse on time: 42.31%, pulse off time: 13.85%, peak current: 36.92%, spark gap voltage: 4.62% and error: 2.31%.

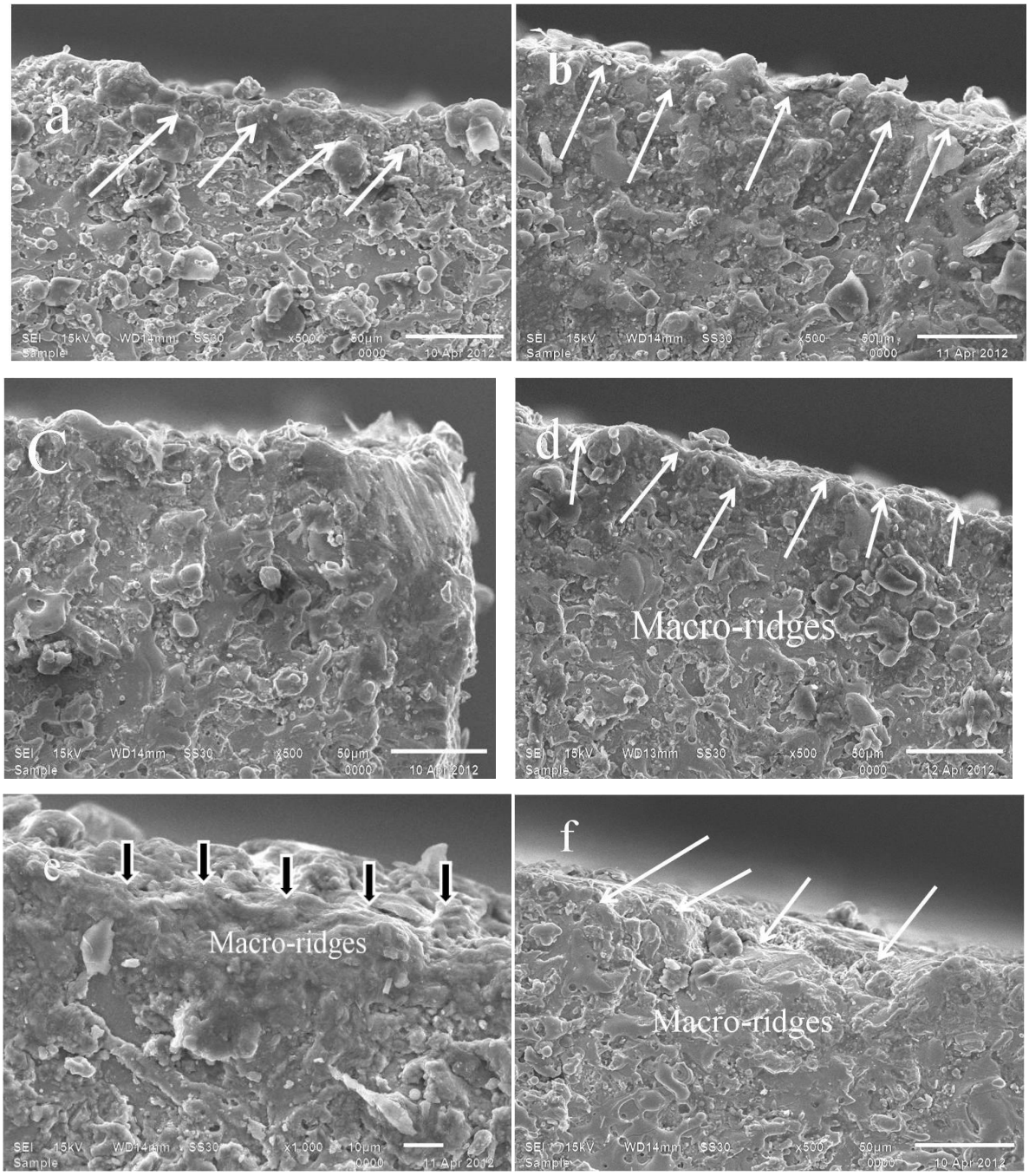

Figure 5.69 Minor hillocks, valleys and macro-ridges at peak current =160A, pulse off time = 26µs and pulse on time = 0.9µs.

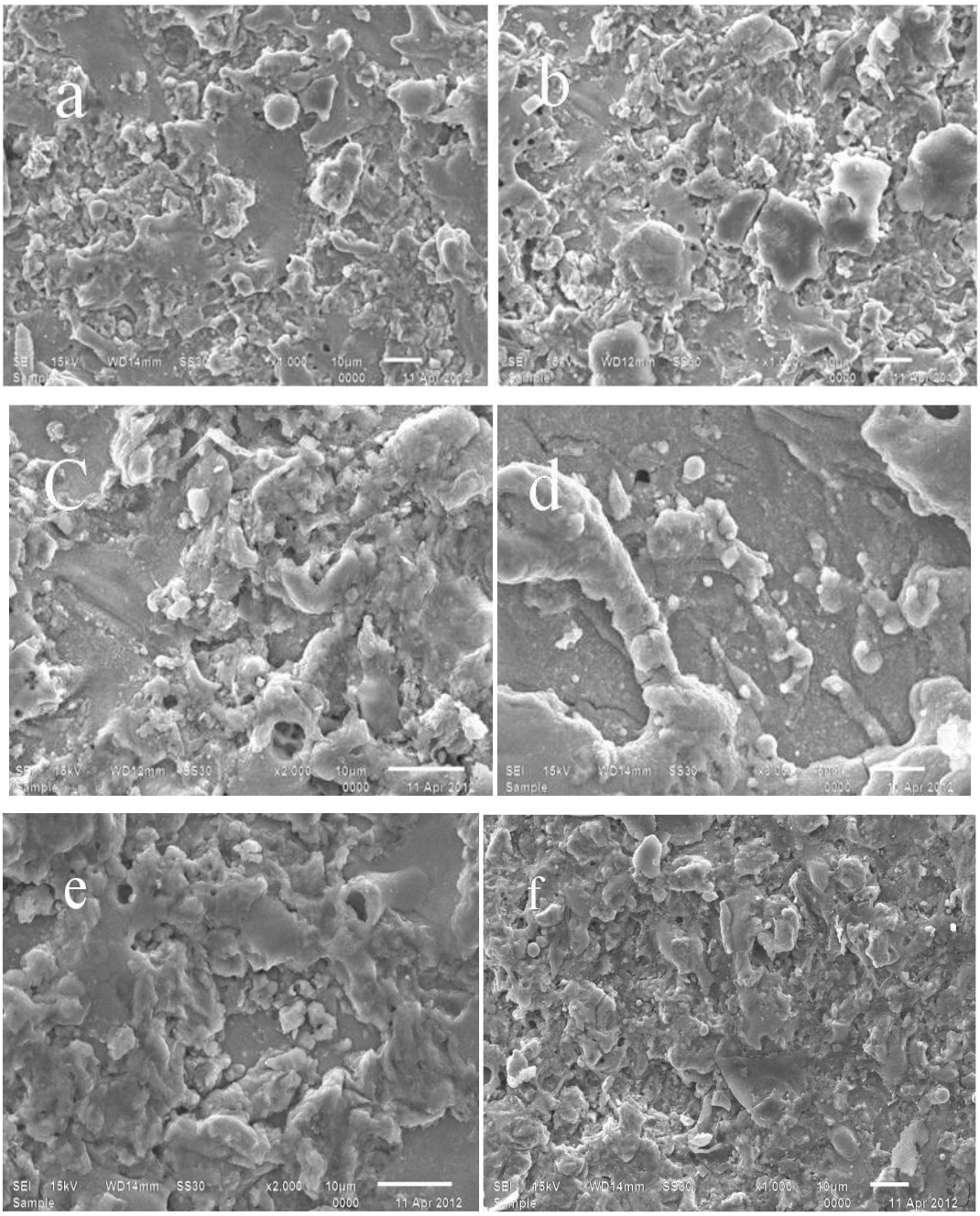

Figure 5.70 SEM micrographs with less number of craters and no cracks were formed at lower peak current =120A,pulse on time= 0.7µs and pulse off time = 38µs and surface roughness = 2.15µm, 2.23µm, 2.48µm, 2.28µm,2.42µm and 2.35µm.

5.5.3 Results and discussion on heat affected zone

The surface integrity of machined samples was also altered by two layers i.e. heat affected zone (HAZ) and recast layer (RL). The dramatic temperature changes in the workpiece associated with WEDM induce change of phase in the material. Regions that achieve the melting point are called fusion or molten region. For the molten areas the phase changes from solid to liquid (and perhaps to gas as well). The neighborhood of the

fusion zone experiences similar rise and fall in temperature but the highest temperature does not necessarily reach the melting point of the workpiece. This region is called the heat-affected region. The heat affected zone is formed below the recast layer. Heat affected zone is formed due to rapid heating and quenching in WEDM process [Lee and Li, 2003]. The work and tool electrode elements melted and resolified near the heat affected zone as observed in Figure 5.71. The thermal residual stresses produced some cracks near this zone [Yadav et al., 2002]. The residuals of spherical nodules in free or compound form were observed in the Figure 5.71 (b, d). These spherical nodules were formed due to high peak current which may result in the formation of martensite α structure. A visible martensite microstructure is formed with lamellar α (light in color)+β (dark in color) structure due to extreme heating caused by discharge and rapid cooling of dielectric as shown in Figure 5.72(a-c). The heat affected zone showed the indication of grain growth and over tempering phenomena. The formation of crack is also observed due to the high peak current (200A) as shown in Figure 5.71(a).

When the induced stress exceeds the material's ultimate tensile strength there is formation of crack in the HAZ surface [Hascalik and Caydas, 2007a, b]. Pure titanium has low thermal conductivity, hence a faint tempered layer is observed in Figure 5.71(d). This may be attributed to slower dissipation of the heat from the region (under the surface) as compared to the upper surface which is exposed to rapid cooling action by dielectric fluid. It is interesting to note that some of spherical deposits, composed of the elements from both wire electrode and titanium workpiece were also observed, as shown in Figure 5.71(d-f). Adjoining to the spherical deposits, an oxygen-rich layer was also observed. These features of deposit can represented as "Bull eye". Moreover theses deposits were consistently covered with oxide layer showed the same effect in WEDM of finish cut for martensitic steel[Huang et al.; 2004].

5.5.4 Results and discussion on recast layer (RL)

The recast layer was observed at the cross section of the WEDM surface. The recast layer is defined as the material melted by electrical discharge and re-solidified on the work surface without being ejected nor removed by dielectric fluid [Lee, 2003]. It is very difficult to remove and its appearance is observed through a scanning electron microscope at different levels of magnification. Below the recast layer there is the heat-affected zone.

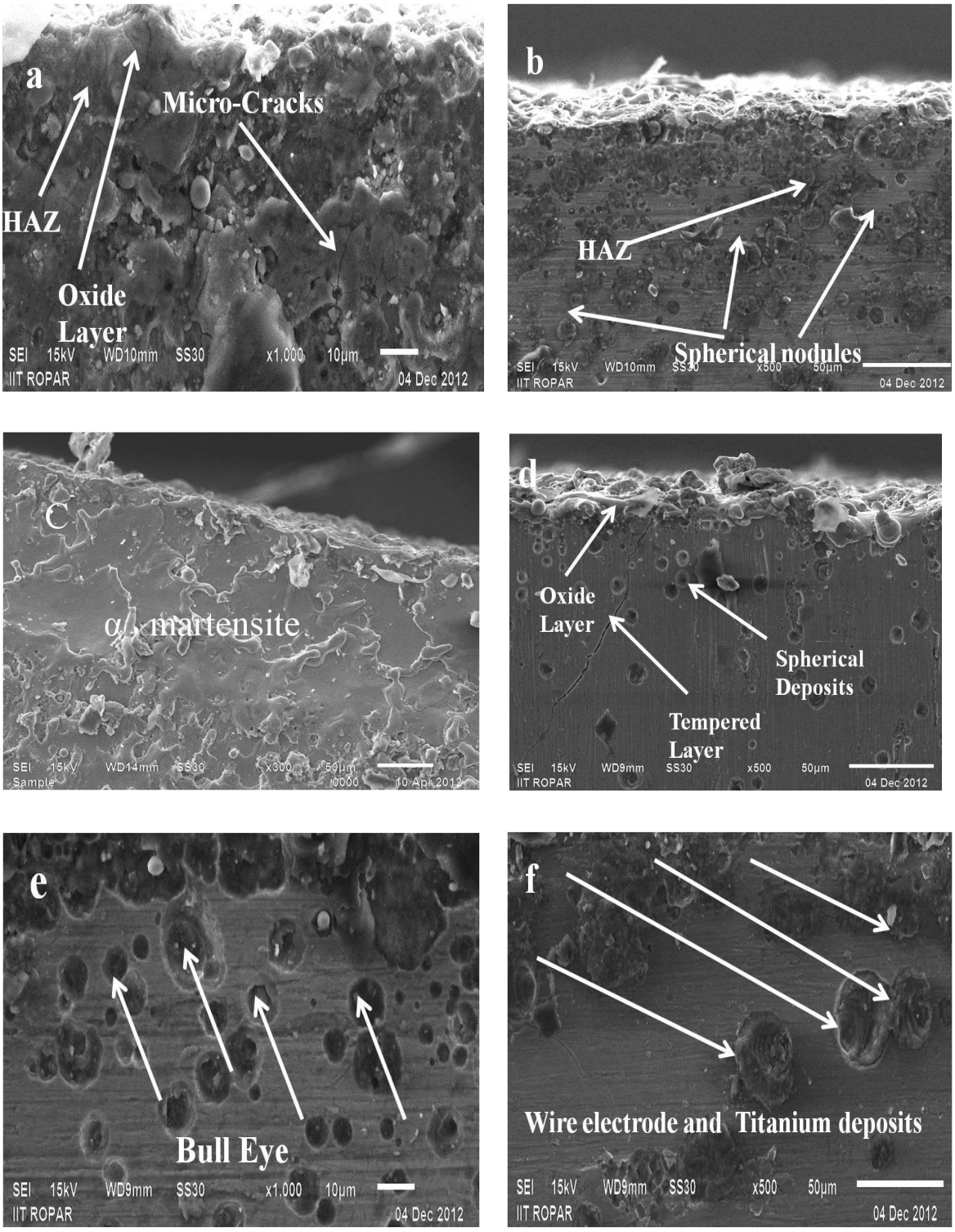

Figure 5.71 SEM micrographs of heat affected zone (HAZ) at higher pulse on time = 0.9µs, pulse off time = 17µs and peak current=200A

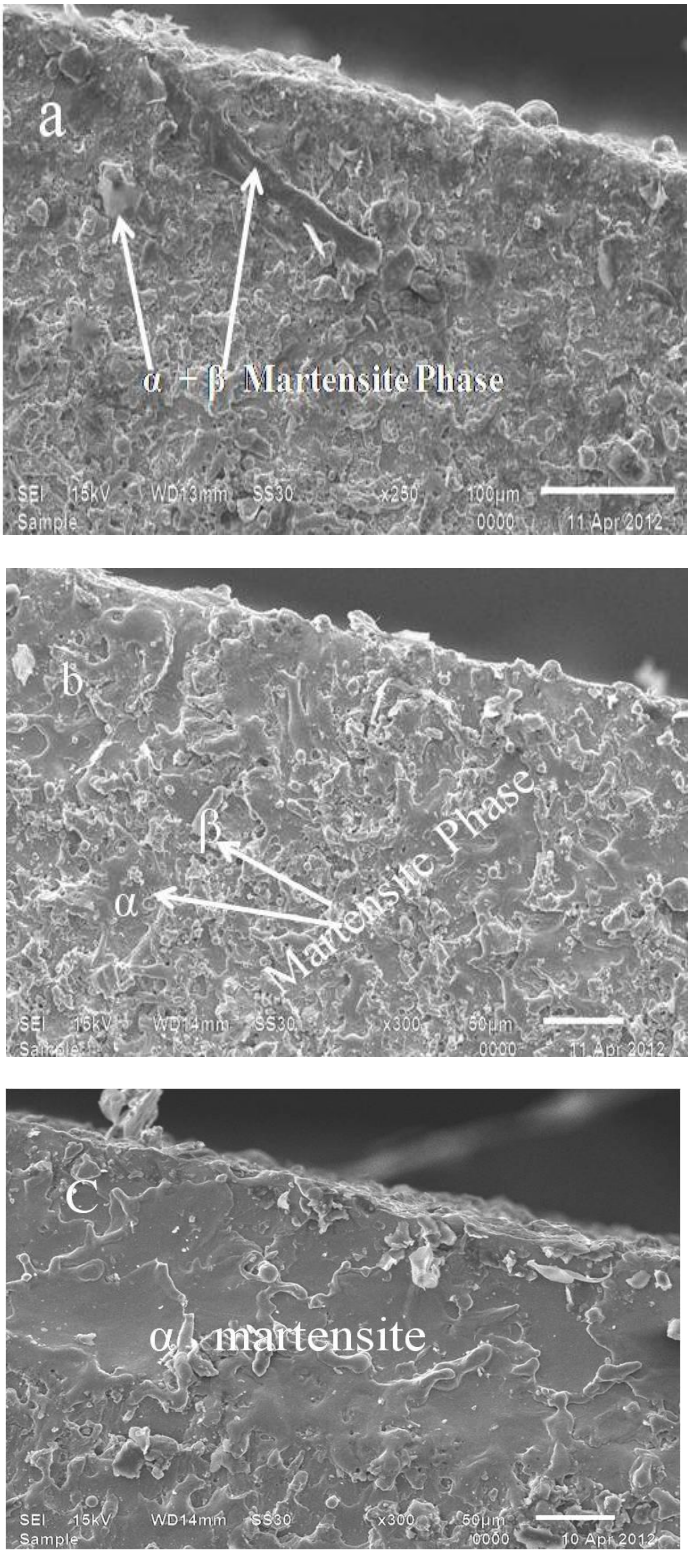

Figure 5.72 SEM micrographs of (α+β) martensite phase

The recast layer thickness was changed due to superficial hardening of the work material by the discharge heat of electrical spark. The intensity of spark depends on peak current, pulse on time and pulse off time. The thickness of recast layer of WEDM surface was increased due to increase of peak current, pulse on time and decrease of pulse off time as

observed in Figure 5.73(a-h). Due to increase of pulse on time and peak current the melting of isothermals becomes more intense, which further penetrates into base metal and the result extends the thickness of recast layer. It is clear that recast layers appear as non-uniform and have wave like pattern. There are some micro-cracks trenchant into recast layer which even cleave into adjacent matrix phase as shown in Figure 5.73(d). The micro-cracks cleaving into matrix have detrimental effects on mechanical properties. The size of the inside crack is approximately 4μm in width. The service life of materials with micro-cracks will be reduced extremely, especially in fatigue and corrosion environment. The micro-cracks in the recast layer were observed due to heat of corrosive debris and formed in a dense, coarse dendrite structure [Rajesha et al., 2012]. Dendrites and sub-layers with different orientations are observed in Figure 5.73(f) marked as A, B, C and D. The average thickness of recast layer, as observed is having a variation of 6μm to 58μm. Due to the variable nature of the recast layer observed, an average must be taken.

The average recast layer thickness was calculated by measuring the area of the recast material and dividing by the length of the recast layer as shown in Figure 5.74. The recast area was always measured at the cross-section in six different locations on the sample. Area and length measurements were made by importing the micrographs into Axio-vision Rel.4.8 software. The average thickness of recast layer is as shown in Figure 5.75. Porosity and spherical deposits was also observed in the interface of the recast layer. EDX analysis of the recast layer is shown in Figure 5.76. Through EDX analysis copper, carbon, calcium, titanium and oxygen elements were detected in the recast layer. This may be due to the melting and re-solidification of titanium and brass wire electrode after WEDM. Before machining, the pure titanium is in cast form and is ground using a diamond grinding wheel so that the calcium may be detected due to this reason. Carbon is mostly transferred from work material due to high discharge energy and deposited on the machined surface as titanium carbide. The titanium carbide formation was observed through XRD analysis. The large amount of oxide can be observed on the surface of samples when machining is performed with de-ionized water, as shown in Figure 5.73(d). This can be recognized due to the decomposition of the water droplets isolated in the discharge gap due to larger pulse on time and peak current. The water droplets which can be easily vaporized by the heat generated by the discharge and consequently reacted with the melted material. The melted metal is further oxidized by oxygen decomposed from water vapours during the discharging time. More oxides exist on the surface of samples

when machining is performed with larger peak current. This indicates that the pulse on time and peak current is an important factor that affects the formation of oxides. Furthermore, the higher discharge energy can result in a higher temperature of the discharge gap, which can accelerate the oxidation reaction rate. The oxidation can intensify the discharge and contribute to a larger crater; therefore the samples machined with de-ionized water have a larger material removal rate (7.70mm^3/min) and surface roughness (3.13μm). Regarding to recast layer thickness analysis the percentage contribution of significant parameters is shown in Figure 5.90(b). The percentage contribution of pulse on time: 48.36%, pulse off time: 16.53%, peak current: 28.37%, spark gap voltage: 2.59% and error: 4.15%.

5.5.5 Results and discussion on micro-cracks formation

Crack formation can be attributed to the presence of thermal stress and tensile stress within the machined component. Thermal stress is produced when the electrode discharges bombard the surface of the sample during the machining process. Tensile stress within the sample is generated because not all of the material which melts during the machining process is swept away from the component's surface by the dielectric. Due to the entrance of carbon, the melted material contracts more than the unaffected parent part during the cooling process, and when the stress in the surface exceeds the material's ultimate tensile strength, cracks are formed. Since both tension cracks and voids form during the cooling stage, there would appear to be some relationship between the two. Although results from previous studies have indicated that cracking increases as the pulse energy increases. The formation of micro-cracks is not only affected by the setting of machining parameters but also depends on materials properties such as tensile strength, thermal conductivity, thermal expansion coefficient and Young modulus [Govindan and Joshi, 2012].

The sub-surface cracks of machined samples indicated that the material is amorphous either in free form and/ or in compound form. The formation of micro cracks is generally accompanied by rapid cooling and heating by dielectric fluid. The heating and cooling process resulted in the formation of stresses which leads to crack formation. The cracks distribution on the machined surface was observed determining the density and mean free path of cracks. The cracks at different settings of peak current and pulse on time were observed on the machined surface as in Figure 5.77(a-f). It was observed from these micrographs that the cracks were developed due to high pulse on time and peak current.

The more density of surface cracks was observed to be due to free path of debris [Tai et al.; 2011]. The cracking phenomena indicated that the surface crack density increases with an increasing of pulse on time and peak current. Since it is not easy to compute the cracking in terms of a judgment of the width, length or the depth of crack, or even by the amount of cracking, this research defines a "surface crack size density", i.e. the total length of cracks (μm) in unit area (μm^2) to evaluate the severity of cracking. Observation of these results showed that surface crack size density varies from 0.0053 to 0.0084μm/μm^2 by increasing pulse on time. On the other hand, due to increase of peak current the surface crack size density varies from 0.014 to 0.019μm/μm^2. This result can be vindicated by increasing discharge energy and impulsive force with peak current and pulse on time that leads to removal of more amount of molten material and therefore produces larger cracks and deeper craters. The surface crack size density is observed in Figure 5.79. Moreover higher carbon content prompts the surface hard and brittle at the grain boundaries, which reinforces the surface cracking effect during solidification. Regarding to surface crack size density analysis the percentage contribution of significant parameters is shown in Figure 5.90(c). The percentage contribution of pulse on time: 22.67%, pulse off time: 7.29%, peak current: 59.26%, spark gap voltage: 6.34% and error: 4.4%. More number of cracks (>20) was observed in experiment no.1, 4, 18, 20, 29, 30, 33, 34, 40, 43, 44, 49 and 52 as shown in Figure 5.78. The study observed no formation of surface cracks if machining is carried out according to the machining conditions pertaining to experiment no.3, 11, 16, 19 as shown in Figure 5.80.

5.5.6 Results and discussion on spalling

Spalling is another main WEDM material removal mechanism (MRM) by which small fraction of material will be alienated from the base material [Lauwers et al., 2004]. This spalling effect is most often related to the generation of larger micro-cracks during WEDM. These larger micro-cracks make the separation of a volume during succeeding discharges much easier. Spalling especially occurs where high energy inputs are used. The regimes with high energy inputs result in larger micro-cracks. The spalling effect can clearly be seen from a debris analysis as shown in Figure 5.81(a-f). Debris analysis shows that they contain the residual elements of copper, Zinc (coming from the electrode) and elements of Ti, carbon (coming from the base material). The particles observed are of irregular in shape, have rounded, spherical as well as sharp edges which clearly indicate spalling as material removal mechanism.

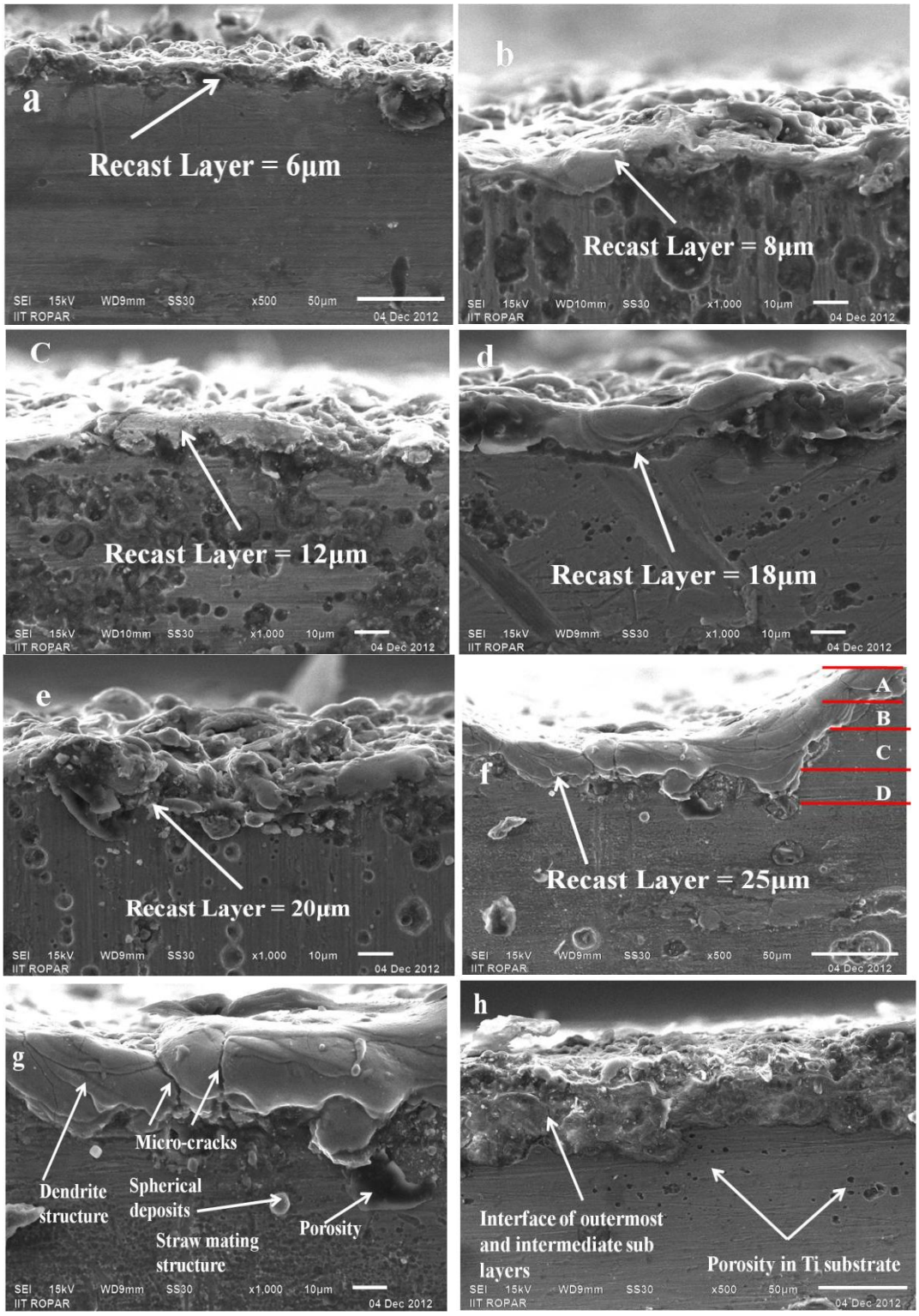

Figure 5.73 Coss-sectional microstructure of recast layer of WEDM samples (a) T_{on} = 0.7µs, T_{off} = 38 µs and I_p = 120A, (b) T_{on} = 0.9µs, T_{off} = 26µs and I_p = 160A, (c) T_{on} = 0.9µs, T_{off} = 17 µs and I_p = 160A, (d) T_{on} = 1.1µs, T_{off} = 26µs and I_p = 160A, (e) T_{on} = 1.1µs, T_{off} = 17µs and I_p = 200A, (f) T_{on} = 1.1µs, T_{off} = 17µs and I_p = 200A(Marker A: Outmost sublayer, B: Intermediate sublayer, C: Innermost recast zone, D: Matrix zone, (g) recast layer with dendrite structure, (h) porosity in Ti substrate

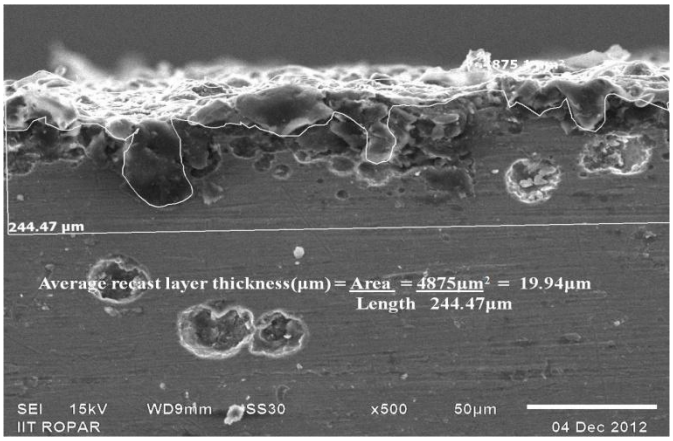

Figure 5.74 Average recast layer thickness measurements

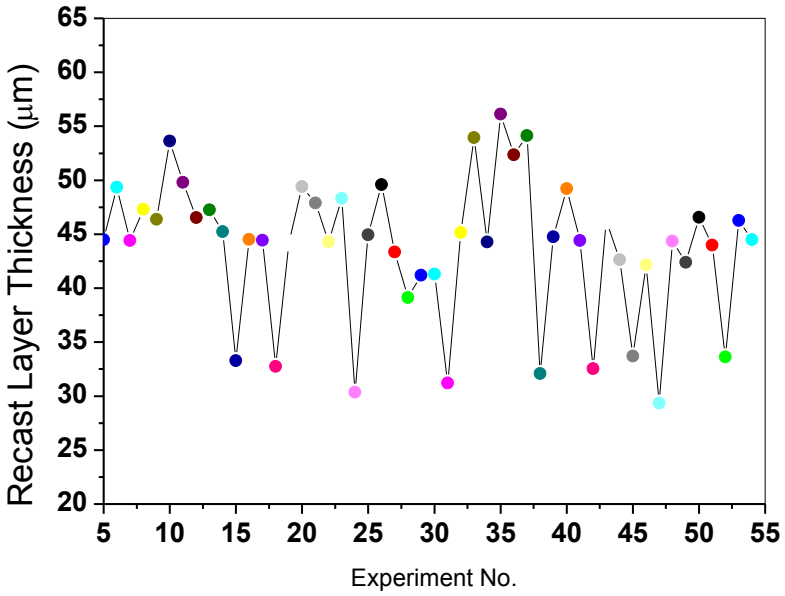

Figure 5.75 Average recast layer thickness(µm)

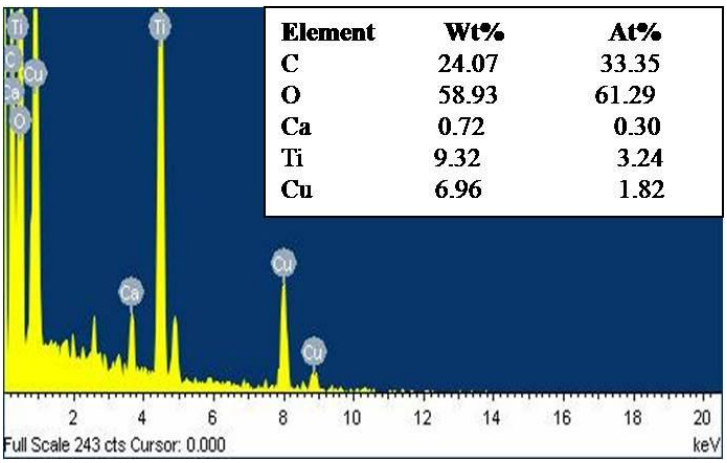

Figure 5.76 EDX analysis of recast layer

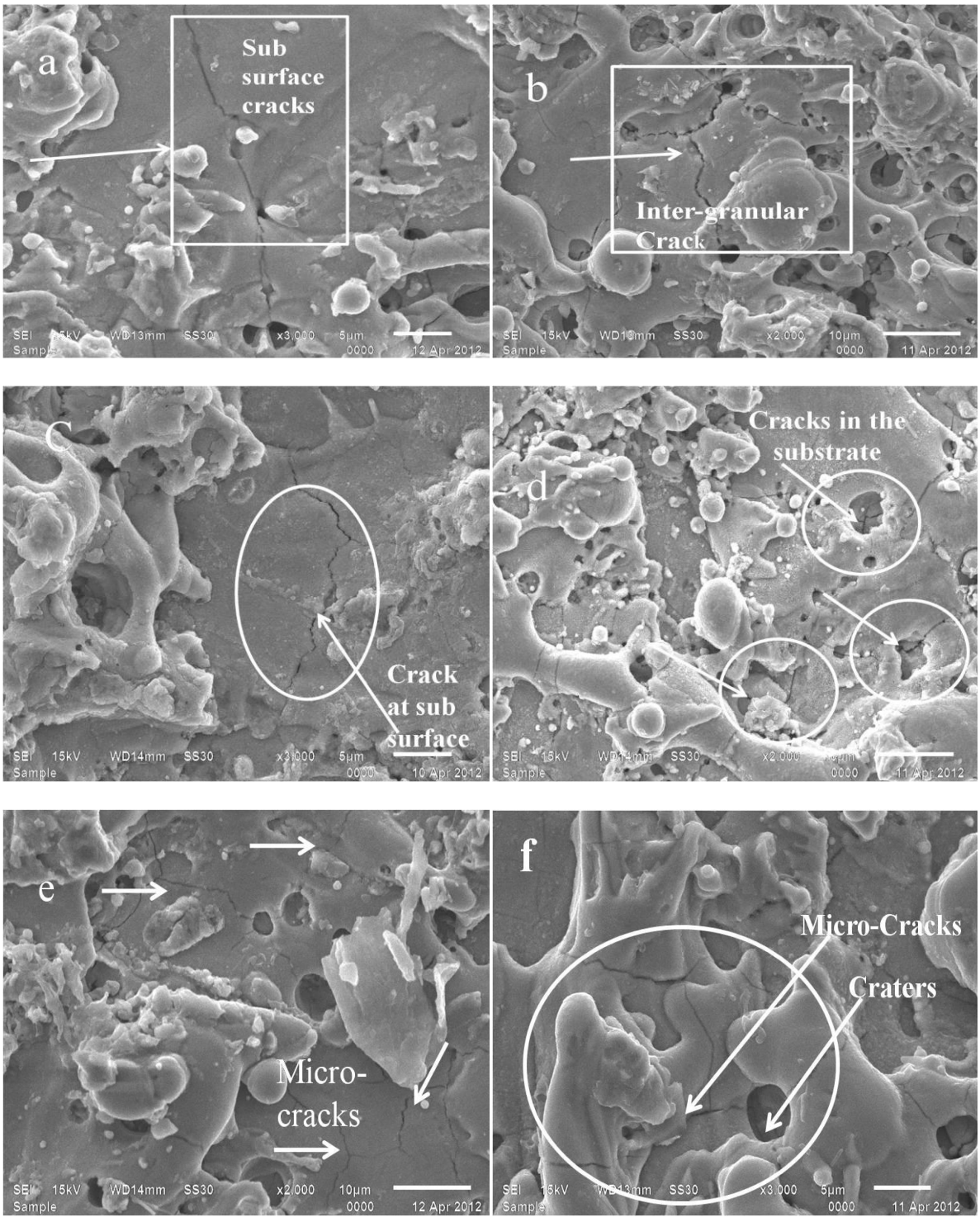

Figure 5.77 SEM micrographs of sub-surface cracks observed at (a) T_{on} = 0.7µs, I_p = 120A, (b) T_{on} = 0.9µs, I_p = 160A, (c) T_{on} = 0.9µs, I_p = 160A, (d) T_{on} = 1.1µs, I_p = 160A, (e) T_{on} = 1.1µs, I_p = 200A, (f) T_{on} = 1.1µs, I_p = 200A

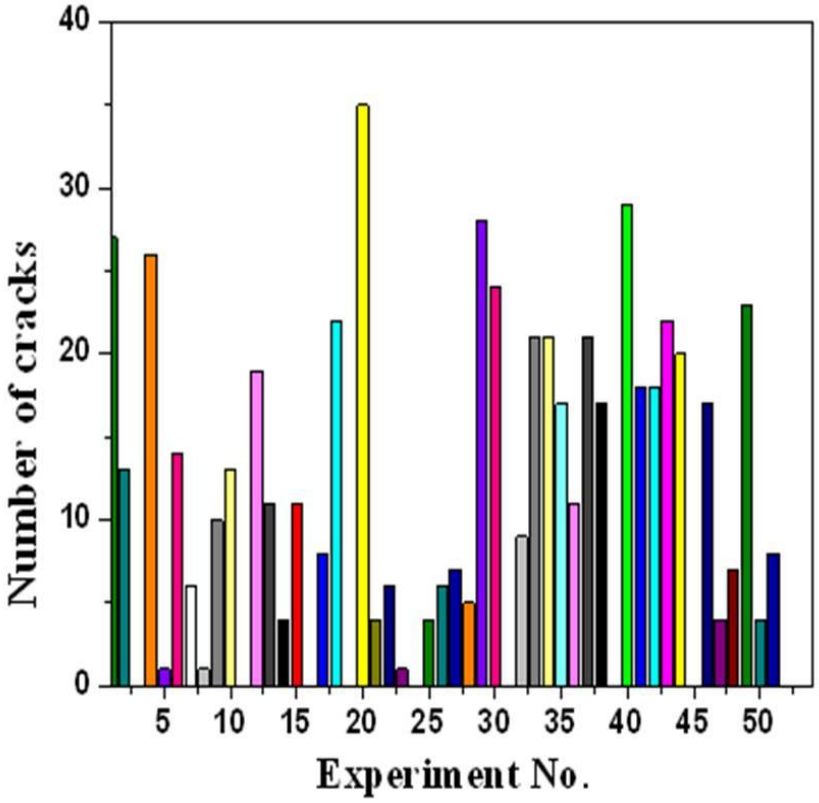

Figure 5.78 Experiment No. Vs Number of Cracks

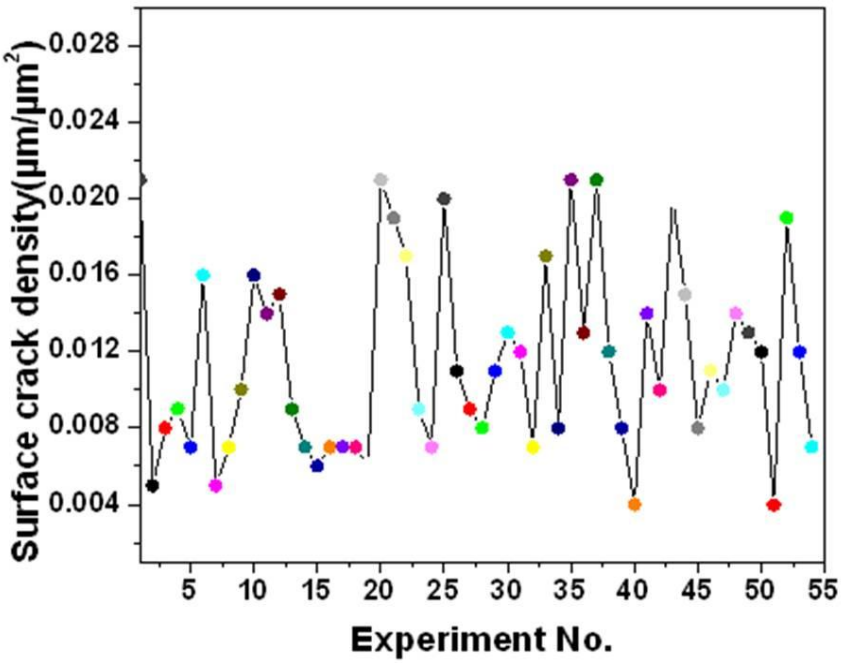

Figure 5.79 Experiment No. Vs. Surface crack size density

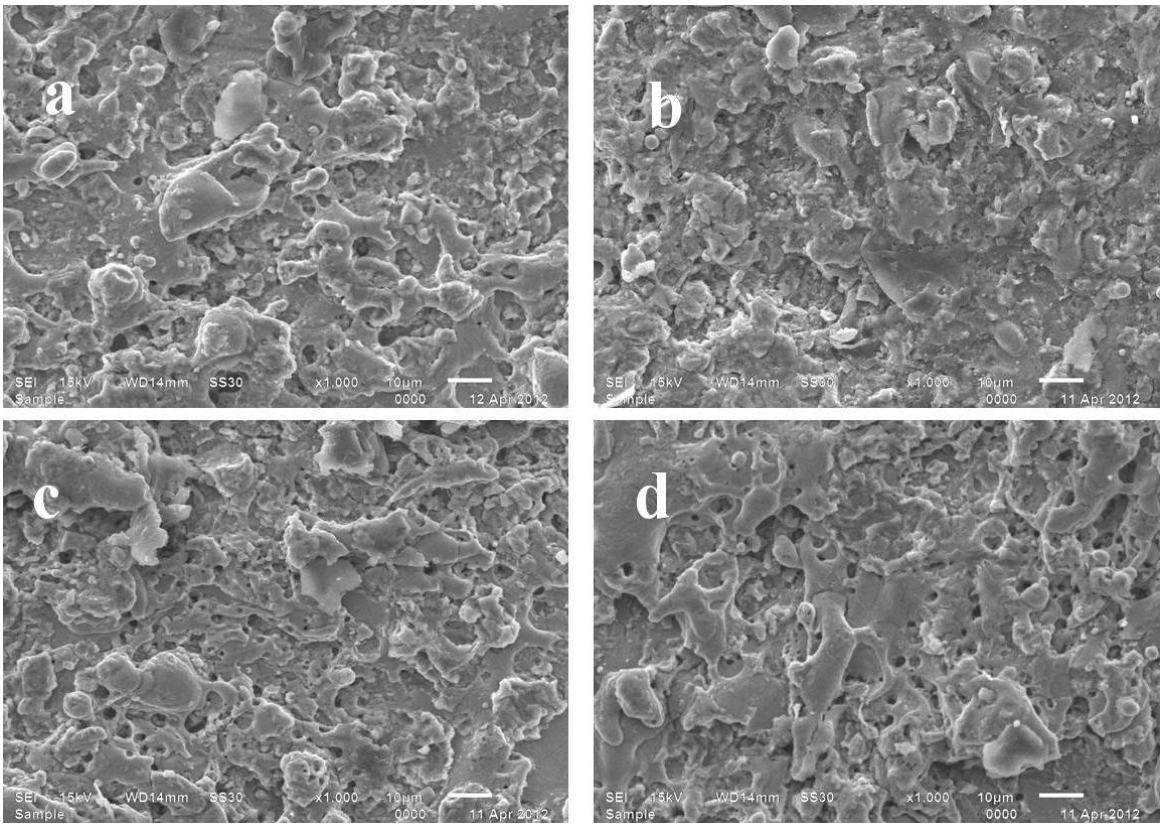

Figure 5.80 SEM micrographs with less number of craters and no cracks were observed at Exp. No. 3,11,16,19

5.6.7 Analysis of wire electrode surface topography

The thermal stresses developed at the interface zone between the tool and work resulted in microstructure changes [Tosun at el., 2003]. Therefore, the material transfer characteristics of wire were investigated. In present study, two types of wire rupture were observed. One is due to high peak current and other is due to increase of spark frequency. Figure 5.82 (a-h) shows the micrographs of worn wire electrode. The different craters and residuals of debris adhered to the surface of wire electrode. The residuals of copper, carbon, oxygen and titanium were detected in wire electrode through EDX as shown in Figure 5.82(i). This may be due to the melting and re-solidification of titanium and brass wire electrode after WEDM. The increase of peak current leads to generation of higher discharge energy in the spark gap. Hence it may result in increase of wear of wire electrode. The presence of debris in the gap not flushed properly by dielectric fluid may result in arcing. This arcing also results in the wire breakage. There are different factors leading to wire breakage such as high wire tension, thermal load, electrical discharge impact and poor flushing. When the developed stresses in wire are more that wire strength, the wire rupture will occur. The developed stresses in wire increase by changing

in wire properties and characteristics, cross-section reduction and the increase in wire temperature. High temperature, work piece varying thickness and process parameters influence the wire strength that affects the wire rupture [Tosun and Cogun, 2003]. The wire used in WEDM should provide some features such as high electrical conductivity, sufficient tensile strength at high temperatures, low melting temperature and high heat conductivity in order to reach to high performance. The high electrical conductivity helps the wire transfers energy to work piece efficiently and minimize energy loss of sparking during machining. The wire with high tensile strength is a good heat resistance in high temperature and maintains straight under vibration and tension. The low melting temperature of wire improves the spark formation and decrease dielectric ionization time.

The higher thermal conductivity of the electrode ensures a better spark discharge energy distribution during the EDM process. This will increase material removal rate (Shah et al.; 2010). Based on the experimental results the percentage contribution of pulse on time: 12.85%, pulse off time: 49.47%, peak current: 28.05% spark gap voltage: 6.72% and error 2.91% as shown in Figure 5.90(d). In this research, pulse on time, pulse off time and peak current are identified as the most significant machining parameters for wire breakage as response. The wire breakage probability increases when pulse on time is increased with a decrease of pulse off time. The number of discharges within a given period of time becomes more when time between two pulses is shorter (i.e. shorter T_{off}) and large peak current leads to higher electrical discharging energy which generates more heat energy. Therefore, due to the excessive thermal load and increased discharge frequency, the wire breakage occurs. On the other hand, wire tension and dielectric pressure are effective parameters for causing reduction in wire breakage. Reduction in wire tension and increase in water pressure may help in decreasing wire rupture possibility while machining. Experiments disclosed that the frequency of wire breakage during machining of pure titanium is more sensitive to changing of process parameters such as pulse on time, pulse off time and peak current. WEDM was performed on pure titanium to identify the location of wire breakage and wire wear ratio as shown in Figures 5.83-5.84. These Figures depict that the wire tends to break at the start, near the middle and end of the experiment at the machined surface. To maximize the efficiency of cutting pure titanium (Grade-2) material by WEDM, the wire breakage during cutting process should be avoided in addition to increased discharge energy. From these results, the optimum setting parameters can be adjusted accordingly in order to minimize the wire

breakage frequency (pulse on time= 0.9µs, pulse off time = 28µs and peak current =160A) during WEDM of pure titanium.

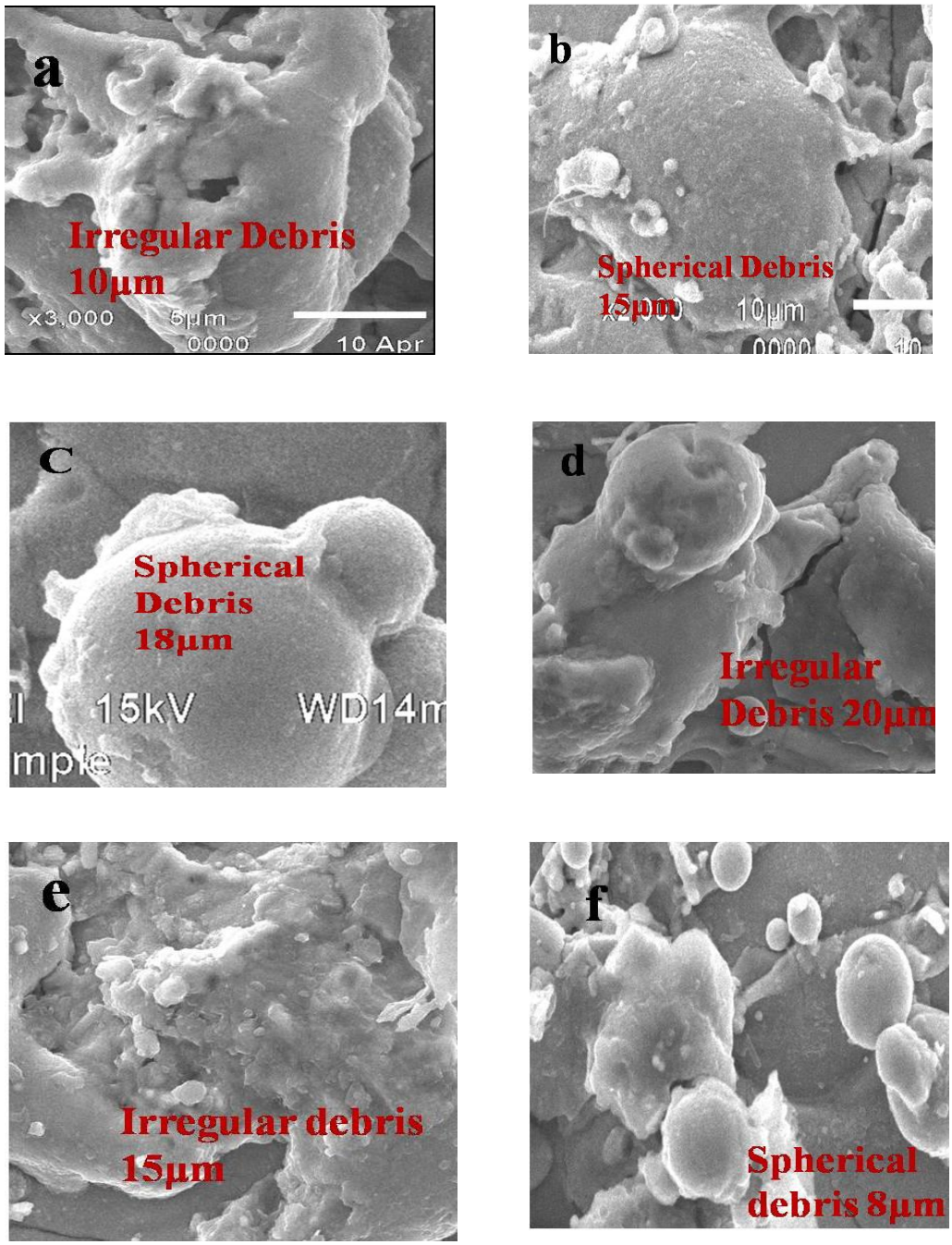

Figure 5.81 Debris collected during WEDM of pure titanium using deionized water (a) MRM: Spalling, (b) MRM: Melting, (c) MRM: Melting, (d) MRM: Spalling, (e) MRM: Spalling, (f) MRM: Melting

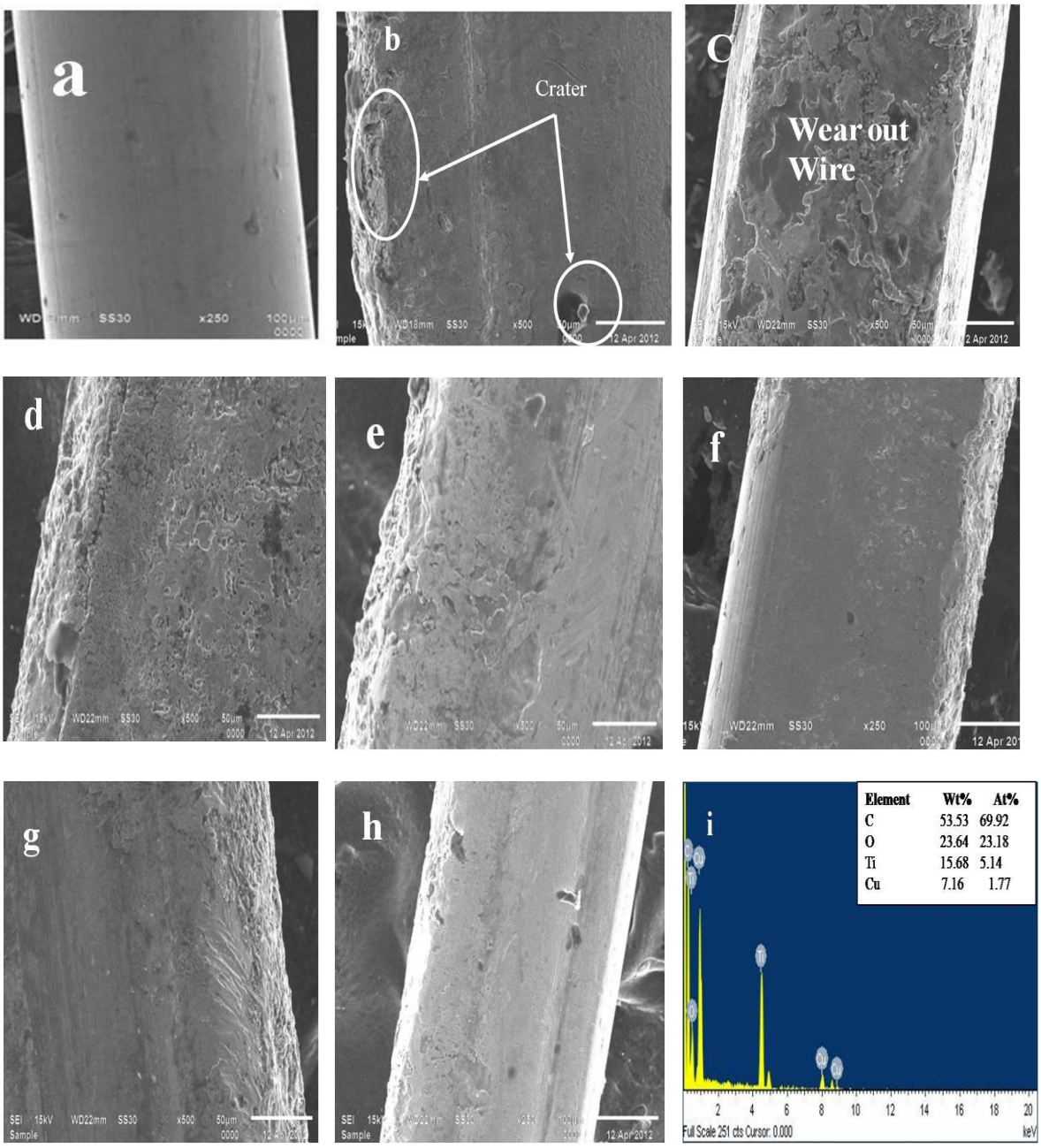

Figure 5.82 SEM micrographs (250X and 500X) of the machined wire electrode surface for machining at (a) T_{on} = 0.7µs, I_p = 120A, (b) T_{on} = 0.9µs, I_p = 160A, (c) T_{on} = 0.9µs, I_p = 160A, (d) T_{on} = 1.1µs, I_p = 160A, (e) T_{on} = 1.1µs, I_p = 200A, (f) T_{on} = 1.1µs, I_p = 200A, (g) wire wear out from the side (h) Debris adhered to wire surface, (i) EDX of wear out wire

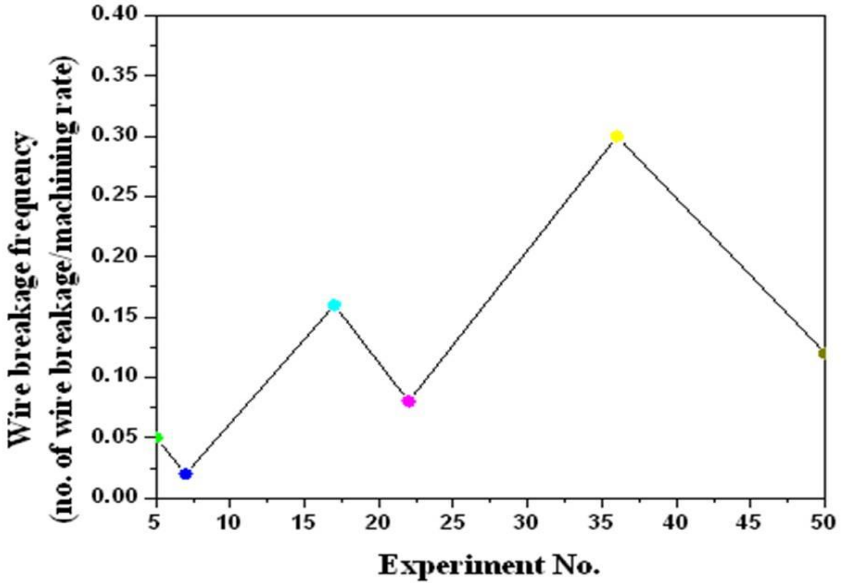

Figure 5.83 Wire breakage frequency Vs Experiment No.

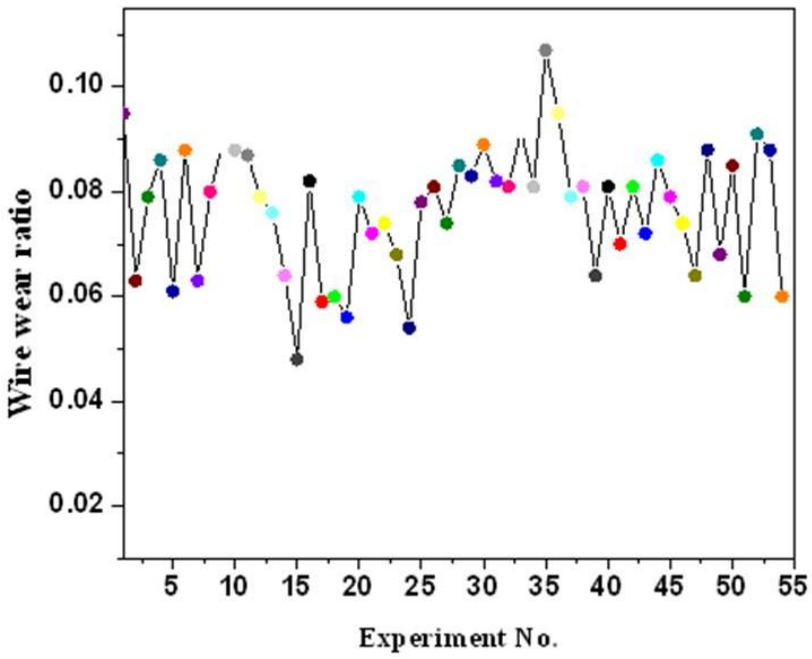

Figure 5.84 Wire wear ratio Vs Experiment No.

5.6.8 Penetrating micro-cracks in the sub-surface

The path followed by the penetrating micro-cracks is so remarkable that they have a trend to follow the temperature isotherms in the solid state at high pulse on time (1.1µs), low pulse off time (17µs) and high peak current (200A) that leads to formation of corresponding cracks as shown in Figure 5.85. This can attributed due to thermal action of electric sparks and extreme temperature gradients that occur at the work surface. With increasing pulse on time, penetrating sub- surface micro-cracks, craters rims and

irregularities is also increased. When pulse on time is increased, the amount of thermal energy which is transferred to the sub-surface of sample as a result of more material is melted that causes increase of immersed volume of molten material in dielectric fluid and in the spark gap. On the other hand, due to low pulse off time during experiments, there is not enough time for proper cleaning of immersed debris and pollution in gap distance, produced by discharges and lead to unstable conditions of electrical discharge and also occurrence of more arcs in gap distance.

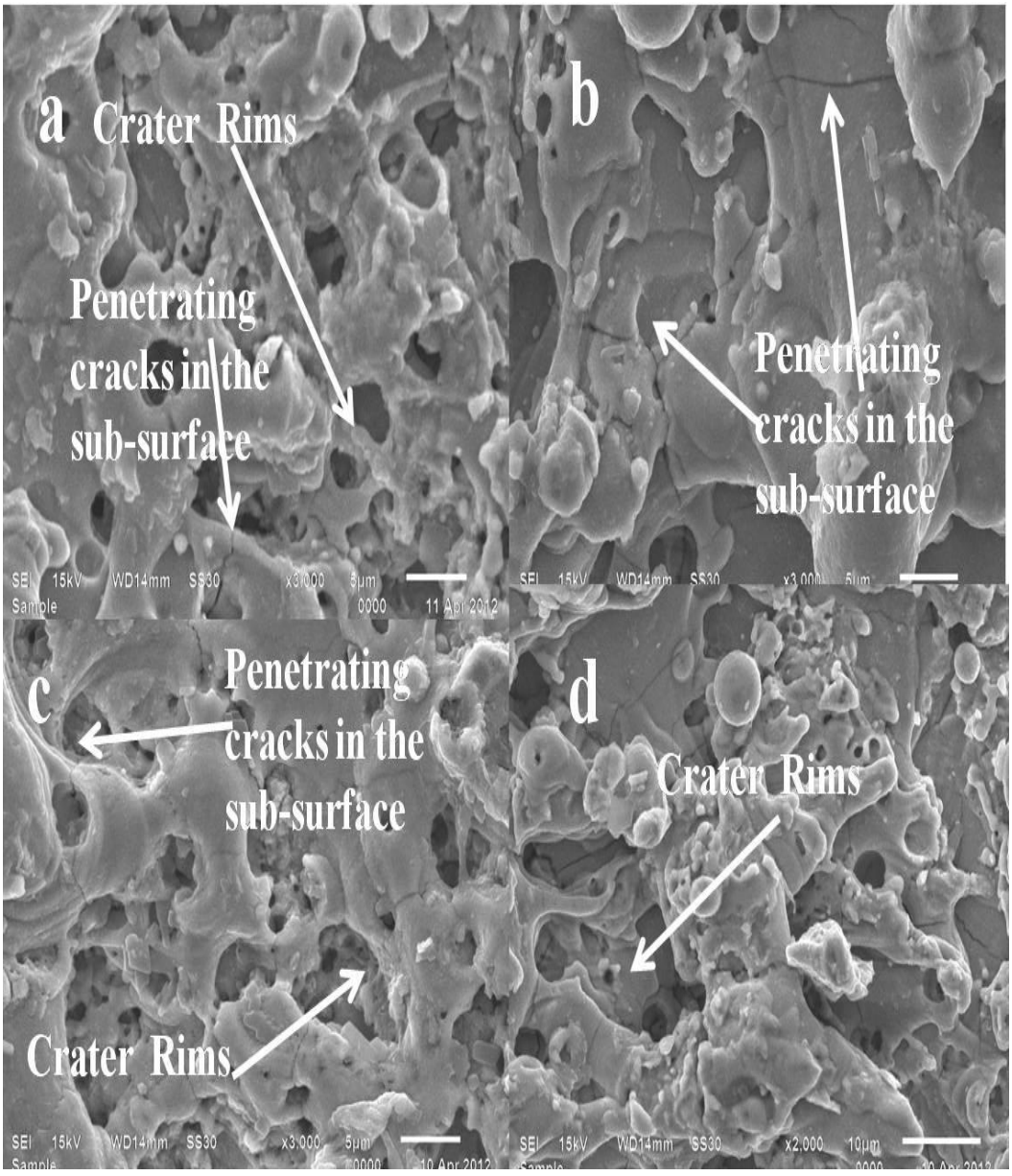

Figure 5.85 SEM micrographs penetrating micro-cracks in the sub-surface at pulse on time = 1.1µs, pulse off time = 17µs, peak current= 200A, spark gap voltage= 40V

5.6.9 Analysis of material migration through energy dispersive X-ray Analysis (EDX)

The surface morphology of WEDM surface is usually rough cut as a result of non-uniform distribution of spherical and non spherical agglomerates. Scanning Electron Microscope/Energy Dispersive X-ray (SEM/EDX) composition analysis of workpiece shows the presence of metal particles other than the base metal. The metal particles transfer from brass wire, decomposition of dielectric to workpiece during WEDM. Since some of the particles cannot be completely flush out of spark gap, part of these materials is deposited on the surface of the workpiece as compound form or free form. This implies that during WEDM, a significant amount of material is transferred from electrode to the workpiece surface. The composition of elements on the workpiece and electrode surfaces was examined by Quantitative Energy Dispersive X-ray (EDX). The compositions of machined samples were determined using EDX technique. The higher peak in the spectrum of EDX presents the more concentrated element in specimen. Figure 5.86(a-d) shows the energy dispersive X-ray (EDX) of machined surfaces as obtained using accelerating voltage of 3KV. The results of the EDX analysis showing the percentage elements migrated from the brass wire electrode to the workpiece are shown in Table 5.22. Results of the EDX analysis show that appreciable amount of Carbon (C), Copper (Cu), Oxygen (O_2), Titanium (Ti), Zinc (Zn) are found to migrate to the surface of the workpiece. The residuals of Cu and Zn were observed in the machined samples due to melting, evaporation and re-solidification of brass wire electrode. The major content of oxygen and carbon was due to decomposition of dielectric, oxidation and mixing of debris at high temperature involved in the process. X-ray diffraction was then used to further analyze the compound deposited as TiC and TiO_2 due to major content of C and O_2. From Table 5.23 the lowest percentage of material migration from electrode to workpiece was found for experiment no. 32, 13, 45 and 46.

The highest percentage of material migration was found at Run no. 2, 8, 10, 26, 33 and 53. From the EDX analysis it is further revealed that the migration of elements from electrode to workpiece is influenced by the pulse on time and decrease of pulse off time as shown in Figure 5.87. This is because, increase in pulse on time results increases spark energy, therefore, more metal is melted from the electrodes which cannot be completely flushed away by the dielectric fluid.

5.5.10 X-ray diffraction analysis (XRD)

The assessment of the XRD patterns allowed to identifying the major phases presents in the WEDM machined samples. The phases are analyzed using X'Pert High Score plus 2.0. The phases have been identified from searches in the PDF-2 database. The plots of identified phases were shown in Table 5.21. The XRD pattern analysis showed the transfer of tool and dielectric fluid elements on the machined surface. The compounds as titanium dioxide (rutile) (TiO_2), ($TiO_{0.325}$), Ti_2O_3, Ilmenite (Fe_2Ti_4O), copper titanium dioxide (Cu_3TiO_4), zinc titanium carbide (Ti_3ZnC), titanium zinc carbide (Zn_2Ti_4C), titanium carbide (TiC), were observed on the machined surface as a free form or combined form as shown in Figure 5.89(a-f). The phases were identified in the form of peaks at 2θ scale values i.e. 35.45, 45.67, 65.70, 85.07 and 105.69 (Cu Kα) respectively. The compounds have been formed due migration of basic workpiece elements, tool elements and with soluble oxygen in dielectric deionized water. The crystal structure (α-phase) of pure titanium at room temperature was hexagonal close packed (HCP). The phase transformation diagram of α + β titanium during cooling is given in Figure 5.88. A visible martensitic microstructure of deformed layer was attributed to extreme heating and rapid cooling as shown in Figure 5.72.

The transformation is depending on the precise thermal behaviour of the material being machined and since the pure titanium has low thermal conductivity, a slightly tempered layer is formed under the heat affected zone as shown in Figure 5.71(d). Additionally, the heat under the surface is retreating from the region more slowly compared to the top surface which is being exposed to immediately cooling action by the surrounding working fluid. The α- phase changed to β -matrix as the molten titanium was rapidly cooled below the β transus temperature by dielectric fluid [Khanna and Sangwan, 2013]. The β transus is the temperature that separates the phase stability of β and α phase in titanium. The amorphous structure developed the cracks due to rapid cooling [Jawahir et al.; 2011].

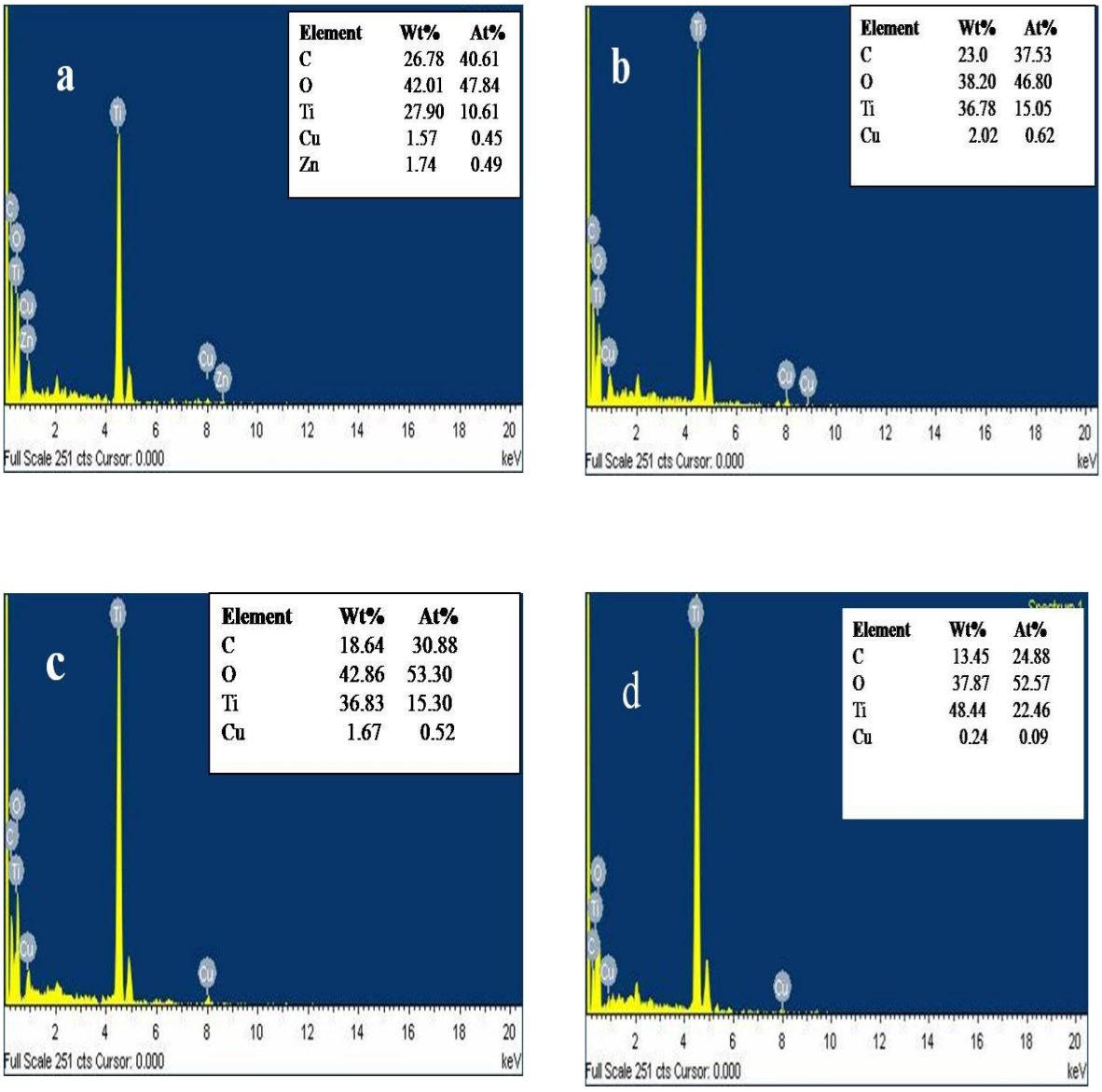

Figure 5.86 EDX analysis of pure titanuim at Exp. No. 3,11,16,19

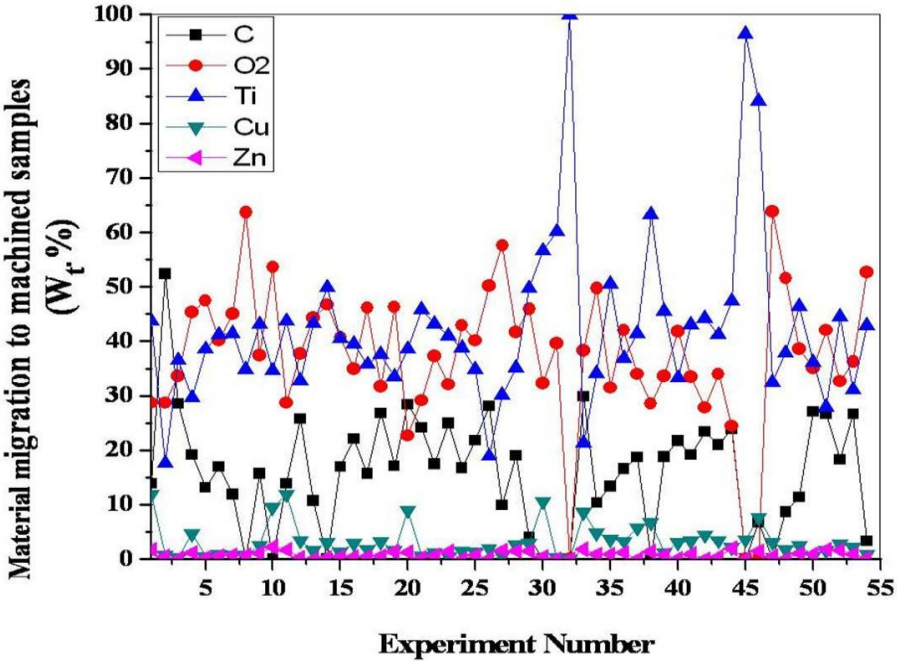

Figure 5.87 EDX analysis of migrated elements at different experiment no. Vs atomic wt.%

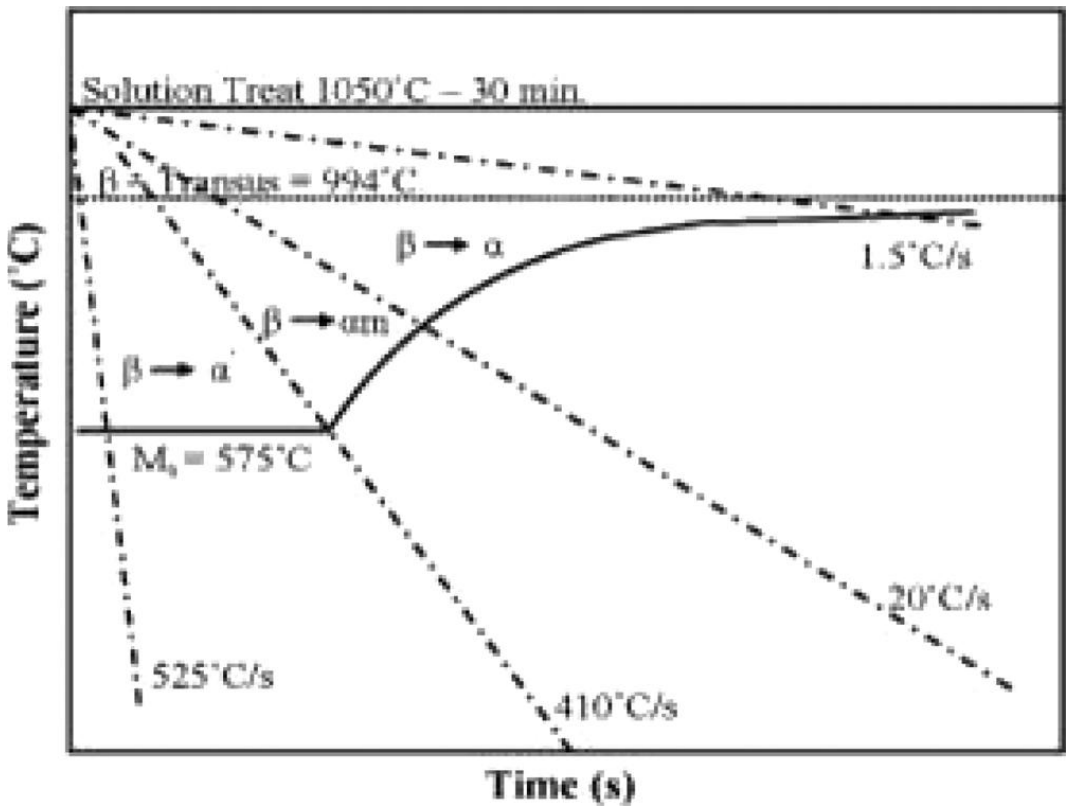

Figure 5.88 The phase transformation diagram of Titanium and its alloys based on cooling rate [Hascalik and Caydas; 2007a].

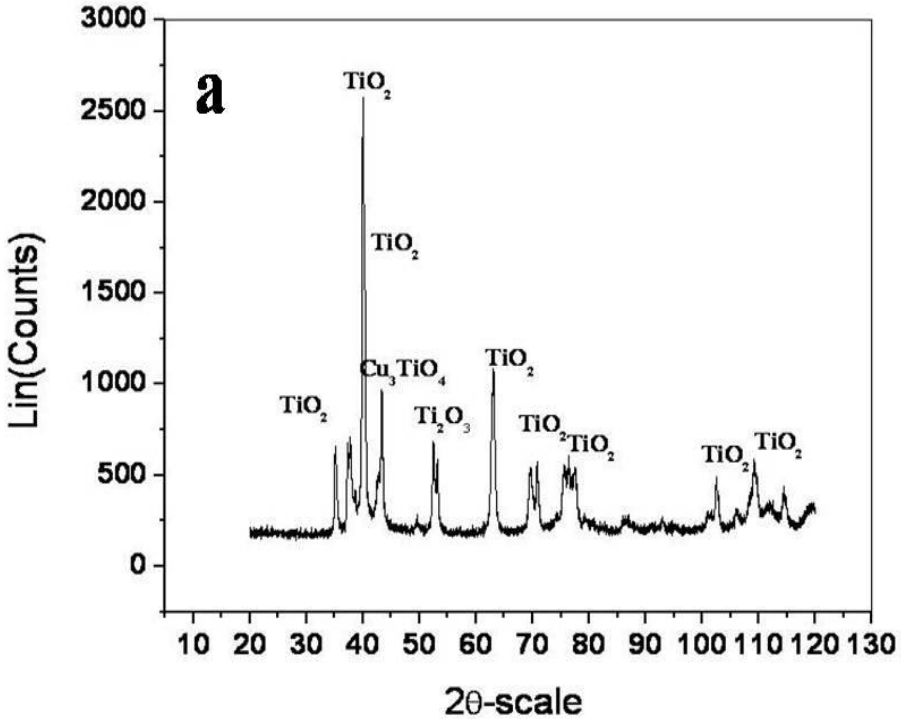

Figure 5.89 (a) XRD phase pattern analysis at Exp. No. 3

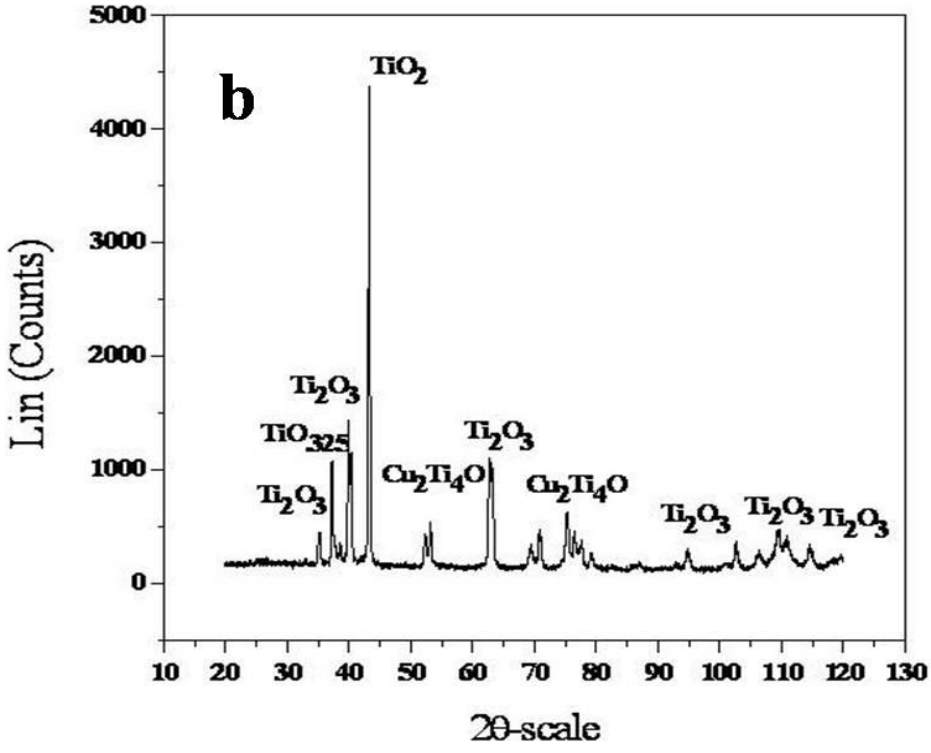

Figure 5.89 (b) XRD phase pattern analysis at Exp. No. 12

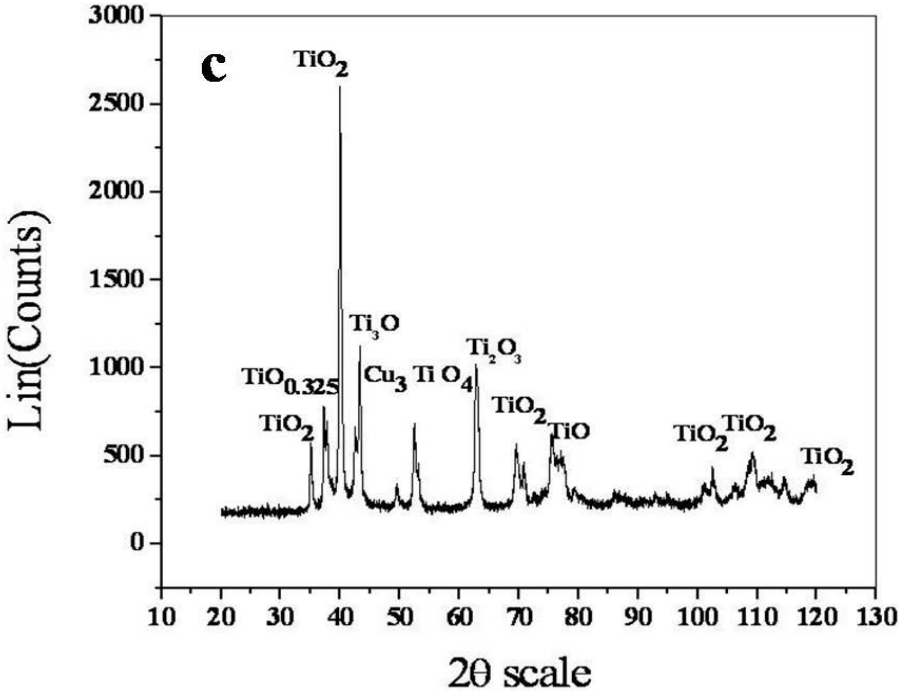

Figure 5.89 (c) XRD phase pattern analysis at Exp. No. 25

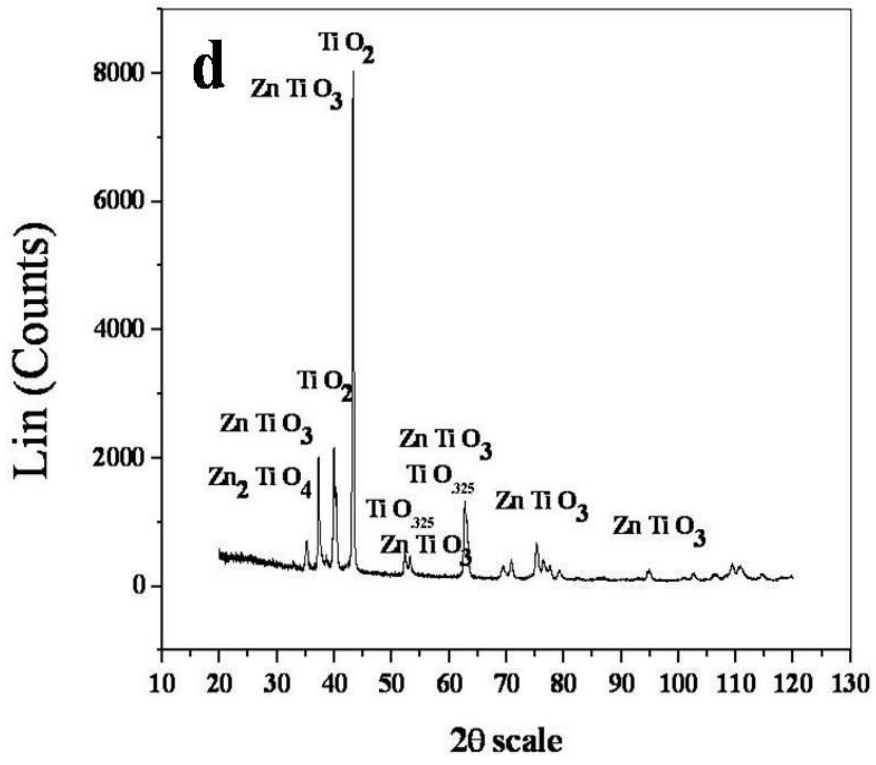

Figure 5.89 (d) XRD phase pattern analysis at Exp. No. 35

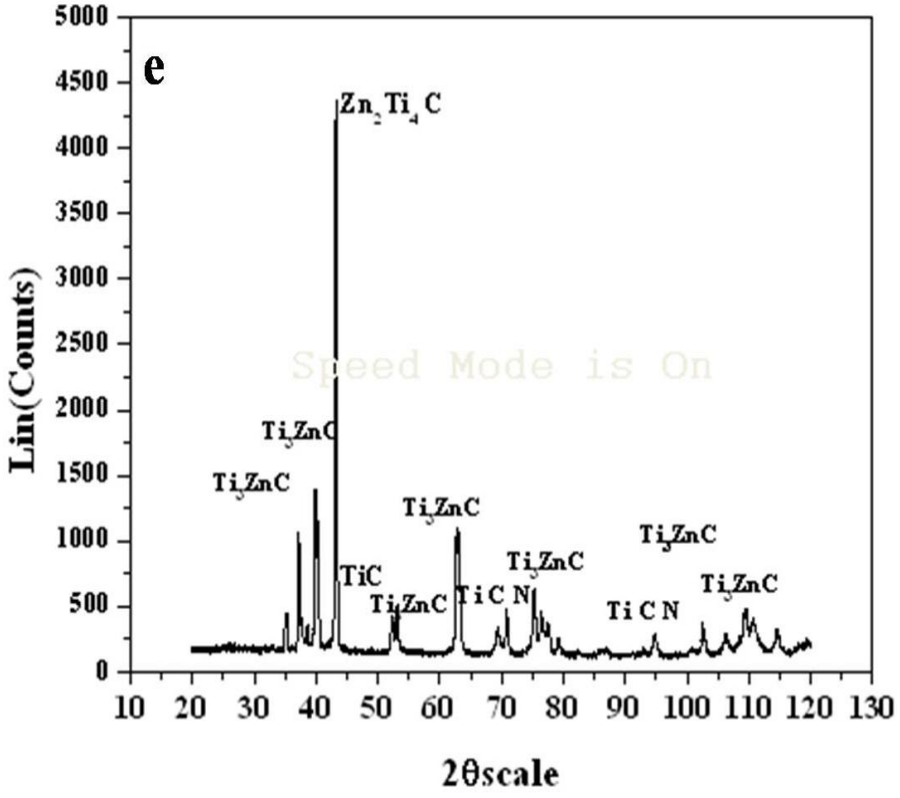

Figure 5.89 (e) XRD phase pattern analysis at Exp. No. 43

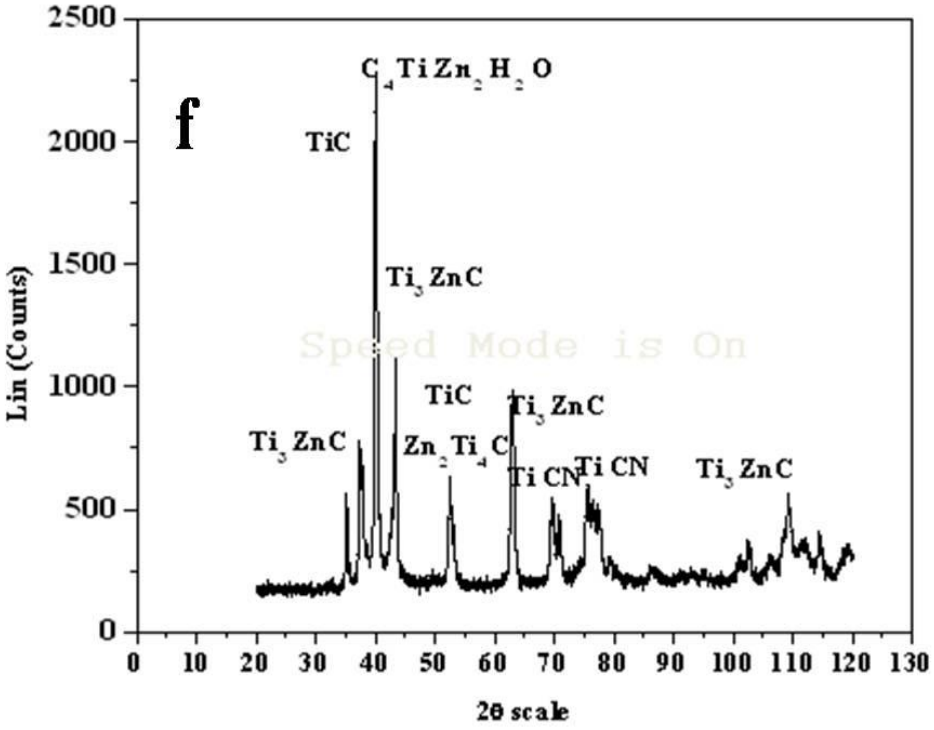

Figure 5.89 (f) XRD phase pattern analysis at Exp. No. 52

Table 5.21 XRD Plot of identified phases

Ref. Code	Compound Name	Crystal system	Chemical Formula
01-073-1581	Titanium Oxide	Hexagonal(225)	$Ti\ O_{.325}$
01-077-2170	Titanium Oxide	Cubic(227)	Ti O
01-083-1284	Copper Titanium Oxide	Rhombohedra(167)	$Cu_3\ Ti\ O_4$
00-010-0063	Titanium Oxide	Cubic(227)	$Ti_2\ O_3$
01-075-0402	Ileminite	Rhombohedra(148)	Fe_2Ti_4O
01-085-0547	Zinc Titanium oxide	Hexagonal(194)	$ZnTiO_3$
00-024-1471	Zinc Titanium Carbide	Cubic (227)	Ti_3ZnC
00-029-1363	Titanium Zinc Carbide	Cubic (227)	Zn_2Ti_4C
00-031-1400	Titanium Carbide	Cubic (225)	TiC
01-076-2484	Titanium Carbide Nitride	Cubic (225)	TiCN

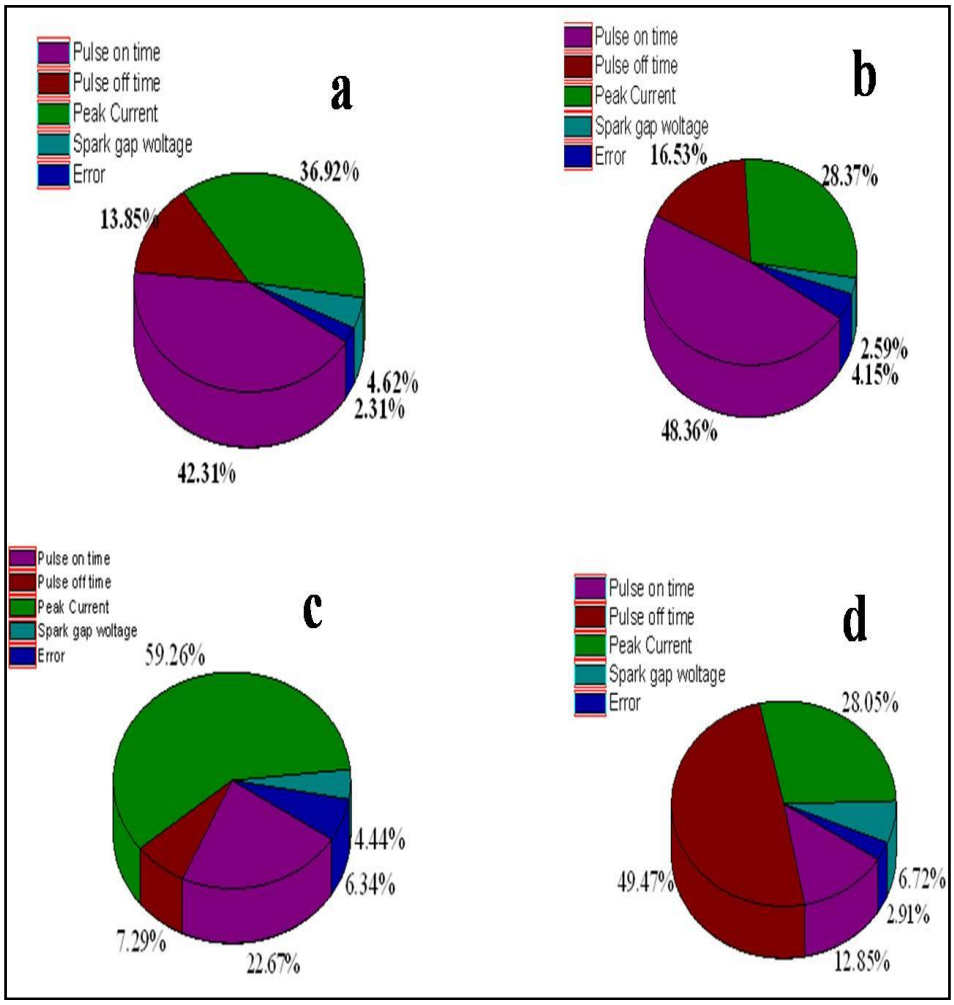

Figure 5.90 Percentage contributions of most significant parameters on surface integrity (a) Surface topography, (b) Recast layer thickness, (c) Surface crack size density, (d) Wire wear topography

5.5.11 Comparison of surface integrity between steel and pure titanium

From the application point of view, WEDM is more suitable candidate for machining of pure titanium as compared to machining of other materials such as steel, as steel can be easily machined using conventional machining. A detailed comparison of surface integrity of pure titanium (in the present study) and other material (such as steel) as reported by other researchers in the literature was difficult to make because all these studies have been reported to make use of different wire cut EDM setups involving different range of machining parameters. However a comparison of surface integrity for pure titanium and steel is done and is presented in Table 5.22. From the Table 5.22 and literature survey it was observed that the published work on the EDM surface characteristics of steel and its alloys is reasonably extensive. After an ample review of literature of different materials it is obvious that the several investigations were performed by early investigators on the following:

1. Much work has been devoted to the EDM of surface integrity in terms of micro-crack analysis, craters, and recast layer thickness.
2. Use of OFTA technique for conducting experimental research.
3. Specifically, no significant literature has been found relating to optimization of surface integrity analysis in terms of surface crack density and recast layer thickness after processing with WEDM using pure titanium.
4. The erosion mechanism of the WEDM process.
5. Much work has been devoted to the EDM of surface integrity in terms of micro-crack analysis, craters, and recast layer thickness [Lin et al.; 2000, Huang and Liao, 2003, Hascalik and Caydas, 2007a, Hascalik and Caydas, 2007b].
6. A few studies have reported the use of ultrasonic machining process for machining of pure titanium [Kumar and Khamba, 2010; Kumar and Khamba, 2009, Kumar and Khamba, 2008].

Table .5.22 A comparison of WEDM surface integrity in steel and pure titanium

<table>
<tr><th colspan="2">Steel</th><th colspan="2">Pure titanium</th></tr>
<tr><td colspan="4">Surface topography</td></tr>
<tr><td colspan="4">a) Crater rims, pockmarks, globules of debris, spherical particles</td></tr>
<tr><td> 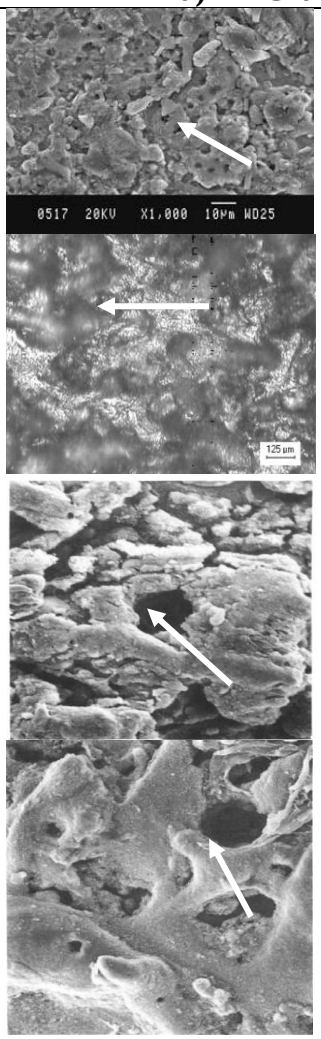
</td><td>In case of steel, the surface integrity was altered due to the impact of machining parameters to a limited extent [Ramakrishnan, and Karunamoorthy, 2006].
The crater size is small, amount of debris has been reported to be less to moderate [Hascalik, and Caydas, 2007].
The quantity of micro holes, pockmarks and pits has been reported less to moderate [Hewidy et al., 2005].</td><td> 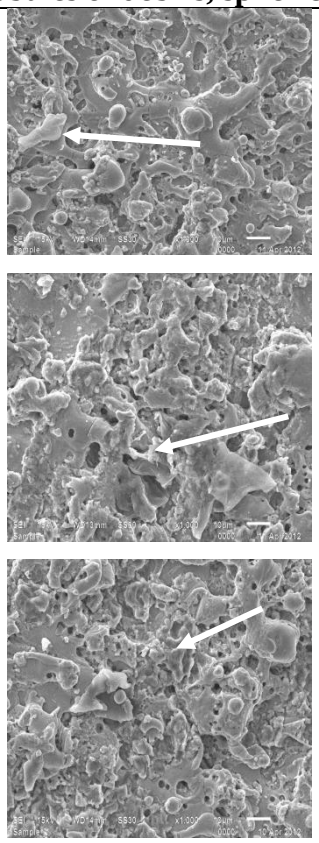 </td><td>The heat which is produced by the discharge is not dissipated quickly and remains entrapped in the cutting zone thus leading to more melting and vaporization of material as compared to steel. Hence, the size of crater is relatively large; globules of debris on the machined surface are more as observed in the present study. Titanium has low thermal conductivity (10-15W/m°K) as compared to steel.</td></tr>
<tr><td colspan="4">b) Recast layer and Heat affected zone</td></tr>
<tr><td> 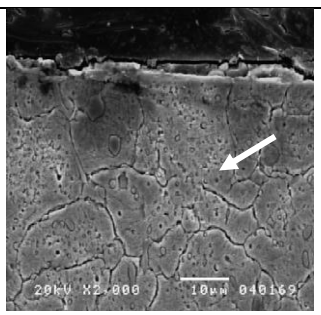
</td><td>A few micro cracks of minor dimension and thin heat affected zone have been observed in the steel. Fewer researchers have been</td><td> 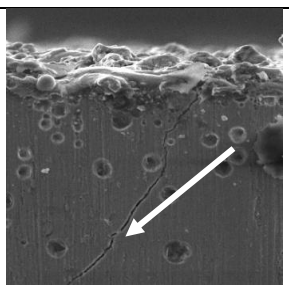 </td><td>Only one micro crack was observed at the heat affected zone. The surface crack density penetrates more deeply into original material.</td></tr>
</table>

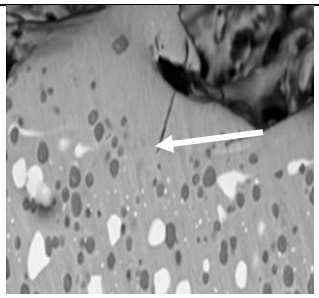

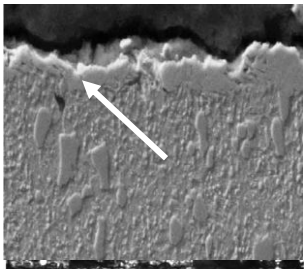

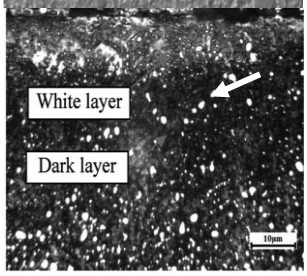

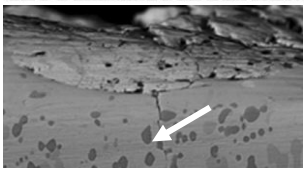

observed that the thickness and density of cracks of in recast layer is less in case of steel [Huang et al., 2004].

Presence of very large amount of black patches in the white layer has been observed [Kanalyasiri, and Boonmung, 2007]

Presence of river lines in the recast layer. The density of cracks in recast layer increase with increased pulse duration and open circuit voltage [Lauwers et al., 2004].

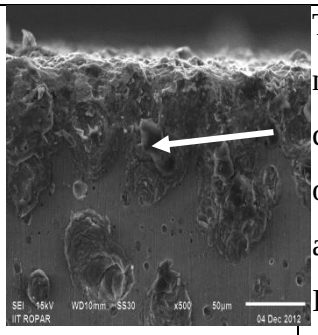

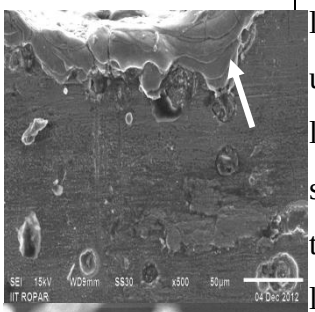

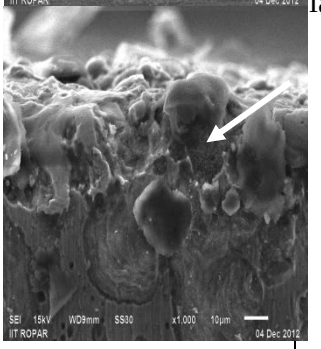

The residuals of spherical nodules in free or compound form are observed near the heat affected zone.

It is clear that recast layers appear as non-uniform and have wave like pattern. There are some micro-cracks trenchant into recast layer.

c) Micro-Cracks

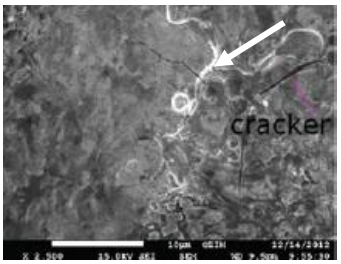

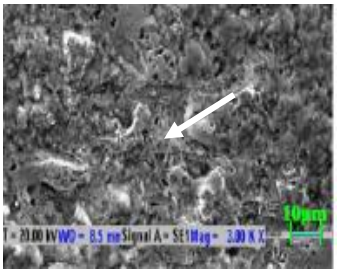

Micro cracks have been less long and no blow holes observed in case of steel [Lee and Li, 2003].

A few regions of spalling effect. Smooth surface with few folding. Micro-cracks formation due to fatigue working condition of splines.

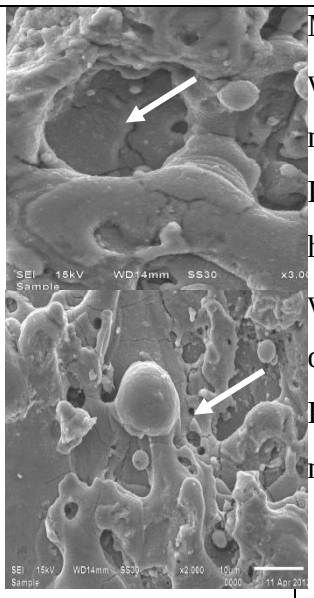

Micro cracks are long, wider and spread over most of the surface. Presence of large blow holes and deposition of work material in the form of debris.

Presence of localized micro cracks.

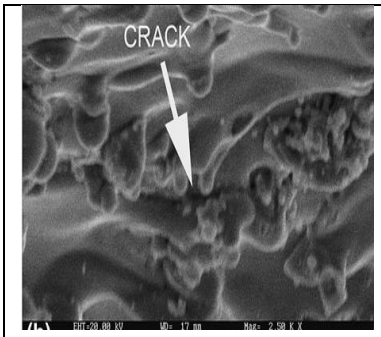	Results prove that local spark and melting on surface while machining are main sources of crack initiation [Liu et al., 2009].		

d) Wire breakage and its surface topography

Many researchers also observed that wire breakage frequency increased due to the influence of pulse on time. In case of steel the active range of pulse on time is more than the pure titanium. No work reported on wire breakage in case of steel. In case of steel wire wear ratio increased at larger values of pulse duration and open circuit voltage.	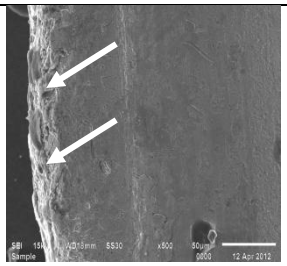 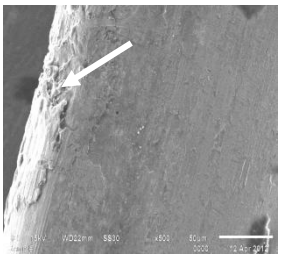 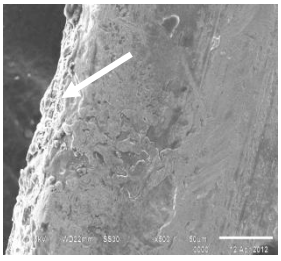	In case of titanium the wire breakage frequency is very large, owing its low thermal conductivity. The range of machining parameters needs to be precisely selected. Accordingly, the present study utilized a moderate range of pulse on time and pulse off time to avoid the wire breakage. In case of pure titanium wire rupturing is affected by pulse on time and spark gap voltage [Hong et al., 2001]. The formation of craters and the residuals of debris adhered to the surface of wire electrode.

Table 5.23 Design of experiments matrix and Material migration

Standard Run no.	Pulse on time T_{on} (µs)	Pulse off time T_{off} (µs)	Peak current Ip (Ampere)	Spark gap voltage SV (Volt)	Wire Feed WF (m/min)	Wire Tension WT (grams)	Material migration to machined samples (%)				
							C	O_2	Ti	Cu	Zn
1	0.9	28	160	50	7	950	13.9	28.7	43.7	11.91	1.67
2	0.9	38	120	50	10	950	52.4	28.7	17.6	0.73	0.49
3	0.9	17	120	50	10	950	28.6	33.6	36.5	0.25	0.07
4	0.9	38	160	50	10	500	19.2	45.3	29.6	4.63	1.13
5	0.9	38	160	50	4	500	13.1	47.5	38.6	0.41	0.24
6	1.1	17	160	60	7	950	17.0	40.2	41.2	0.81	0.57
7	1.1	28	200	50	7	1400	11.9	45.1	41.5	0.79	0.69
8	0.7	38	160	60	7	950	0.0	63.7	34.8	0.72	0.75
9	0.9	28	200	60	7	1400	15.7	37.4	43.1	2.50	1.11
10	1.1	28	160	60	10	950	0.0	53.6	34.6	9.46	2.25
11	0.9	28	160	50	7	950	13.9	28.7	43.7	11.91	1.67
12	0.7	38	160	40	7	950	25.8	37.7	32.78	3.38	0.26
13	0.9	28	120	60	7	500	10.7	44.3	43.3	1.61	0.0
14	0.7	28	200	50	7	500	0.0	46.7	49.9	2.98	0.32
15	1.1	28	160	60	4	950	17.0	40.7	40.5	1.27	0.38
16	1.1	17	160	40	7	950	22.1	34.9	39.5	2.88	0.42
17	0.7	28	120	50	7	1400	15.7	46.1	35.8	1.83	0.42
18	0.9	28	160	50	7	950	26.8	31.7	37.6	3.15	0.61
19	0.9	28	160	50	7	950	17.1	46.3	33.5	1.52	1.38
20	0.9	28	200	40	7	1400	28.4	22.7	38.6	8.94	1.25
21	0.7	17	160	40	7	950	24.1	29.1	45.8	0.61	0.21
22	0.9	28	160	50	7	950	17.5	37.27	43.2	1.21	0.68
23	1.1	28	120	50	7	500	24.9	32.1	41.0	0.49	1.36
24	0.7	28	200	50	7	1400	16.7	42.9	38.8	1.49	0.0
25	0.9	28	200	60	7	500	21.8	40.1	34.8	1.31	0.74
26	0.9	38	120	50	4	950	28.1	50.2	18.9	1.91	0.08
27	0.9	17	160	50	4	1400	9.9	57.6	30.1	0.59	1.65
28	0.9	28	160	50	7	950	19.0	41.7	35.1	2.64	1.45
29	0.9	17	160	50	10	1400	4.0	45.9	49.7	2.86	1.50
30	1.1	38	160	40	7	950	0.0	32.3	56.6	10.6	0.37
31	0.9	28	160	50	7	950	0.0	39.6	60.1	0.22	0.0
32	0.9	28	160	50	7	950	0.0	0.0	100.0	0.0	0.0
33	0.9	28	160	50	7	950	29.9	38.3	21.3	8.57	1.82
34	0.9	17	160	50	10	500	10.4	49.7	34.1	4.82	0.82
35	0.9	17	200	50	10	950	13.4	31.5	50.5	3.58	0.88
36	0.7	28	160	40	10	950	16.6	42.0	36.9	3.30	1.14
37	0.9	17	160	50	4	500	18.7	34.0	41.4	5.76	0.0
38	0.9	38	200	50	4	950	0.0	28.5	63.3	6.71	1.38
39	0.9	28	120	40	7	500	18.8	33.6	45.6	1.18	0.72
40	0.9	17	200	50	4	950	21.7	41.8	33.3	2.98	0.05
41	0.7	28	160	60	10	950	19.1	33.5	43.0	3.32	0.91
42	0.9	17	120	50	4	950	23.4	27.8	44.2	4.45	0.0
43	0.7	28	160	40	4	950	21.0	34.0	41.2	3.41	0.36
44	0.9	38	160	50	10	1400	23.9	24.4	47.4	2.20	1.97
45	1.1	28	160	40	10	950	0.0	0.0	96.4	3.54	0.0
46	1.1	28	120	50	7	1400	6.79	0.0	84.1	7.66	1.43
47	0.9	28	200	40	7	500	0.0	63.8	32.5	3.11	0.50
48	0.9	38	200	50	10	950	8.68	51.6	37.8	1.78	0.0
49	0.7	28	120	50	7	500	11.4	38.6	46.4	2.50	1.01
50	0.7	17	160	60	7	950	27.1	35.1	36.2	0.57	0.88
51	1.1	28	200	50	7	500	26.7	42.0	27.9	1.57	1.74
52	0.7	28	160	60	4	950	18.3	32.6	44.5	2.80	1.66
53	1.1	28	160	40	4	950	26.6	36.3	31.1	2.20	0.87
54	0.9	38	160	50	4	1400	3.27	52.7	42.9	0.94	0.18

CHAPTER 6

MICRO-MODELING OF RESULTS

6.1 MICRO-MODEL FOR PREDICTION OF MATERIAL REMOVAL RATE (MRR)

It has been demonstrated that the material removal rate (MRR) can be predicted using micro model such as response surface model. However, the validity this model is limited to the range of the machine parameters used in the investigation. Therefore, it was decided to develop a model which could predict the machining characteristics (MRR) beyond the range of the input parameters used in the study. The present work uses the technique of dimensional analysis to develop a micro model of material removal rate in WEDM of pure titanium. Dimensional analysis is a method by which we deduce information about a phenomenon from the single premise that the phenomenon can be described by a dimensionally correct equation among certain variables. The theory of dimensional analysis is the mathematical theory which is purely algebraic. The application of dimensional analysis to a practical problem is based on the hypothesis that the solution of the problem is expressible by means of a dimensionally homogeneous equation in terms of specified variables.

The developed micro model for WEDM to predict the values of material removal rate (MRR) over a wide range of input parameters such as pulse on time, pulse off time, peak current, spark gap voltage, wire feed and wire tension. All of the input parameters selected for developing the model have been found to be significant for MRR, as observed from the results of ANOVA test.

6.2 BUCKINGHAM'S Π THEOREM

If there are n variables in a problem and these variables contain m primary dimensions (for example M, L, T) the equation relating all the variables will have (n-m) dimensionless groups. Buckingham referred to these groups as π groups. The final equation obtained is in the form of:

$$\pi_1 = f(\pi_2, \pi_3, \ldots \pi_{n-m}) \quad (6.1)$$

The π groups must be independent of each other and no one group should be formed by multiplying together powers of other groups. This method offers the advantage of being

simpler than the method of solving simultaneous equations for obtaining the values of the indices (the exponent values of the variables). In this method of solving the equation, there are 2 conditions:

1. Each of the fundamental dimensions must appear in at least one of the m variables
2. It must not be possible to form a dimensionless group from one of the variables within a recurring set. A recurring set is a group of variables forming a dimensionless group.

By applying dimensional analysis, the material removal rate (MRR) 'Z' depends upon five significant input parameters: pulse on time, pulse off time, peak current, spark gap voltage and wire feed. Again, by selecting:

M (mass)

L (length)

T (time)

I (current)

as basic dimensions, the dimensions of the foregoing quantities would then be:

1. *The MRR "Z" (mm^3/min), $M^0L^3T^{-1}$*
2. *Pulse on time "T_{on}" (μs), $M^0L^0T^1$*
3. *Pulse off time "T_{off}" (μs), $M^0L^0T^1$*
4. *Peak current "Ip" (A),$M^0L^0T^0I^1$*
5. *Spark gap voltage "SV" (Volt), $M^1L^2T^{-3}I^{-1}$*
6. *Wire feed rate "WF" (m/min),$M^0L^1T^{-1}$*
7. *Wire tension "WT"(gram), $M^1L^0T^0$*

Now,

$$Z = f(T_{on}, T_{off}, Ip, SV, WF, WT) \quad (6.2)$$

In this case, n=7 and m=4, hence, we can have (n-m=3) π_1, π_2, and π_3 respectively, we obtain three dimensionless groups.

$$\pi_1 = Z\,(T_{off})^{\alpha 1}\,(Ip)^{\beta 1}\,(SV)^{\gamma 1}\,(WT)^{\delta 1} \quad (6.3)$$

$$\pi_2 = T_{on}\,(T_{off})^{\alpha 2}\,(Ip)^{\beta 2}\,(SV)^{\gamma 2}\,(WT)^{\delta 2} \quad (6.4)$$

$$\pi_3 = WF\,(T_{off})^{\alpha 3}\,(Ip)^{\beta 3}\,(SV)^{\gamma 3}\,(WT)^{\delta 3} \quad (6.5)$$

Substituting the dimensions of each quantity and equating to zero, the ultimate exponent of each basic dimension is achieved, since the "π_{is}" are dimensionless groups.

Solving for π_1, we get,

$$\pi_1 = M^0L^3T^{-1}(M^0L^0T^1)^{\alpha 1}\,(M^0L^0T^0I^1)^{\beta 1}\,(M^1L^2T^{-3}I^1)^{\gamma 1}\,(M^1L^0T^0)^{\delta 1} \qquad (6.6)$$

Here,

$\gamma_1 + \delta_1 = 0$

$3 + 2\gamma_1 = 0$

$-1 + \alpha_1 - 3\gamma_1 = 0$

$\beta_1 - \gamma_1 = 0$

On solving,

$\alpha_1 = 3.5,\ \beta_1 = -1.5,\ \gamma_1 = -1.5,\ \delta_1 = 1.5$

Hence,

$$\pi_1 = Z\,(T_{off})^{3.5}\,(Ip)^{-1.5}\,(SV)^{-1.5}\,(WT)^{1.5} \qquad (6.7)$$

Solving for π_2, we get,

$$\pi_2 = M^0L^0T^1\,(M^0L^0T^1)^{\alpha 2}\,(M^0L^0T^0I^1)^{\beta 2}\,(M^1L^2T^{-3}I^1)^{\gamma 2}\,(M^1L^0T^0)^{\delta 2} \qquad (6.8)$$

Here,

$\gamma_2 + \delta_2 = 0$

$2\gamma_2 = 0$

$1 + \alpha_2 - 3\gamma_2 = 0$

$\beta_2 - \gamma_2 = 0$

On solving,

$\alpha_2 = -1, \beta_2 = 0, \gamma_2 = 0, \delta_2 = 0$

Hence,

$$\pi_2 = Ton\ (Toff)^{-1} \tag{6.9}$$

Similarly, we get,

$$\pi_3 = M^0L^0T^{-1}\ (M^0L^0T^1)^{\alpha 3}\ (M^0L^0T^0I^1)^{\beta 3}\ (M^1L^2T^{-3}I^{-1})^{\gamma 3}\ (M^1L^0T^0)^{\delta 3} \tag{6.10}$$

Here,

$\gamma_3 + \delta_3 = 0$

$1+2\gamma_3 = 0$

$-1 + \alpha_3 - 3\gamma_3 = 0$

$\beta_3 - \gamma_3 = 0$

On solving,

$\alpha_3 = -0.5, \beta_3 = 0.5, \gamma_3 = -0.5, \delta_3 = 0.5$

Thus,

$$\pi_3 = WF\ (T_{off})^{-0.5}\ (Ip)^{0.5}\ (SV)^{-0.5}\ (WT)^{0.5} \tag{6.11}$$

The functional relationship is of the form,

$\pi_1 = f(\pi_2, \pi_3)$

Hence,

$$Z\,(T_{off})^{3.5}\,(Ip)^{-1.5}\,(SV)^{-1.5}\,(WT)^{1.5} = f\,[(T_{on}\,(T_{off})^{-1}]\,[WF\,(T_{off})^{-0.5}\,(Ip)^{0.5}\,(SV)^{-0.5}\,(WT)^{0.5}] \quad (6.12)$$

$$Z = C\,[WF^{1}\,T_{on}{}^{1}T_{off}{}^{-5}\,Ip^{2}\,SV^{1}] \quad (6.13)$$

Where, C is a constant of proportionality. To calculate "C", experiments were performed by keeping remaining parameters set at constant level and varying one parameter.

6.2.1 Case I (WF=8m/min, T_{off} =36µs, Ip=160A, and SV=45V)

To know the effect of pulse on time on MRR, experiments were performed by "changing one factor at a time approach" thus with changing pulse on time and keeping all other parameters at constant level. The actual data presented in Table 6.1. Thus the equation for C and fitted line plot as shown in Figure 6.1.

Table 6.1 Effect of process parameters on material removal rate (MRR)

Parameters	Range	Units	Mean MRR(mm^3/min)
Pulse on time (T_{on})	0.35	µs	1.26
	0.6	µs	2.15
	0.85	µs	3.38
	1.1	µs	5.40
	1.35	µs	7.87
	1.6	µs	10.65
Peak current (Ip)	40	A	3.18
	80	A	4.35
	120	A	5.42
	160	A	6.12
	200	A	7.00
	230	A	7.18
Spark gap voltage (SV)	5	V	10.40
	15	V	8.30
	25	V	7.20
	35	V	7.05
	45	V	6.75
	55	V	6.22
	65	V	5.44
Wire feed rate (WF)	2	m/min	3.89
	4	m/min	3.92
	6	m/min	3.95
	8	m/min	4.02
	10	m/min	4.10
	12	m/min	4.12

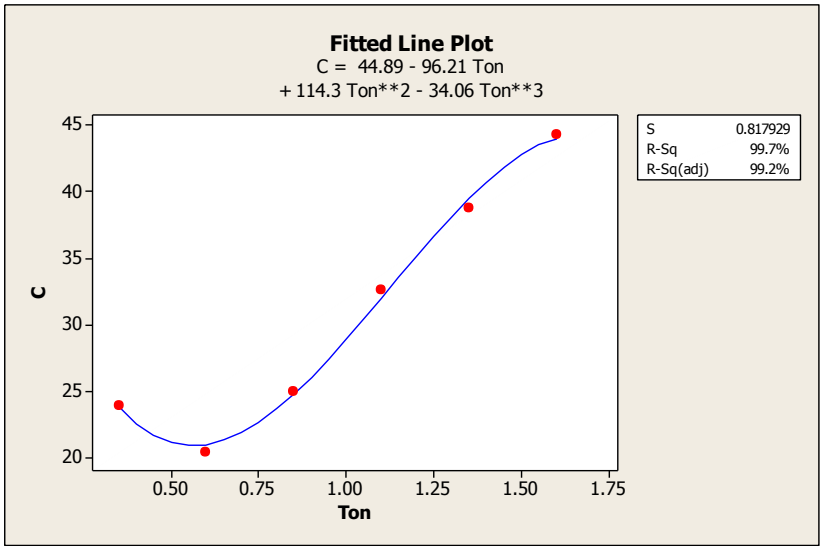

Figure 6.1 Fitted line plot for MRR by varying T_{on}

The data has been further used for finding the best fitting line as depicted in Figure 6.2. Thus the regression equation for MRR in this case is.

$$Z= (44.89-96.21T_{on} + 114.3T_{on}^{2} - 34.06T_{on}^{3}) \times WF^{1}\ T_{on}^{1}\ T_{off}^{-5} Ip^{2}\ SV^{1} \quad (6.14)$$

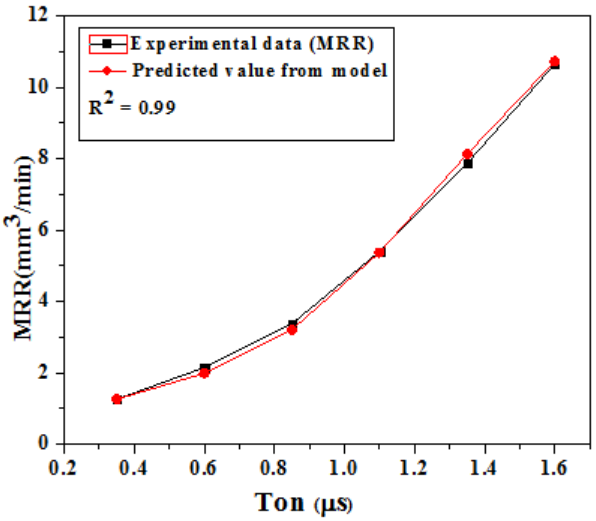

Figure 6.2 MRR values proposed by experimental and micro- model for T_{on}

6.2.2 Case II (WF=8m/min, T_{on} =0.85µs, T_{off} =36µs, and SV=45V)

To know the effect of peak current on MRR, experiments were performed by "changing one factor at a time approach" thus with changing peak current and keeping all other

parameters at constant level. Thus the equation for C and fitted line plot as shown in Figure 6.3.

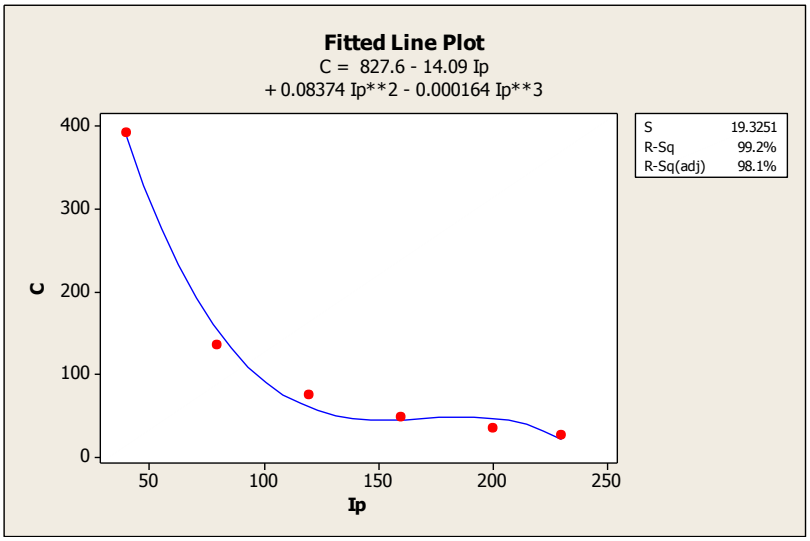

Figure 6.3 Fitted line plot for MRR by varying Ip

The data has been further used for finding the best fitting line as depicted in Figure 6.4. Thus the regression equation for MRR in this case is.

$$Z = (827.4\text{-}14.09Ip + 0.08374Ip^2\text{-}0.000164Ip^3) \times WF^1 T_{on}^1 T_{off}^{-5} Ip^2 SV^1 \quad (6.15)$$

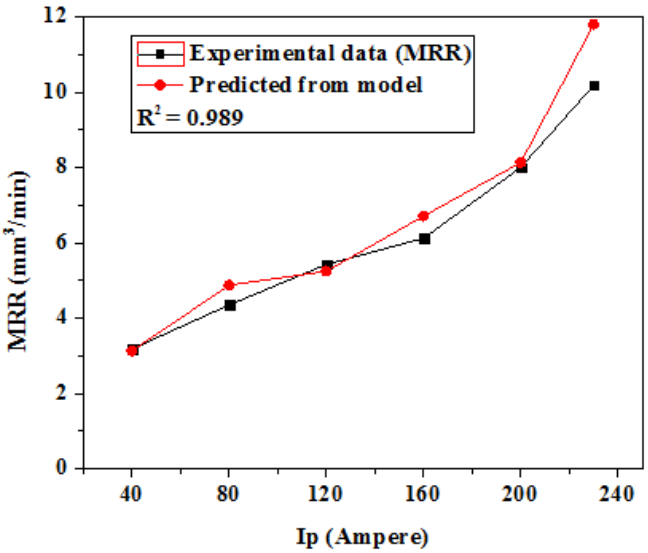

Figure 6.4 MRR values proposed by experimental and micro- model for Ip

6.2.3 Case III (WF=8m/min, T_{on} =0.85µs, T_{off} =36µs, and Ip=160A)

To know the effect of spark gap voltage on MRR, experiments were performed by "changing one factor at a time approach" thus with changing spark gap voltage and keeping all other parameters at constant level. Thus the equation for C and fitted line plot as shown in Figure 6.5.

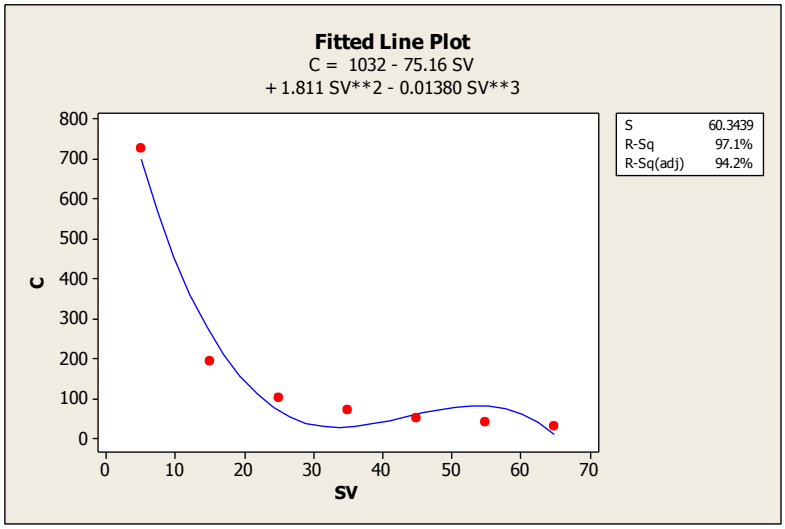

Figure 6.5 Fitted line plot for MRR by varying SV

The data has been further used for finding the best fitting line as depicted in Figure 6.6. Thus the regression equation for MRR in this case is.

$$Z = (1032\text{-}75.16SV+1.811SV^{2}\text{-}0.01380SV^{3}) \times WF^{1}\ T_{on}^{\ 1}\ T_{off}^{\ -5} Ip^{2}\ SV^{1} \qquad (6.16)$$

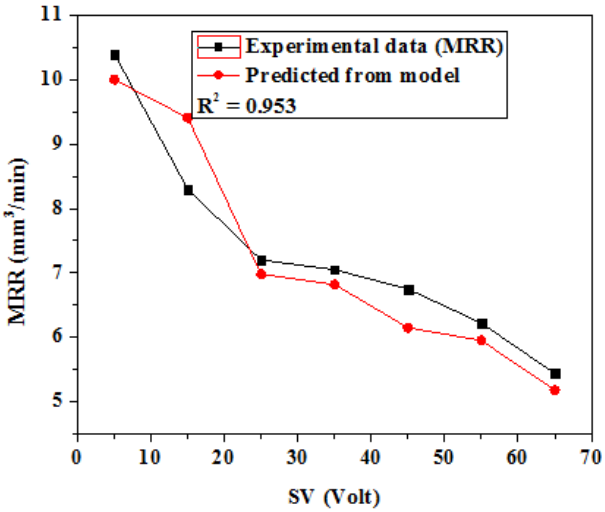

Figure 6.6 MRR values proposed by experimental and micro- model for SV

6.2.4 Case IV (T_{on} =0.85µs, T_{off} =36µs, Ip = 160A and SV=45V)

To know the effect of wire feed rate on MRR, experiments were performed by "changing one factor at a time approach" thus with changing wire feed rate and keeping all other parameters at constant level. Thus the equation for C and fitted line plot as shown in Figure 6.7.

The data has been further used for finding the best fitting line as depicted in Figure 6.8. Thus the regression equation for MRR in this case is.

$$Z = (218.4\text{-}61.31WF+6.691WF^{2}\text{-}0.246WF^{3}) \times WF^{1}\ T_{on}^{\ 1}\ T_{off}^{\ -5} Ip^{2}\ SV^{1} \qquad (6.17)$$

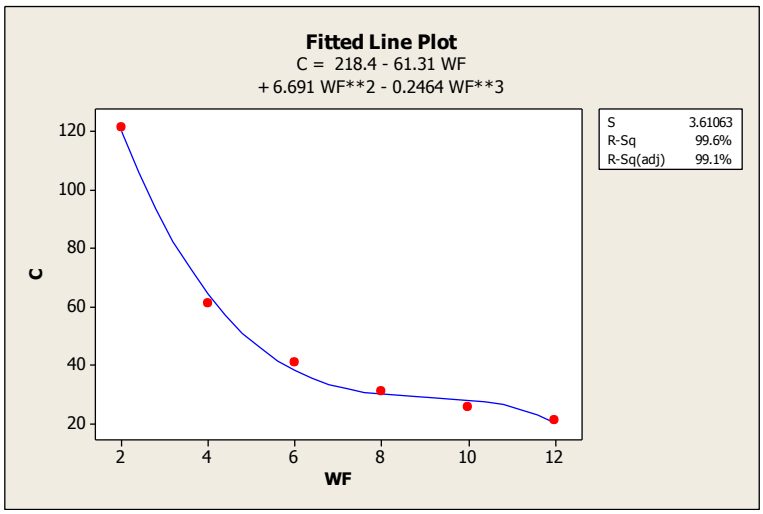

Figure 6.7 Fitted line plot for MRR by varying WF

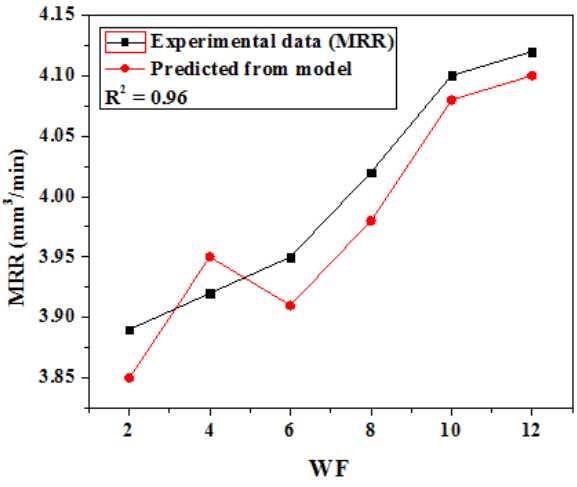

Figure 6.8 MRR values proposed by experimental and micro- model for WF

The developed model has been validated by comparing the predictions of the model with the experimental values of MRR and a good agreement between the two has been obtained. The model might be very useful for prediction of MRR over a wide range of input parameters of WEDM process. The model would find application in parameter selection for profile cutting operation of pure titanium parts in industrial sectors such as aerospace or heat exchanger manufacturing

6.3 MICRO-MODEL FOR PREDICTION OF SURFACE ROUGHNESS (Ra)

The Buckingham π theorem states that it is possible to assemble all variables appearing in a problem into a number of dimensionless products (π_i). In addition, the required relations connecting the individual variables are determined by algebraic expressions relating each π_i. According to the breakdown mechanism of WEDM, the dissipated energy in the cathode depends upon the ionization voltage, cathode drop, and work function of the cathode materials. In contrast, the energy dissipated into the anode depends only on the anode voltage drop and the work function of the anode materials. The effects of electric polarity on wire erosion can therefore be expressed in terms of the work function, the ionization potential, and the cathode or anode drop, either from the view point of the cathode or the anode. Based on a theoretical conjecture, the work metal is removed essentially by evaporation, but a small amount of molten metal remains in the crater. Part of the crater may be ejected owing to the various forces operating in the spark region based on observations in the past. Therefore, it seems justified to assume that the effects of the latent heat of fusion and the melting temperature can be neglected. By applying dimensional analysis, the surface roughness 'Ra' depends upon six significant input parameters: pulse on time, pulse off time, peak current, spark gap voltage and wire tension .Since the dimensionless homogeneous equation of quality characteristics has 7 variables and only 4 fundamental dimensionless coefficients. According to the Buckingham π theorem, the dimensional formula on the surface roughness (Ra) of work can now be written as:

Again, by selecting:

M (mass)

L (length)

T (time)

I (current)

as basic dimensions, the dimensions of the foregoing quantities would then be:

1. *The surface roughness "Ra" (μm),* $M^0L^1T^0$
2. *Pulse on time "Ton" (μs),* $M^0L^0T^1$
3. *Pulse off time "Toff" (μs),* $M^0L^0T^1$
4. *Peak current "Ip" (A),* $M^0L^0T^0I^1$
5. *Spark gap voltage "SV" (Volt),* $M^1L^2T^{-3}I^1$
6. *Wire feed rate "WF" (m/min),* $M^0L^1T^{-1}$
7. *Wire tension "WT" (gram),* $M^1L^0T^0$

Now,

$$Ra = f(T_{on}, T_{off}, Ip, SV, WF, WT) \quad (6.18)$$

In this case, n=7 and m=4, hence, we can have (n-m=3) π_1, π_2, and π_3 respectively, we obtain three dimensionless groups.

$$\pi_1 = Ra\,(T_{off})^{\alpha 1}\,(Ip)^{\beta 1}\,(SV)^{\gamma 1}\,(WT)^{\delta 1} \quad (6.19)$$

$$\pi_2 = T_{on}\,(T_{off})^{\alpha 2}\,(Ip)^{\beta 2}\,(SV)^{\gamma 2}\,(WT)^{\delta 2} \quad (6.20)$$

$$\pi_3 = WF\,(T_{off})^{\alpha 3}\,(Ip)^{\beta 3}\,(SV)^{\gamma 3}\,(WT)^{\delta 3} \quad (6.21)$$

Substituting the dimensions of each quantity and equating to zero, the ultimate exponent of each basic dimension is achieved, since the "π_{is}" are dimensionless groups.

Solving for π_1, we get,

$$\pi_1 = M^0L^1T^0(M^0L^0T^1)^{\alpha 1}\,(M^0L^0T^0I^1)^{\beta 1}\,(M^1L^2T^{-3}I^{-1})^{\gamma 1}\,(M^1L^0T^0)^{\delta 1} \quad (6.22)$$

Here,

$$\gamma_1 + \delta_1 = 0$$

$$1 + 2\gamma_1 = 0$$

$$\alpha_1 - 3\gamma_1 = 0$$

$\beta_1 - \gamma_1 = 0$

On solving,

$\alpha_1 = -1.5, \beta_1 = -0.5, \gamma_1 = -0.5, \delta_1 = 0.5$

Hence,

$$\pi_1 = Ra\ (T_{off})^{-1.5}\ (Ip)^{-0.5}\ (SV)^{-0.5}\ (WT)^{0.5} \quad (6.23)$$

Solving for π_2, we get,

$$\pi_2 = M^0L^0T^1\ (M^0L^0T^1)^{\alpha 2}\ (M^0L^0T^0I^1)^{\beta 2}\ (M^1L^2T^{-3}I^{-1})^{\gamma 2}\ (M^1L^0T^0)^{\delta 2} \quad (6.24)$$

Here,

$\gamma_2 + \delta_2 = 0$

$2\gamma_2 = 0$

$1 + \alpha_2 - 3\gamma_2 = 0$

$\beta_2 - \gamma_2 = 0$

On solving,

$\alpha_2 = -1, \beta_2 = 0, \gamma_2 = 0, \delta_2 = 0$

Hence,

$$\pi_2 = T_{on}\ (T_{off})^{-1} \quad (6.25)$$

Similarly, we get,

$$\pi_3 = M^0L^0T^{-1}\ (M^0L^0T^1)^{\alpha 3}\ (M^0L^0T^0I^1)^{\beta 3}\ (M^1L^2T^{-3}I^{-1})^{\gamma 3}\ (M^1L^0T^0)^{\delta 3} \quad (6.26)$$

Here,

$\gamma_3 + \delta_3 = 0$

$1+2\gamma_3 = 0$

$-1 + \alpha_3 - 3\gamma_3 = 0$

$\beta_3 - \gamma_3 = 0$

On solving,

$\alpha_3 = -0.5, \beta_3 = 0.5, \gamma_3 = -0.5, \delta_3 = 0.5$

Thus,

$$\pi_3 = WF\ (Toff)^{-0.5}\ (Ip)^{0.5}\ (SV)^{-0.5}\ (WT)^{0.5} \quad (6.27)$$

The functional relationship is of the form,

$\pi_1 = f(\pi_2, \pi_3)$

Hence,

$$Ra\ (T_{off})^{-1.5}\ (Ip)^{-0.5}\ (SV)^{-0.5}\ (WT)^{0.5} = f\ [(T_{on}\ (T_{off})^{-1}]\ [WF\ (T_{off})^{-0.5}\ (Ip)^{0.5}\ (SV)^{-0.5}\ (WT)^{0.5}] \quad (6.28)$$

$$Ra = C\ [T_{on}^{1}\ WF^{1}\ Ip^{1}] \quad (6.29)$$

Where, C is a constant of proportionality.

To calculate "C", experiments were performed by using one factor at a time approach (OFTA).

6.3.1 Case I (WF=8m/min, T_{off} =36µs, Ip=160A, and SV=45V)

To know the effect of pulse on time (T_{on}) on surface roughness (Ra), experiments were performed by "changing one factor at a time approach" thus with changing pulse on time (Ton) by keeping all other parameters at constant level. The actual data presented in Table.2. Thus the equation for C and fitted line plot as shown in Figure 6.9.

Table 6.2 Effect of process parameters on surface roughness (Ra)

Parameters	Range	Units	Ra(µm)
Pulse on time (T_{on})	0.35	µs	1.57
	0.6	µs	1.87
	0.85	µs	1.95
	1.1	µs	2.24
	1.35	µs	2.78
	1.6	µs	3.25
Peak current (Ip)	40	A	1.58
	80	A	1.76
	120	A	2.41
	160	A	2.39
	200	A	2.54
	230	A	2.58
Wire feed rate (WF)	2	m/min	2.20
	4	m/min	2.31
	6	m/min	2.25
	8	m/min	2.27
	10	m/min	2.30
	12	m/min	2.24

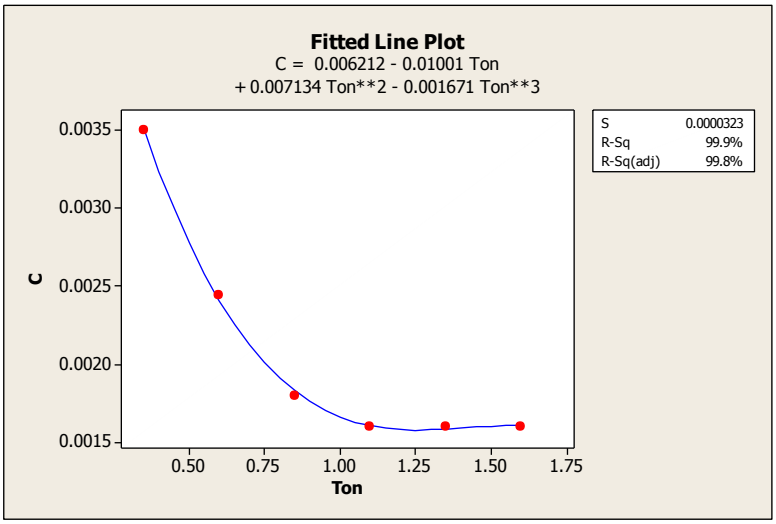

Figure 6.9 Fitted line plot for Ra by varying Ton

The data has been further used for finding the best fitting line as depicted in Figure 6.10. Thus the regression equation for Ra in this case is.

$$Ra = (0.006212 - 0.01001T_{on} + 0.007134T_{on}^{2} - 0.001671T_{on}^{3}) \times T_{on}^{1}\, WF^{1}\, Ip^{1} \qquad (6.30)$$

6.3.2 Case II (WF=8m/min, T_{on} =0.85µs, Toff =36µs, and SV=45V)

To know the effect of peak current on surface roughness (Ra), experiments were performed by "changing one factor at a time approach" thus with changing peak current and keeping all other parameters at constant level. Thus the equation for C and fitted line plot as shown in Figure 6.11.

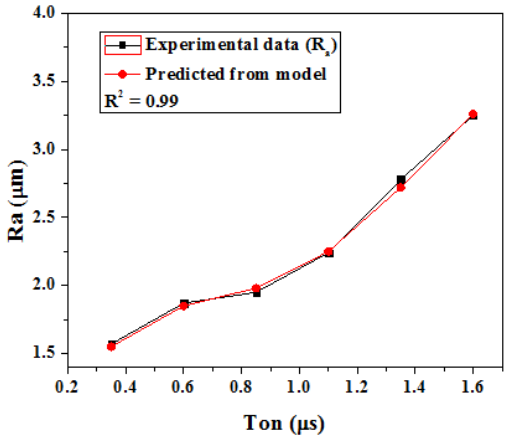

Figure 6.10 Ra values proposed by experimental and micro- model for T_{on}

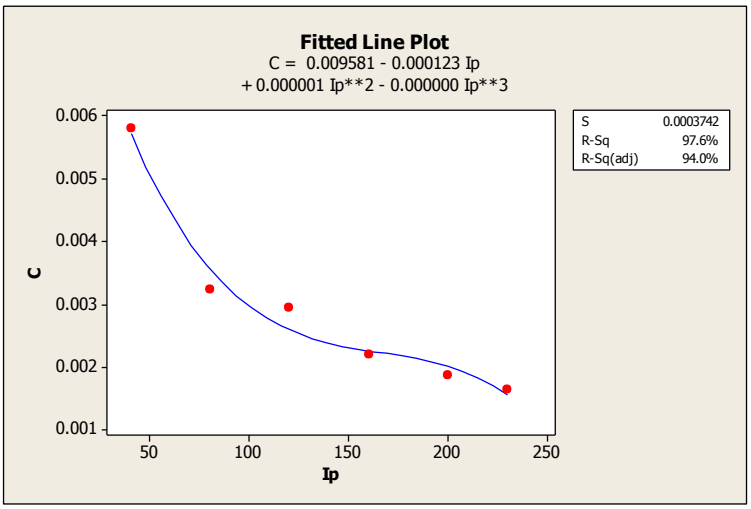

Figure 6.11 Fitted line plot for Ra by varying Ip

The data has been further used for finding the best fitting line as depicted in Figure 6.12. Thus the regression equation for Ra in this case is.

$$Ra = (0.009581 - 0.000123Ip + 0.000001Ip^2 - 0.000000Ip^3) \times Ton^1 WF^1 Ip^1 \quad (6.31)$$

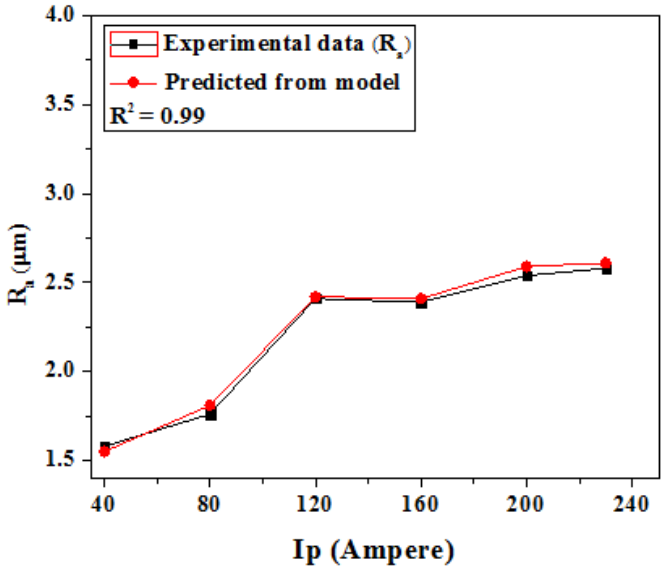

Figure 6.12 Ra values proposed by experimental and micro- model for Ip

6.3.3 Case III (Ton =0.85µs, Toff =36µs, Ip = 160A and SV=45V)

To know the effect of wire feed rate on surface roughness (Ra), experiments were performed by "changing one factor at a time approach" thus with changing wire feed rate and keeping all other parameters at constant level. Thus the equation for C and fitted line plot as shown in Figure 6.13.

The data has been further used for finding the best fitting line as depicted in Figure 6.14. Thus the regression equation for Ra in this case is.

$$Ra = (0.01426 - 0.003884WF + 0.000415WF^2 - 0.000015WF^3) \times T_{on}^1 WF^1 Ip^1 \quad (6.32)$$

The micro-model developed for prediction of both the MRR and surface roughness is found to yield precise results, as established from the values of R^2 obtained in each case. The model could find application on the shop floor for prediction of the machining performance of WEDM over a wide range of input parameters.

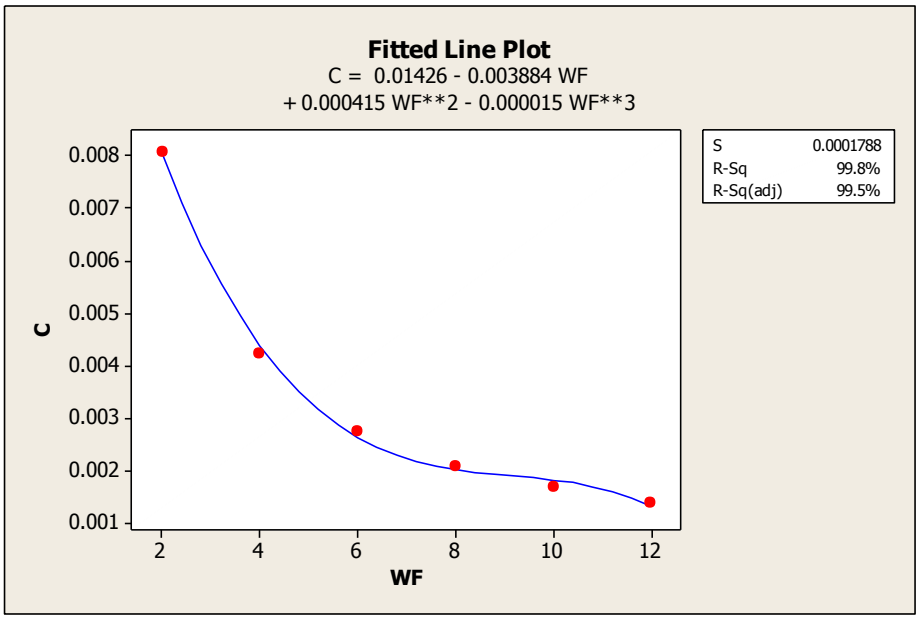

Figure 6.13 Fitted line plot for Ra by varying WF

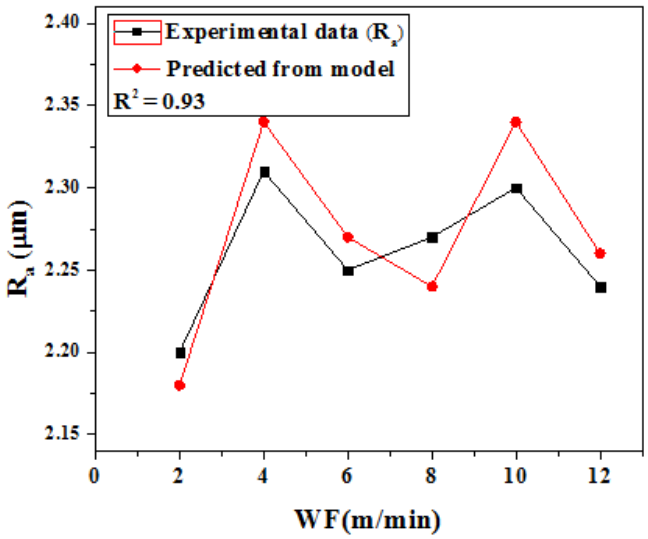

Figure 6.14 Ra values proposed by experimental and micro- model for WF

CHAPTER 7

CONCLUSIONS AND SCOPE FOR FUTURE WORK

7.1 CONCLUSIONS

In previous chapters, details of preliminary investigations and finalization of working range of WEDM process parameters, main experimentation using Box-Behnken Design approach, and optimization of WEDM process parameters using RSM with desirability approach are presented. This investigation as a whole is successful in identifying parameters that require attention from operational viewpoint during machining of pure titanium. This chapter list down general conclusions drawn from the present research work. The future research directions are also discussed.

7.1.1 Conclusions drawn from the pilot investigation

1. Pulse on time, pulse off time, peak current and spark gap set voltage mainly affect the machining rate obtained. The effect of wire feed rate and wire tension on machining rate is found to be insignificant.
2. The pulse on time, pulse off time, peak current and spark gap voltage affects the surface roughness of the machined surface. A little effect of wire feed rate and wire tension was also observed on surface roughness.
3. The pilot study concluded the range of process parameters as; pulse on time from 0.7μs to 1.1μs, pulse off time from 17μs to 38μs, peak current from 120 A to 200 A, spark gap voltage from 40V to 60V, wire feed rate from 4m/min to 10 m/min and wire tension from 500g to 1400g, as the outcome to carry out further investigation on WEDM of pure titanium.

7.1.2 Conclusions drawn from main experimentation

1. The machining rate obtained was ranged between 0.446 mm/min and 0.916 mm/min. The percentage contribution of input factors is given as; pulse on time: 54%, pulse off time: 26%, peak current: 9%, spark gap voltage: 7% and error: 4%.
2. Material removal rate (MRR) was found to be increased approximately 53.45% when pulse on time was increased from 0.7 μs to 1.1 μs. Meanwhile, when pulse off

time was decreased from 38 to 17μs, the increment of material removal rate is obtained 33.41%. When peak current was increased from 120 to 200A showed the marginal increment of material removal rate is 23.38%.

3. The surface roughness varied between 2.48μm to 2.62μm. The surface roughness was mainly affected by interaction between pulse on time and peak current. The decrement of surface roughness was about 13.1%, when spark gap voltage was increased from 40 to 60V.
4. The dimensional deviation was decreased from 153.80μm to 149.32 μm on increasing the spark gap voltage from 40V to 60V. When peak current was increased from 120 to 200A, it showed the less significant effect on dimensional deviation, i.e. 151 to 154μm.The overcut was decreased from 26.85μm to 34.07μm when spark gap voltage decreased from 60V to 40V. The optimum parametric combination obtained for overcut is; pulse on time = 0.7μs, pulse off time =36μs, peak current =160A, spark gap voltage = 50V, wire feed = 7m/min and wire tension = 950 gram.
5. Wire rupturing was observed due to higher peak current and spark frequency. The formation of craters and the residuals of debris adhered to the surface of wire electrode was observed using the EDX analysis.
6. This study describes the average white layer thickness and surface crack density at machined surface using SEM. It is found that the pulse on time, pulse off time and peak current are the most significant parameters for these responses.
7. The surface crack density increased from 0.0066μm/μm^2 to 0.010μm/μm^2 by decreasing the pulse off time from 38 to 17μs. On increasing the peak current from 120A to 200A, the surface crack density increasing from 0.0065μm/μm^2 to 0.015μm/μm^2.
8. Recast layer thickness was increased from 34.07μm to 48.78μm, on increasing the pulse on time (0.7μs-1.1μs), it was found to be decreased on increasing the pulse off time (17μs-38μs) from 49.35μm to 48.32μm.
9. A mechanistic model was developed for prediction of material removal rate and surface roughness; cover a wide range of significant input parameters. The predicted results were found to be in good agreement with the experimental results.

7.1.3 Conclusions drawn from surface characterization

1. The surface integrity was studied using scanning electron microscope (SEM). It was observed that higher pulse on time and peak current deteriorated the surface integrity of machined samples. It resulted in the formation of deep and wide overlapping craters, pock marks, globules of debris and micro cracks.
2. The residuals of spherical nodules in free or compound form were observed near the heat affected zone. These nodules were developed due to thermal affects and surface tension. The spherical nodules were formed due to higher discharge energy and rapid quenching resulted in martensite α structure.
3. The recast layer was developed due to higher peak current, pulse on time and low pulse off time. The micro-cracks in the recast layer were formed due to higher discharge energy. The average thickness of recast layer was found to vary between 6μm to 58μm.
4. The crack density was increased due to rapid cooling and heating in the spark zone. Due to melting and vaporization, solidified material was observed as amorphous either in free form or in compound form. Higher carbon content revealed that the machined surface becomes hard and brittle at the grain boundaries, which reinforces the surface cracking effect during solidification.
5. The residuals of copper, carbon and zinc were detected in the machined samples using EDX analysis. The major content of oxygen and carbon was due to decomposition of dielectric fluid, oxidation and mixing of debris at high temperature involved in the process. From the EDX analysis, it was observed that the migration of elements from electrode to workpiece is influenced by pulse on time and pulse off time parameters.
6. Using XRD analysis, the chemical compounds and phases of titanium dioxide (rutile) (TiO_2), ($TiO_{0.325}$), Ti_2O_3, Ilmenite (Fe_2Ti_4O), copper titanium tetra-dioxide (Cu_3TiO_4), zinc titanium carbide (Ti_3ZnC), titanium zinc carbide (Zn_2Ti_4C), titanium carbide (TiC) have been studied. The compounds have been formed due to migration of workpiece elements, tool elements and soluble oxygen in dielectric (deionized water).

6.2 LIMITATIONS OF THE RESEARCH

1. In the present work, only straight cutting of pure titanium using WEDM has been done. Efforts can be directed towards parametric optimization for the curved profile.
2. In the present work, diffused brass wire of Ø 0.25 mm is used as the tool electrode. Process analysis can be done using wire of different diameters and different material.
3. Present work optimized process parameters considering rough cutting. Trim cutting operation of pure titanium can be investigated.
4. There is further scope of process simulation (Finite element analysis) in for dry WEDM.

6.3 SCOPE FOR FUTURE WORK

The results presented by the present work can be used directly for effective and economical machining of pure titanium in industrial applications. The future research directions in WEDM machining as follows:

1. In the future work, wire impregnated with abrasives such as Al_2O_3 and SiC can be experimented, if major changes in machine set-up are permitted.
2. The issues such as residual stress after machining with WEDM may be investigated.
3. The present work is an attempt towards the investigation of machinability characteristics of pure titanium using WEDM. The research work could be further extended over a variety of some more advanced materials such as MMC's, shape memory alloys.
4. The results can be analyzed using other optimization techniques such as neural network, fuzzy logic, genetic algorithm, particle swarm optimization etc., and their effectiveness can be compared.
5. The possible use of cryogenic treated wire electrode for machining of non conductive and composite materials (Ceramic, fiberglass etc.) could also be investigated.

REFERENCES

1. Abdulkareem, S., Khan, A. A. and Zain, Z.M., (2011), "Effect of machining parameters on surface roughness during wet and dry wire EDM of stainless steel", *Journal of Applied Sciences*, pp. 1-5.

2. Adler, Y. P., Markova, E.V. and Granovosky, Y.V., (1975), "The design of experiments to find optimal conditions", Mir Publishers, Moscow.

3. Aggarwal, A., Singh H., Kumar, P. and Singh, M.(2008), "Modeling of machining parameters and cooling conditions in hard turning of AISI P-20 tool steel using response surface methodology and desirability graphs", *International Journal of Machining & Machinability of Materials* , Vol. 4, No. 1, pp. 95-110.

4. Ahmet, H., Ulas, C., (2004), "Experimental study of wire electrical discharge machining of AISI D5 tool steel", *Journal of Materials Processing Technology*, Vol. 148, pp. 362–367.

5. Ali, T., (2006), " Parametric study and optimization of wire electrical discharge machining of AI-Cu-TiC-Si P/M composite", *International Journal of Machining and Machinability of Materials*, Vol. 1, No. 4, pp. 380-395.

6. Almeida, I.A., Rossi de, W., Lima, M.S.F., Berretta, J.R., Wetter N.U., Vieira, N.D., (2006), "Optimization of titanium cutting by factorial analysis of the pulsed Nd: YAG laser parameters", *Journal of Materials Processing Technology*, Vol. 179, pp. 105-110.

7. Amin, A.K.M.; Ismail, F.A. and Khairushima, M.K., (2007), "Effectiveness of uncoated WC-Co and PCD inserts in end milling of titanium alloy Ti-6Al-4V", *Journal of Materials Processing Technology*, Vol. 192-193, pp. 147-158.

8. Antony, (2003), "Design of experiments for engineers and scientists", Butterworth and Heinman, USA.

9. ASM Material Data Sheet (Aerospace Specification Metals Inc), 26 /12/2008, www.asm.com.

10. Aspinwall, Soo, D.K., Berrisford, S.L, Walder, G., (2008), "Work piece surface roughness and integrity after WEDM of Ti-6Al-4V and Inconel-718 using minimum damage generator technology", *CIRP Annals Manufacturing Technology*, Vol. 57, pp. 187-190.

11. Asokan, T., Sudhakar, R.S., and De Costa, P. (2000), "Electrical discharge drilling of titanium alloys for aerospace applications", *Manufacturing Technology Proceeding of 19th AIMTDR Conf.,* Narosa Publishing House, pp. 161-165.

12. Beltrami, I., Dauw, D., (1996), "A simplified post process for wire cut EDM", *Journal of Materials Processing Technology*, Vol. 58, No. 4, pp. 385-389.

13. Benedict, G.F., (1987), "Electrical discharge machining (EDM)", Nontraditional manufacturing processes", Marcel Dekker, New York and Basel, pp. 231-232.

14. Box G.E.P. and Hunter J. S. (1957), "Multifactor Experimental Designs for Exploring Response Surface", Annals of Mathematical. Statistics, 28, pp 195-241.

15. Box G.E.P., (1952) ,"Multilayer design of first order", Biometrics, Vol. 39, pp. 49-57.

16. Box, G.E., Behnken, D.W., (1960), "Some new three level designs for the study of quantitative variables", Technometrics, Vol. 2, pp. 455–475.

17. Box, G.E.P., Hunter, W.G. and Hunter, J.S., (1978), "Statistics for experimenters", Wiley, New York.

18. Cabanes, I., Portillo, E., Macros, M., Sanchez, J. A., (2008), "On line prevention of wire breakage in wire electro discharge machining", *Robotics and Computer Integrated Manufacturing*, Vol. 24, pp. 287-298.

19. Chiang, K.T. and Chang, F.P., (2006) "Optimization of the WEDM process of particle-reinforced material with multiple performance characteristics using grey relational analysis". *Journal of Materials Processing Technology*, Vol. 180, pp. 96-101.

20. Chow, H.M., Yan, B.H., Huan, F.Y., and Hung, J.C. (2000), " Study of added powder in kerosene for the micro slit machining of titanium alloy using electro discharge machining", *Journal of Material Processing Technology* 101 pp. 95-103.

21. Chen, S.L., Yan, B.H., Huang, F.Y. (1999), "Influence of kerosene and distilled water as dielectric on the electric discharge machining characteristics of Ti-6Al-4V", *Journal of Materials Processing Technology* 87, pp. 107–111.

22. Datta, S. and Mahapatra, S.S., (2010), "Modelling, simulation and optimization of Wire EDM process using response surface methodology coupled with Grey Taguchi", *International Journal of Engineering Science and Technology*, Vol. 2, No.5, pp. 162-183.

23. Dauw, D.F. and Beltrami, I., (1994), "High-precision wire-EDM by online wire positioning control", *Annals of CIRP*, Vol. 43, No. 1, pp. 193–197.

24. Derringer, G. and Suich, R., (1980), "Simultaneous optimization of several response variables", *Journal of Quality Technology*, Vol. 12, pp. 214-219

25. Dixit, U.S., Risbood, K.A. and Sahasrabudhe, A.D., (2003), "Prediction of surface roughness and dimensional deviation by measuring cutting forces and vibrations in turning process", *Journal of Materials Processing Technology*, Vol. 132, No. 1–3, pp. 203-214.

26. Donachie, M. J., (2000), "Titanium: A technical guide", 2nd ed., ASM international, OH, USA.

27. Hamed, E. and Sarkar, A., (2001), "Application of multiple response optimization technique to extended release formulations design", Journal of Control, Vol. 73, pp. 329–338.

28. Ekmekci, B., (2009), "White layer composition, heat treatment and crack formation in electric discharge machining process", *Journal of Materials Processing Technology*, Vol. 40, pp. 70-81.

29. Electronica Machine Tools Ltd. (2010), "Technology manual for Wire cut EDM-Electronica Sprintcut 734", pp. 1-2.

30. Ezugwu, E. O. and Wang, Z. M., (1997), "Titanium alloys and their machinability – a review", *Journal of Materials Processing Technology*, Vol. 68, pp. 262-274.

31. Ferreira, S.L., Bruns, R.E., Ferreira, H.S., Matos, G.D., David, J.M., Brandao, G.C., Da Silva, E.G., Portugal, L.A., Dos Reis, P.S., Souza, A.S. and Dos Santos, W.N., (2007), "Box–Behnken design: an alternative for the optimization of analytical methods". *Anal. Chim. Acta*, Vol. 597, pp. 179–186.

32. Fonda, Peter, Wang, Zhigang, Yamazaki, Kazuo, Akutsu, Yuji (2008), "A fundamental study on Ti–6Al–4V's thermal and electrical properties and their relation to EDM productivity", *Journal of Materials Processing Technology* 202, pp. 583-589.

33. Garg, R.K., Singh, K.K., Sachdeva, A., Sharma, V.S., Ojha, K. and Singh, S., (2010), "Review of research work in sinking EDM and WEDM on metal matrix composite materials", *International Journal of Advanced Manufacturing Technology*, Vol. 50, No. 5-8, pp. 611-624.

34. Gauri, S. K. and Chakraborty, S., (2010), "A study on the performance of some multi response optimization methods in WEDM processes", *International Journal of Advanced Manufacturing Technology*, Vol. 49, pp. 155-166.

35. Ginting, A. and Nouari, M., (2007), "Optimal cutting conditions when dry end milling the aero engine material Ti-6242Si", *Journal of Materials Processing Technology*, Vol. 184, pp. 319-324.

36. Goldberg, D. E., (1989), "Genetic algorithm in search, optimization and machine learning", Addison Wesley Reading, Massachusetts.

37. Guitrau, B., (1997), "The EDM Handbook", Hansen Gardner Publications, Cincinnati, OH, pp. 174.

38. Govindan, P., and Joshi, S.S., (2012), "Analysis of micro-cracks on machined surfaces in dry electrical discharge machining", *Journal of Manufacturing Processes*, Vol.14, pp. 277–288.

39. Gunaraj, V. and Murugan, N., (1999), "Application of response surface methodologies for predicting weld base quality in submerged arc welding of pipes", *Journal of Materials Processing Technology*, Vol. 88, pp. 266–275.

40. Guo, Z. N., Wang, X., Huang, Z. G. and Yue, T. M., (2002), "Experimental investigation into shaping particle-reinforced material by WEDM", *Journal of Materials processing Technology*, Vol.129, pp. 56-59.

41. Han, F., Jiang, J. and Yu, D., (2007), "Influence of machining parameters on surface roughness in finish cut of WEDM", *International Journal of Advanced Manufacturing Technology*, Vol. 34, pp. 538-546.

42. Hascalyk, A. and Caydas, U., (2004), "Experimental study of wire electrical discharge machining of AISI D5 tool steel", *Journal of Materials Processing Technology*, Vol. 148, pp. 362–367.

43. Hascalik, Ahmet; Caydas, Ulas (2007a), "Electrical discharge machining of titanium alloy (Ti-6Al-4V)", *Applied Surface Science*, Vol. 253, pp. 9007-9016.

44. Hascalik, Ahmet; Caydas, Ulas (2007b), "A comparative study of surface integrity of Ti-6Al-4V alloy machined by EDM and AECG", *Journal of Material Processing Technology*, Vol. 190, pp.173-180.

45. Hewidy, M.S., El-Taweel, T.A. and El-Safty, M.F., (2005), "Modelling the machining parameters of wire electrical discharge machining of Inconel-601 using RSM", *Journal of Materials Processing Technology*, Vol. 169, pp. 328-336.

46. Ho, K.H., Newman, S.T. and Rahimifard, S., A., (2004), "State of the art in wire electrical discharge machining (WEDM)", *International Journal of Machine tools and Manufacture*, Vol.44, pp.1247-1259.

47. Hseigh S.F., Chen, S.L.,Lin, M.H.,(2009),"The machining characteristics and shape recovery ability of Ti Ni X(X= Zr, Cr) ternary shape memory alloys using WEDM" , *International Journal of Machine Tools and Manufacturing*, Vol. 49, pp. 509-514.

48. Hu, Y. H. and Hwang, J. N., (2002), "Handbook of neural network signal processing", CRC Press, New York.

49. Huang, J.T. and Liao, Y.S., (1997), "A study of finish-cutting operation number and machining parameters setting in wire electrical discharge machining", Proceedings of the International Conference on Precision Engineering (ICPE 97), pp. 671-676.

50. Huang, J.T., Liao, Y.S. and Hsue, W.J., (1999), "Determination of finish – cutting operation number and machining parameters setting in wire electrical discharge machining", *Journal of Materials Processing Technology*, Vol. 87, pp. 69-81.

51. Huang, C.A; Tu, G.C.; Yao, H.T.; Kuo, H.H. (2004), " Characteristics of the rough cut surface quenched and tempered maternsitic stainless steel using wire electric discharge machining", *Metallurgical and Materials Transactions A*, Vol.35A, pp.1351-1357.

52. Hunter, R.G., Sutherland, J.W and Devor, R.E., (1989), "A methodology for robust design using models for mean, variance and loss", The American Society of Mechanical Engineers, California, Dec. 10-15.

53. Hong, S.Y., Markus, I, and Jeong, W. (2001), "New cooling approach and tool life improvement in cryogenic machining of titanium alloy Ti-6Al-4V", *International Journal of Machine Tool Manufacture*, Vol. 41, pp. 2245-2260.

54. Huang, Yu, Ming, Wuyi, Guo, Jianwen, Zhang, Zhen, Liu, Guangdou, Li, Mingzhen and Zhang, Guojun, (2013), "Optimization of cutting conditions of YG15 on rough and finish cutting in WEDM based on statistical analyses", *International Journal of Advanced Manufacturing Technology,* DOI 10.1007/s00170-013-5037-3.

55. Ikram Adeel, Mufti, Nadeem Ahmad, Saleem, Muhammad Qaiser and Khan , Ahmed Raza, (2013), "Parametric optimization for surface roughness, kerf and MRR in wire electrical discharge machining (WEDM) using Taguchi design of experiment", *Journal of Mechanical Science and Technology,* Vol.27 No.7, pp. 2133-2141.

56. Jain, V.K, (2002), "Advance machining processes", Allied publishers Pvt. Ltd, New Delhi. pp. 1-5.

57. Jain, V.K, Jain, N.K.,. and Deb, K., (2007), "Optimization of process parameters of mechanical type Advance machining processes using genetic algorithms", *International Journal of Machine Tools and Manufacture*, Vol. 47, pp. 900-919.

58. Jameson, E.C., (2001), "Description and development of electrical discharge machining (EDM)", *Society of Manufacturing Engineers,* Dearben, Michigan, pp. 16.

59. Jeelani, S., (1983), "Subsurface plastic deformation in machining 6Al-2Sn-4Zr-2Mo Titanium alloy", *Wear*, Vol. 85, pp.121-130.

60. Jin, Y., Wang, K., Tao, Y. and Fang, M., (2008), "Reliable multi-objective optimization of high speed WEDM process based on Gaussian process regression", *International Journal of Machine Tools and Manufacture,* Vol. 48, pp. 47-60.

61. Joshi, S.S. and Das, S., (2010), "Modeling of spark erosion rate in micro- wire EDM", *International Journal of Advanced Manufacturing Technology*, Vol. 48, pp. 581-596.

62. Jawahir, I.S., Brinksmeier, E., Saoubi, R. M., Aspinwall, D.K., Outeiro, J.C., Meyer, D., Umbrello, D., Jayal, A.D. (2011), "Surface integrity in material removal processes: Recent advances", *CIRP Annals - Manufacturing Technology*, Vol. 60, pp. 603-626.

63. Jackson, M.J., (2006), "Atomic scale machining of surfaces", *Proceedings of 5th international surface engineering congress*, May 15-17, USA.

64. Kanalyasiri, K., and Boonmung, S., (2007), "Effects of wire-EDM machining variables on surface roughness of newly developed DC 53 die steel: Design of experiments and regression model", *Journal of Materials Processing Technology*, Vol. 192-193, pp. 459-464.

65. Kanangarajan, D., Kartthikeyan, R., Palanikumar, K. and Davim, J. P., (2008), "Optimization of electrical discharge machining characteristics of WC/Co composites using non dominated sorting genetic algorithm (NSGA-II)", *International Journal of Advanced Manufacturing Technology*, Vol. 36, pp.1124-1132.

66. Kinoshita, N., Fukui, M., Gamo, G., (1982), "Control of wire EDM preventing electrode from breaking", *Annals CIRP*, Vol.31, pp.111-114.

67. Kinsohita, N., Fukui, M., Kimura, Y., (1984), "Study on Wire-EDM: in process measurement of mechanical behavior of electrode wire", Annals of *CIRP*, Vol. 33, No.1, pp. 89–92.

68. Kondayya, D. and Krishna, A. G., (2010), "An integrated evolutionary approach for modelling and optimization of wire electrical discharge machining", *Proceedings of I Mech E Part B: Journal of Engineering Manufacture*, Vol. 225, pp. 549-567.

69. Kozak, J., Rajurkar,K.P. and Chandrana, N., (2004), "Machining of low electrical conductive materials by wire electrical discharge machining", *Journal of Materials Processing Technology*, Vol.149, pp. 266-271.

70. Kuang,Y. K. and Chiang, K.T., (2008), “Modeling and analysis of machinability evaluation in the wire electrical discharge machining (WEDM) Process of Aluminum Oxide-based ceramic”, *Materials and Manufacturing Processes*, Vol. 23, pp. 241–250.

71. Kumar, A., Kumar, V., and Kumar, J., (2012), “An investigation into machining characteristics of commercially pure titanium (grade-2) using CNC WEDM”, *Applied Mechanics of Materials*, Vol. 159, pp. 56-68.

72. Kumar, C.S., Ganesan, G. and Kartthikeyan, R., (2011), “Parametric optimization of electro chemical machining of Al/15%SiC C composites using NSGA-II”, *Transactions of Non Ferrous metal Society, China*, Vol. 21, pp. 2294-2300.

73. Kumar, J., (2009), “Investigating the machining characteristics of titanium using ultrasonic machining”, Ph. D thesis, Thapar University, Patiala.

74. Kumar, M., Babu, S., Venkatasamy, R. and Raajenthiren, M., (2010), “Optimization of the WEDM Parameters on Machining Inconel 800 super alloy with Multiple Quality Characteristics”, *International Journal of Engineering Science and Technology*, Vol. 2, No. 6, pp. 1538-1547.

75. Kuriakose, S. and Shunmugam, M. S., (2005), “Multi -objective optimization of wire electro- discharge machining process by non-dominated sorting genetic algorithm”, *Journal of Materials Processing Technology*, Vol. 170, No. 1-2, pp. 133-141.

76. Khanna, N., Sangwan, K.S., (2013), "Comparative machinability study on Ti54M titanium alloy in different heat treatment conditions", *Proc I. Mech. E, Part B: J Engineering Manufacture*, Vol. 227, No. 1, pp. 96-101.

77. Kwak, J.S., (2005), “Application of Taguchi and response surface methodologies for geometric error in surface grinding process”, *International Journal of Machine Tools Manufacturing*, Vol. 45, pp. 327–334.

78. Lee, S.H., Li, X.P., (2003), “Study of surface integrity of machined work piece in EDM of tugesten carbide”, *Journal of Materials Processing Technology*, Vol. 139, pp. 315-321.

79. Liao, Y. S., Huang, J. T. and Chen, Y. H., (2004), "A study to achieve a fine surface finish in wire-EDM", *Journal of Materials Processing Technology*, Vol.149, pp.165-171.

80. Liao, Y.S. and Woo, J.C., (1997), "The effect of machine settings on the behavior of pulses in the WEDM process", *Journal of Materials Processing Technology*, Vol. 71, pp. 433-439.

81. Liao, Y.S., and Yu, Y.P., (2003), "Study of specific discharge energy in WEDM and its application", *International Journal of Machine Tools and Manufacture*, Vol. 44, No. 12-13, pp. 1373–1380.

82. Lauwers, B.; Kruth, J.P.; Liu, W.; Eeraerts, W.; Schacht, B.; Bleys, P. (2004), "Investigation of material removal mechanisms in EDM of composite ceramic materials", *Journal of Material Processing Technology*, Vol.149, pp.347-352.

83. Liu, J. W., Yue, T. M, and Guo, Z. N, (2009), "Wire electro- chemical discharge machining of Al2O3 particle reinforced aluminum alloy 6061", *Materials and Manufacturing Processes*, Vol. 24, No. 4 , pp. 446-453.

84. Lok, Y. K. and Lee, T. C., (1997), "Processing of Advanced ceramics using the wire-cut EDM process", *Journal of Materials Processing Technology*, Vol.63, pp.839-843.

85. Luo. Y.F., (1995), "An energy distribution strategy in fast cutting wire EDM", *Journal of Materials Processing Technology*, Vol.55, pp. 380-390

86. Mahapatra, S. S. and Patnaik, A., (2007), "Optimization of wire electrical discharge machining (WEDM) process parameters using Taguchi method", *International Journal of Advanced Manufacturing Technology*, Vol.34, No. 9-10, pp. 911-925

87. Minami, H., Masui, K., Tsukahara, H., Hagino, H. (1998), "Coloring method of titanium alloy using EDM process", *VDI Berichte*, 1405, pp. 503–512.

88. Lee, Jyh-Wei (2003), " Microstructure evaluation and phase transformation of recast layers in electrical discharge machined dual phase Fe-Mn-Al alloy", *Journal of Material Science*, Vol. 38, pp.1679-1687.

89. Mandal, D., Pal, S. K.,and Saha, P., (2007), "Modeling of electrical discharge machining process using back propagation neural network and multi objective

optimization using non dominating sorting genetic algorithm-II", *Journal of Material Processing Technology*, Vol. 186, pp. 154-162.

90. Manna, A. and Bhattacharya, B., (2006), "Taguchi and gauss elimination method: a dual response approach for parametric optimization of CNC wire cut EDM of PRAISiCMMC", *International Journal of Advanced Manufacturing Technology*, Vol. 28, pp. 67-75.

91. Manna, A., (2009), "A study on electrode wear of WEDM during cutting of E-0300 alloy steel", *Journal of Institution of Engineers*, Vol. 89, pp. 30-35.

92. McGeough, J.A., (1988), "Electro discharge machining, advanced methods of machining", Chapman and Hall, London, pp. 130.

93. Montgomery D.C (2002), " Design and Analysis of Experiments", 4th ed. Wiley New York.

94. Miller, S. F., Chen, C. K., Albert J. S. and Jun, Q., (2005), "Investigation of wire electric discharge machining of thin cross sections and compliant mechanisms", *International Journal of Machine Tools and Manufacture*, Vol. 45, pp. 1717-1725.

95. Mohammadi, A., Tehrani, A., Fadaei, E., E. and Karini, D., (2008), "Statistical analysis of wire electric discharge turning on material removal rate", *Journal of Materials Processing Technology*, Vol. 205, pp.283-289.

96. Mukherjee, R., Chakarboraty, S. and Samanta, S., (2012), "Selection of wire electric discharge machining process parameters using nontraditional optimization algorithms", *Applied Soft Computing*, Vol.12, pp. 2506-2516.

97. Myers, R.H. and Montgomery, D.C., (2002), "Response Surface Methodology – Process and Product Optimization Using Designed Experiments", John Wiley & Sons, New York.

98. Nabhani, F., (2001), "Machining of aerospace Titanium alloys", *Robotics and Computer Integrated Manufacturing*, Vol. 17, pp. 99-106.

99. Newton, T. R., Melkote, S. N. , Watkins, T. R. , Trejo, R. M. and Reister, L., (2009), "Investigation of the effect of process parameters on the formation and characteristics of recast layer in wire-EDM of Inconel 718", *Materials Science and Engineering* , Vol. 513–514, pp. 208–215.

100. Ozdemir, N. and Ozek, C., (2006), "An investigation on machinability of nodular cast iron by WEDM", *International Journal of Advanced Manufacturing Technology*, Vol. 28, pp. 869-872.

101. Pal, S.K, Saha, P., Tarafdar, D., Saha, P., Srivastiva, A.K and Das, K., (2009),"Modelling of wire electro discharge machining of TiC/Fe in metal matrix composite using normalized RBFN with enhanced K means clustering technique, *International Journal of Advanced Manufacturing Technology*, Vol. 43, pp. 107-116.

102. Parashar, V., Rehman ,A., Bhagoria,J. L. and Puri,Y. M., (2010), "Kerfs width analysis for wire cut electro discharge machining of SS 304L using design of experiments", *Indian Journal of Science and Technology*, Vol. 3, No. 4, pp. 369-373.

103. Pasam, V., Battulla, S. B., Madar, V. P. and Swapna, M., (2010), " Optimizing surface finish in WEDM using the Taguchi parameter design method". *Journal of Brazilian Society of Mechanical Science & Engineerin*g, Vol. 32, No.2, pp. 107-113.

104. Patil, G.N. and Brahmakar, P. K., (2010), "Determination of material removal rate in wire electric discharge machining of metal matrix composites using dimensional analysis", *International Journal of Advanced Manufacturing Technology*, Vol. 51, pp. 599-610.

105. Pecas, P., Henriques, E.A., (2003), "Influence of silicon powder nixed dielectric on conventional discharge machining", *International Journal of Machine Tools and Manufacture*, Vol.43, pp. 1465-1471.

106. Peterson, R.G., (1985), "Design and analysis of experiments", Marcell Dekker, New York.

107. Piexto, J.L., (1987), "Hierarchical model selection in polynomial regression models", *Am. Stat*., Vol. 41, pp. 311-313.

108. Porous D. and Zaboruski, S., (2009), "Semi empirical model of efficiency of wire electric discharge machining of hard to machine materials", *Journal of Material Processing Technology*, Vol. 209, No. 3, pp. 1247-1253.

109. Pragya, S., Jain, P.K. and Jain, N. K., (2012), "On wire breakage and micro structure in WEDC of SiCP/6061 aluminum metal matrix composites", *International Journal of Advanced Manufacturing Technology*, Vol. 61, No.9-12, pp.1199-1207.

110. Prasad, D.V.S.S.S.V. and Krishna, A.G., (2009), "Empirical modeling and optimization of wire electrical discharge machining", *International Journal of Advanced Manufacturing Technology*, Vol. 43, pp. 914-925.

111. Puri, A. B., Bhattacharya, B., (2005), "Modelling and analysis of white layer depth in wire cut EDM process through response surface methodology", *International Journal of Advanced Manufacturing Technology*, Vol. 25, pp. 301-307.

112. Puri, A. B. and Bhattacharyya, B., (2003, a), "An analysis and optimization of the geometrical inaccuracy due to wire lag phenomenon in WEDM", *International Journal of Machine tools and Manufacture*, Vol.43, pp.151-159.

113. Puri, A. B. and Bhattacharyya, B., (2003, b), "Modeling and analysis of the wire tool vibration in wire-cut EDM", *Journal of Materials Processing Technology*, Vol.141, pp. 295-301.

114. Pandey, P.C and Shan, H.S., (1980), "Non Traditional machining methods", Tata Mcgraw Hill.

115. Qin, G.W, Smith, G.D.W. and Hao, S.M., (2003), "Wire electric discharge machining induced titanium hydride in Ti-46Al-2Cr alloy", *Intermetallics*, Vol.11, pp. 907-910.

116. Rajurkar, K. P. and Wang, W. M., (1991), "On line monitor and control for wire breakage in WEDM", *Annals CIRP*, Vol. 40, No.1, pp. 219-222.

117. Rajurkar, K.P. and Wang, W.M., (1993), "Thermal Modeling and online monitoring of wire EDM", *Journal of Materials Processing Technology*, Vol. 38, No. 1-2, pp. 417-430.

118. Rajesha, S., Sharma, A.K. and Kumar, P., (2012), "On electro-discharge machining of Inconel- 718 with hollow tool", *Journal of Materials Engineering and Performance*, Vol. 21, pp. 882-891.

119. Rakwal, D. and Bamberg, E., (2009), "Slicing, cleaning and kerf analysis of germanium wafers machined by wire electric discharge machining, *Journal of Materials Processing Technology*, Vol. 209, pp. 3740-3751.

120. Ramakrishna, R. and Karunamoorthy, L., (2008), "Modeling and multi response optimization of Inconel-718 on machining of CNC WEDM process", *Journal of Materials Processing Technology*, Vol. 207, pp. 343-349.

121. Ramakrishnan, R. and Karunamoorthy, L., (2006), "Multi response optimization of wire EDM operations using robust design of experiments", *International Journal of Advanced Manufacturing Technology*, Vol. 29, pp.105-112.

122. Rao, P., Sarkar, S. (2009), "Evaluation of optimal parameters for machining brass with wire cut EDM", J*ournal of Scientific and Industrial Research*, Vol. 68, pp. 32-35.

123. Rao, P. V., Suresh, P.V.S. and Deshmukh, S.G., (2002), "A genetic algorithmic approach for optimization of surface roughness prediction model", *International Journal of Machine Tools & Manufacture*, Vol. 42, pp. 675–680.

124. Rao, R. V. and Pawar, P.J., (2010), "Modelling and optimization of process parameters of wire electric discharge machining", *Proceedings of I. Mech. E, Part B; Journal of Engineering Manufacture*, Vol. 223, pp. 1431-1440.

125. Rao, S., Pujari, R. K. and Satyanarayana, B., (2010), "Prediction of material removal rate for Aluminum BIS-24345 alloy in wirecut EDM", International Journal Engineering Science and Technoogy., Vol. 2, No. 12, pp. 7729-7739.

126. Regener, B., Krempaszky, C., Werner, E., Berhuber, E. and Stockinger, M., (2010), "Characterization of residual stresses by WEDM-assisted dissectioning", *Materials Science and Engineering*, Vol.10, pp. 1-10.

127. Roger, K., (2010), "Wire EDM deionizing resin", *EDM Today*, pp. 10-16.

128. Rozenek, M., Kozak, J., Dabrowski, L. and Lubkowski, K., (2001), "Electrical discharge machining characteristics of metal matrix composites", *Journal of Materials Processing Technology*, Vol.109, pp. 367-370.

129. Sadeghi, M., Razavi, H., Esmaeilzadeh, A. and Kolahan, F., (2011), "Optimization of cutting conditions in WEDM process using regression modeling

and Tabu search algorithm", *Proceedings of IMechE Part B: Journal of Engineering Manufacture*, Vol. 225, pp. 1825-1834.

130. Saha, P., Singha, A., Pal, S.K.and Saha,P., (2009), "Soft computing models based prediction of cutting speed and surface roughness in wire electro-discharge machining of tungsten carbide cobalt composite", International *Journal of Advanced Manufacturing Technology*, Vol. 39, No. 1-2, pp. 74-84.

131. Sanchez, J.A., Rodil, J. L., Herrero, A., Lopez L. N. and Lamikiz, A., (2007), "On the influence of cutting speed limitation on the accuracy of wire-EDM corner-cutting", *Journal of Materials Processing Technology*, Vol. 182, pp. 574–579.

132. Sardinas, R. Q., Santana, M. R. and Beindis, E. A., (2006), "Genetic algorithm based multi objective optimization of cutting parameters in turning processes", Engineering Applications in Artificial Intelligence, Vol. 19, pp. 127-133.

133. Sarkar, S., Mitra, S. and Bhattacharyya B., (2005), "Parametric analysis and optimization of wire electrical discharge machining of γ-titanium aluminide alloy", *Journal of Materials Processing Technology*, Vol. 159, No. 3, pp. 286-294.

134. Sarkar, S., Mitra, S. and Bhattachyraya, B., (2006), "Parametric optimization of wire electric discharge machining of γ titanium alumnide alloy through an artificial neural network model", *International Journal of Advanced Manufacturing Technology*, Vol. 27, pp. 501-508.

135. Sarkar, S., Sekh, M., Mitra, S. and Bhattacharyya, B., (2008), "Modeling and optimization of wire electrical discharge machining of γ-TiAl in trim cutting operation", *Journal of Materials Processing Technology*, Vol. 205, pp. 376-387.

136. Sarkar, S., Ghosh, K., Mitra, S. and Bhattacharya B (2010), "An integral approach to optimization of WEDM combining single pass and multi pass cutting operations", *Materials and Manufacturing Processes*, Vol. 25, pp. 799-807.

137. Satish, K. D., Kanthababu, M., Vajjiravelu, V., Anburaj, R., Sundarragan, N.T. and Arul, H., (2011), "Investigation of wire electrical discharge machining characteristics of Al 6063/SiCP composites", *International Journal of Advanced Manufacturing Technology*, Vol.56, pp. 975-986.

138. Scott F. Miller, Albert J, Shih Jun Qu, (2004), "Investigation of spark cycle on material removal rate in wire electrical discharge machining of advanced materials", *International Journal of Machine Tools and Manufacture* 44, pp. 391-400.

139. Scott, D., Boyina, S. and Rajurkar, K.P., (1991), "Analysis and optimization of parameter combination in wire electrical discharge machining", *International Journal of Production Research*, Vol. 29, No. 11, pp. 2189-2207.

140. Shabgard, M., Olivei, S.N.B., Seyedzavuar, M. and Najadekrahimi, A., (2011), "Experimental investigation and 3D finite element prediction of white layer thickness, heat effected zone and surface roughness in EDM process", Journal of Mechanical Science and Technology, Vol. 25, No. 12, pp. 3173-3183.

141. Shah, A., Nadeem, A., Rakwal, D. and Bamberg, E., (2009), "Material removal rate, kerf, and surface roughness of tungsten carbide machined with wire electric discharge machining", *Journal of Materials Engineering and Performance* , Vol. 20, No. 1, pp. 71-76.

142. Somashekhar, K.P., Mathew, J. and Ramachandran, N., (2012), "A feasibility approach by simulated annealing on optimization of micro wire electric discharge machining parameters", *International Journal of Advanced Manufacturing Technology*, Vol.61, No. 9-12, pp. 1209-1213.

143. Souza, A.S., Dos S., Walter, N.L., Ferreira, S.L.C., (2005), "Application of Box–Behnken design in the optimization of an on-line pre-concentration system using knotted reactor for cadmium determination by flame atomic absorption spectrometry". *Spectrochimica Acta Part-B*, Vol. 609, pp. 737–742.

144. Spedding, T. A. and Wang, Z. Q., (1997), "Parameter optimization and surface characteristics of wire electrical discharge machining process", *International Journal of Precision Engineering*, Vol.20, pp. 5-15.

145. Sreejith, P.S. and Nagoi, B.K.A., (2000), "Dry machining: machining of future", *Journal of Materials Processing Technology*, Vol. 101, pp. 287-291.

146. Takeyama, H. and Murata, R. (1962), "Study on machinability of pure titanium", *Journal of JSPE*, Vol. 28, No. 6, pp. 331.

147. Tarng, Y. S., Ma, S. C. and Chung, L. K., (1995), "Determination of optimal cutting parameters in wire electrical discharge machining", *International Journal of Machine Tools and Manufacture*, Vol. 35, pp.1693-1701.

148. Tosun, N., Cogun. C and Inan, A., (2003), "The effect of cutting parameters on work piece surface roughness in wire EDM", *Machining Science and Technology*, Vol.7, No. 2, pp. 209-219.

149. Tosun, N., Cogun, C. and Pihtili, H. (2003, a), "The Effect of cutting parameter on wire crater sizes in wire EDM", *International Journal of Advanced Manufacturing Technology*, Vol.21, pp. 857-865.

150. Tzeng, C. J., Yang, Y. K., Hseigh, M. H. and Jeng, M. C., (2010), "Optimization of wire electrical discharge machining of pure tungsten using neural network and response surface methodology", *Proceedings of I Mech E, Part B: J. Engineering Manufacture*, Vol. 225, pp. 841-852.

151. Taweel,T.A.(2009), "Multi-response optimization of EDM with Al–Cu–Si–TiC P/M composite electrode, *International Journal of Advanced Manufacturing Technology*, Vol. 44, pp.100-113.

152. Tai, Tzu-Yao; Lu, S.J.; Chen, Y.H. (2011), "Surface crack susceptibility of electro discharge-machined steel surfaces", *International journal of Advance Manufacturing Technology*, Vol.57, pp.983-989.

153. Yadav, V., Jain, V.K., Dixit, P.M., (2002), "Thermal stresses due to electrical discharge machining", *International Journal of Machine Tools & Manufacture*, Vol. 42, pp. 877-888.

154. Wang, J., Ravani, B., (2003), "Computer aided contouring operation for travelling wire electric discharge machining (EDM)", *Computer- Aided Design*, Vol. 35, No.10, pp. 925–934.

155. Weingartner, G., Konard, W. and Friedrich, K., (2012), "Wire electric discharge machining applied to rotating work pieces", *Journal of Materials Processing Technology*, Vol. 23, pp.1298-1304.

156. Wong, Y.S., Lim, L.C. and Lee, L.C., (1995), "Effect of flushing on electro discharged machined surfaces, Journal of Materials Processing Technology, Vol. 48, pp. 299-305.

157. Wood, R.A., and Favor, R.J. (1972), "Titanium alloys handbook", Air Force Materials Laboratory, Ohio, pp. 45-46.

158. Wansheng, Z., Zhenlong, W., Shichun, D., Guanxin, C., Hongyu, W. (2002), "Ultrasonic and electric discharge machining to deep and small hole on titanium alloy", *Journal of Materials Processing Technology* 120, pp. 101–106.

159. Yang, Xiaoping and L.C., Richard (1999), "Machining titanium and its alloys", *Machining Science and Technology*, Vol.3 (1), pp.107-139.

160. Yadav, V., Jain, V.K., Dixit, P.M., (2002), "Thermal stresses due to electrical discharge machining", *International Journal of Machine Tools & Manufacture*, Vol. 42, pp. 877-888.

161. Yan, B. H., Tsai, H. C., Huang, F. Y. and Lee, L.C., (2005), "Examination of wire electrical discharge machining of Al_2O_3p/6061Al composites", *International Journal of Machine tools and Manufacture*, Vol. 45, pp. 251-259

162. Yang, R. T., Tzeng, C. J., Yang, Y. K. and Hseigh, M. H., (2012), "Optimization of wire electric discharge machining process parameters for cutting Tungsten", *International Journal of Advanced Manufacturing Technology*, Vol. 60, pp. 135-147.

163. Yeh, Chin-Chang, Wu, Kun-Ling, Lee, Jyh-Wei and Yan, Biing-Hwa, (2013), "Study on surface characteristics using phosphorous dielectric on wire electrical discharge machining of polycrystalline silicon," *International Journal of Advanced Manufacturing Technology,* DOI 10.1007/s00170-013-4995-9.

164. Zhang, Yanzhen, Liu,Yonghong, Ji,Renjie, and Cai, Baoping, (2011), " Study of the recast layer of a surface machined by sinking electrical discharge machining using water-in-oil emulsion as dielectric",. *Applied Surface Science,* Vol. 257, pp. 5989-5997.

APPENDIX I

Table A: Conversional table for pulse on Time from machine Units (mu) to micro seconds (µs)

T_{on} (mu)	T_{on} (µs)	T_{on} (mu)	T_{on} (µs)	T_{on} (mu)	T_{on} (µs)	T_{on} (mu)	T_{on} (µs)
100	0.1	108	0.5	116	0.9	124	1.3
101	0.15	109	0.55	117	0.95	125	1.35
102	0.2	110	0.6	118	1	126	1.4
103	0.25	111	0.65	119	1.05	127	1.45
104	0.3	112	0.7	120	1.1	128	1.5
105	0.35	113	0.75	121	1.15	129	1.55
106	0.4	114	0.8	122	1.2	130	1.6
107	0.45	115	0.85	123	1.25	131	1.65

Legend: TON- Pulse on time, mu- machine units, µs- micro seconds

Table B: Conversional table for pulse off time from machine units (mu) to micro seconds (µs)

T_{off} (mu)	T_{off} (µs)	T_{off} (mu)	T_{off} (µs)	T_{off} (mu)	T_{off} (µs)	T_{off} (mu)	T_{off} (µs)
0	2	16	6	32	10	48	22
1	2.25	17	6.25	33	10.5	49	24
2	2.5	18	6.5	34	11	50	26
3	2.75	19	6.75	35	11.5	51	28
4	3	20	7	36	12	52	30
5	3.25	21	7.25	37	12.5	53	32
6	3.5	22	7.5	38	13	54	34
7	3.75	23	7.75	39	13.5	55	36
8	4	24	8	40	14	56	38
9	4.25	25	8.25	41	14.5	57	40
10	4.5	26	8.5	42	15	58	42
11	4.75	27	8.75	43	16	59	44
12	5	28	9	44	17	60	46
13	5.25	29	9.25	45	18	61	48
14	5.5	30	9.5	46	19	62	50
15	5.75	31	9.75	47	20	63	52

Legend: T_{off}- Pulse off time, mu- machine units, µs- micro seconds

Table C: Conversional table for wire tension from machine units (mu) to grams (gram)

WT (mu)	WT (gram)	WT (mu)	WT (gram)	WT (mu)	WT (gram)	WT (mu)	WT (gram)
0	450	4	500	8	1000	12	1800
1	450	5	600	9	1200	13	2000
2	450	6	700	10	1400	14	2200
3	450	7	850	11	1600	15	2500

Legend: WT- Wire Tension, mu- machine units, µs- micro seconds